Publishing House ASV
begell house, inc. publishers
РААСН
Scientific coordination is carried out by the Russian Academy of Architecture and Construction Sciences (RAACS)

Volume 18 • Issue 3 • 2022

ISSN 2588-0195 (Online)
ISSN 2587-9618 (Print) Continues ISSN 1524-5845

International Journal for
Computational Civil and Structural Engineering

Международный журнал по расчету гражданских и строительных конструкций

http://raasn.ru/public.php
http://ijccse.iasv.ru/index.php/IJCCSE

DOI: 10.22337/2587-9618
GICID: 71.0000.1500.2830

Scientific coordination is carried out by the Russian Academy of Architecture and Construction Sciences (RAACS)

PUBLISHER

ASV Publishing House
(ООО «Издательство АСВ»)
19/1,12, Yaroslavskoe Shosse, 120338, Moscow, Russia
Tel. +7(925)084-74-24; E-mail: iasv@iasv.ru; Интернет-сайт: http://iasv.ru/

ADVISORY EDITORIAL BOARD

EDITORIAL TEAM

INVITED REVIEWERS

AIMS AND SCOPE

The aim of the Journal is to advance the research and practice in structural engineering through the application of computational methods. The Journal will publish original papers and educational articles of general value to the field that will bridge the gap between high-performance construction materials, large-scale engineering systems and advanced methods of analysis.

The scope of the Journal includes papers on computer methods in the areas of structural engineering, civil engineering materials and problems concerned with multiple physical processes interacting at multiple spatial and temporal scales. The Journal is intended to be of interest and use to researches and practitioners in academic, governmental and industrial communities.

ОБЩАЯ ИНФОРМАЦИЯ О ЖУРНАЛЕ

International Journal for Computational Civil and Structural Engineering

(Международный журнал по расчету гражданских и строительных конструкций)

Международный научный журнал “International Journal for Computational Civil and Structural Engineering (Международный журнал по расчету гражданских и строительных конструкций)” (IJCCSE) является ведущим научным периодическим изданием по направлению «Инженерные и технические науки», издаваемым, начиная с 1999 года (ISSN 2588-0195 (Online); ISSN 2587-9618 (Print) Continues ISSN 1524-5845). В журнале на высоком научно-техническом уровне рассматриваются проблемы численного и компьютерного моделирования в строительстве, актуальные вопросы разработки, исследования, развития, верификации, апробации и приложений численных, численно-аналитических методов, программно-алгоритмического обеспечения и выполнения автоматизированного проектирования, мониторинга и комплексного наукоемкого расчетно-теоретического и экспериментального обоснования напряженно-деформированного (и иного) состояния, прочности, устойчивости, надежности и безопасности ответственных объектов гражданского и промышленного строительства, энергетики, машиностроения, транспорта, биотехнологий и других высокотехнологичных отраслей.

В редакционный совет журнала входят известные российские и зарубежные деятели науки и техники (в том числе академики, члены-корреспонденты, иностранные члены, почетные члены и советники Российской академии архитектуры и строительных наук). Основной критерий отбора статей для публикации в журнале − их высокий научный уровень, соответствие которому определяется в ходе высококвалифицированного рецензирования и объективной экспертизы, поступающих в редакцию материалов.

Журнал входит в Перечень ВАК РФ ведущих рецензируемых научных изданий, в которых должны быть опубликованы основные научные результаты диссертаций на соискание ученой степени кандидата наук, на соискание ученой степени доктора наук по научным специальностям и соответствующим им отраслям науки:

- 1.1.8 – Механика деформируемого твердого тела (технические науки),
- 1.2.2 – Математическое моделирование численные методы и комплексы программ (технические науки),
- 2.1.1 – Строительные конструкции, здания и сооружения (технические науки),
- 2.1.2 – Основания и фундаменты, подземные сооружения (технические науки),
- 2.1.5 – Строительные материалы и изделия (технические науки),
- 05.23.07 – Гидротехническое строительство (технические науки),
- 2.1.9 – Строительная механика (технические науки)

В Российской Федерации журнал индексируется Российским индексом научного цитирования (РИНЦ).

Журнал входит в базу данных Russian Science Citation Index (RSCI), полностью интегрированную с платформой Web of Science. Журнал имеет международный статус и высылается в ведущие библиотеки и научные организации мира.

Издатели журнала – *Издательство Ассоциации строительных высших учебных заведений /АСВ/* (Россия, г. Москва) и до 2017 года *Издательский дом Begell House Inc*. (США, г. Нью-Йорк). Официальными партнерами издания является *Российская академия архитектуры и строительных наук* (РААСН), осуществляющая научное курирование издания, и *Научно-исследовательский центр СтаДиО* (ЗАО НИЦ СтаДиО).

Цели журнала – демонстрировать в публикациях российскому и международному профессиональному сообществу новейшие достижения науки в области вычислительных методов решения фундаментальных и прикладных технических задач, прежде всего в области строительства.

Задачи журнала:

• предоставление российским и зарубежным ученым и специалистам возможности публиковать результаты своих исследований;

• привлечение внимания к наиболее актуальным, перспективным, прорывным и интересным направлениям развития и приложений численных и численно-аналитических методов решения фундаментальных и прикладных технических задач, совершенствования технологий математического, компьютерного моделирования, разработки и верификации реализующего программно-алгоритмического обеспечения;

• обеспечение обмена мнениями между исследователями из разных регионов и государств.

Тематика журнала. К рассмотрению и публикации в журнале принимаются аналитические материалы, научные статьи, обзоры, рецензии и отзывы на научные публикации по фундаментальным и прикладным вопросам технических наук, прежде всего в области строительства. В журнале также публикуются информационные материалы, освещающие научные мероприятия и передовые достижения Российской академии архитектуры и строительных наук, научно-образовательных и проектно-конструкторских организаций.

Тематика статей, принимаемых к публикации в журнале, соответствует его названию и охватывает направления научных исследований в области разработки, исследования и приложений численных и численно-аналитических методов, программного обеспечения, технологий компьютерного моделирования в решении прикладных задач в области строительства, а также соответствующие профильные специальности, представленные в диссертационных советах профильных образовательных организациях высшего образования.

Редакционная политика. Политика редакционной коллегии журнала базируется на современных юридических требованиях в отношении авторского права, законности, плагиата и клеветы, изложенных в законодательстве Российской Федерации, и этических принципах, поддерживаемых сообществом ведущих издателей научной периодики.

За публикацию статей плата с авторов не взымается. Публикация статей в журнале бесплатная. На платной основе в журнале могут быть опубликованы материалы рекламного характера, имеющие прямое отношение к тематике журнала.

Журнал предоставляет непосредственный открытый доступ к своему контенту, исходя из следующего принципа: свободный открытый доступ к результатам исследований способствует увеличению глобального обмена знаниями.

Индексирование. Публикации в журнале входят в системы расчетов индексов цитирования авторов и журналов. «Индекс цитирования» – числовой показатель, характеризующий значимость данной статьи и вычисляющийся на основе последующих публикаций, ссылающихся на данную работу.

Авторам. Прежде чем направить статью в редакцию журнала, авторам следует ознакомиться со всеми материалами, размещенными в разделах сайта журнала (интернет-сайт Российской академии архитектуры и строительных наук (http://raasn.ru); подраздел «Издания РААСН» или интернет-сайт Издательства АСВ (http://iasv.ru); подраздел «Журнал IJCCSE»): с основной информацией о журнале, его целями и задачами, составом редакционной коллегии и редакционного совета, редакционной политикой, порядком рецензирования направляемых в журнал статей, сведениями о соблюдении редакционной этики, о политике авторского права и лицензирования, о представлении журнала в информационных системах (индексировании), информацией о подписке на журнал, контактными данными и пр. Журнал работает по лицензии Creative Commons типа cc by-nc-sa (Attribution Non-Commercial Share Alike) – Лицензия «С указанием авторства – Некоммерческая – Копилефт».

Рецензирование. Все научные статьи, поступившие в редакцию журнала, проходят обязательное двойное слепое рецензирование (рецензент не знает авторов рукописи, авторы рукописи не знают рецензентов).

Заимствования и плагиат. Редакционная коллегия журнала при рассмотрении статьи проводит проверку материала с помощью системы «Антиплагиат». В случае обнаружения многочисленных заимствований редакция действует в соответствии с правилами COPE.

Подписка. Журнал зарегистрирован в Федеральном агентстве по средствам массовой информации и охраны культурного наследия Российской Федерации. Индекс в общероссийском каталоге РОСПЕЧАТЬ − 18076.

По вопросам подписки на международный научный журнал “International Journal for Computational Civil and Structural Engineering (Международный журнал по расчету гражданских и строительных конструкций)” обращайтесь в Агентство «Роспечать» (Официальный сайт в сети Интернет: http://www.rosp.ru/) или в издательство Ассоциации строительных вузов (АСВ) в соответствии со следующими контактными данными:

ООО «Издательство АСВ»

Юридический адрес: 129337, Россия, г. Москва, Ярославское ш., д. 26, офис 705;

Фактический адрес: 129337, Россия, г. Москва, Ярославское ш., д. 19, корп. 1, 5 этаж, офис 12 (ТЦ Соле Молл);

Телефоны: +7 (925) 084-74-24, +7 (926) 010-91-33;

Интернет-сайт: www.iasv.ru. Адрес электронной почты: iasv@iasv.ru.

Контактная информация. По всем вопросам работы редакции, рецензирования, согласования правки текстов и публикации статей следует обращаться к главному редактору журнала члену-корреспонденту РААСН *Сидорову Владимиру Николаевичу* (адреса электронной почты: sidorov.vladimir@gmail.com, sidorov@iasv.ru, iasv@iasv.ru, sidorov@raasn.ru) или к техническому редактору журнала советнику РААСН *Кайтукову Таймуразу Батразовичу* (адреса электронной почты: tkaytukov@gmail.com; kaytukov@raasn.ru). Кроме того, по указанным вопросам, а также по вопросам размещения в журнале рекламных материалов можно обращаться к генеральному директору ООО «Издательство АСВ» *Никитиной Надежде Сергеевне* (адреса электронной почты: iasv@iasv.ru, nsnikitina@mail.ru, ijccse@iasv.ru).

Журнал становится технологичнее. Издательство АСВ с сентября 2016 года является членом Международной ассоциации издателей научной литературы (Publishers International Linking Association (PILA)), осуществляющей свою деятельность на платформе CrossRef. Оригинальным статьям, публикуемым в журнале, будут присваиваться уникальные номера (индексы DOI – Digital Object Identifier), что значительно облегчит поиск метаданных и местонахождение полнотекстового произведения. DOI – это система определения научного контента в сети Интернет.

С октября 2016 года стал возможен прием статей на рассмотрение и рецензирование через онлайн систему приема статей Open Journal Systems на сайте журнала (электронная редакция): http://ijccse.iasv.ru/index.php/IJCCSE.

Автор имеет возможность следить за продвижением статьи в редакции журнала в личном кабинете Open Journal Systems и получать соответствующие уведомления по электронной почте.

В феврале 2018 года журнал был зарегистрирован в Directory of open access journals (DOAJ) (это один из самых известных поисковых сервисов в мире, который предоставляет открытый доступ к материалам и индексирует не только заголовки журналов, но и научные статьи), в сентябре 2018 года включен в продукты EBSCO Publishing.

В ноябре 2020 года журнал начал индексироваться в международной базе Scopus.

International Journal for
Computational Civil and Structural Engineering
(Международный журнал по расчету гражданских и строительных конструкций)
Volume 18, Issue 3 ***2022***

Scientific coordination is carried out by the Russian Academy of Architecture and Construction Sciences (RAACS)

CONTENTS

International Journal for
Computational Civil and Structural Engineering
(Международный журнал по расчету гражданских и строительных конструкций)
Volume 18, Issue 3 ***2022***

Scientific coordination is carried out by the Russian Academy of Architecture and Construction Sciences (RAACS)

СОДЕРЖАНИЕ

DOI:10.22337/2587-9618-2022-18-3-14-24

NUMERICAL SIMULATION OF THE PROCESS OF DIRECTED TRANSFORMATION OF A REGULAR HINGE-ROD SYSTEM

***Peter P. Gaydzhurov* [1], *Nadezhda G. Tsaritova* [2], *Abacar I. Kurbanov* [2], *Anastasia A. Kurbanova* [2], *Elvira R. Iskhakova* [2]**

[1] Don State Technical University, Rostov-on-Don, RUSSIA
[2] Platov South-Russian State Polytechnic University, Novocherkassk, RUSSIA

Abstract. The process of forming new architectural solutions in the field of regular frame-rod systems necessitates the development of the concept of creating original spatial structures through the directed transformation of kinematically changeable truss-type objects. The article presents a numerical study of kinematic parameters during the gradual shaping of a rod system, which in its initial state is a flat hinge-rod network of repeating fragments in the form of equilateral triangles. The controlled kinematic effect on the object was modeled using actuators that were placed on the peripheral sections of the studied grids.
The wide variability of the hinge-rod forms, the economical installation process using the principle of "self-extension" allow us to speak about the relevance of research in this direction.

Keywords: hinge-rod structures, finite element method, matrix stiffness, the stress-strain state, actuators

ЧИСЛЕННОЕ МОДЕЛИРОВАНИЕ ПРОЦЕССА НАПРАВЛЕННОЙ ТРАНСФОРМАЦИИ РЕГУЛЯРНОЙ ШАРНИРНО СТЕРЖНЕВОЙ СИСТЕМЫ

***П.П. Гайджуров* [1], *Н.Г. Царитова* [2], *А.И. Курбанов* [2], *А.А. Курбанова* [2], *Э.Р. Исхакова* [2]**

[1] Донской государственный технический университет, Ростов-на-Дону, РОССИЯ
[2] «Южно-Российский государственный политехнический университет (НПИ) имени М.И. Платова», Новочеркасск, РОССИЯ

Аннотация. Процесс формирования новых архитектурных решений в области регулярных каркасно-стержневых систем обуславливает необходимость разработки концепции создания оригинальных пространственных структур путем направленной трансформации кинематически изменяемых объектов ферменного типа. В статье выполнено численное исследование кинематических параметров при постепенном формоизменении стержневой системы, представляющей в исходном состоянии плоскую шарнирно-стержневую сеть из повторяющихся фрагментов в форме равносторонних треугольников. Управляемое кинематическое воздействие на объект моделировалось с помощью актуаторов, которые размещались на периферийных участках исследуемых сеток.
Широкая вариативность шарнирно-стержневых форм, экономичный процесс монтажа с использованием принципа «самовыдвижения» позволяют говорить об актуальности исследований в данном направлении.

Ключевые слова: шарнирно-стержневая система, метод конечных элементов, матрица жесткости, напряженно-деформированное состояние, актуаторы.

INTRODUCTION

The process of forming new architectural solutions in the field of regular frame-rod systems necessitates the development of the concept of creating original spatial structures through the directed transformation of kinematically changeable truss-type objects.
Currently, folding in two directions have become widespread (S_x, S_y) cover formed from hinge-rod kinematic pairs (Fig. 1).

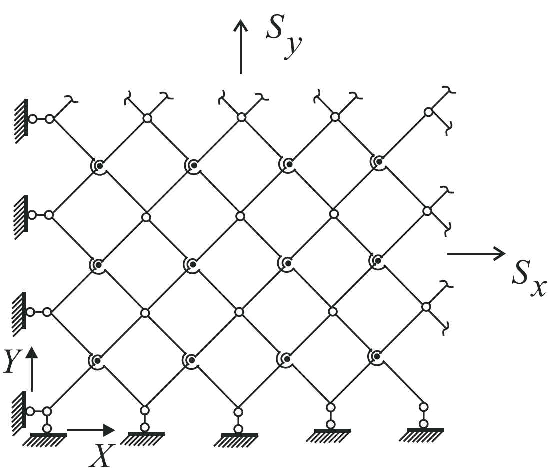

Figure 1. Kinematic scheme of a collapsible covering

A separate category consists of hinge-rod systems (HRS) of large-sized transformable space structures, the disclosure of which occurs automatically in zero gravity [1].
Works [2, 3] are devoted to the problem of finite element analysis of the stress-strain state of hinge-rod systems taking into account large displacements. In particular, in [2] a two-rod instantaneously kinematically variable HRS is considered, the design scheme of which is shown in Fig.2. For numerical simulation of the behavior of the HRS in a geometrically nonlinear formulation, the authors have developed an algorithm based on a step-by-step loading scheme and the formation at each step of a mixed system of equations in the form of the displacement method and the force method. The configuration of this HRS corresponding to a statically unchangeable state (the rightmost position of the second link) is shown in Fig. 3. In order to verify the algorithm proposed in [2, 3] we will perform the calculation of the two-rod HRS for the initial position A, B, C and configuration of the system in the position A', B', C (Fig. 3). Figures 4 and 5 show the patterns of vertical displacement distribution $u_y^{(A)}$ and longitudinal forces N in rods, derived using a nonlinear solver of the software package ANSYS Mechanical. Comparing these data with the results of [2], we establish that the value of $u_{y\,max}^{(A)}$ corresponding to the calculation of an instantaneously changeable system (Fig. 4) is in both calculations -4,97 m. when geometrically nonlinear calculation of HRS in position $\alpha = 90^0$ также получены the results are similar [2]. The coincidence of the results is also observed when comparing the longitudinal forces in the rods for the two positions of the system.

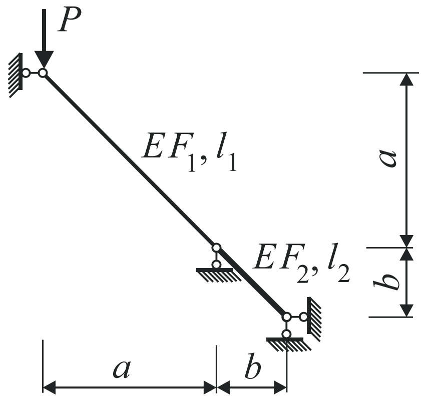

Figure 2. Two - rod HRS

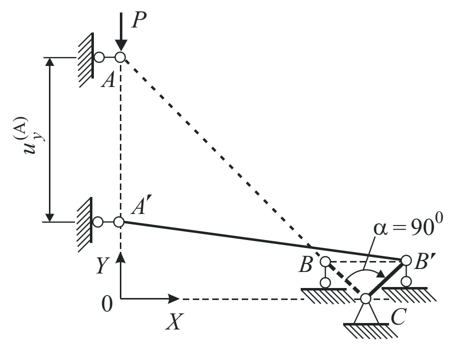

Figure 3. Configuration HRS

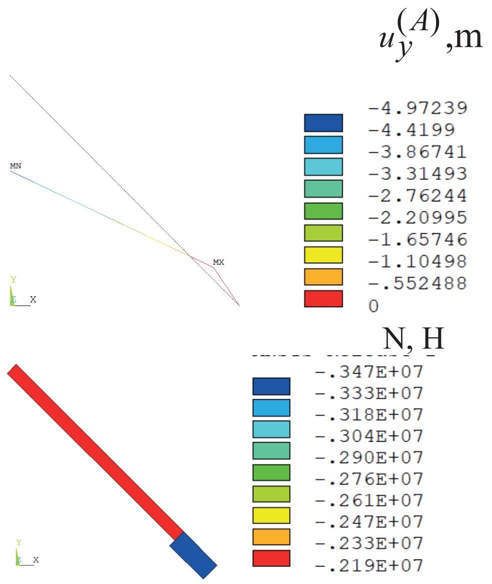

Figure 4. Distribution patterns $u_y^{(A)}$ и N for the initial instantaneously changeable state HRS

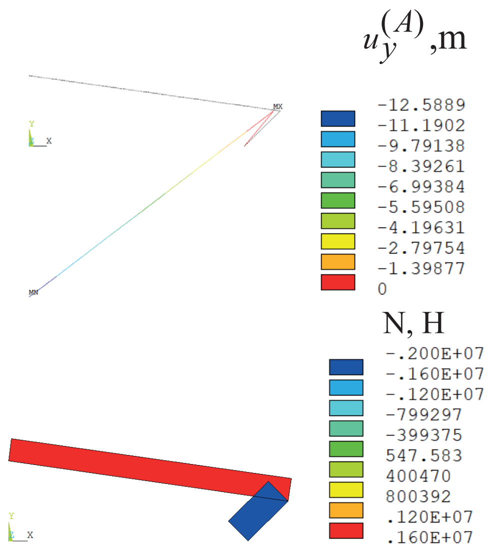

Figure 5. Distribution patterns $u_y^{(A)}$ и N for a statically immutable state HRS

Thus, it can be argued that the ANSYS software package allows for the simulation of HRS with sufficient accuracy, taking into account large displacements.

The article presents a numerical study of the kinematic parameters of the rod system with its gradual formalization. In its initial state, the system is a flat hinge-rod network of repeating fragments in the form of equilateral triangles. The controlled kinematic effect on the object was modeled using actuators that were placed on the peripheral sections of the studied grids. The wide variability of hinge-rod forms, the economical installation process using the principle of "self-extension" allow us to speak about the relevance of research in this direction.

MATERIALS AND METHODS

As an object of research, we consider a hinge-rod system (HRS), the initial state of which (before transformation) is shown in Figure 6. Each rod of the SHSS is modeled by one three-dimensional truss finite element [4]. We set the geometry of the SHSS in the global axes X, Y, Z. We believe that the stiffness of all the rods of the system is the same.

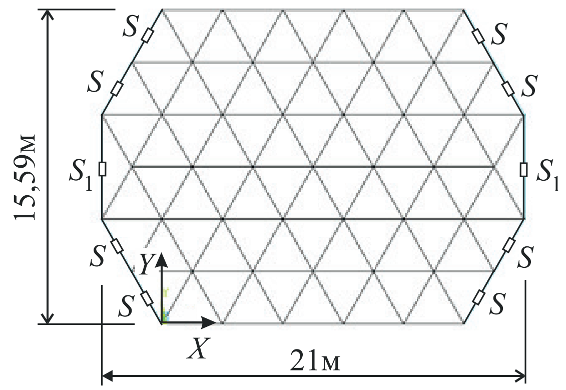

Figure 6. Hinge-rod system in the initial state

In Fig. 6, the links with actuators are marked with rectangles and marked with the letters S и S_1. Synchronous axial movements can be created on the hinges of the actuators, causing shortening / elongation of the links. We model the actuators with combined finite elements [3]. Figure 7 shows a repeating fragment of the HRS. In the initial state, the positive direction of the normals $\overline{n}$ of all fragments coincides with the orientation of the Z axis. For each rod of a repeating fragment, we introduce a local system of axes so that the axis $\overline{x}, \overline{y}, \overline{z}$ so that the direction of the axis $\overline{z}$ coincided with normal $\overline{n}$, and the axis $\overline{x}$ was directed from the node

i to the node k provided that the node numbers are arranged in this sequence $j > k > i$. Axle $\overline{y}$ are pointing away from the center of the fragment.

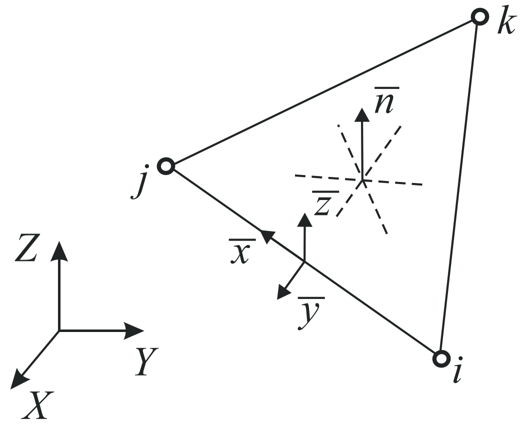

Figure 7. A repeating fragment of the hinge-rod system

The calculation scheme for modeling the process of transformation of the HRS is shown in Fig. 8. In this drawing, the symbols «+», «Δ», «▷» the connections prohibiting movement are marked, respectively, in the direction of the axes *Z*, *Y*, *X*. Letters *a* and *b* denote nodes, movements u_z which will be observed during directed transformation HRS. The letter *e* denotes an element, the kinematic parameters of which will also be investigated in the process of shaping the HRS.

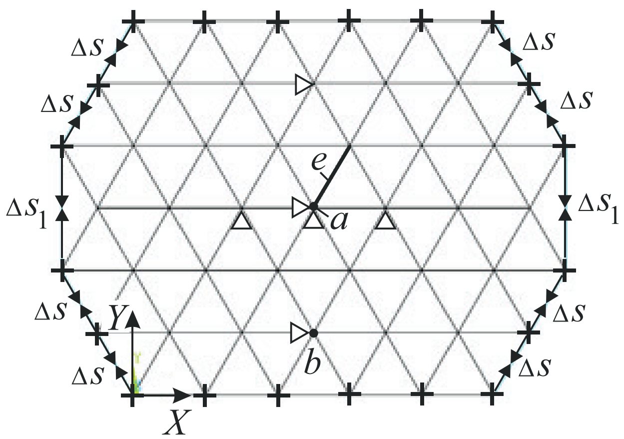

Figure 8. Calculation scheme for modeling the process of shaping HRS

We accept the following assumptions [5, 6, 7]:

- the process of transformation of the structure is a quasi-static sequence of steps $k = 1, 2, ..., n$ discrete changes in the lengths of combined finite elements by small values Δs, Δs_1 (Fig. 8);
- in the process of transformation of the structure, the achieved level of stress state of the rods is inherited.

We emphasize that the transition from the current position of the rod k to the subsequent provision $k+1$ it is accompanied by small increments of the values of the nodal coordinates. Based on this, the calculation of the stress-strain state at each step of the transformation of the HRS is carried out within the framework of the linear theory of elasticity.

For the software implementation of the proposed concept of the transformation of the HRS, we use the programming language APDL [8], built into the ANSYS Mechanical software package [4]. An application macro created on the basis of this language is entered into the command window, after which each line of the macro is processed by the APDL interpreter and, in case of a positive result, it is immediately launched for execution. Thus, the macro allows you to automatically create the geometry of the structure, build a finite element grid, set boundary conditions and load, run the solver to perform calculations, as well as perform intermediate operations related to extracting information from the ANSYS database at the current loading step and forming working arrays by performing the necessary algebraic procedures. In addition to the listed actions, the macro contains commands to delete and rebuild the finite element model at each step of the calculation.

RESULTS OF FINITE ELEMENT MODELING

First of all, it should be noted that the design scheme of the HRS (Fig. 8) is geometrically changeable. Therefore, the process of transformation of the HRS from the position when the coordinates of all nodes $z_i = 0$, it will not lead to the expected rise of repeating fragments, i.e. it is necessary to start (begin transformation) with a pre-prepared dome-shaped geometry of the HRS (Fig. 9).

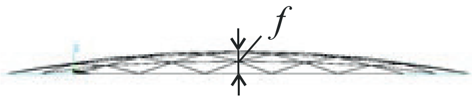

Figure 9. Pre - launch domed shape HRS

In this connection, the question arises: at what minimum value of the lifting boom *f* the arch effect occurs and how to make the transition from a flat configuration of the HRS (*f* = 0) to a domed shape (*f* > 0) with the preservation of the original lengths of the rods?

To transition from the initial flat shape of the SHSS to the starting dome-shaped configuration, we use kinematic boundary conditions, which are reduced to setting displacements in the direction of the axis *Z* in the non-support nodes of the grid:

$$u^*_{zi} = f\varphi_i(\xi,\eta),$$

marked: $\varphi_i(\xi,\eta) = 1-\xi^2-\eta^2+\xi^2\eta^2$ – approximating polyquadratic polynomial; $\xi = \dfrac{2(x_i-7,5)}{21}$; $\eta = \dfrac{2(y_i-7,794)}{15,59}$ – normalized coordinates that take into account the dimensions HRS; x_i, y_i – coordinates of nodes truss finite element in global axes.

Based on the accepted kinematic boundary conditions, the stiffness matrix is adjusted according to standard technology and the corresponding vector of the right part of the resulting system of equations is formed. To solve the corrected system of equations, we use the nonlinear solver of the ANSYS complex, i.e. we perform the calculation taking into account large (finite) displacements. The obtained data on the new geometry of the nodes and the corresponding topology of the model are recorded in intermediate files.

In order to test the proposed approach to obtaining the domed shape of the HRS, a computational experiment was conducted for the values of the parameter *f* equals 0,1m, 0,25m, 0,5m, 1,0m, 1,5m. The calculations were carried out taking into account geometric nonlinearity (large displacements). As an evaluation criterion, we used control over the immutability of the lengths of the rods of the model during the transition from the initial (flat) shape to the domed shape of the HRS. It was found that the iterative process in the investigated range of the parameter f converges and the lengths of the rods before and after the calculation coincide.

The next step was to study the obtained dome-shaped shapes of the HRS for the presence of an arched effect under the boundary conditions shown in Fig. 5 and the action of only the own weight of the rods. As a result, it was found that the iterative process does not diverge, starting with *f* = 1 m. Visualization of the picture of the deformed state of the SSS and the distribution of the corresponding displacements u_z shown in Fig. 10.

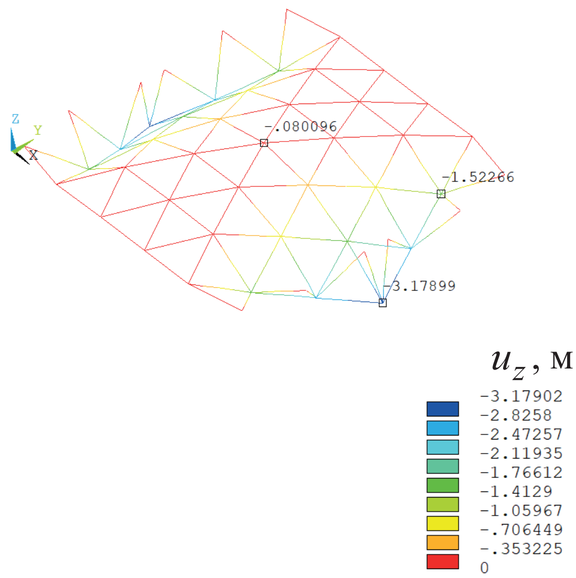

Figure 10. The picture of the distribution of movements in HRS u_z when f = 1m

Next, a simulation of the process of kinematic shaping of the HRS was performed using a specially developed step algorithm. Fig. 11 shows the results of modeling this process for the

SHSS with the initial boom of the dome f = 0,1 m, with the same movements Δs in all actuators. The following parameters were taken into account in the calculation: the course at each step of the transformation Δs =0,01 m; number of transformation steps n = 80. Visualization of vertical movements u_z at points a and b, the HRS is shown in Fig. 12. As can be seen for the accepted parameter value Δs there is a rise of peripheral repeating fragments and a deflection of the central part HRS.

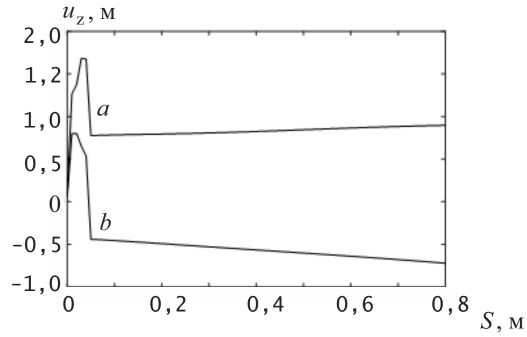

Figure 12. Charts $u_z \sim s$ at point a and b when f = 0,1 m; Δs =0,01 m; n = 80

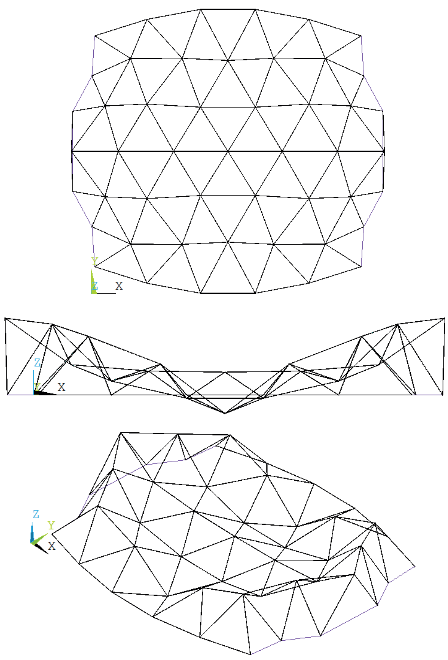

Figure 11. The result of modeling the shape change HRS when f = 0,1 m; Δs =0,01 m; n = 80

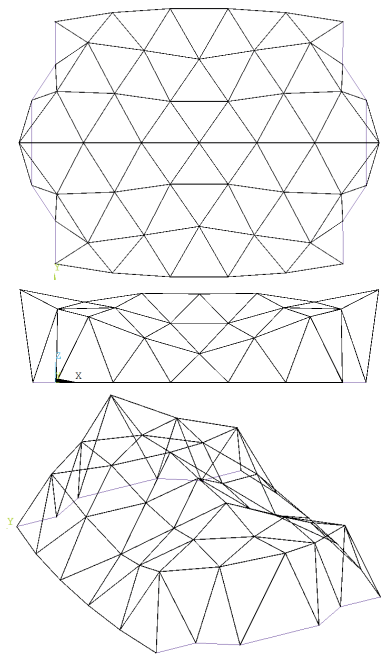

Figure 13. The result of modeling the shape change HRS when f = 0,1 m; Δs =0,02 m; n = 40

To achieve the lifting of the rods in the center of the SHSS, it was necessary to double the parameter Δs. Figure 13 shows the model of the HRS in the transformed state obtained for the variant with Δs =0,02 m и n = 40. Graphs of vertical movements in nodes *a* and *b* of the grid are shown in Fig. 14. From the presented graphs it can be seen that the dependencies $u_z \sim s$ at points *a* and *b* have clearly defined three sections. Moreover, in the last section, the displacement at point a continues to monotonically increase, and the displacement at point *b* monotonically decreases.

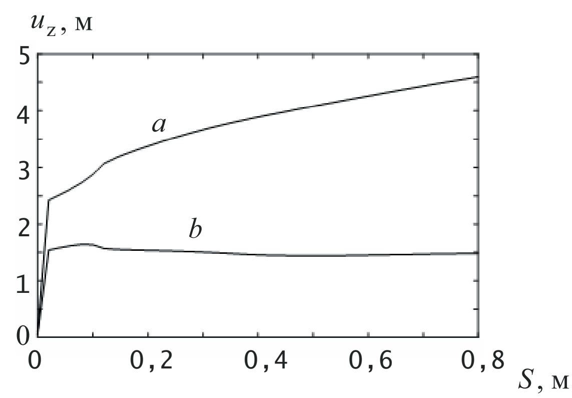

Figure 14. Charts $u_z \sim s$ at point a and b when f = 0,1 m; Δs =0,02 m; n = 40

Based on the simulation data of the transformation process with variable stroke of the actuators $S_1 = 1,2S$ it is established that the final form of the HRS in this case differs little from the result of the previous calculation $(S_1 = S)$.

Important for the practical implementation of the concept of the shape of the HRS is the information about the kinematics of angular displacements of rods. In this regard, a study of the behavior of the rod was carried out *e*, adjacent to the node *a* in the process of transformation (Fig. 8). Figure 15 shows graphs of changes in the guiding cosines $cos(y\overline{x})$, $cos(z\overline{x})$, $cos(x\overline{x})$ the observed rod depending on the stroke *S* actuators. Visualization of plume projections of rod positions *e* during the transformation, the HRS is shown in Fig. 16.

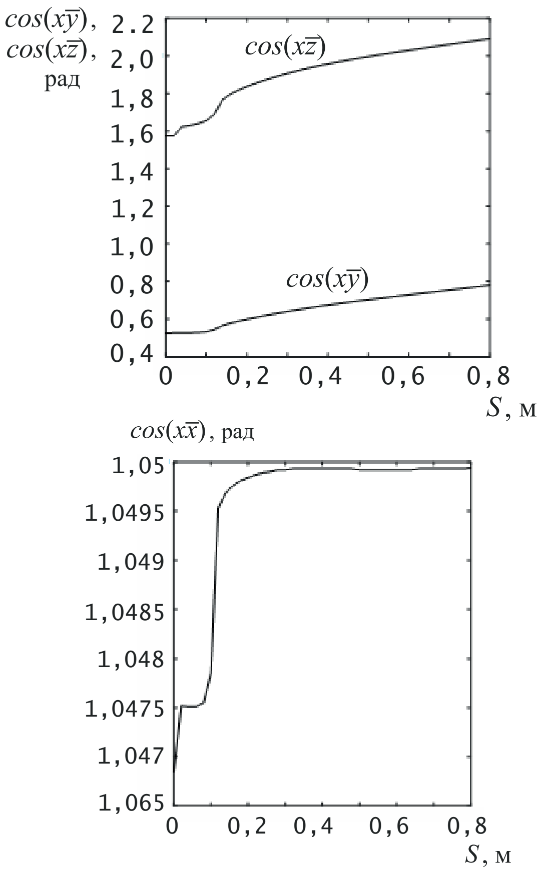

<u>Figure 15.</u> *Charts* $cos(x\overline{x})$, $cos(y\overline{x})$, $cos(z\overline{x})$ *of rod e to option f = 0,1 m; Δs = 0,02 m; n = 40*

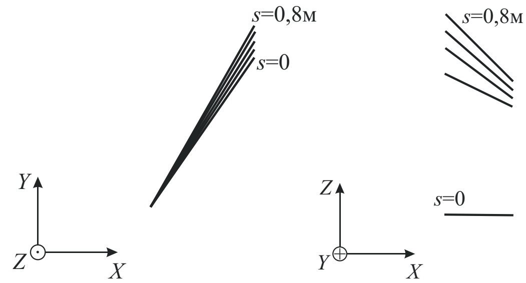

<u>Figure 16.</u> *Visualization of plume projections of rod positions e*

It follows from the presented data that the design of the hinge assembly should provide rotations relative to global axes. Naturally, this circumstance complicates the design of the hinge assembly. In the works [9,10,11], the design of a universal node providing the transformation of the HRS is proposed.

Let's consider a variant of the modified design scheme of the HRS, which differs from the previous scheme in that its rods located along the extreme rectilinear sides are replaced with actuators (Fig. 17). This arrangement of actuators allows for comprehensive compression of the structure. The boundary conditions are similar to those introduced earlier.

Visualization of a finite element model of a modified HRS circuit having an initial bend *f* = 0,1 m, after the transformation is shown in Fig. 18. The values of the stroke at each step of the transformation in all actuators were assumed to be the same $\Delta S_1 = \Delta S$. The result of the corresponding calculation in the form of graphs of the dependence of vertical movements at points *a* and *b* from the stroke of the actuators for the parameters, Δs =0,02 m; *n* = 30 presented in fig. 18.

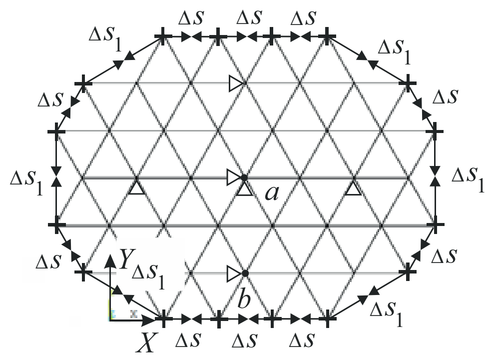

<u>Figure 17.</u> *A modified calculation scheme for modeling the process of shaping HRS*

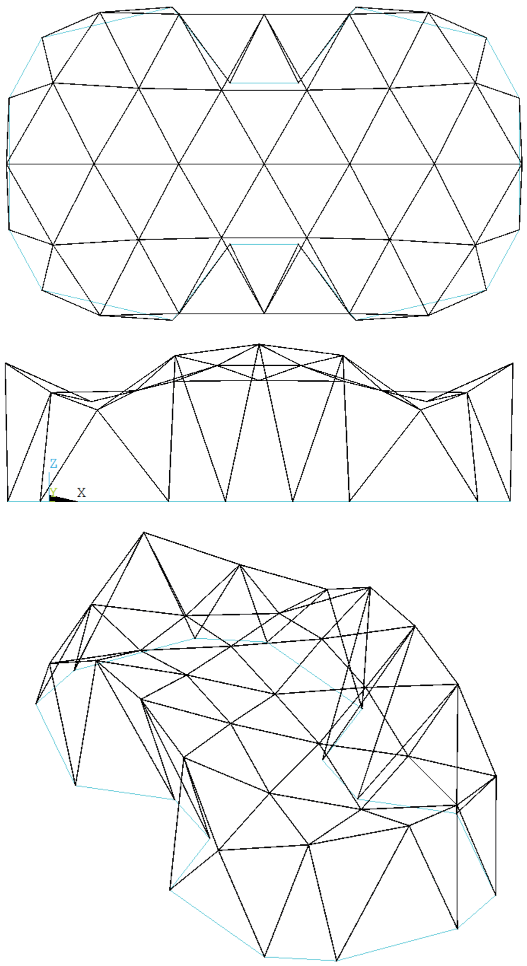

Figure 18. The result of modeling the shape change HRS when f = 0,1 m; Δs *=0,02 m; n = 30*

From the graphs of Fig. 19 it can be seen that the greatest rise $u_{z\ max}$ = 4,8m observed in a section of a repeating fragment adjacent to the node *b*.

Visualization of the modified HRS circuit after transformation in the case of variable stroke values $\Delta S_1 = 1,2\Delta S$ is presented in Fig. 20. The corresponding graphs $u_z \sim s$ shown in Fig. 21.

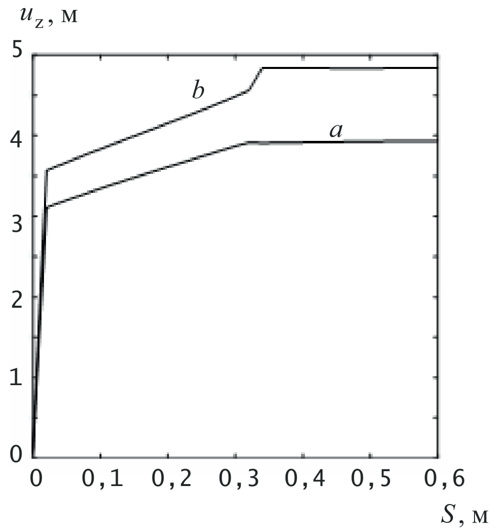

Figure 19. Charts $u_z \sim s$ *at point a and b when f = 0,1 m;* Δs *=0,02 m; n = 30*

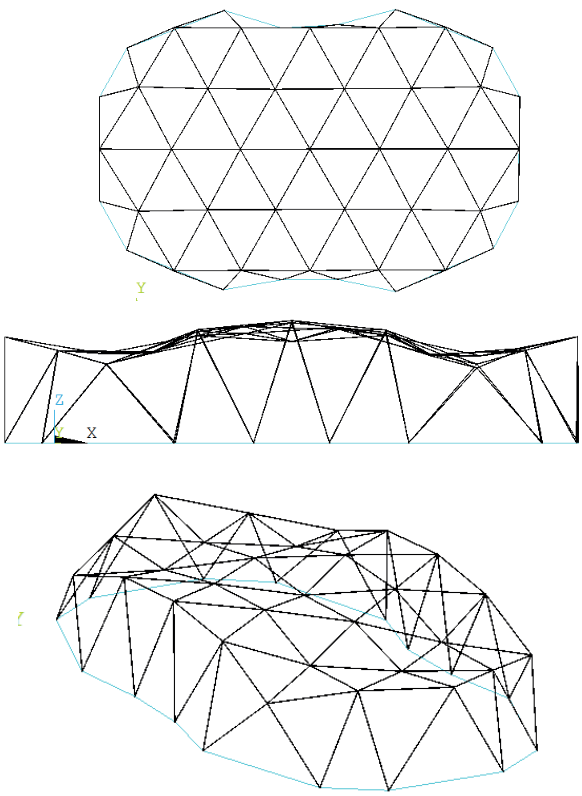

Figure 20. The result of modeling the shape change HRS when f = 0,1 m; Δs *= 0,02 m;* $\Delta S_1 = 1,2\Delta S$ *; n = 30*

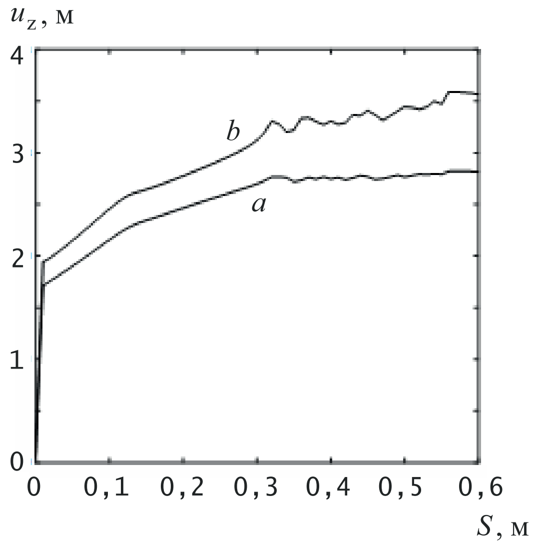

Figure 21. Charts $u_z \sim s$ at point a and b when f = 0,1 m; Δs =0,02 m; $\Delta S_1 = 1{,}2\Delta S$; n = 30

Analyzing displacement curves u_z in Fig. 20, we conclude that starting from S > 0,3m there is a zone of unstable transformation HRS.

CONCLUSIONS

1. A method of step-by-step modeling of the transformation process of a regular hinge-rod system formed by flat equilateral triangular fragments of the truss type has been developed and tested on test examples.
2. The range of geometric and kinematic parameters providing vertical lifting of the rods of the structure is established.

REFERENCES

1. **Usyukin V.I.** Stroitel'naya mekhanika konstrukcij kosmicheskoj tekhniki [Construction mechanics. of space technology constructions]. Moscow: Mashinostroenie Publ., 1988. 392 pages (in Russian).
2. **Ignatiev A.V., Ignatiev V.A. and Onishchenko E.V.** The possibility of using the finite element method in the form of a classical mixed method for geometrically nonlinear analysis of hinge-rod systems. Vestnik MGSU, No. 12, 2015, pp. 47-58. (in Russian).
3. **Ignatiev A.V., Ignatiev V.A. and Onishchenko E.V.** Solution of geometrically nonlinear static problems of hinge-rod systems based on the finite element method in the form of a classical mixed method. Vestnik MGSU, 2016, No. 2, pp. 20-33 (in Russian).
4. **Basov K.A.** ANSYS: user's guide. – M.: DMK Press, 2012. 248 pages (in Russian).
5. **Gaydzhurov, P.P., Iskhakova E.R., Tsaritova N.G.** Study of Stress-Strain States of a Regular Hinge-Rod Constructions with Kinematically Oriented Shape Change. International Journal for Computational Civil and Structural Engineering. 2020. Vol. 16. No 1. pp. 38-47 (in Russian).
6. **Gaydzhurov, P.P.** Finite element modeling of the formation process of a hinge-rod system under controlled kinematic action / P. P. Gaydzhurov, E. R. Iskhakova, N. A. Savelyeva, N. G. Tsaritova // News of higher educational institutions. The North Caucasus region. Technical sciences. 2020, № 3(207), pp. 5-12 (in Russian).
7. **Gaydzhurov, P.P**. Modeling of the process of directed transformation of regular hinge-rod systems / P. P. Gaydzhurov, N. G. Tsaritova // News of higher educational institutions. The North Caucasus region. Technical sciences. 2021, № 1(209). pp. 5-11 (in Russian).
8. **Morozov E.M., Muizemnek A.Yu., Shadsky A.S**. ANSYS in the hands of an engineer: Mechanics of Destruction. M.: LENAND, 2008, 456 pages (in Russian).
9. The regular hinged structure: The patent of Russia № 2586351: IPC E04B 1/58 / **N.G. Tsaritova, N.A. Buzalo**; applicant and patentee of Platov South-Russian State Polytechnic University – № 2015100939/03; declare 01.12.15; publ. 06.10.16, Bulletin № 16 (in Russian).

10. **Buzalo, N.A., Alekseev, S., & Tsaritova, N.** Numerical Analysis of Spatial Structural Node Bearing Capacity in the View of the Geometrical and Physical Nonlinearity. 2016, Procedia Engineering, 150, pp.748-1753.
11. **Tsaritova N., Buzalo N.** Creating a solid model of the spatial structure node with application of solidworks complex. 2015. Construction and Architecture, 3, pp. 1-6 (in Russian).

СПИСОК ЛИТЕРАТУРЫ

1. **Усюкин В.И.** Строительная механика конструкций космической техники. М.: Машиностроение, 1988. 392 с.
2. **Игнатьев А.В., Игнатьев В.А., Онищенко Е.В.** Возможность использования метода конечных элементов в форме классического смешанного метода для геометрически нелинейного анализа шарнирно-стержневых систем // Вестник МГСУ. 2015. № 12. С. 47-58.
3. **Игнатьев А.В**. Решение геометрически нелинейных задач статики шарнирно-стержневых систем на основе метода конечных элементов в форме классического смешанного метода / А. В. Игнатьев, В. А. Игнатьев, Е. В. Онищенко // Вестник МГСУ. – 2016. – № 2. – С. 20-33.
4. **Басов К.А**. ANSYS для конструкторов.-М.:ДМК Пресс,2012.-248 с.
5. **Гайджуров Р., Исхакова Е., & Царитова N.** Исследование напряженно-деформированного состояния регулярной шарнирно-стержневой конструкции при кинематически ориентированном изменении формы. International Journal for Computational Civil and Structural Engineering, 2020, 16(1), 38–47.
6. **Гайджуров П.П.** Конечно-элементное моделирование процесса формоизменения шарнирно-стержневой системы при управляемом кинематическом воздействии / П.П. Гайджуров, Э.Р. Исхакова, Н.А. Савельева, Н.Г. Царитова // Известия высших учебных заведений. Северо-Кавказский регион. Технические науки. – 2020. – № 3(207). – С. 5-12.
7. **Гайджуров, П.П.** Моделирование процесса направленной трансформации регулярных шарнирно-стержневых систем / П. П. Гайджуров, Н. Г. Царитова // Известия высших учебных заведений. Северо-Кавказский регион. Технические науки. – 2021. – № 1(209). – С. 5-11.
8. **Морозов Е.М., Муйземнек А.Ю., Шадский А.С.** ANSYS в руках инженера // Механика разрушения. М.: ЛЕНАНД, 2008. 456 с.
9. Патент № 2586351 C1 Российская Федерация, МПК E04B 1/58. Шарнирный узел пространственной стержневой конструкции регулярной структуры : № 2015100939/03 : заявл. 12.01.2015 : опубл. 10.06.2016 / **Н.Г. Царитова, Н.А. Бузало** ; заявитель федеральное государственное бюджетное образовательное учреждение высшего профессионального образования "Южно-Российский государственный политехнический университет (НПИ) имени М.И. Платова".
10. **Buzalo, N. A.** Numerical Analysis of Spatial Structural Node Bearing Capacity in the View of the Geometrical and Physical Nonlinearity / **N. A. Buzalo, S. A. Alekseev, N. G. Tsaritova** // Procedia Engineering, Chelyabinsk, 19–20 мая 2016 года. – Chelyabinsk: Elsevier Ltd, 2016. – P. 1748-1753.
11. **Бузало, Н.А.** Создание твердотельной модели узла пространственной стержневой системы с использованием комплекса SolidWorks / **Н. А. Бузало, Н. Г. Царитова** // Строительство и архитектура. – 2015. – Т. 3. – № 1. – С. 1-6.

Peter P. Gaydzhurov, PhD, DSc, Professor of the Department «Technical mechanics», Don State Technical University, Rostov-on-Don

Гайджуров Петр Павлович, доктор технических наук, профессор кафедры «Техническая механика» Донского государственного технического университета, г. Ростов-на-Дону

Nadezhda G. Tsaritova, PhD, Associate Professor of the Department «Urban development, designing of buildings and structures», Platov South-Russian State Polytechnic University, (NPI), Novocherkassk, e-mail: ncaritova@yandex.ru

Царитова Надежда Геннадьевна, кандидат технических наук, доцент кафедры «Градостроительство, проектирование зданий и сооружений», Южно-Российского государственного политехнического университета им. М.И.Платова (НПИ), г. Новочеркасск

Abacar I. Kurbanov, PhD student of the Department «Urban development, designing of buildings and structures», Platov South-Russian State Polytechnic University, (NPI), Russian Federation. Novocherkassk

Курбанов Абакар Ибрагимович, аспирант кафедры «Градостроительство, проектирование зданий и сооружений», Южно-Российского государственного политехнического университета им. М.И.Платова (НПИ), г. Новочеркасск

Anastasia A. Kurbanova, PhD student of the Department «Urban development, designing of buildings and structures», Platov South-Russian State Polytechnic University, (NPI), Russian Federation. Novocherkassk

Курбанова Анастасия Алексеевна, аспирант кафедры «Градостроительство, проектирование зданий и сооружений», Южно-Российского государственного политехнического университета им. М.И.Платова (НПИ), г. Новочеркасск

Elvira R. Iskhakova, PhD student of the Department «Urban development, designing of buildings and structures», Platov South-Russian State Polytechnic University, (NPI), Russian Federation. Novocherkassk

Исхакова Эльвира Рашидовна, аспирант кафедры «Градостроительство, проектирование зданий и сооружений», Южно-Российского государственного политехнического университета им. М.И.Платова (НПИ), г. Новочеркасск

DOI:10.22337/2587-9618-2022-18-3-25-36

ON THE CALCULATIONS FOR THE STABILITY OF BEAMS, FRAMES, AND CYLINDRICAL SHELLS IN THE ELASTO-PLASTIC STAGE

Gaik A. Manuylov, Sergey B. Kosytsyn, Maxim M. Begichev

Russian University of Transport, Moscow, RUSSIA

Abstract. The problems of stability of some beams, П-shaped frames and cylindrical shells with the elasto-plastic material are considered. The possibility of modeling bars using finite elements of various types is studied. Plate elements and even one-dimensional beam finite elements can be used for modelling compressed rods with geometric and physical nonlinearity. For the problem of stability of a circular cylindrical shell is given the comparison of the authors' results obtained using the FEM with the experimental results of V.G. Sazonov and the calculations of A.V. Karmishin.

Keywords: stability, geometric nonlinearity, physical nonlinearity, finite element method

О РАСЧЕТАХ НА УСТОЙЧИВОСТЬ СТЕРЖНЕЙ, РАМ И ЦИЛИНДРИЧЕСКИХ ОБОЛОЧЕК В УПРУГО ПЛАСТИЧЕСКОЙ СТАДИИ

Г.А. Мануйлов, С.Б. Косицын, М.М. Бегичев

Российский университет транспорта, Москва, РОССИЯ

Аннотация. В работе рассматриваются вопросы устойчивости некоторых стержней, П-образных рам и цилиндрических оболочек в упруго пластической стадии работы материала. Рассмотрена возможность моделирования стержней при помощи конечных элементов различных типов. Показано, что для расчета сжатых стержней с учетом геометрической и физической нелинейности можно использовать плоские и даже одномерные конечные элементы. Для задачи устойчивости круговой цилиндрической оболочки приведено сравнение результатов авторов, полученных при помощи МКЭ с результатами экспериментов В.Г. Сазонова и расчетами А.В. Кармишина.

Ключевые слова: устойчивость, геометрическая нелинейность, физическая нелинейность, метод конечных элементов

1. ANALYSIS OF DIFFERENT TYPES OF FINITE ELEMENTS IN THE STABILITY PROBLEMS WITH GEOMETRIC AND PHYSICAL NONLINEARITIES

Let us investigate the possibilities of various finite element models concerning the geometrically and physically nonlinear problem of stability of a cantilever beam. The beam had a length *l*=100 cm and a square cross section 10×10 cm, beam flexibility

$$\lambda = Ml/\sqrt{EJ} = 69.$$

This value is less than the limiting flexibility for a beam with such geometrical parameters made of steel 10HSND ($\lambda_* = 72$). The study used the model of an ideal Prandtl elasto-plastic material (σ_{yeiled}=400 MPa). Four types of finite element models are considered:

1. Using solid finite elements (FE) in the NASTRAN complex (Hex8);
2. Using plate FE with loss of stability in the element plane;

3. Using plate FE with loss of stability out of the element plane;

4. Using beam FE.

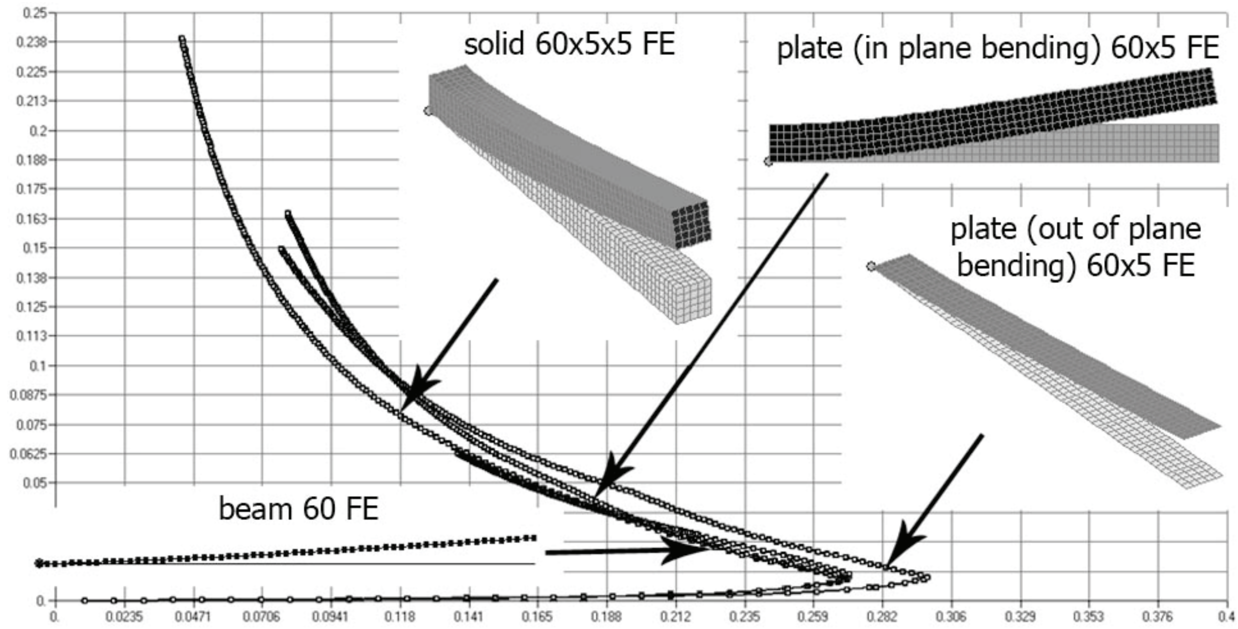

Figure 1. Curves of deformation development of an axially compressed cantilever beam

It was found that when using a three-dimensional model (5x5x60 cubic elements) of the above-described axially compressed beam, a model of 60 one-dimensional beam elements, as well as flat square four-node FE (5 plate elements along the height of the section, located in the plane of loss of stability), the critical loss of stability loads at limiting points and post-critical curves of unstable equilibrium states, almost coincided (Fig. 1).

A slightly higher compression load ($\Delta P_{cr} \approx 9\%$) had the model of a plate elements, bending at loss of stability "out of its plane". It follows from this that to solve physically and geometrically nonlinear stability problems it is not necessary to use models of beams from three-dimensional finite elements. Two-dimensional plate elements (and even one-dimensional beam elements) make it possible to obtain acceptable results in majority of loss of stability problems taking with elasto-plastic material behavior. The use of such elements significantly reduces the dimension of stability problems (in comparison with solid FE), and, as a consequence, reduces the time for their solution.

2. ECCENTRICALLY COMPRESSED CANTILEVER BEAM

In this paragraph, on the model (1200 flat four-node FE) of the cantilever beam (lenght l = 1,2 m) which has a nonlinear material diagram with hardening (Fig. 2, $\sigma = \varepsilon E - -k\varepsilon^3/3\,, E = 2{,}1 \cdot 10^6\ kg/cm^2$) and unloading according to a linear law, the influence of the initial imperfections in the application of a compressive force (offset) to the end section by the value of the loss of stability critical load.

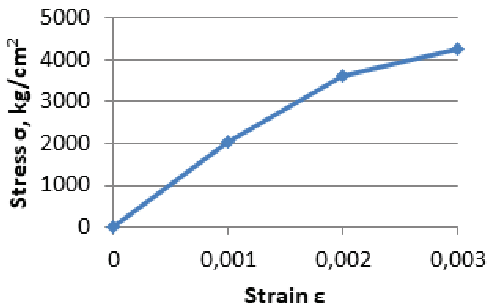

Figure 2. Stress-strain diagram for the material of the cantilever beam

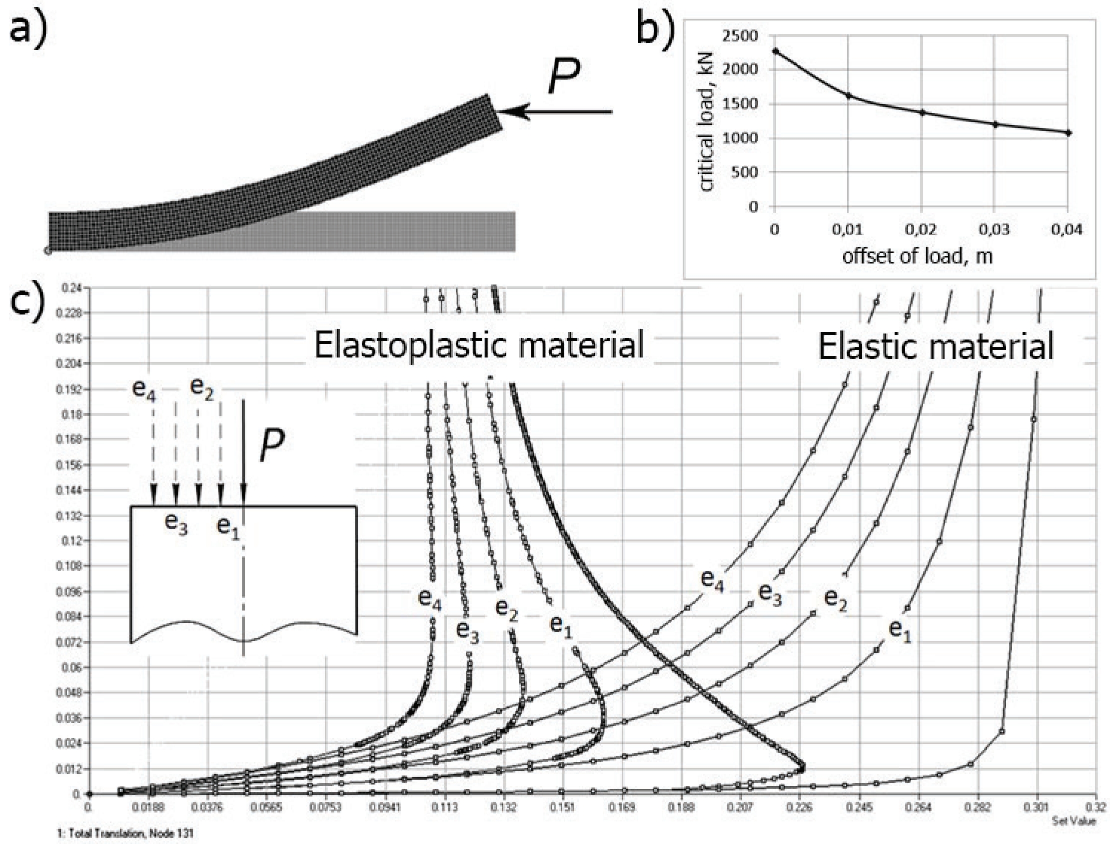

Figure 3. Elasto-plastic buckling of a cantilever axially compressed beam: a) deformed form of the beam; b) a graph of reduction of the values of critical loads; c) curves of displacement of the end of the beam

Imperfections in this problem were set in the form of different values of the offset of the point of the force application with respect to the center line of the beam (Fig. 3). A series of curves of equilibrium states was obtained for a beam made of an linear elastic material and for an elastoplastic rod made of a material with the above mentioned deformation law (Fig. 2). For a beam with a linear elastic material model, the curves of equilibrium states increase smoothly with increasing load, since the loss of stability of a linear elastic axially compressed beam occurs at the point of symmetric stable bifurcation [1,2].

When the material of the beam obeys the diagram of elasto-plastic deformation, the bifurcation point becomes unstable (in the formulation of the Euler-Karman problem), and the cantilever axially compressed beam loses its stability «in large» (Fig. 3a). In this case, the drop in the critical loads values turns out to be strongly dependent on the magnitude of the initial imperfections (indicated offsets) (Fig. 3c). The graph of the dependence of the critical loads at the limiting points on the offset value shown in Fig. 3b demonstrates that when the load was displaced from the axis by 0.01 m (the minimum used offset value) its critical value decreased by ~ 30%, and at a maximum offset of 0.04 m by ~ 52%. This confirms the well-known statement of T. Karman about the extremely high sensitivity of short beams (beams that lose their stability in the elasto-plastic stage of material operation) to the initial application of compressive load' offsets [3].

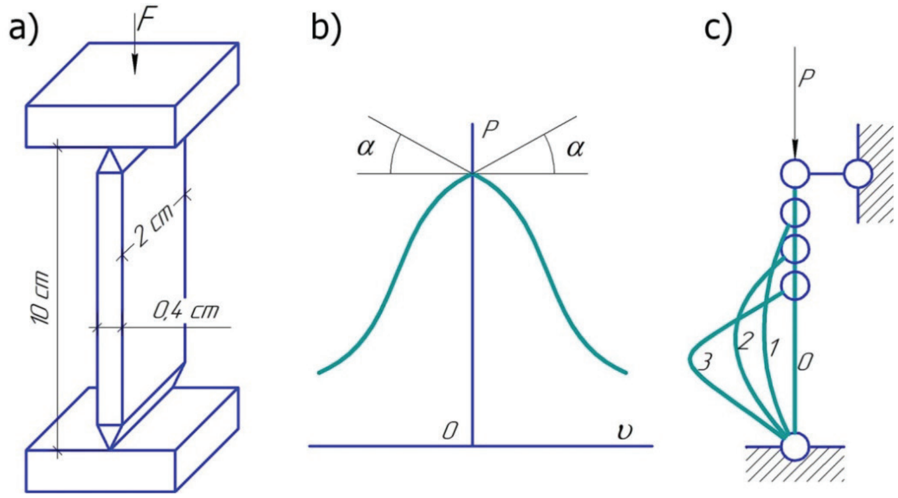

Figure 4. Compressed pivotally supported beam

3. ON THE LOSS OF STABILITY OF A COMPRESSED PIVOTALLY SUPPORTED BEAM IN THE ELASTO-PLASTIC STAGE

A flat steel beam 10×2×0.4 cm (St. 3) is used to qualitatively demonstrate the loss of stability effects in the elastoplastic stage under kinematic loading in a press (Fig. 4a). Beam characteristics $A = 0{,}8\ cm^2,\ J_{min} = 1{,}07\ cm^4$, $\lambda = 86{,}6 < 100$.

The beam had hinged boundary conditions. According to the Tetmayer's formula:

$$\sigma_{crit} = 3100 - 11{,}4{,} = 2112{,}7\ kg/cm^2,$$
$$P_{crit} = \sigma_{crit}\,A = 1690{,}2\ kg$$

The actual critical load observed during experiment is less than 1690 kg. This is explained by the high sensitivity of the critical load to the initial offsets of load, since here the curve of the initial post-critical equilibrium is unstable (with a bend at the apex at P = P_{crit}, Fig. 4b).

The moment of loss of stability of the elasto-plastic beam onset corresponds to the maximum load. At the beginning of buckling, the beam is slightly bent along a curve close to a sinusoid. But unlike elastic loss of stability, the "new" compressed-bent equilibrium is unstable. The beam, as it were, "slips out" of the decreasing pressure in the press. At the same time, its shape is changing. The curvature of the middle zone of the beam becomes larger and larger. On the contrary, the zones adjacent to the supports try to “straighten out”. In the end, the rod takes the shape of an angle of $\sim 130° - 140°$ with a concentration of curvature near the middle section (Fig. 4c). In fact, a plastic hinge is formed here.

The calculation of such a beam was carried out with the NASTRAN (2520 FE plate) to construct the equilibrium diagrams shown in Fig. 5. The calculated diagram σ – ε was taken as Prandtls diagram with a yield point $\sigma_{yield} = 2400\ \mathrm{kg/cm^2}$. The critical load was 1800 kg. But this is not the result of loading in the form of pure compression. The beam bending was provoked by a "small" lateral force Q = 30 kg. When performing a geometrically nonlinear calculation, such a “disturbing” force is required. But this force causes imperfections, to which the "elasto-plastic" beam is very sensitive.

Fig. 5 shows the sequential development of stresses and deformations in the middle zone of the test sample after loss of stability in the elasto-plastic stage of material operation. The beginning of the formation of the plastic hinge - points 1 and 2. But if point 1 corresponds to the maximum load, then in point 2 the load dropped to $\sim 0{,}3\ P_{max}$. In points 3 and 4, the compressive load is even smaller. However, the zone of compressive stresses (blue) has increased (along the depth of the section). Finally, for point 5, the plastic hinge extended about ¼ along the length of the sample.

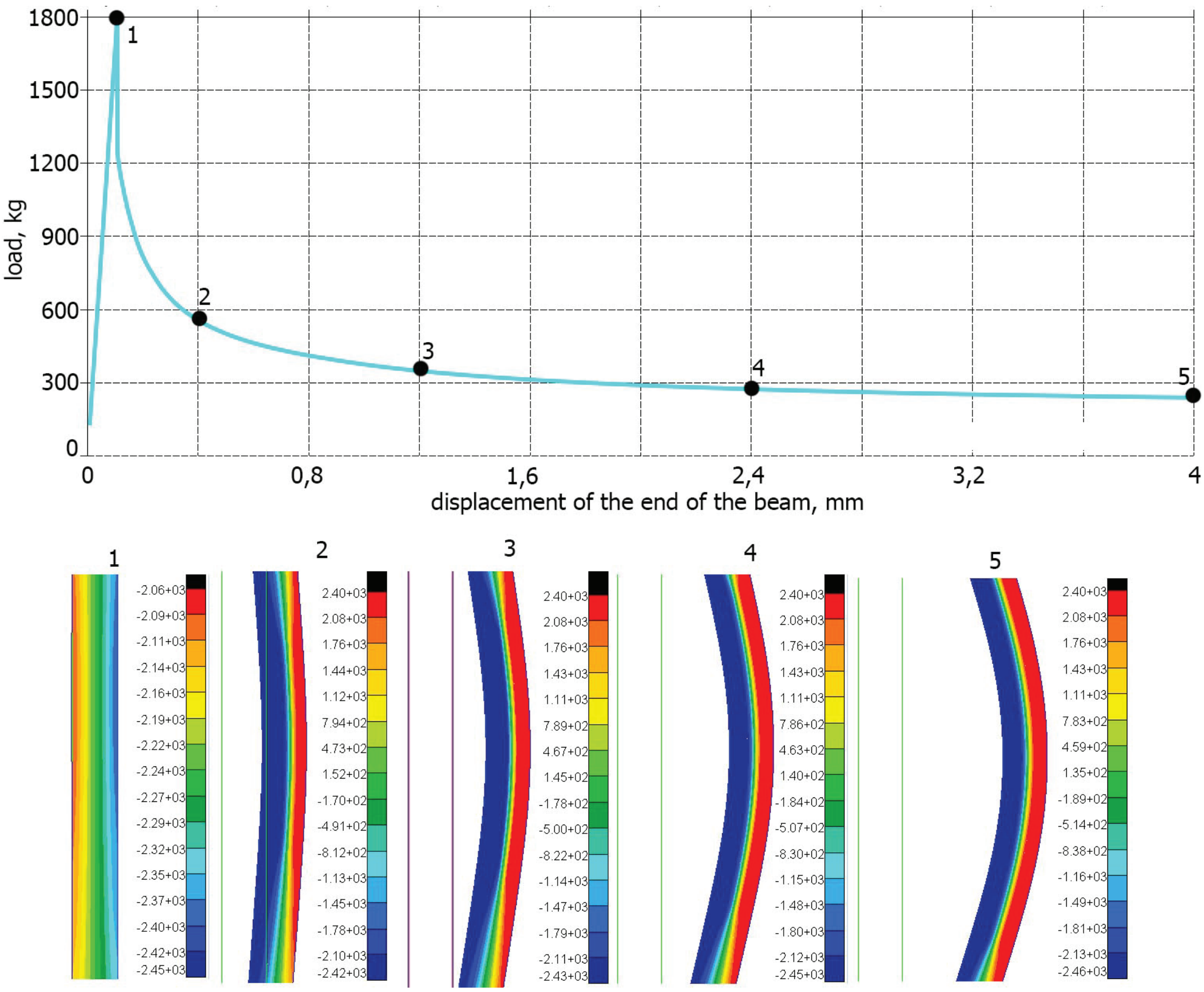

Figure 5. The equilibrium diagram for the compressed pivotally supported beam

4. ON SOLUTIONS OF ELASTO-PLASTIC PROBLEMS OF STABILITY OF FRAMES

It is known that the solution of elastoplastic problems can be determined using two different approaches: the theory of small elastoplastic deformations and using the flow theory. According to the first theory, the relationship between stresses and deformations turns out to be finite; according to the flow theory, these relations are differential.

If the loading is simple, then both theories of plasticity give the same results.

If the loading is not simple, then the results obtained using the flow theory, usually, match better the experimental data in comparison with the results given by the theory of small elasto-plastic deformations.

Solutions for both theories are obtained as a result of the convergence of iterative processes. The FE-complex NASTRAN implements the solving procedure according to the flow theory. In the semi-automatic version of the stability problems for frame systems in the elasto-plastic stage solution, it is convenient to use the theory of small elasto-plastic deformations with

iterations by the method of elastic solutions with variable elastic parameters.
The convergence of this iterative process in the general case has not been rigorously proven. However, numerous calculations show that for ordinary "convex" (broken or smooth) $\sigma - \varepsilon$ diagrams, the iterations converge to such a solution.

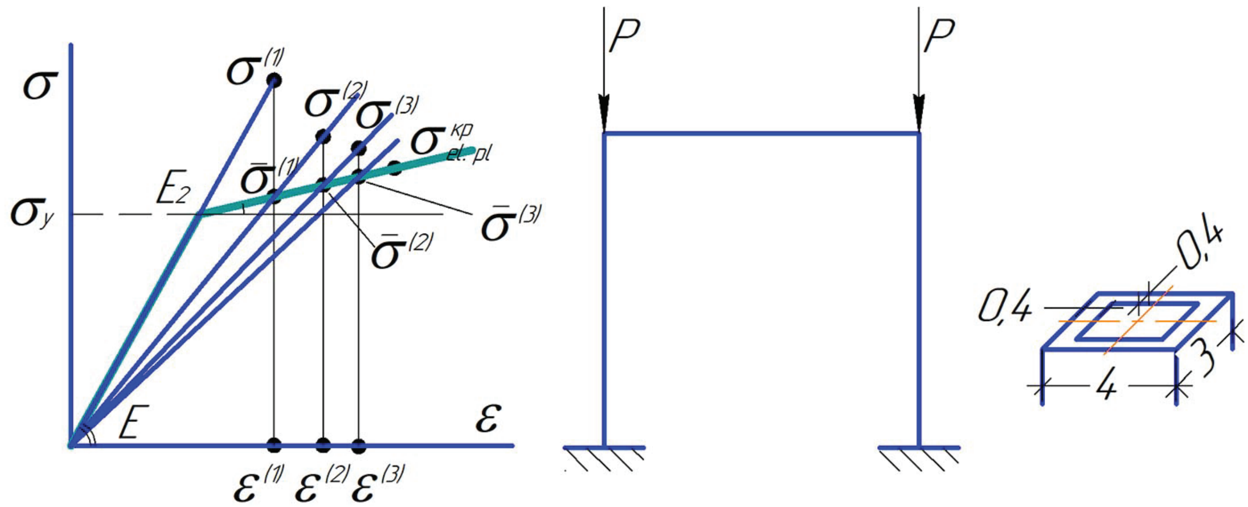

Figure 6. The variable parameters of elasticity method.

The essence of the variable parameters of elasticity in stability problems method will be explained using Fig. 6.
Let the material have a bilinear $\sigma - \varepsilon$ diagram with modules E and E_2. The first approximation is the result of solving the elastic stability problem. If the critical "elastic" stresses of the first approximation

$$\sigma^{(1)} = \frac{P_{cr\ elast}}{A} = \frac{P^{(1)}}{A}$$

is greater than the yield stress $\sigma_{yieled}\left(\sigma^{(1)} > \sigma_{yieled}\right)$this means that the frame loses its stability in the elastoplastic stage. The stress $\sigma^{(1)}$ is the first upper approximation for $\sigma^{cr}_{elast-pl}$. Next, we find the relative deformation

$$\varepsilon^{(1)} = \frac{\sigma^{(1)}}{E},$$

and stress $\bar{\sigma}^{(1)}$ in the second section of the $\sigma - \varepsilon$ diagram

$$\bar{\sigma}^{(1)} = \sigma_{yieled} + (\varepsilon^{(1)} - \varepsilon_{yieled})E_2$$

Here $E_2$is the slope modulus in the second section. The stress $\bar{\sigma}^{(1)}$ gives lower bound $\sigma^{cr}_{elast-pl}$. As a result, we have the first two-sided estimates

$$\bar{\sigma}^{(1)} < \sigma^{cr}_{elast-pl} < \sigma^{(1)}$$

Next, a new elasticity modulus is calculated $E^{(2)}$

$$E^{(2)} = \frac{\bar{\sigma}^{(1)}}{\varepsilon^{(1)}} < E^{(1)}$$

This module takes into account the decrease in the bending stiffness of the compressed beams at the second iteration compared to the original module E. The reduction factor

$$\Psi^{(1)} = \frac{E^{(2)}}{E} < 1$$

is a multiplier as well in the bending stiffness of compressed beams,

$$\frac{EJ}{l} \to \frac{\Psi EJ}{l},$$

as in the new force parameter $\nu^{(2)}$

$$\nu^{(2)} = l\sqrt{\frac{N}{\Psi E\mathrm{T}}} = \frac{\nu}{\sqrt{\Psi^{(2)}}}$$

The solution of the characteristic equation of the second approximation gives the critical parameter $\nu_{cr}^{(2)}$ and the critical force $P^{(2)}$

$$P^{(2)} = \left(\nu_{cr}^{(2)}\right)^2 \Psi^{(2)} \frac{E\mathrm{T}}{l^2}$$

Then all calculations of $\sigma^{(2)}, \varepsilon^{(2)}$and $\bar{\sigma}^{(2)}$ are repeated. As a result, we obtain new improved two-sided estimates ($\sigma^{(2)} < \sigma^{(1)}, \bar{\sigma}^{(2)} > \bar{\sigma}^{(1)}$).

$$\bar{\sigma}^{(2)} < \sigma_{elast-pl}^{cr} < \sigma^{(2)}$$

Iterations continue until the first few digits match in the values $\sigma^{(n)}$and $\sigma^{(-n)}$. Usually, two or three correct signs are enough for $\sigma_{elast-pl}^{cr}$.

As an example, let us consider the solution of the elasto-plastic stability of a U-shaped frame with a box-shaped cross-section of 3×4 cm and 0.4 cm thick walls by the method of variable elastic parameters problem. Here: $l = 100$ cm, $A = 4{,}96$ cm^2, $J = 10\ cm^4$, $E_1 = 2 \cdot 10^6\ kg/cm^2$, $E_2 = 0{,}6 \cdot 10^6\ kg/cm^2$. The stress $\sigma_{yieled} = 2000$ кг/см^2 (bilinear diagram).

The characteristic equation of the first approximation (elastic problem) and its solution is

$$6\frac{EJ}{l} + \frac{EJ}{l} * \frac{\nu}{tg\,\nu} = 0,\ \ \nu^{(1)} = 2{,}716,$$

$$\nu = l\sqrt{\frac{P}{EJ}}.$$

$$P^{(1)} = \frac{2{,}716^2 * 2 * 10^6 * 10}{10^4} = 14753{,}3\ kg,$$

$$\sigma^{(1)} = \frac{P^{(1)}}{A} = 2974{,}4\ kg/cm^2$$

$$\varepsilon^{(1)} = \frac{\sigma^{(1)}}{E_1} = 1{,}48723_{-3},\ \ \varepsilon_{prop} = 10^{-3},$$

$$\bar{\sigma}^{(1)} = 2000 + (1{,}48723_{-3} - 1_{-3})0{,}6 * 10^6 = 2292{,}3\ kg/cm^2$$

Thus, after the first iteration step, we have the estimates

$$\left(2292{,}3 < \sigma_{elast-pl}^{cr} < 2974{,}4\right)\ kg/cm^2$$

The new elasticity modulus for the second iteration

$$E^{(2)} = \frac{\bar{\sigma}^{(1)}}{\varepsilon^{(1)}} = \frac{2294{,}3}{1{,}48723_{-3}} \cong 1541347\,\frac{\text{кг}}{\text{см}^2},$$

$$\Psi^{(2)} = \frac{E^{(2)}}{E} = 0{,}77$$

Characteristic equation of the second iteration

$$6\frac{EJ}{l} + 0{,}77\frac{EJ}{l} * \frac{\nu_2}{tg\,\nu_2} = 0,\ \ \nu_{2\,cr} \cong 2{,}8, \nu_{cr}^{(2)} = \frac{\nu_{2\,cr}}{1{,}139} = 2{,}458$$

Continuing the calculations, we obtain the estimates

$$\left(2348{,}4 < \sigma_{elast-pl}^{cr} < 2436\right)\ kg/cm^2$$

The third iteration gives

$$\left(2353 < \sigma_{elast-pl}^{cr} < 2360\right)\ kg/cm^2$$

We restrict ourselves to the third approximation and assume that $\sigma_{elast-pl}^{cr} \cong 2356\ kg/cm^2$. Critical load $P_{cr.\ elast-pl} = 11688{,}6$ kg.

It is interesting to note that according to the solution using a beam FE at $\varepsilon = 1/100000$, the critical load turned out to be very close to the calculated one ($P^{cr}_{elast-pl}\,(beam) = 11739\,kg$). However, when comparing with the results ($P^{cr}_{elast-pl}$~$9880{,}5\,kg$) obtained with the help of plate FE, one can see the difference (~16.5%) in the critical force. There are no convincing explanations for this discrepancy yet. It is impossible to explain the difference between the flow theory and the theory of small elasto-plastic deformations, since the result $P^{cr}_{elast-pl}$, obtained using the beam FE was calculated according to the theory of flows ($P^{cr}_{elast-pl} = 11739\,kg$), and, as shown above, is in good agreement with the value of $P^{\text{ск}}_{elast-pl}$ obtained on the basis of the theory of small elasto-plastic deformations ($P^{cr}_{elast-pl} = 11688\,kg$). Let us consider additional solutions to the problem of elasto-plastic buckling of a U-shaped frame (Fig. 7), composed of 100 cm long beams and having 4 × 3 cm rectangular tubular sections 0.4 cm thick. The analytic model of the frame is made up of 10492 plate FE (NASTRAN). The lower sections of the frame struts are sealed. Nodal load (two vertical compressive forces P). The diagram of material operation is bilinear with module $E = 2 \cdot 10^6\ kg/cm^2$ in the first section and module $E_2 = 0{,}3\,E = 0{,}6 \cdot 10^6\ kg/cm^2$ for the second section ($\sigma_T = 2000\ kg/cm^2$). The imperfections were specified in the form of 2 small horizontal nodal forces εP, where ε = 0.0000022; 0.00001; 0.0001; 0.001 and 0.01. With such imperfections, the critical loads are 98.805; 98.7; 97.65; 90.36 and 71.04 (kN). As can be seen from the above results, with the loss of stability in the elasto-plastic stage, the drop in the critical load with an increase in the "forced" initial imperfections is quite noticeable. This is a significant difference from the "elastic" loss of stability (stable symmetric bifurcation), the curves of the initial supercritical equilibrium at ε = 0 and ε = 0.001 are very close to each other (Fig. 7).

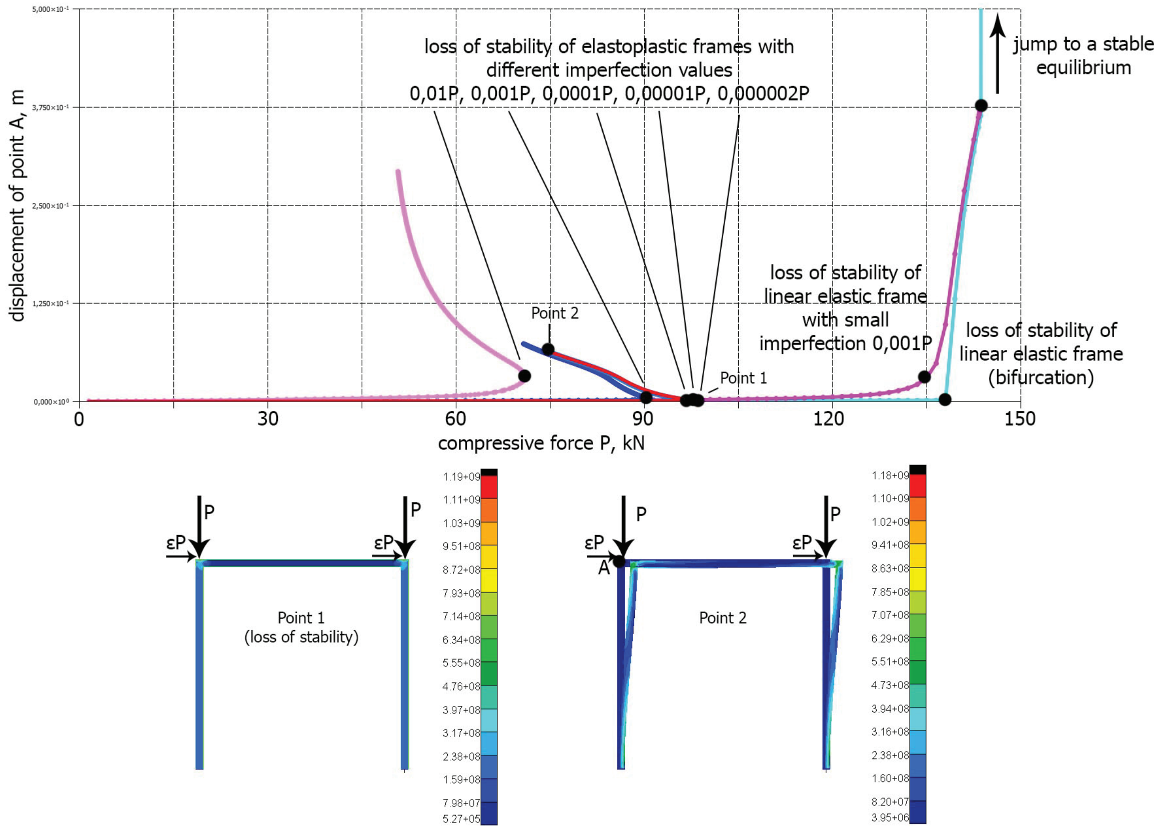

Figure 7. Deformation diagrams of U-shaped frame with different initial imperfections

The sensitivity of the elasto-plastic critical load to initial imperfections exists due to the fact that the post-critical equilibrium of the frame after elasto-plastic loss of stability is unstable.
The nature of a sharp decrease in elasto-plastic critical loads is clearly visible in Fig. 7. At ε = 0.01 ΔPcr% = (98.8−71.04)/98, 8·100% ≅ 28%. That is quite a lot.
Note that when using plate elements and a nonlinear elastic material model, the critical loads (98.2 kN at ε = 0.00001 and 98.65 kN at $\varepsilon = \frac{1}{500000}$) practically coincided with the corresponding values from the elastic-plastic calculation.
An attempt was made to use a beam FE element. For a linearly elastic material, the results of calculating $P_{кр}$ turned out to be quite close to those calculated "manually".

$$P_{cr\ elast} = 147{,}54\ kN\ =>$$
$$2{,}716^2 \cdot 2 \cdot 10^6 \cdot \frac{10}{10^4}\ kg = 147533\ kg$$

However, the elasto-plastic calculation gave a significantly lower critical force ($P_{cr\ elast-pl} \cong 117{,}4\ kN$). The obtained value of the critical load on the NASTRAN is in good agreement with the result of the calculation by the method of variable parameters of elasticity (~ 117 kN).

5. STABILITY OF A CIRCULAR CYLINDRICAL SHELL UNDER AXIAL COMPRESSION

Let us compare the study results on the stability of a circular cylindrical shell under axial compression made by the author (numerical simulation according to the NASTRAN FEM) with the results of experiments by V.G. Sazonov and the calculations of A.V. Karmishin, given in the book [4].
Three series (each with six samples) of shells with length L = 136 mm, outer diameter d = 79 mm and thicknesses h = 1.0; 1.5; 2.0 mm were subjected to tests. The shells were made from pipes and checked for wall thickness differences (± 2%). The shell material - AMG6. The material diagram is shown in Fig. 8, the values of ε and σ are given in Table 1.

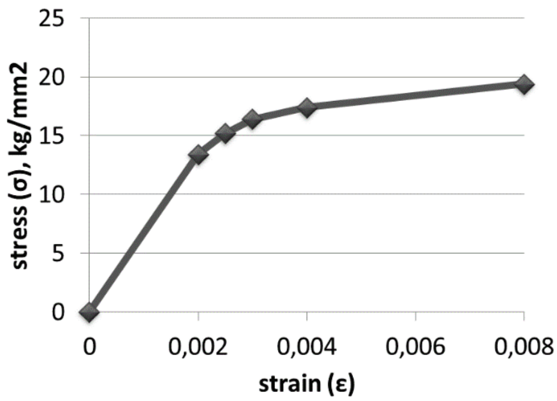

Figure 8. Stress-strain diagram of the elastoplastic material AMG6

Table 1. Coordinates of the AMG6 stress-strain diagram

Point №	strain	stress, kg/mm^2
1	0	0
2	0,002	13,40
3	0,0025	15,20
4	0,003	16,40
5	0,004	17,40
6	0,008	19,40

Tests of shells with h = 1 mm and h = 1.5 mm were carried out on a laboratory machine with a mechanical wire ZDM-10, shells with h = 2 mm - on a machine with a Sapper-100 hydraulic drive. The alignment of the models was ensured by marking the machine plates. To prevent distortions, ball joints were used (this is evidenced by stable test results). The models loading was carried out in stages at a low speed. Fig. 8 shows the $\sigma_c(\varepsilon_c)$ diagrams obtained by recalculating the $P(\Delta)$ diagram using the formulas

$$\sigma_c = \frac{P}{2\pi Rh}, \qquad \varepsilon_c = \frac{\Delta}{L}.$$

At loads close to $\sigma_{\text{А}}$ (Fig. 8), a pronounced bending deformation state is observed at the edges of the shell. The maximum deflection amplitude before the loss of stability reaches approximately 0.1 h.

When $\sigma = \sigma_{\text{А}}$ for shells with h = 1 mm and h = 1.5 mm, at one of the edges of the shell, the loss of stability occurs in an asymmetric shape, accompanied by a drop in stresses to $\sigma = \sigma_{\text{Б}}$, and the maximum deflection at the edge increases approximately up to 0.3h. However, the shell does not lose its bearing capacity, continuing to perceive the load. Then, at $\sigma = \sigma_{\Gamma}$, the buckling shapes change and the shell loses its bearing capacity.

Shells with h = 2 mm also lose stability in their asymmetric shape, but no sharp drop in the load is observed. The buckling begins with the formation of four regular indentations along the ring, which increase with additional loading, and the load decreases.

When modeling cylinders by the finite element method, two material models were considered: an infinitely elastic and an elasto-plastic one based on the digitization of the diagram given in [4] (Fig. 8). The load was applied kinematically to the upper end of the shell through a rigid-element (absolutely rigid plate).

The obtained calculations results compared with the results of experiments by V.G. Sazonov and calculations by A.V. Karmishin are given in table 2.

The loss of stability in the experiment of V.G. Sazonov occurred at stresses corresponding to the flat section of the diagram.

Calculation using a nonlinear elastic model by A.V. Karmishin gave a good correlation with the experimental results (columns 2 and 3).

The curve of subcritical and supercritical equilibrium states for a shell 1 mm thick, obtained by NASTRAN, is shown in Fig. 10.

When using an elastic model of the material, the critical load on the shell was 22.8 kN (point 1 in Fig. 10, stress 93.2 kg / mm^2).

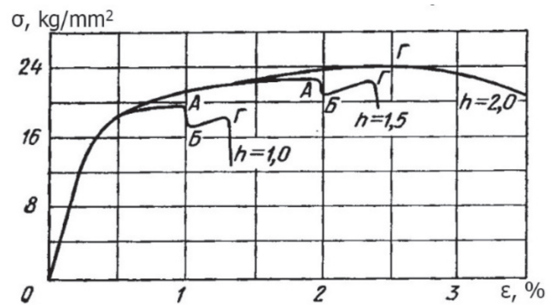

Figure 9. Experimentally obtained deformation diagrams of cylindrical shells

The subcritical equilibrium of the shell is axisymmetric; a nonlinear edge effect exists near the edges of the shell. Then the loss of stability occurs, and the shell goes into a distant stable equilibrium, characterized by the formation of a two-row belt of the rhombic-triangular indentations [5, 6] (Fig. 10 point 2). The compression load was reduced to 8.4 kN. With further loading, a secondary bifurcation occurs the restructuring of this belt into a three-row one (Fig. 10 point 3). After the loss of stability at point 2 (and under conditions of further loading), it turned out that the rigid element shifted and a skew appeared towards one part of the lateral surface of the shell. Cyclic symmetry has been lost.

The elasto-plastic equilibrium curve of the shell is completely different. Up to a load of $\sim 3{,}9\ kN$, the relationship between load and shortening is linear. Further, with a compression of $\sim 3{,}9\ kN$, a sharp increase in shortening was observed with a very weak increase in the load up to the limit point 4. (Fig. 10). Then the equilibrium of the shell became unstable. The development of dents was not along the entire lateral surface, but only near the end sections, in the zone of the elasto-plastic edge effect (point 5, Fig. 10).

Thus, it can be concluded that with the compressed circular cylindrical shells' elasto-plastic loss of stability, there is no "jump" in the load. However, it is 3.5-4 times less than the critical loads of elastic loss of stability.

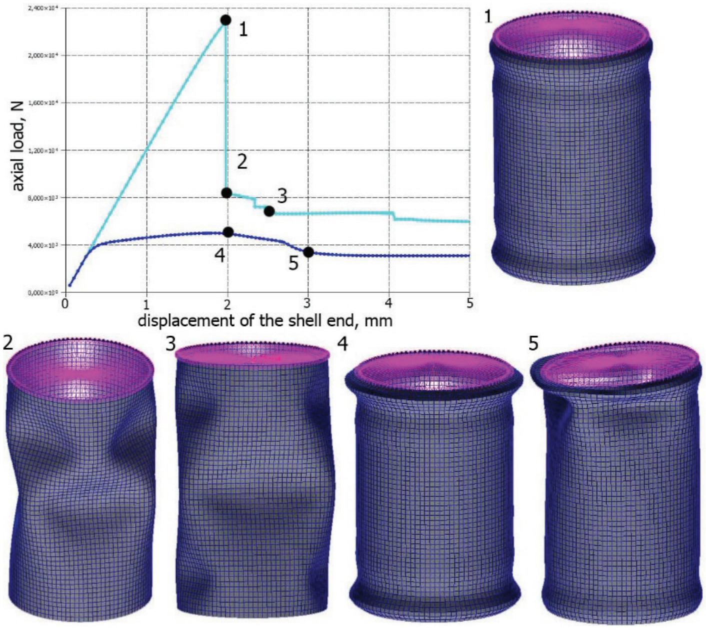

Figure 10. The diagram of the cylinder's deformation with a 1 mm thickness and a view of the model at characteristic points

Table 2. comparison of results of authors the results of experiments by V.G. Sazonov and calculations by A.V. Karmishin

Shell's thickness, mm	Critical stresses, kg/mm^2			
	Expiriment (V.G. Sazonov)	Plastic shell buckling (A.V. Karmishin)	Elastic analysis (Nastran)	Elasto-plastic analysis
1	2	3	4	5
1	19,5	19,2	93,20	20,45
1,5	22,6	21,4	148,11	25,75
2	23,9	22,6	178,84	30,55

REFERENCES

1. **Manuylov G.A., Kositsyn S.B., Begichev M.M.** Chislennoye modelirovaniye protsessov poteri ustoychivosti ravnovesiya tonkostennykh elementov konstruktsiy v usloviyakh uprugoplasticheskikh deformatsiy. Trudy Mezhdunarodnoy nauchno-prakticheskoy konferentsii «Inzhenernyye sistemy – 2011», Moscow, 05 – 08 april 2011. – Moscow: RUDN. – 2011. – p. 377-383.
2. **Manuylov G.A., Kositsyn S.B., Begichev M.M.** Sravnitel'nyy analiz ustoychivosti nekotorykh tonkostennykh konstruktsiy pri uprugikh i uprugo-plasticheskikh deformatsiyakh // Tezisy doklada 70 Nauchno-metodicheskoy i nauchno-issledovatelskoy konferentsii MADGTU (MADI). 30 january – 03 february 2012, Moscow: MADI, 2012 – p. 21 – 22.
3. **Timoshenko S.P.** Ustoychivost uprugikh sistem / M.: Ogiz, Gostekhizdat. – 1946. – 533 p.
4. **Karmishin A.V., Lyaskovets V.A., Myachenkov V.I., Frolov A.N.** Statika i dinamika tonkostennykh obolochechnykh

konstruktsiy. – Moscow: Mashinostroyeniye. – 1975. – 376 p.

5. **Manuylov G.A., Kositsyn S.B., Begichev M.M.** O yavlenii poteri ustoychivosti prodol'no szhatoy krugovoy tsilindricheskoy obolochki. chast 1: O poslekriticheskom ravnovesii obolochki // International Journal for Computational Civil and Structural Engineering Volume 12, Issue 3. – 2016. – p. 58-72.
6. **Manuylov G.A., Kositsyn S.B., Begichev M.M.** O yavlenii poteri ustoychivosti prodol'no szhatoy krugovoy tsilindricheskoy obolochki. chast II. Maksvellova sila i energeticheskiy bar'yer // International Journal for Computational Civil and Structural Engineering) Volume 12, Issue 4. – 2016. – p. 103-115.

СПИСОК ЛИТЕРАТУРЫ

1. **Мануйлов Г.А., Косицын С.Б., Бегичев М.М.** Численное моделирование процессов потери устойчивости равновесия тонкостенных элементов конструкций в условиях упругопластических деформаций // Труды Международной научно-практической конференции «Инженерные системы – 2011», Москва, 05 – 08 апреля 2011 г., М.: РУДН, 2011. С. 377 – 383.
2. **Мануйлов Г.А., Косицын С.Б., Бегичев М.М.** Сравнительный анализ устойчивости некоторых тонкостенных конструкций при упругих и упруго-пластических деформациях // Тезисы доклада 70 Научно-методической и научно-исследовательской конференции МАДГТУ (МАДИ). 30 января – 03 февраля 2012 г., М.: МАДИ, 2012 – С. 21 – 22.
3. **Тимошенко С.П.** Устойчивость упругих систем / М.: Огиз, Гостехиздат. 1946. - 533 с.
4. **Кармишин А.В., Лясковец В.А., Мяченков В.И., Фролов А.Н.** Статика и динамика тонкостенных оболочечных конструкций. – М.: Машиностроение. – 1975 г. – 376 с.
5. **Мануйлов Г.А., Косицын С.Б., Бегичев М.М.** О явлении потери устойчивости продольно сжатой круговой цилиндрической оболочки. часть 1: О послекритическом равновесии оболочки // International Journal for Computational Civil and Structural Engineering Volume 12, Issue 3. – 2016. – p. 58-72.
6. **Мануйлов Г.А., Косицын С.Б., Бегичев М.М.** О явлении потери устойчивости продольно сжатой круговой цилиндрической оболочки. часть II. Максвеллова сила и энергетический барьер // International Journal for Computational Civil and Structural Engineering) Volume 12, Issue 4. – 2016. – p. 103-115.

Gaik A. Manuylov, Ph.D., Associate Professor, Department of Structural Mechanics, Russian University of Transport; 127994, Russia, Moscow, 9b9 Obrazcova Street; phone/fax +7(499)972-49-81.

Sergey B. Kosytsyn, Dr.Sc., Professor, Head of Department of Theoretical Mechanics, Russian University of Transport; 127994, Russia, Moscow, 9b9 Obrazcova Street; phone/fax: +7(499) 978-16- 73; E-mail: kositsyn-s@yandex.ru, kositsyn-s@mail.ru

Maxim M. Begichev, Ph.D., Associate Professor, Department of Theoretical Mechanics, Russian University of Transport; 127994, Russia, Moscow, 9b9 Obrazcova Street; phone/fax: +7(499) 978-16-73; E-mail: noxonius@mail.ru.

Мануйлов Гайк Александрович, кандидат технических наук, доцент, доцент кафедры «Строительная механика» Российского университета транспорта; 127994, г. Москва, ул. Образцова, 9, стр. 9; тел./факс +7(499) 972-49-81

Косицын Сергей Борисович, доктор технических наук, профессор, заведующий кафедрой «Теоретическая механика» Российского университета транспорта; 127994, г. Москва, ул. Образцова, 9, стр. 9; тел./факс +7(499) 978-16-73; E-mail: kositsyn-s@yandex.ru, kositsyn-s@mail.ru

Бегичев Максим Михайлович, кандидат технических наук, доцент кафедры «Теоретическая механика» Российского университета транспорта; 127994, г. Москва, ул. Образцова, 9, стр. 9; тел./факс +7(499) 978-16-73; E-mail: noxonius@mail.ru.

DOI:10.22337/2587-9618-2022-18-3-37-43

INFLUENCE STIFFNESS OF SHEAR BONDS ON THE STRESS-STRAIN STATE OF MULTISTOREY BUILDINGS

Valery A. Lyublinskiy

National Research Moscow State University of Civil Engineering, Moscow, RUSSIA

Abstract. The paper considers issues the nonlinear behavior of shear bonds affecting the changes in the distribution of stresses and strains in vertical structures, as well as to compare these stresses and strains with the linear statement of the problem solution in which the compliance of the bonds is constant.

In a complex multiconnected system of the multistory building, the new redistribution of stresses arises, which does not coincide with the original distribution of stresses. To correct the stiffness value for the bonds, the experimental data were used. A secant module was used to determine the stiffness for vertical joints. Loading was performed by the step method. At the extreme stage of loading, the redistribution of stresses in the load-bearing elements of the building showed their significant leveling. The issue of ultimate deformations of shear bonds limiting the process of redistribution of stresses and deformations requires discussion.

Keywords: multistory building, shear bonds, stiffness, nonlinear deformation, bearing system

ВЛИЯНИЕ ЖЕСТКОСТИ СВЯЗЕЙ СДВИГА НА НАПРЯЖЕННО-ДЕФОРМИРОВАННОЕ СОСТОЯНИЕ МНОГОЭТАЖНЫХ ЗДАНИЙ

В.А. Люблинский

Национальный исследовательский Московский государственный строительный университет, Москва, РОССИЯ

Аннотация: В работе рассмотрены вопросы нелинейного поведения сдвиговых связей, влияющих на изменение распределения напряжений и деформаций в вертикальных конструкциях, а также сопоставление этих напряжений и деформаций с линейной постановкой решения задачи, в которой податливость связей постоянна.

В сложной многосвязной системе многоэтажного здания возникает новое перераспределение напряжений, не совпадающее с первоначальным распределением напряжений. Для корректировки значения жесткости связей использовались экспериментальные данные. Модуль секущей использовался для определения жесткости вертикальных швов. Загрузка производилась ступенчатым методом. На предельной стадии нагружения перераспределение напряжений в несущих элементах здания показало их значительное нивелирование. Требует обсуждения вопрос о предельных деформациях связей сдвига, ограничивающих процесс перераспределения напряжений и деформаций.

Ключевые слова: многоэтажные здания, связи сдвига, жесткость, нелинейная деформация, несущая система

INTRODUCTION

The bearing system of a multi-story buildings consists of vertical structures united into a spatial system by floors slabs and vertical connections with certain stiffness. Vertical shear bonds (lintels, welded joints, floor areas) can be used as connections in a multi-story building.

Existing mathematics models of load-bearing systems of multistory buildings, in most cases, are guided by the elastic work of load-bearing elements and their connections [1-3]. In the

classical calculation models of a building the relationships between stresses and strains are specified by the Hooke elastic-linear law. However, they do not allow sufficient use of the safety margins of the entire load-bearing system or can distort the assessment of the real state of this load-bearing system of the building. The important feature of the real work of materials is the nonlinear nature of the relationship between stress and deformation of
both vertical load-bearing structures and the elements connecting them.
Deformation diagrams are used to consider the nonlinear properties of structural materials.
Proposals for concrete deformation diagrams are contained in a number of works [4-7]. Description of the diagrams of concrete deformation in compression is contained in the design standards [8,9]. Various studies are devoted to the analysis of the work of shear bonds [10-12], welded butts, vertical concrete joints [13-14].
The aim of this work is to conduct a comparative analysis of the stress-strain state multistory building with linear and nonlinear deformation of shear bonds. The main task of the work is to establish changes in the stress-strain state of the multistory building taking into account the experimental data work shear bonds as lintels.

METHOD

In this work, the object of the study was a 30-storey residential building made of monolithic concrete. A multistorey building with the building system is shown in Figure 1. The diagram shows 16 walls W and 14 shear bonds Shb. The building consists of 30 floors and basement and attic premises. Type B25 concrete was used, the walls 30 cm thick were connected by lintels with a cross-sectional size of 20 by 40 cm and a length of 2 m, the columns were taken as 40 by 40 cm and 40 by 6 cm.
The building was subjected to permanent, temporary and wind loads. The calculation was carried out using the ETABS software package based on the finite element method [15-17]. For walls, a finite element of the shell type was adopted, for shear bonds - an elastic element, the stiffness of which was refined at each stage of the calculation. The maximum size of the wall finite element was 85 x 85 cm. The base of the building was assumed to be non-deformable. To correct the value of the shear modulus, the experimental deformation diagram « shear force Q - displacement Δ» [13,18] was used. A secant module was used to determine the stiffness K for shear bonds. The loading was carried out by the stepwise method (Fig. 2.).

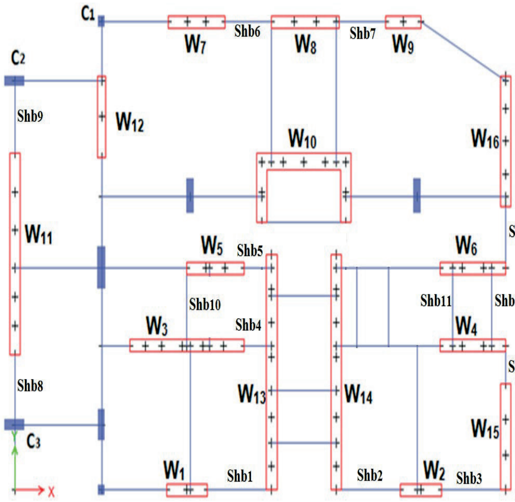

Figure 1. The design scheme of the building (communication)

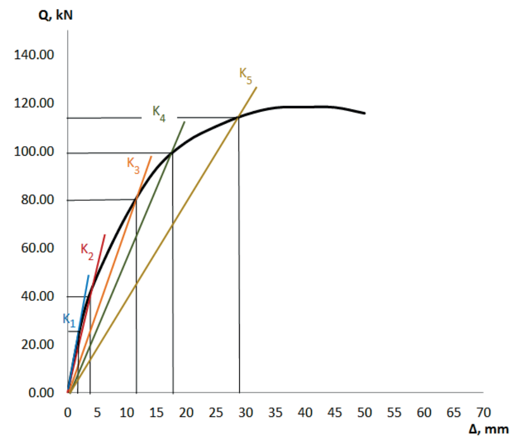

Figure 2. Experimental strain diagram deformation "Q-Δ" for shear joints

The loading was carried until hinged joint is formed in one of the shear bonds. During loading, shear forces and corresponding deformations were recorded.

RESULTS

The initial calculation of the bearing system multistory building with constant stiffness of shear bonds is designated K0. The subsequent steps of changing the stiffness of the shear bonds and the corresponding recalculations of the bearing system multistory building are designated K1 – K5.

As an example, the stress-strain state of wall W7, wall W2 and the adjacent shear bonds are shown.

Table 1. Change in maximum stresses and percentage of reinforcement in wall W7

	K0	K1	K2	K3	K4	K5
б (kN/m²)	8881.46	9769.61	10480.13	11013.01	11457.09	11634.72
Δб%		-10.0	-7.3	-5.1	-4.0	-1.6
μ%	0.48	1.03	1.47	1.80	2.08	2.19
Δμ%		0.55	0.44	0.33	0.28	0.11

Table 2. Change in maximum stresses and percentage of reinforcement in wall W2

	K0	K1	K2	K3	K4	K5
б (kN/m²)	16980.82	14773.32	13414.85	12396.00	11716.77	11207.34
Δб%		13.0	9.2	7.6	5.5	4.3
μ%	2.72	1.70	1.08	0.62	0.31	0.07
Δμ%		-1.01	-0.62	-0.47	-0.31	-0.23

Determination of the actual stress-strain state of structural elements of the bearing system was evaluated on the basis of comparing the results of linear and nonlinear calculations.

The maximum change in normal stresses occurred in the wall W2, W7, W10, W11, W12, W13, W14, W15. For wall W7 (Fig 3, Table 1), the difference was 33.2%, in the first case the value was 8881.46 kN / m^2, in the second case it was 11827.25 kN / m^2. For wall W2 (Fig. 4, Table 2), the difference between the calculations was -37.6%, in the first case the value is 16980.82 kN / m^2, in the second - 10601.57 kN / m^2.

For wall W8 the difference was 21.5%, in the first case the value was 9758.06 kN / m^2, in the second case it was 11852.45 kN / m^2. for wall W9 the difference was -8%, in the first case the value is 12803.33 kN / m^2, in the second 11774.36 kN / m^2.

Bending moments have changed in almost all walls. For the W7 wall (Fig.5), the difference between the calculations was 37.3%, in the first case the value was 77.88 kN. m, in the second it was 106.9 kN. m, for the W8 wall the difference was 27.1%, in the first case the value was 180.45 kN. m, in the second 229.3 kN. m, for the W9 wall the difference was 131.1%, in the first case the value was 50.27 kN. m, in the second 116.3 kN. m.

The shear forces in the shear bonds have changed. In a number of connections, efforts increased (Shb6, Shb7), in some (Shb2) – decreased.

Reinforcement of vertical construction s of the bearing system was also calculated based on a comparison of the results of linear and non-linear calculations. Of course, the maximum change in reinforcement occurred in the walls with the largest change in normal stresses, in the wall W2, W7, W10, W11, W12, W13, W14, W15, where in the first case the percentage of reinforcement in the walls W2, W12 was close to the maximum allowable percentage of reinforcement, in the second case, the minimum percentage of reinforcement 1% became less, where it changed by -2.9% and -2.16%.

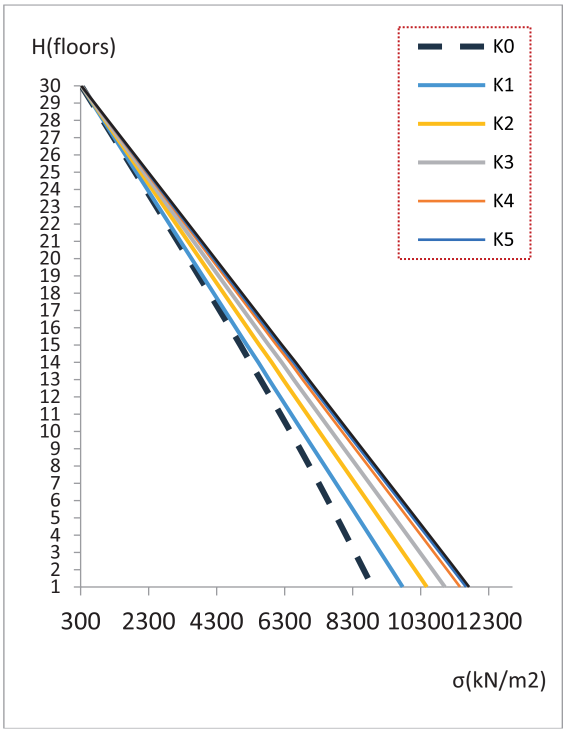

Figure 3. Changes vertical stresses in the wall (W7) depending on changes in the stiffness of shear bonds (K)

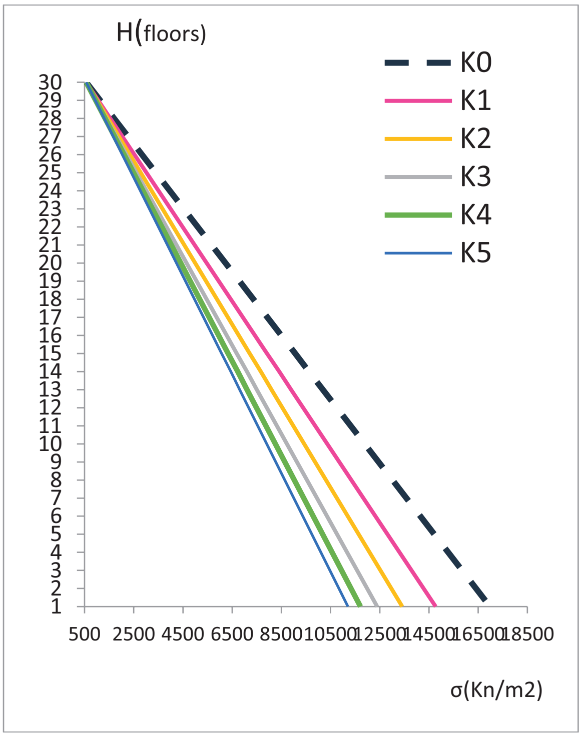

Figure 4. Changes vertical stresses in the wall (W2) depending on changes in the stiffness of shear bonds (K)

For wall W7 the difference in calculations was 1.8%, for wall W8 the difference in calculations was 1.32%, for wall W9 the difference in calculations was -0.6%, for wall W13 the difference in calculations was 2.32%, for wall W14 the difference in calculations amounted to 2.7%. This was due to a redistribution of stresses.

In the process of redistribution of stresses and deformation during the nonlinear operation of shear bonds, changes occur in all load-bearing elements of a multistory building. There is a relative equalization of stress levels in all vertical bearing structures (Fig. 6). Redistribution of stresses from more loaded elements to less loaded ones took place. To the extent that the stiffness parameters of the shear bonds allowed it. Further redistribution stresses is impossible. Shear bonds gradually reach ultimate deformations (Fig. 6).

Due to the decrease in the stiffness of the shear bonds, the bending moment in the walls of the bearing system increases. There is an increase in the deflection of the bearing system the multistorey building.

CONCLUSIONS

The bearing system of multistorey buildings is experiencing a turn in the plan and a flat bend in two directions. Stress-strain state multistory buildings are determined by position of vertical constructions in the building plan and by the stiffness characteristics walls and shear bonds.

In the bearing system, all walls and shear bonds are in a spatial interaction. They cannot be deformed and destroyed independently of other elements, their deformations are constrained by neighboring shear bonds, walls and overlaps.

When the bearing capacity of one or several elements of the bearing system is reached, the bearing capacity of the system as a whole is not exhausted. The numerical experiments carried out have shown that with an increase in the load, the stresses are redistributed in all elements of the bearing system.

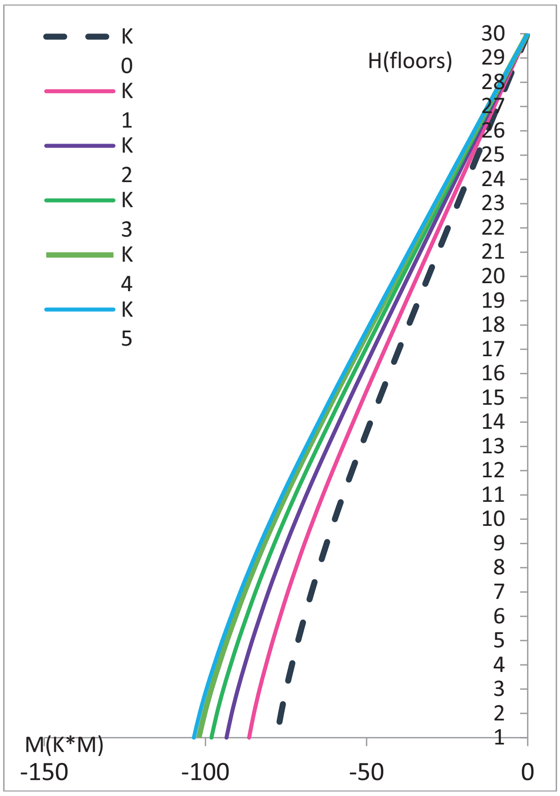

Figure 5. Changes bending moment in the wall (W7) depending on changes in the stiffness of shear bonds (K)

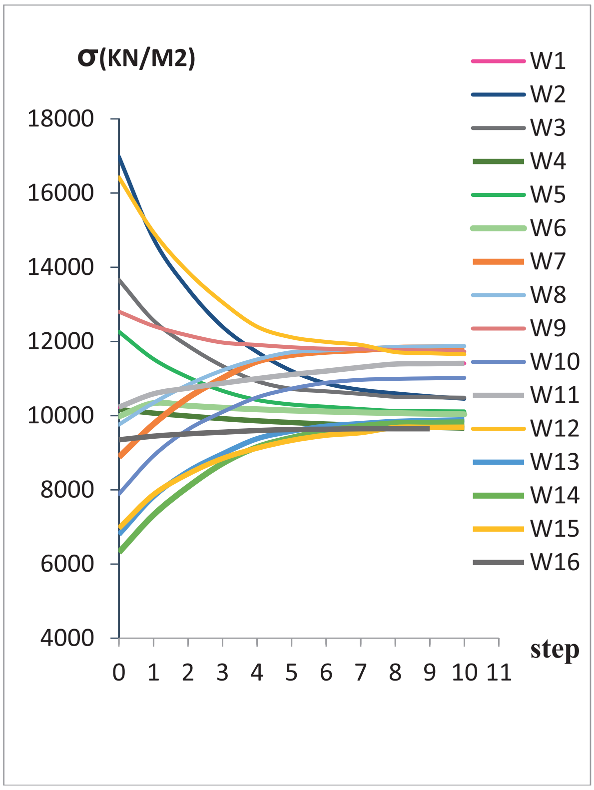

Figure 6. Changing the normal stresses in the walls W1- W16 in accordance with the change in the stiffness of the shear bonds at each step Ki

The maximum value of change in normal stresses -10% occurred in wall W7. The percentage of reinforcement increases significantly in wall W14 - 2.33%.

The spatial work of shear bonds is a mechanism for the spatial redistribution of stresses in vertical structures. The stiffness shear bonds are important for the determination of deformations and stresses in vertical bearing structures.

REFERENCES

1. **Zolotov A.B., Akimov P.A., Sidorov V.N., Mozgaleva M.L.** Discrete-continual finite element method. Applications in Construction, ASV, Moscow, 2010, 336 p.
2. **Senin N.I., Akimov P.A.** Mathematical fundamentals of linear three-dimensional analysis of load bearing structures of multistory buildings with the use of discrete-continual model. // Vestnik MGSU, 2, 2011, P. 44-49.
3. **Tamrazyan A., Avetisyan L**. Comparative analysis of analytical and experimental results of the strength of compressed reinforced concrete columns under special combinations of loads. // MATEC Web of Conferences, doi:10.1051/matecconf/20168601029.
4. **Blokhina N., Galkin A.** The application of ANSYS software package in limit load analysis of structures made from anisotropic nonlinear elastic materials. // MATEC Web of Conferences, doi:10.1051/matecconf/ 201711700019.
5. **Panfilof D.A., Pischulev A.A., Givadetdinov K.I.** Review of diagrams of concrete deformation under compression in

national and foreign concrete codes. // Ind. & Civ. Eng., 2014, 3, pp. 80-84.
6. **Karpenko N.I., Sokolov B.S, Radaykin O.V.** Analysis and enhancement of curvilinear diagrams of concrete deformations for calculation of reinforced concrete structures on the basic of a deformation model. // Ind. & Civ. Eng., 2013, 1, pp. 28-30.
7. **Murashkin V., Murashkin G.** Application of concrete deformation model for calculation of bearing capacity of reinforced concrete structures. // MATEC of Web Conference, doi:10.1051/matecconf/201819604008.
8. Building Code of RF SP 63.13330.2018 Concrete and reinforced concrete structures. General provisions, Moscow, 2019, p. 170.
9. **Shuvalov A., Gorbunov I., Kovalev M., Faizova A**. Experimental studies of compliance of vertical joints used in construction of high-rise panel buildings. // MATEC Web of Conferences, doi:10.1051/matecconf/201819602049.
10. **Zimos D.K., Papanikolaou V.K., Kappos A.J., Mergos P.E.** Shear-Critical Reinforced Concrete Columns under Increasing Axial Load. // ACI Structural Journal, 2020, 117(5), pp. 29 - 39.
11. **Blazhko V**. About determination of ductility of Connections when forming calculation models of panel buildings. // Hous. Constr. 2017, v. 3, pp. 17-21.
12. **Sokolov B., Mironova Y.** Strength and compliance of vertical joints of wall panels using flexible loops. // Housing construction, 2014, v. **5** pp 60-62.
13. **Lyublinskiy V.**, TO test vertical weldid butt joints of panel buildings. // Build. & Reconst., 2019 v. 5, pp. 17-22, doi:10.33979/2073-7416-2019-85-5-17-22.
14. **Tamrazyan A., Popov D.** Reduce of bearing strength of the bent reinforce-concrete elements on a sloping section with the corrosive damage of transversal armature. // MATEC Web of Conferences, 2017, doi:10.1051/matecconf/201711700162.
15. **Зенкевич О**. Finite element and approximation., МИР, Moscow, 1986, p. 318.
16. **Zienkiewicz O.C, Taylor R.L., Zhu J.Z.** The Finite Element Method Set, sixth Edition. Butterworth-Heinemann, 2005, p. 435.
17. **Klovanich S.F., Bezushko D.I.** The finite element method in the calculation of spatial reinforced concrete structures. // Publishing house of ONMU, Odessa, 2009, p. 89.
18. **Lyublinskiy V., Tomina M.** Experimental study of the strength and suppleness of a vertical welded joint. // Syst. Technol. Met. 2018, v. 5, pp. 17-19.

СПИСОК ЛИТЕРАТУРЫ

1. **Золотов А.Б., Акимов П.А., Сидоров В.Н.** Дискретно-континуальный метод конечных элементов. Приложения в строительстве, М., Изд-во АСВ, 336 с.
2. **Сенин Н.И., Акимов П.А.** Некоторые математические основы расчета пространственных несущих систем многоэтажных зданий в линейной постановке в рамках дискретно-континуальной модели. Вестник МГСУ, №2, 2011, с. 44-49.
3. **Tamrazyan A., Avetisyan L**. Comparative analysis of analytical and experimental results of the strength of compressed reinforced concrete columns under special combinations of loads. // MATEC Web of Conferences, doi:10.1051/matecconf/20168601029.
4. **Blokhina N., Galkin A.** The application of ANSYS software package in limit load analysis of structures made from anisotropic nonlinear elastic materials. // MATEC Web of Conferences, doi:10.1051/matecconf/201711700019.
5. **Панфилов Д.А., Пищулев А.А., Гимадетдинов К.И.** Обзор существующих диаграмм деформирования бетона при сжатии в отечественных и зарубежных нормативных документах. Промышленное

и гражданское строительство, 2014, №3, с. 80-84.

6. **Карпенко Н.И., Соколов Б.С., Радайкин О.И.** Анализ и совершенствование криволинейных диаграмм деформирования бетона для расчета железобетонных конструкций по деформационной модели. Промышленное и гражданское строительство, 2013, №1, с. 28-30.
7. **Murashkin V., Murashkin G.** Application of concrete deformation model for calculation of bearing capacity of reinforced concrete structures. // MATEC of Web Conference, doi.org/10.1051/matecconf/20181960400
8. СП 63.13330.2018 Бетонные и железобетонные конструкции. Основные положения. М., 2018, с. 170.
9. **Shuvalov A., Gorbunov I., Kovalev M., Faizova A**., Experimental studies of compliance of vertical joints used in construction of high-rise panel buildings. // MATEC Web of Conference, doi:10.1051/matecconf/201819602049.
10. **Zimos D.K., Papanikolaou V.K, Kappos A.J., Mergos P.E.**, Shear-Critical Reinforced Concrete Columns under Increasing Axial Load. // ACI Structural Journal, 2020, 117(5), pp. 29 - 39.
11. **Блажко В.П.** Об определении податливости связей при формировании расчетных моделей панельных зданий. Жилищное строительство, 2017, №3, с.17-21.
12. **Соколов Б.С., Миронова Ю.В.** Прочность и податливость вертикальных соединений стеновых панелей с использованием гибких петель. Жилищное строительство, 2014, №5, с. 60-62.
13. **Люблинский В.А**. К испытанию вертикальных сварных стыковых соединений панельных зданий. // Строительство и реконструкция, 2019, № 5, с. 17-22.
14. **Tamrazyan A., Popov D.** Reduce of bearing strength of the bent reinforce-concrete elements on a sloping section with the corrosive damage of transversal armature. // MATEC Web of Conferences, 2017, doi:10.1051/matecconf/201711700162
15. **Зенкевич О**. Конечные элементы и аппроксимация, М.: МИР, 1986, с. 318.
16. **Zienkiewicz O.C, Taylor R.L., Zhu J.Z.** The Finite Element Method Set, Sixth Edition. Butterworth-Heinemann, 2005, p. 435.
17. **Клованич С.Ф., Безушко Д.И.** Метод конечных элементов в нелинейных расчетах пространственных железобетонных конструкций, Одесса, ОНМУ, 2009, 89с.
18. **Люблинский В.А., Томина М.В.** Экспериментальное исследование прочности и податливости вертикального сварного стыка, Системы, технологии, методы. 2018, №3, с. 154-158.

Valery A. Lyublinskiy, Associate Professor, Ph.D.; Professor Department of reinforced concrete constructions, National Research Moscow State University of Civil Engineering; 26, Yaroslavskoe Shosse, Moscow, 129337, Russia; phone: +7(495) 287-49-19 (3036); Email: LyublinskiyVA@mgsu.ru.

Люблинский Валерий Аркадьевич, кандидат технических наук, профессор кафедры железобетонных конструкций Национального исследовательского Московского государственного строительного университета; 129337, Россия, г. Москва, Ярославское шоссе, дом 26; телефон: +7(495) 287-49-19(3036); Email: LyublinskiyVA@mgsu.ru.

DOI:10.22337/2587-9618-2022-18-3-44-53

MODELING OF THE MICROCLIMATE OF A RESIDENTIAL COURTYARD DURING RENOVATION

Valery I. Telichenko [1], *Yurii A. Sumerkin* [2]

[1] Moscow State University of Civil Engineering, Moscow, RUSSIA
[2] "Megastoy" LLC, Moscow, RUSSIA

Abstract. The article provides an example of modeling the microclimate of a residential courtyard during renovation in conditions of high-density urban development. Modeling is carried out on the basis of a bioclimatic indicator - the environmental heat load index (TNS-index). The calculations are based on the method for analysis temperature radiation and determining the angel factors between a black glob temperature to the surrounding the given platforms of side of residential courtyard. The method shows a good reflection on changes in spatial planning, architectural and construction solutions, landscaping, aeration of the yard, etc. This allows to comprehensively assessing the degree of comfort of the microclimate of the courtyard for specific weather conditions.

Keywords: renovation, urban planning, microclimate of urban areas, radiation

МОДЕЛИРОВАНИЕ МИКРОКЛИМАТА ТЕРРИТОРИИ ДВОРА ПРИ РЕНОВАЦИИ

В.И. Теличенко [1], *Ю.А. Сумеркин* [2]

[1] Национальный исследовательский московский государственный строительный университет, Москва, РОССИЯ
[2] ООО «Мегастрой», Москва, РОССИЯ

Аннотация: В статье приводится пример моделирования микроклимата территории жилого двора при реновации в условиях высокоплотной городской застройки. Моделирование осуществляется на основе биоклиматического показателя - индекса тепловой нагрузки окружающей среды (ТНС-индекса). В основе вычислений используется метод расчета радиационной температуры с применением коэффициентов облученности с шарового термометра на окружающие приведенные площадки ограждений жилого двора. Метод расчета показывает хорошую рефлексию на изменения объемно-планировочных, архитектурно-строительных решений, способов озеленения, аэрации двора и др. Это дает возможность комплексной оценки степени комфортности микроклимата территории двора для конкретных метеоусловий.

Ключевые слова: реновация, градостроительство, микроклимат городских территорий, радиационная температура

1. INTRODUCTION

The program of Housing Renovation in Moscow, launched in 2017, is systemic and multi-purpose. The renovation should improve the living conditions of more than a million residents for the formation and development of a modern urban environment [1].

As a part of the environment-forming of open urban areas is its climate [2].

Interest increases to the quantitative and qualitative analysis of changes in the indicators of the microclimate of the courtyard area after renovation, for example, for the warm season with a significant increase in building density, and, if necessary, its melioration by various methods to achieve comfort [3].

With an increase in building density, streets, squares, adjacent territories, courtyards, etc. sink to the bottom of "urban canyons". The visible part of the sky decreases. Therefore, the intense heat exchange with it, as with the coldest surface of the surrounding space, descends. Among other things, the result of this microclimatic process is an increase in radiation temperatures due to the surrounding surfaces. The increasing of radiation temperatures, the deterioration of the aeration of the urban active layer, air pollution and technogenic heat lead to the effect known as an urban heat island [4].

This article provides a number of simulation results for a bioclimatic indicator - the environmental heat load index (TNS-index) based on the method for analysis the radiation temperature using the irradiance coefficients obtained from a spherical bulb thermometer to the surrounding reduced areas of fences of a residential yard [5]. Based on the obtained simulation results, recommendations have been proposed to increase comfort in the courtyard of a residential building planned for renovation in Moscow.

2. PROBLEM FORMULATION

Simulation of the TNS-index was carried out for the space-planning solution of the residential yard, proposed by the Moscow Committee for Architecture, and was based on:

- variability of the use of materials in the decoration of the facade and their areas;
- variability of materials used in paving, landscaping;
- rational landscaping of yard areas and landscaping of vertical surfaces;
- changes in the aeration mode during the installation of "windows" in the perimeter (well) building.

2.1 ENVIRONMENTAL HEAT LOAD INDEX (TNS-INDEX)

According to SanPiN 2.2.4.548-96 "Hygienic requirements to occupational microclimate" TNS-index is calculated from the formula:

$$TNS=0.7\times tw+0.3\times tg, \qquad (1)$$

where

t_w is the wet bulb temperature, °C;

t_g is the spherical bulb temperature, °C.

Simulation of the microclimatic conditions of a residential court yard for the warm period of the year based on the TNS-index is not random, since the TNS-index has established itself as a universal tool for evaluation the environment indoors and outdoors during the warm season among other widely used bioclimatic indicators containing the radiation component. The TNS-index is easy to calculate. Many installations for field surveys using a spherical bulb thermometer determine these indicators automatically [6, 7].

As Figure 1 shows, the TNS-index has good compatibility with the WBGT index (ISO 7243) and the operational (equivalent) temperature, which is used to determine thermal comfort based on the predicted mean vote (PMV) according to ISO 7730. However unlike the latter one, it has no restrictions in its application with a significant local asymmetry of radiation temperatures.

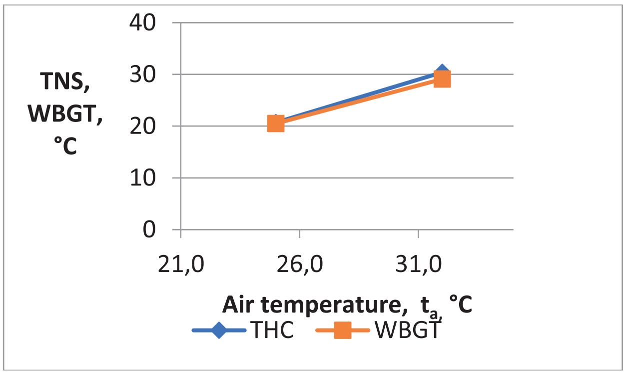

Figure 1. Graphs for TNS-index and WBGT-index under the same meteorological conditions.

3. ALGORITHM FOR ANALYSIS

3.1. Step 1. Calculation of radiation temperatures (tr) for i point of the yard at a height of 1.5m

Based on the determination of the average radiation temperature inside the room, in accordance with the formula (12) ISO 7726:1998 "Ergonomics of the thermal environment — Instruments for measuring physical quantities" and earlier numerical results, confirmed by field studies, an equation has been proposed for determining the average radiation temperature of the environment using the irradiance coefficients from a spherical bulb thermometer to the surrounding reduced areas of fences of a residential court yard [5].

The formula for the average radiation temperature of the environment for the *i* point of a residential court yard from the influence of all six fences looks like this:

$$t_{ri}=\sum_{1}^{6}\sum_{n=1}^{N}t_{\text{пл.}}\times\varphi_{\text{сф}-\text{пл.}} \qquad (2)$$

where $\varphi_{sph-y.}$ is the irradiance coefficient from a spherical bulb thermometer towards the reduced area of a particular fence;

$t_{пл.}$ is the temperature of the reduced area, °C;

N is the number of reduced areas on the fence.

3.2. Step 2. Calculation of the indication of a spherical thermometer (tg) for the i point of the yard

According to ISO 7243, the relationship between the temperature of a bulb thermometer and the radiation temperature of the environment during natural convection, i.e. $\bar{\upsilon} < 0.15$ m/s is defined as:

$$t_{\text{g}}=\frac{t_R+2.44\times t_{\text{a}}\times\sqrt{\bar{\upsilon}}}{1+2.44\times\sqrt{\bar{\upsilon}}}, \qquad (3)$$

where t_R is the ambient radiation temperature, °C; t_a is the air temperature, °C; t_{g} is the spherical bulb thermometer readings, °C; $\bar{\upsilon}$ is the wind velocity, m/s.

3.3. Step 3. Calculation of the TNS index for the i point of the yard

The TNS-index is calculated according to formula 1.

Field studies of new residential microdistricts have shown that the average values of the wet thermometer readings (tw) amounted to +18.0 ° C at an average relative humidity of 46% [7] for the absence of tree and shrub plantations or their insufficiency, as well as the absence of water surfaces at an outdoor temperature of +26.0 ° C. Formula 1 takes the form:

$$THC_i=0{,}7\times(+18°C)+0{,}3\times t_{gi}$$

3.4. Step 4. Construction of areas of the TNS-index of a residential yard and determination of the level of comfort/discomfort according to Table 1

Table 1. Working conditions in terms of TNS-index (°C) for working premises with a heating microclimate, regardless of the period of the year and open areas in the warm season (upper limit)

Category of work *	Working conditions					
	Permissible *	Harmful				Dangerous (extreme)
		3.1	3.2	3.3	3.4	
Ia	26,4	26,6	27,4	28,6	31,0	31,0
Ib	25,8	26,1	26,9	27,9	30,3	30,3
IIa	25,1	25,5	26,2	27,3	29,9	29,9
IIb	23,9	24,2	25,0	26,4	29,1	29,1
III	21,8	22,0	23,4	25,7	27,9	27,9

* According to app. 1 SanPiN 2.2.4.548-96 "Hygienic requirements to occupational microclimate"

4. OBJECT OF SIMULATION

The object of the study was two identical residential courtyards planned for placement in zones 18.1 and 22.1 in accordance with the Planning Project for the Perovo district of Moscow, proposed by the Moscow Architecture Committee under the renovation program

(Figure 2). The building density is 52.59 thousand sq. m/ha (super dense) [8].

The size of the space of the residential yard after renovation is 104.4 × 122.4 m; h=10-55-65-95 m.

4.1. Initial data:

The residential group is assumed to be latitudinal (Figure 2.).

- period of the year: July
- time period: 11.00-13.00 hours
- air temperature +26.0 °C - with a security of 0.98;
- wind speed up to 0.06 m/s;
- clear.

The solar component coming to the spherical bulb thermometer is +21.5 °C

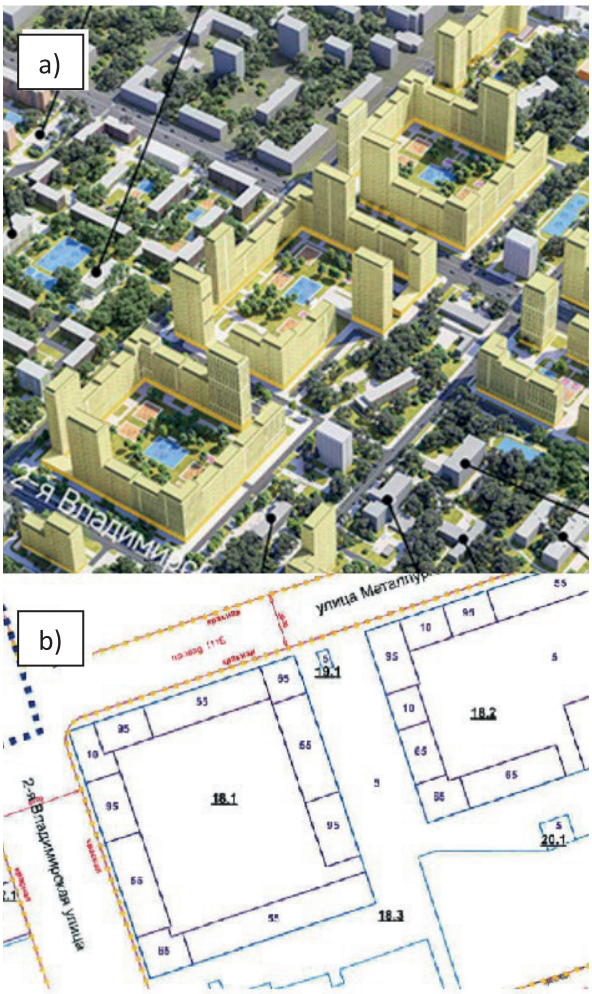

Figure 2. urban planning solution a) 3D vizualization; b) scheme

On the basis of field studies of similar objects (Table 2) [7], the surface temperatures of various coatings (t_{melt}) corresponding to the above mentioned meteorological conditions were obtained:

Table 2. Surface temperatures of urban planning solution coating for air temperature +26,0°C.

No	Coating	Surface temperature, C
1	2	3
1	Facade "light" - concrete surface painted in light colors	+30.0
2	The facade is dark	+36.0
3	Window	+28.0
4	Concrete pavers "light"	+36.0
5	Concrete pavers "dark"	+38.0
6	Rubber coating, brown, recreation and sports grounds	+40.0
7	Lawn	+32.0

The temperature of the sky was calculated by formula 4 [9]:

$$T_{sky}=0.0552\times T_{air}^{3/2} \qquad (4)$$

$$T_{sky}=0.0552\times(273+26.0)^{3/2}=285{,}4°K \text{ or } +12{,}4°C$$

Specifically, for the area under consideration, the equation for calculating the radiation temperature of the environment for the i point considering the irradiance coefficient from the sphere bulb thermometer towards the given sites after its renovation (104.4×122.4×95.0 m), takes the following form:

$$t_{ri}=\sum_1^{3654} t_{av.ar.ins.f.} \times \varphi_{sph-ar.ins.f.}+\sum_1^{3654} t_{av.ar.shady.f.} \times \varphi_{sph-ar.shady.f.} + +\sum_1^{4284} t_{av.ar.right.f.} \times \varphi_{sph-ar.right.f.} + \sum_1^{4284} t_{av.ar.left.f.} \times \varphi_{sph-ar.left.f.}+ +\sum_1^{3944} t_{av.ar.land.f.} \times \varphi_{sph-ar.land.f.}+\sum_1^{3944} t_{av.ar.sky.f.} \times \varphi_{sph-ar.sky.f.} \qquad (5)$$

where

$t_{av.ar.f.}$ is the average surface temperature of the reduced area of a particular fence of an imaginary yard space;

$\varphi_{sph-ar.f.}$ is the irradiance coefficient from a sphere bulb thermometer in the direction of the reduced areas of a specific fence of an imaginary yard space

5. NUMERICAL RESULTS AND CONCLUSIONS FOR THE MOSCOW ARCHITECTURE OPTION

The TNS index calculation grid is 1.8 × 1.8 m. In accordance with Table 1, three areas of the TNS-index were built on the yard plan (Figure 3.):
- in the sun above +25.1°C;
- in the sun in the range of +24.2°C <……≤ +25.1°C
- in the shade less than +24.2°C.

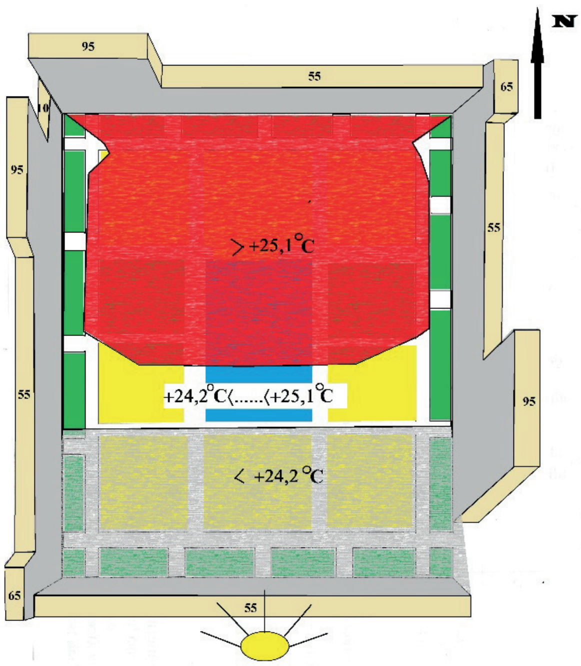

<u>Figure 3.</u> Areas of the TNS-index (°C) for the projected urban planning solution

Using the obtained TNS-index (Table 1.) (R 2.2.2006-05 "Occupational health. Guidelines for the hygienic assessment of factors of the working environment and the labor process. Criteria and classification of working conditions"), we can draw the following conclusions about the bioclimatic impact on a person from due to such urban planning solutions for specific weather conditions:

1. Throughout the yard it is comfortable to be in a state of rest and unhurried walks with an intensity of energy consumption up to 200 Kcal / h.
2. Fast walking (>5 km/h), carrying a grocery bag (more than 1 kg), light jogging, etc. with energy consumption up to 220 Kcal/h will cause uncomfortable heat sensations such as: slightly warm - warm in half of the yard.
3. Physical activity with energy consumption over 220 Kcal / h, for example: volleyball, gymnastics, badminton, will cause uncomfortable heat sensations such as: warm-hot in half of the yard.

6. CLIMATOMELIORATIVE MEASURES, SIMULATION RESULTS

6.1. Coating materials, paving

Calculations of radiation temperatures and field studies show the surface-ground provides main “contribution” to the resulting radiation temperature from the surrounding surfaces (42÷46%), regardless of the height of the yard building [5]. Since the degree of heating of materials in the sun is related to the absorption coefficient of short-wave radiant energy (Equation 5.), It should be noted that the materials of coatings, paving must have absorption coefficients (a_p) of no more than 0.5, for example: white sand; yellow brick; polished marble. Well-maintained lawns can also be used to reduce the resulting radiation temperatures.

Additional sun heating of surfaces (ti), according to IEC 60721-2-4:1987 “Classification of environmental conditions. Part 2: Environmental conditions appearing in natural. Solar radiation and temperature" is determined by the formula:

$$t_i = t_a + (a_p \times E)/h_{to}, \qquad (6)$$

where t_a is the air temperature, °C;
a_p is the absorption coefficient of radiant energy;
E is the solar flux density, W/m²;
h_{to} is the heat transfer coefficient of the surface, W/m²×C°.

6.2. Facade finishing materials

The previous section also applies to the issue of finishing insolated facades. As you approach the sunlit facade, its synergistic effect on the resulting radiation temperatures increases to 35% of the total "contribution" (Figure 4).

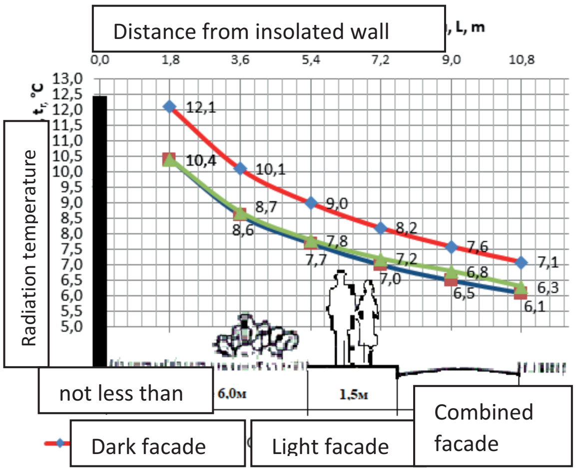

Figure 4. Graphs of radiation temperatures generated by an insulated facade with various architectural and construction solutions

This means the pedestrian paths fall into the zone of active influence of the insolated facade. There are cases when, in the absence of an extensive pavement-path network, a person is experienced the maximum thermal load while moving along a fire-prevention passage along a multi-meter wall illuminated by the sun. It is recommended to provide shortest paths to the entrances to the building and objects in the yard when planning it (Figure 5).

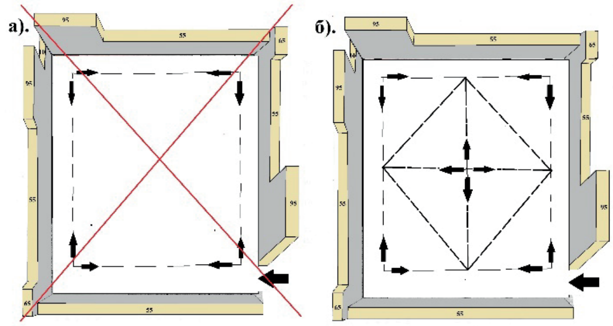

Figure 5. a). in the planning structure of the yard only fire lanes with sidewalks; b). in the planning structure of the courtyard, a developed sidewalk and path network

If it is necessary to use "dark" (radiant energy absorption coefficient of the material ~ 0.8) facade elements in architectural and construction solutions, it is advisable to make the facing of the first five floors from "light" material (radiant energy absorption coefficient is not more than 0.6). At the same time, at least 50% of the thermal radiation generated by the insolated facade falls on the first five floors (Figures 4, 6).

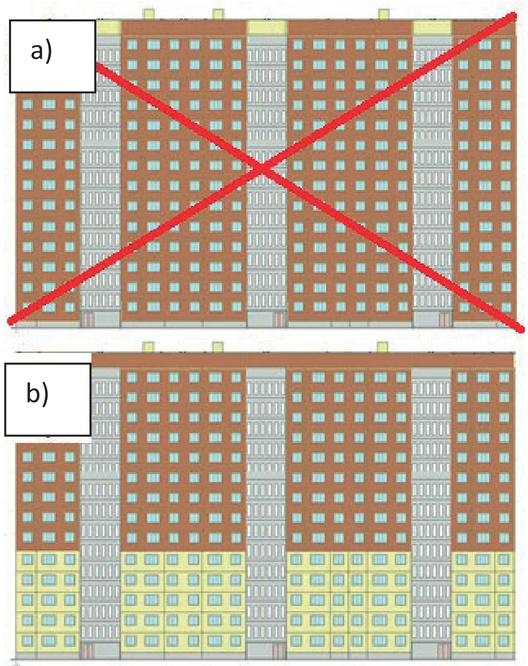

Figure 6. Variants of the architectural and construction solution for the insolated facade: a) "dark"; b) "combined" with the first floors of "light" cladding

6.3. Landscaping area

Since 2020, the planning structure of the adjoining and courtyard areas of residential buildings has been standardized including landscaping area. However, these requirements are only quantitative.

Simulation of the thermal load of the environment to residential yard shows the green areas should be quantitative and applied nature. For example, the even distribution of green areas allows you to evenly distribute the heat load isotherms of the yard. In the future, individual trees or groups of trees can be grown in these areas, which will improve the microclimate in the warm season (Figure 7) [10].

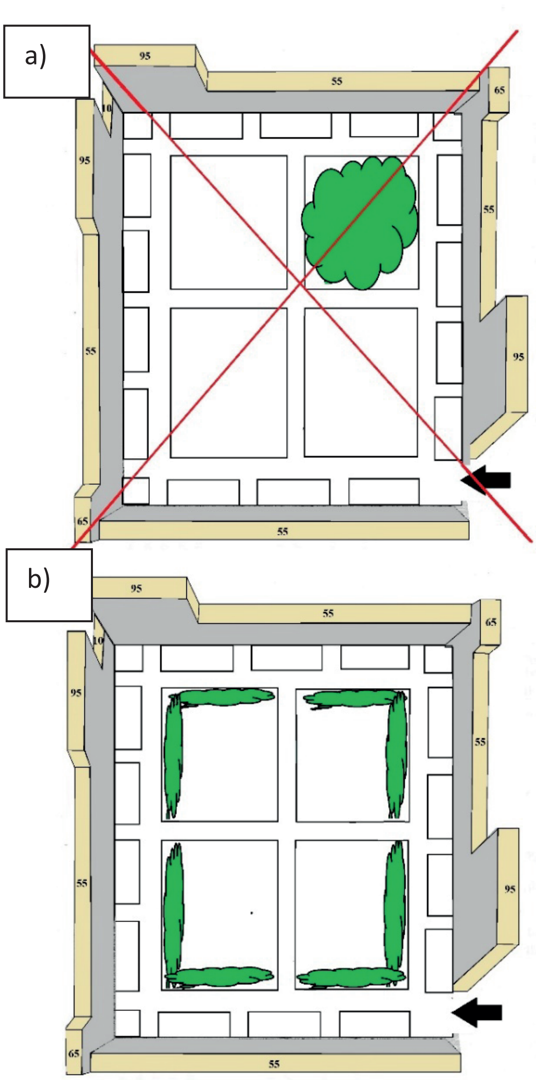

Figure 7. a) quantitative nature of landscaping; b) applied nature of landscaping

For landscaping vertical insolated surfaces, climbing grapes were chosen as the most common fast-growing plant of medium latitude with well-studied properties (Figure 8) [11]. Moreover, a plant height of 6 to 8.0 meters is sufficient, because a further increase in the height of vertical gardening does not lead to significant changes in the heat load (calculation data).

The calculation of the TNS-index for wall landscaping showed that it becomes more comfortable on the walking route (Figure 9). The shift of the increased area of the TNS-index (> +25.1°C) to the central part of the yard is due to the use of molded rubber coating with a high absorption coefficient of solar energy (~0.8) in the coating of playgrounds, recreation and sports grounds. It is recommended to replace the coating material of the sites with materials with a solar energy absorption coefficient (0.5÷0.6).

Figure 8. The example of green facade of building

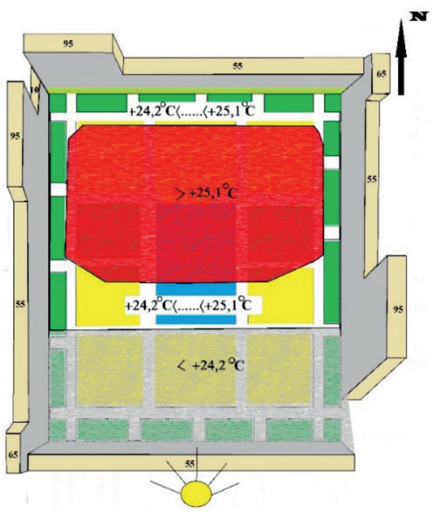

Figure 9. TNS-index areas (°C) for the designed urban planning solution

6.4. Aeration mode

The variant of urban planning proposed by the Moscow Committee for Architecture is a semi-closed morphotype of the yard [12]. There is practically no aeration in such yards, the temperature fields are more stable than in sparse buildings. Simulation of the TNS-index shows that in order to improve the thermal conditions of the yard, it is enough to increase the air velocity in the surface (active) layer up to 0.1 m/s. The TNS-index will drop to a favorable +24.8 °C. To aerate the residential yard, it is proposed to make an additional gap in the perimeter building and several through arches, considering the wind rose of the warm period of the year (Figure 10).

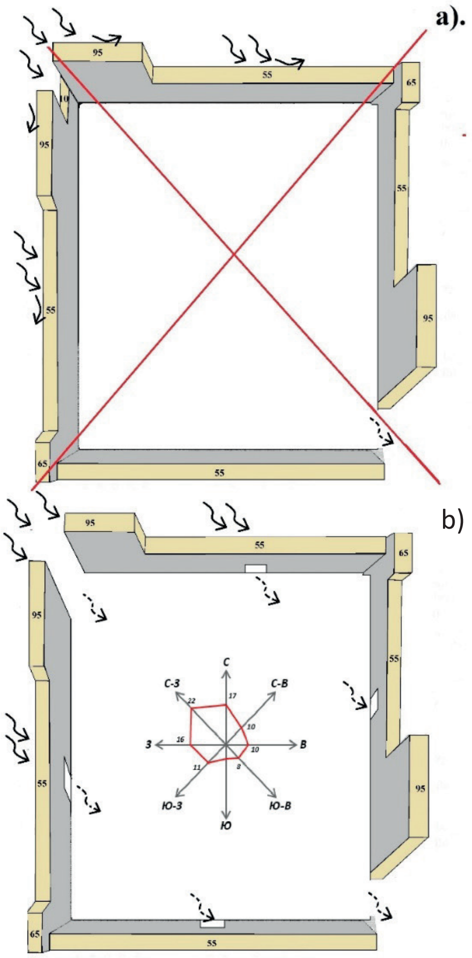

Figure 10. a). there is not aeration of the yard; b). aeration of the yard

7. CONCLUSIONS

The possibility of the radiation temperatures' calculation for the environment of the yard in regard with the urban planning solution of the surrounding buildings, allows to simulate the microclimate of its territory and assess the degree of its comfort based on the bioclimatic indicator of the TNS-index.

This simulation allows you give a comprehensive recommendation for improving the microclimate for typical meteorological conditions during the warm season in the renovation area of Moscow, such as follows:

- development of the system of sidewalk and footpath network of the yard;
- rational placement of landscaping areas on the territory of the yard and landscaping of the insolated facade;
- thermal performance of materials used in coatings, paving and facade cladding;
- space-planning solution in order to improve the aeration of the yard.

REFERENCES

1. **Telichenko V.I.** Renovatsiya - sozdaniye sovremennoy gorodskoy sredy [Renovation - creating modern urban environment] // Vestnik MGSU. – 2020. – T. 15. – No 1. – P. 11. – EDN JXFWEE.
2. **Myagkov M.S., Gubernskiy YU.D., Konova L.I., Litskevich V.K.** Gorod, arkhitektura, chelovek i klimat [City, architecture, human and climate] //Arkhitektura-S. Moscow, 2007.
3. **Myagkov M.S.** Normirovaniye i normativy mikroklimaticheskikh usloviy territoriy gorodskoy zastroyki. Realizatsiya trebovaniy bioklimaticheskoy komfortnosti v proyektnoy podgotovke stroitel'stva [Rationing and standards for microclimatic conditions in urban areas. Implementation of the requirements of bioclimatic comfort in the design preparation of construction] //

https://marhi.ru/kafedra/techno/phisics/myagkov_climat.pdf (available on 01.08.2022).
4. **Oke T.R**. The urban energy balance / T.R. Oke//Progress in Physical Geography 1988; 12; 471 DOI: 10.1177/030913338801200401 https://www.researchgate.net/publication/275590257_The_urban_energy_balance_Prog_Phys_Geogr (accessed 10.07.2022) (In Russian).
5. **Sumerkin YU.A.** Raschet radiatsionnoy temperatury okruzhayushchey sredy gorodskoy zastroyki [Calculation of the radiation temperature of the urban development environment] // Promyshlennoye i grazhdanskoye stroitel'stvo. 2020. No 4. P. 34-40. DOI: 10.33622/0869-7019.2020.04.34-40.
6. **Fedorovich G.V.** Otsenka teplovoy obstanovki s pomoshch'yu sharovogo termometra [Assessment of the thermal situation using spherical bulb thermometer] // Bezopasnost' i okhrana truda. 2011. No 1. P. 68-71.
7. **Sumerkin YU.A.** Naturnoye obsledovaniye zhiloy zastroyki na predmet energeticheskogo vliyaniya zdaniy na mikroklimaticheskiye usloviya dvorovogo prostranstva [Field Surveys of Residential Development on the Subject of Energy Impact of Buildings on Microclimatic Conditions of Courtyard Space] // Promyshlennoye i grazhdanskoye stroitel'stvo. 2017. No 5. P. 76-80.
8. Moskomarkhitektura. Proyekt planirovki territorii mikrorayonov 11-12, 21-22, 23-24, chasti mikrorayonov 29, 68 rayona Perovo goroda Moskvy [Moscow Architecture Committee. Draft planning of the territory of microdistricts 11-12, 21-22, 23-24, parts of microdistricts 29, 68 of the Perovo district of Moscow] URL:https://www.mos.ru/authority/documents/doc/44599220/ (available on 05.07.2022)
9. Metodika rascheta soprotivleniya teploperedachi ograzhdayushchey konstruktsii zdaniya s uchetom pokrytiya «mikrosfera-svyazuyushcheye» [Method for calculating the heat transfer resistance of the building envelope, taking into account the "microsphere-binder" coating] //URL:http://inoteck.net/metodika_rascheta_soprot (available on 10.07.2022)
10. **Berezin D.V.** Snizheniye peregreva na pridomovoy territorii putem ratsional'nogo razmeshcheniya zelenykh nasazhdeniy [Reduction of overheating in the local area by rational placement of green spaces] / D.V. Berezin // Vestnik YUUrGU. Seriya «Stroitel'stvo i arkhitektura». – 2013. – Vol. 13, No 2. – P. 16-21.
11. **Sandifer S., Givoni B.** Thermal effects of vines on wall temperatures- comparing laboratory and field collected data // https://www.sbse.org/sites/sbse/files/attachments/scholarships/Sandifer.pdf (data obrashcheniya 10.05.2022).
12. **Kozhayeva L.YU.** Morfotipy zastroyki v teorii i na praktike [Building morphotypes in theory and practice]. Arkhitekturnyy vestnik, No 4. - 2011. - P. 43-47.

СПИСОК ЛИТЕРАТУРЫ

1. **Теличенко В.И.** Реновация – создание современной городской среды // Вестник МГСУ. – 2020. – Т. 15. – № 1. – С. 11. – EDN JXFWEE.
2. **Мягков М.С., Губернский Ю.Д., Конова Л.И., Лицкевич В.К.** Город, архитектура, человек и климат //Архитектура-С. Москва 2007.
3. **Мягков М.С.** Нормирование и нормативы микроклиматических условий территорий городской застройки. Реализация требований биоклиматической комфортности в проектной подготовке строительства // https://marhi.ru/kafedra/techno/phisics/myagkov_climat.pdf (дата обращения 01.08.2022).
4. **Oke T.R.** The urban energy balance / T.R. Oke//Progress in Physical Geography 1988; 12; 471 DOI: 10.1177/030913338801200401

https://www.researchgate.net/publication/275590257_The_urban_energy_balance_Prog_Phys_Geogr (accessed 10.07.2022) (In Russian).
5. **Сумеркин Ю.А.** Расчет радиационной температуры окружающей среды городской застройки // Промышленное и гражданское строительство. 2020. № 4. С. 34–40. DOI: 10.33622/0869-7019.2020.04.34-40.
6. **Федорович Г.В.** Оценка тепловой обстановки с помощью шарового термометра // Безопасность и охрана труда. 2011. № 1. С. 68–71.
7. **Сумеркин Ю.А.** Натурное обследование жилой застройки на предмет энергетического влияния зданий на микроклиматические условия дворового пространства // Промышленное и гражданское строительство. 2017. № 5. С. 76-80.
8. Москомархитектура. Проект планировки территории микрорайонов 11-12, 21-22, 23-24, части микрорайонов 29, 68 района Перово города Москвы URL:https://www.mos.ru/authority/documents/doc/44599220/ (дата обращения: 05.07.2022)
9. Методика расчета сопротивления теплопередачи ограждающей конструкции здания с учетом покрытия «микросфера-связующее» //URL:http://inoteck.net/metodika_rascheta_soprot (дата обращения 10.07.2022)
10. **Березин Д.В.** Снижение перегрева на придомовой территории путем рационального размещения зеленых насаждений / Д.В. Березин // Вестник ЮУрГУ. Серия «Строительство и архитектура». – 2013. – Том. 13, №2. – С. 16-21.
11. **Sandifer S., Givoni B.** Thermal effects of vines on wall temperatures- comparing laboratory and field collected data // https://www.sbse.org/sites/sbse/files/attachments/scholarships/Sandifer.pdf (дата обращения 10.05.2022).
12. **Кожаева Л.Ю.** Морфотипы застройки в теории и на практике. Архитектурный вестник, № 4. – 2011. – С. 43–47.

Telichenko Valery Ivanovich, full member of Russian Academy of Architectural and Construction Sciences, Doctor of Technical Science, Professor of the Department of Structures and facilities for thermal and nuclear power generation of National Research Moscow State University of Civil Engineering (NRU MGSU), 129337, Moscow, Yaroslavskoye shosse, 26; ph.: +7(495) 781-80-07

Sumerkin Yurii Alekseevich, Deputy Head of the Production and Technical Department of Megastroy LLC, 111024, Moscow, st. Aviamotornaya, 50, building 2, ph.: +7(903)730-68-63, sumerk1n@mail.ru

Теличенко Валерий Иванович, академик Российской академии архитектуры и строительных наук (РААСН), доктор технических наук, профессор кафедры «Сооружения, объекты тепловой и атомной энергетики» Московского государственного строительного университета (МГСУ), 129337, г. Москва, Ярославское шоссе, д. 26; тел.: +7(495) 781-80-07

Сумеркин Юрий Алексеевич, зам. Нач. ПТО ООО «Мегастрой», 111024, г. Москва, ул. Авиамоторная, д. 50, стр. 2; тел.: +7(903)730-68-63, sumerk1n@mail.ru

DOI:10.22337/2587-9618-2022-18-3-54-64

ON THE QHASI CLASS AND ITS EXTENSION TO SOME GAUSSIAN SHEETS

***Charles El-Nouty* [1], *Darya V. Filatova* [2]**

[1] LAGA, UMR 7539, F-93430, Université Sorbonne Paris Nord, Paris, FRANCE
[2] National Research Moscow State University of Civil Engineering, Moscow, RUSSIA

Abstract. Introduced in 2018 the generalized bifractional Brownian motion is considered as an element of the quasi-helix with approximately stationary increment class of real centered Gaussian processes conditioning by parameters. This paper proves that the generalized bifractional Brownian motion is an element of the above mentioned class with no condition on parameters. The quasi-helix with approximately stationary increment class of real centered Gaussian processes is extended to two-dimensional processes as the fractional Brownian sheet, the sub-fractional Brownian sheet, and the bifractional Brownian sheet. This generalized presentation of the class of stochastic processes is used to augment the training samples for generative adversarial networks in computer vision problem.

Keywords: centered Gaussian process, generalized bifractional Brownian motion, Gaussian sheet, generative adversarial network, computer vision

О КВАЗИ КЛАССЕ И ЕГО РАСШИРЕНИИ К НЕКОТОРЫМ ГАУССОВЫМ ЛИСТАМ

***Шарль Эль-Нути* [1], *Дарья Филатова* [2]**

[1] ЛАГА, УМР 7539, Ф-93430, Университет Сорбонны Париж-Норд, Париж, ФРАНЦИЯ
[2] Национальный исследовательский Московский государственный строительный университет, Москва, РОССИЯ

Аннотация. Введенное в 2018 году обобщенное бифрактальное броуновское движение рассматривается как элемент квазиспирали класса действительных центрированных гауссовских процессов, обладающих приблизительно стационарными приращениями, обусловленных параметрами. В данной работе доказывается, что обобщенное бифракционное броуновское движение является элементом указанного выше класса без каких-либо условий на параметры. Свойство квазиспирали этого класса центрированных гауссовских процессов распространяется на двумерные процессы, такие как фрактальный броуновский лист, субфрактальный броуновский лист и бифрактальный броуновский лист. Это обобщенное представление класса процессов используется для расширения обучающих выборок для генеративно-состязательных сетей в задаче компьютерного зрения.

Ключевые слава: центрированный гауссовский процесс, обобщенное бифракционное броуновское движение, гауссовский листгенеративно-состязательная сеть, компьютерное зрение

1. INTRODUCTION

Trends in the development of information technology are changing the classical idea of how to solve many problems that arise in civil engineering. Accelerated analysis of large information flows of multivariate solutions from the concept of the project to the decommissioning moment for a certain construction object requires the use of artificial intelligence methods. It is clear that machine learning, deep learning, and reinforcement learning are becoming the leading information technologies. For example, the development of neural networks makes it possible to more accurately solve the problem of finding and classifying defects or pathologies hidden from the human eye on the surface of a structure, even at an early stage of the destruction process. In pursuit of the goal of increasing the reliability of the solutions obtained, the solution methodology itself is modified [1]. Popular in computer vision, convolutional neural networks very often use the so-called pseudo-samples for training, which result from generating data using various random noises [2]. This approach to training neural networks has led to the creation of generative adversarial networks (GANs) [3]. The main idea of the GAN is to compete with two neural networks in a zero-sum game, i.e. one network generates information and the other tries to please it. This competitive process must change over time to avoid overfitting the guessing network. When writing a scenario for generating pseudo data, it is necessary to use some universal multidimensional (even if two-dimensional) stochastic process or a class of processes that allows you to display reality as closely as possible - stationary or non-stationary dynamics of the phenomenon under study. The modern development of the theory of stochastic processes makes it possible to introduce a certain class of processes that can be successfully used to create a GAN, and as a result, to increase the reliability of solving computer vision problems.

In [4], a new class of centered Gaussian processes was introduced. More precisely, a centered Gaussian process $\{X(t), t \in I \subset \mathsf{R}\}$ belongs to the quasi-helix with approximately stationary increments (QHASI) class if it fulfills the five following assumptions:

- **A1**: $X(0) = 0$ with probability 1;
- **A2**: there exists $\lambda > 0$ such that X is self-similar with index λ;
- **A3**: there exist

$$0 < C_1 \le C_2 < +\infty;$$

such that $\forall\, (s,t) \in I^2$

$$C_1 \,|\, t-s\,|^{2\lambda} \le \mathsf{E}(X(t) - X(s))^2 \le C_2 \,|\, t-s\,|^{2\lambda};$$

- **A4**: there exists

$$C_3 \in [C_1, C_2]$$

such that $\forall\, (s,t) \in I^2$, $t \ge s$, $st \ne 0$, when $t - s \to 0$, $\mathsf{E}(X(t) - X(s))^2 \sim C_3\, (t-s)^{2\lambda}$,

- A5: there exists

$$C_4 \in [C_1, C_2]$$

such that $\forall\, t \in I$, $\mathsf{E}\, X(t)^2 = C_4 \,|\, t\,|^{2\lambda}$.

Let us make some comments about the assumptions. Assumptions (**A1**) and (**A5**) are done for sake of convenience. Then, assumption (**A2**) means that the process X is an attractive one. Finally, assumption (**A3**) means that the process X is a λ-quasi-helix in the sense of [5], whereas assumption (A4) means that the increments of X are approximately stationary for small increments, this notion having been introduced in [6]. The underlying idea of the QHASI class is to replace the stationary increments property by assumptions (**A3**) and (**A4**).

The QHASI class contains some famous Gaussian processes such that the fractional Brownian motion (fBM), the bifractional Brownian motion (bBM) and the sub-fractional Brownian motion (sfBM). The values of the associated constants $\left(\lambda, C_1, C_{2,} C_3, C_4\right)$ can be found in [4] for each of these processes. We refer on one hand to [6] for further information on the bBm and on the other hand to [7] for further information on the sfBm. Note also that the following processes are also elements of the QHASI class:

- the sub bifractional Brownian motion (sbBm) (see [8])
- the generalized fBM (gfBm) (see [9], [10])

In [10], the generalized bifractional Brownian motion (gbBm) $Y := Y_{\alpha,\beta,H,K}$, was introduced. It is defined as follows:

$$Y(t) := Y_{\alpha,\beta,H,K}(t) = \alpha\, B_{H,K}(t) + \beta\, B_{H,K}(-t), \quad t \ge 0,\ \alpha > 0,\ \beta > 0,$$

where $\{B_{H,K}(t), t \in \mathsf{R}\}$ is a bBm with indices $0 < H < 1$ and $0 < K \le 1$.

Set $\alpha(K)=\frac{1}{2^{(2-K)/2}}$, $0<K\le 1$. We insist on the fact that the process Y was already introduced for specific values of α, β, and K. More precisely, the sfBm corresponds to $Y_{\alpha(1),\alpha(1),H,1}$, the sbBm to $Y_{\alpha(K),\alpha(K),H,K}$ and the gfBm to $Y_{\alpha,\beta,H,1}$.
In [10], it was proved that the gbBm was an element of the QHASI class under some conditions on H and K. More precisely, the following result was established.

Theorem 1. *Assume that $2HK\le 1$. Then the gbBm is an element of the QHASI class, with*

- $\lambda = HK$,
- $C_1=(\alpha+\beta)^2-2^{2-K}\alpha\beta$,
- $C_2=2^{1-K}((\alpha+\beta)^2-2^{2HK}\alpha\beta)$,
- $C_3=2^{1-K}\left(\alpha^2+\beta^2\right)$,
- $C_4=\alpha^2+2(1-2^{2HK-K})\alpha\beta+\beta^2$.

■

The first aim of this paper is to show that the gbBm is an element of the QHASI class for any

$$(\alpha,\beta,H,K)\in]0,+\infty[\times]0,+\infty[\times]0,1[\times]0,1].$$

Our first result is stated in the following theorem.

Theorem 2. *Assume that $2HK>1$. Then the gbBm is an element of the QHASI class, with*

- $\lambda = HK$,
- $C_1=2(1-2^{2HK-1-K})(\alpha^2+\beta^2)$,
- $C_2=2^{1-K}(\alpha^2+\beta^2)$,
- $C_3=2^{1-K}\left(\alpha^2+\beta^2\right)$,
- $C_4=\alpha^2+2(1-2^{2HK-K})\alpha\beta+\beta^2$.

■

Let us make some comments on the above theorems. As it was already observed in [4], [8] and [12], the hyperbola $2HK=1$ plays a key role. It has also an influence on the values of the constants C_1 and C_2. Let focus our attention on two specific cases. First, when $\alpha=\beta=\alpha(K)=\frac{1}{2^{(2-K)/2}}$, theorem 2 generalizes proposition 1.1 in [8]. Next, when $K=1$ and $2H>1$, the values of the constant C_2 given in the above theorem and in [9] are similar, but the value of C_1 given in Theorem 2 is less precise than the value of C_1 given in [9]. It can be explained by the fact that, when $K=1$, direct computations are available.
The second aim of this paper is to answer to the following question: can we extend the QHASI class to two-dimensional processes? To this purpose, we introduce the following notation.

Let

$$\left\{X_1(s),s\ge 0\right\}$$

and

$$\left\{X_2(t),t\ge 0\right\}$$

be two elements of the QHASI class. For any $i\in\{1,2\}$, we denote by $\left(\lambda_i,C_{i1},C_{i2},C_{i3},C_{i4}\right)$ the associated constants. Set

$$\sigma_1^2\left(s_1,s_2\right)=\mathsf{E}\left(X_1(s_1)-X_1(s_2)\right)^2$$

and

$$\sigma_2^2\left(t_1,t_2\right)=\mathsf{E}\left(X_2(t_1)-X_2(t_2)\right)^2.$$

Set $u=(s,t)$ and $u_{ij}=(s_i,t_j)$, $1\le i,j\le 2$. We consider some Gaussian sheets $\left\{X(u),u\in\mathsf{R}^+\times\mathsf{R}^+\right\}$ such that

$$\mathsf{E}\left(X\left(u_{ij}\right)X\left(u_{i'j'}\right)\right)=\mathsf{E}\left(X_1\left(s_i\right)X_1\left(s_{i'}\right)\right)\times\mathsf{E}\left(X_2\left(t_j\right)X_2\left(t_{j'}\right)\right).$$

We can easily derive the variance of the process X. We have

$$\mathsf{E}\left(X(u)^2\right)=\mathsf{E}\left(X_1(s)^2\right)\times\mathsf{E}\left(X_2(t)^2\right)=C_{X4}s^{2\lambda_1}t^{2\lambda_2},$$

where $C_{X4} = C_{14} \times C_{24}$.

Note that when the process X_1 is a fBm with Hurst index $0 < H_1 < 1$ and the process X_2 is a fBm with Hurst index $0 < H_2 < 1$, the process X is a fractional Brownian sheet (fBS) with indexes H_1 and H_2. There is a huge literature on the fBs. We refer to [13] for further information on this process.
The rest of the paper is organized as follows. In section 2, we prove Theorem 2, whereas the properties of the two-dimensional process X are studied in section 3. In section 4, we focus our attention on specific sheets and illustrations for the computer vision problem related to the surface anomalies detection. Section 5 concludes the main results of this research.

2. PROOF OF THEOREM 2

Recall first that $1 < 2HK < 2$, and therefore $H > 1/2$ and $K > 1/2$. Note that the values of λ, C_2, C_3 and C_4 were already given in [CEN18]. The proof of the theorem will be divided into four steps.

Step 1. Let us determine the value of the constant C_1. Combining proposition 10 with lemma 12 presented in [10], we have for $t \ge s \ge 0$

$$\begin{aligned}\sigma^2(s,t) &:= \sigma^2_{\alpha,\beta,H,K}(s,t) \\ &= \mathsf{E}\left(\left(Y_{\alpha,\beta,H,K}(t) - Y_{\alpha,\beta,H,K}(s)\right)^2\right) \\ &= 2^{1-K}\left(\alpha^2+\beta^2\right)(t-s)^{2HK} \\ &\quad -(\alpha+\beta)^2 F_{H,K}(s,t) \\ &\quad -2^{1-K+2HK}\alpha\beta\left|F_{1/2,2HK}(s,t)\right|\end{aligned}$$

where

$$F_{H,K}(s,t) = 2\left(\frac{t^{2H}+s^{2H}}{2}\right)^K - t^{2HK} - s^{2HK} \ge 0,$$

$$F_{1/2,2HK}(s,t) = 2\left(\frac{t+s}{2}\right)^K - t^{2HK} - s^{2HK} \le 0.$$

Let us establish a suitable upper bound of

$$(\alpha+\beta)^2 F_{H,K}(s,t) + 2^{1-K+2HK}\alpha\beta\left|F_{1/2,2HK}(s,t)\right|.$$

Recall that

$$2\,\alpha\,\beta \le \alpha^2+\beta^2 \le (\alpha+\beta)^2 \le 2\,(\alpha^2+\beta^2).$$

Thus, we have

$$\begin{aligned}&(\alpha+\beta)^2 F_{H,K}(s,t) + 2^{1-K+2HK}\alpha\,\beta\left|F_{1/2,2HK}(s,t)\right| \\ &\quad\le 2\left(\alpha^2+\beta^2\right)\Big(F_{H,K}(s,t) \\ &\qquad +2^{2HK-1-K}\left|F_{1/2,2HK}(s,t)\right|\Big)\end{aligned}$$

Note that $2HK-1-K = (2H-1)K-1 < 0$.
Next, combining inequality (2.4) in [8] with straight computations, we get

$$\begin{aligned}&F_{H,K}(s,t) + 2^{2HK-1-K}\left|F_{1/2,2HK}(s,t)\right| \\ &\quad= \tfrac{1}{2^K}\Big(2\left(t^{2H}+s^{2H}\right)^K \\ &\qquad -\left(2^K-2^{2HK-1}\right)\left(t^{2HK}+s^{2HK}\right)-(t+s)^{2HK}\Big) \\ &\quad\le \tfrac{1}{2^K}\left((t-s)^{2HK}-\left(2^K-2^{2HK-1}\right)(t-s)^{2HK}\right).\end{aligned}$$

Hence, we get

$$\begin{aligned}\sigma^2(s,t) &\ge 2^{1-K}\left(\alpha^2+\beta^2\right)(t-s)^{2HK} - 2\left(\alpha^2+\beta^2\right) \\ &\quad \tfrac{1}{2^K}\left((t-s)^{2HK}-\left(2^K-2^{2HK-1}\right)(t-s)^{2HK}\right) \\ &= 2\left(1-2^{2HK-1-K}\right)\left(\alpha^2+\beta^2\right)(t-s)^{2HK}.\end{aligned}$$

The constant C_1 is now determined.

Step 2. The aim of this step is to show that $C_1 \le C_3 = C_2$. Since $1 < 2HK < 2$ and $0 < K \le 1$, we have

$$2^K \le 2 \le 1 + 2^{2HK-1},$$

and therefore

$$2 - 2^{2HK-K} \le 2^{1-K}.$$

The last inequality can be rewritten as follows

$$2\,(1 - 2^{2HK-K-1}) \le 2^{1-K}.$$

Hence $C_1 \le C_3 = C_2$.

Step 3. Let us show that $C_4 \le C_2 = C_3$. To determine the sign of $C_3 - C_4$, it suffices to study the function $T_{H,K}$ defined by

$$T_{H,K}(x) = (2^{1-K} - 1)x^2 + 2(2^{2HK-K} - 1)x + 2^{1-K} - 1, \quad x \in \mathrm{R}.$$

We will distinguish the following two cases.

Case 1. $K = 1$ and $2H > 1$.
We have $T_{H,1}(x) = 2(2^{2H-1} - 1)x$. Keep in mind that $\alpha > 0$ and $\beta > 0$. Once $x > 0$, it follows that $T_{H,1}(x) > 0$. Thenceforward, $C_3 > C_4$.

Case 2. $K < 1$ and $1 < 2HK$.
The function $T_{H,K}$ has a unique minimum at the point

$$x_0 = -\frac{2^{2HK-K} - 1}{2^{1-K} - 1}.$$

Since

$$2HK - K > 0,$$

we obviously have $x_0 < 0$. Moreover, recall that, when $x \le x_0$, $T_{H,K}$ is a non-increasing function, otherwise a non-decreasing one. Note that

$$T_{H,K}(0) = 2^{1-K} - 1 > 0.$$

Thus we have $T_{H,K}(x) > 0$ for any $x > 0$, and therefore $C_3 > C_4$.

Step 4. Let us show that $C_1 \le C_4$. It suffices to verify

$$2\left(1 - 2^{2HK-1-K}\right)\left(\alpha^2 + \beta^2\right) \le \alpha^2 + 2\left(1 - 2^{2HK-K}\right)\alpha\beta + \beta^2.$$

This inequality can be rewritten in the form

$$\left(1 - 2^{2HK-K}\right)\left(\alpha^2 + \beta^2\right) \le 2\left(1 - 2^{2HK-K}\right)\alpha\beta,$$

which is equivalent to

$$\left(1 - 2^{2HK-K}\right)\left(\alpha - \beta\right)^2 \le 0.$$

Since $2HK - K > 0$, $C_1 \le C_4$.
This completes the proof of the theorem.

3. PROPERTIES OF THE PROCESS X

Let us state some basic properties of the process X

Proposition 3. *We have*

- $X(\cdot,\cdot)$ *is a Gaussian process,*
- $X(s,0) = X(0,t) = 0$,
- *for any* $s_0 > 0$, *the one-dimensional process* $\left\{s_0^{-\lambda_1} X\left(s_0, t\right), t \ge 0\right\}$ *is a* $\sqrt{C_{14}} \times X_2$ *process,*
- *for any* $t_0 > 0$, *the one-dimensional process* $\left\{t_0^{-\lambda_2} X\left(s, t_0\right), s \ge 0\right\}$ *is a* $\sqrt{C_{24}} \times X_1$ *process.*
-

Proof. The first two points are obvious. To prove the third point, it suffices to compute

$$\mathrm{E}\left(s_0^{-\lambda_1} X\left(s_0, t_1\right) s_0^{-\lambda_1} X\left(s_0, t_2\right)\right).$$

We have

$$\begin{aligned}
&\mathsf{E}\left(s_0^{-\lambda_1}X(s_0,t_1)s_0^{-\lambda_1}X(s_0,t_2)\right)\\
&\quad=s_0^{-2\lambda_1}\mathsf{E}\left(X_1(s_0)X_1(s_0)\right)\times\mathsf{E}\left(X_2(t_1)X_2(t_2)\right)\\
&\quad=s_0^{-2\lambda_1}C_{14}s_0^{2\lambda_1}\times\mathsf{E}\left(X_2(t_1)X_2(t_2)\right)\\
&\quad=C_{14}\times\mathsf{E}\left(X_2(t_1)X_2(t_2)\right).
\end{aligned}$$

We omit the proof of the last point. ■

Keep in mind that the flavor of the QHASI class consists in the quasi-helix property in the sense of Kahane [2] and its approximately stationary one. To extend these concepts to two-dimensional processes, let us recall that the increment Δ of X between the points $u_{11}=(s_1,t_1)$ and $u_{22}=(s_2,t_2)$ is defined as follows

$$\Delta=X(u_{11})+X(u_{22})-X(u_{12})-X(u_{21}),$$

where $u_{12}=(s_1,t_2)$ and $u_{21}=(s_2,t_1)$.
Set

$$\mathsf{E}\Delta^2=\sigma^2(u_{11},u_{22}).$$

We can establish the following essential proposition.

Proposition 4. *We have*

$$\sigma^2(u_{11},u_{22})=\sigma_1^2(s_1,s_2)\times\sigma_2^2(t_1,t_2).$$

Proof. As far as we know, the above proposition has not been written yet. Therefore we will prove it. Direct computations yield

$$\begin{aligned}
&\sigma^2(u_{11},u_{22})=\\
&\left(\mathsf{E}X_1^2(s_1)+\mathsf{E}X_1^2(s_2)\right)\times\left(\mathsf{E}X_2^2(t_1)+\mathsf{E}X_2^2(t_2)\right)\\
&+2\times\mathsf{E}\left(X_1(s_1)X_1(s_2)\right)\times\mathsf{E}\left(X_2(t_1)X_2(t_2)\right)\\
&-\left(\mathsf{E}X_1^2(s_1)+\mathsf{E}X_1^2(s_2)\right)\times\mathsf{E}\left(X_2(t_1)X_2(t_2)\right)\\
&-\left(\mathsf{E}X_2^2(t_1)+\mathsf{E}X_2^2(t_2)\right)\times\mathsf{E}\left(X_1(s_1)X_1(s_2)\right).
\end{aligned}$$

Since

$$\begin{aligned}
\sigma_1^2(s_1,s_2)=\mathsf{E}X_1^2(s_1)-2\,\mathsf{E}\left(X_1(s_1)X_1(s_2)\right)\\
+\mathsf{E}X_1^2(s_2)
\end{aligned}$$

and

$$\begin{aligned}
\sigma_2^2(t_1,t_2)=\mathsf{E}X_2^2(t_1)-2\,\mathsf{E}\left(X_2(t_1)X_2(t_2)\right)\\
+\mathsf{E}X_2^2(t_2),
\end{aligned}$$

we have

$$\begin{aligned}
&\sigma^2(u_{11},u_{22})=\\
&\left(\mathsf{E}X_1^2(s_1)+\mathsf{E}X_1^2(s_2)\right)\left(\mathsf{E}X_2^2(t_1)+\mathsf{E}X_2^2(t_2)\right)\\
&-2\times\sigma_1^2(s_1,s_2)\mathsf{E}\left(X_2(t_1)X_2(t_2)\right)\\
&-\left(\mathsf{E}X_2^2(t_1)+\mathsf{E}X_2^2(t_2)\right)\mathsf{E}\left(X_1(s_1)X_1(s_2)\right)\\
&=-2\times\sigma_1^2(s_1,s_2)\times\mathsf{E}\left(X_2(t_1)X_2(t_2)\right)\\
&\quad+\left(\mathsf{E}X_2^2(t_1)+\mathsf{E}X_2^2(t_2)\right)\\
&\quad\times\left(\mathsf{E}X_1^2(s_1)+\mathsf{E}X_1^2(s_2)-2\mathsf{E}\left(X_1(s_1)X_1(s_2)\right)\right)\\
&=-2\times\sigma_1^2(s_1,s_2)\times\mathsf{E}\left(X_2(t_1)X_2(t_2)\right)\\
&\quad+\left(\mathsf{E}X_2^2(t_1)+\mathsf{E}X_2^2(t_2)\right)\times\sigma_1^2(s_1,s_2)\\
&=\sigma_1^2(s_1,s_2)\times\left(\mathsf{E}X_2^2(t_1)+\mathsf{E}X_2^2(t_2)\right.\\
&\quad\left.-2\times\mathsf{E}\left(X_2(t_1)X_2(t_2)\right)\right)\\
&=\sigma_1^2(s_1,s_2)\times\sigma_2^2(t_1,t_2).
\end{aligned}$$

The proof of the proposition is now complete. ■

Combining the above proposition with the fact that the processes X_1 and X_2 are elements of the QHASI class, we get the following results.

Proposition 5. *We have*

$$\begin{aligned}
C_{X1}\left|s_1-s_2\right|^{2\lambda_1}\left|t_1-t_2\right|^{2\lambda_2}\le\sigma^2(u_{11},u_{22})\\
\le C_{X2}\left|s_1-s_2\right|^{2\lambda_1}\left|t_1-t_2\right|^{2\lambda_2},
\end{aligned}$$

where $C_{X1}=C_{11}\times C_{21}$ *and* $C_{X2}=C_{12}\times C_{22}$.

Proposition 6. *When* $s_2 - s_1 \to 0$, $s_2 \geq s_1 > 0$, *and* $t_2 - t_1 \to 0$, $t_2 \geq t_1 > 0$, *we have*

$$\sigma^2(u_{11}, u_{22}) \sim C_{X3}(s_2 - s_1)^{2\lambda_1}(t_2 - t_1)^{2\lambda_2},$$

where $C_{X3} = C_{13} \times C_{23}$.

It is obvious that $C_{X1} \leq C_{X3} \leq C_{X2}$ and $C_{X1} \leq C_{X4} \leq C_{X2}$. Roughly speaking, we can say that the process X is a quasi-helix in the sense of Kahane [2] and has approximately stationary increments. We can associate to X the six constants $(\lambda_1, \lambda_2, C_{X1}, C_{X2,} C_{X3}, C_{X4})$. Thus, we answer to the question stated in the introduction. Indeed we are able, on one hand to extend the definition of the QHASI class to two dimensional processes, and on the other hand to create new Gaussian sheets.

4. SOME SPECIFIC SHEETS

4.1. The fractional Brownian sheet

Let X_1 be a fBm with Hurst index $0 < H_1 < 1$ and X_2 be a fBm with Hurst index $0 < H_2 < 1$. As already mentioned, the process X constructed as described earlier is the fBs. Note that its six associated constants are $(H_1, H_2, 1,1,1,1)$. It implies that calculi are quite convenient for the fBs. This partially explains its popularity.

4.2. The subfractional Brownian sheet

Let X_1 be a sfBm with Hurst index $0 < H_1 < 1$ and X_2 be a sfBm with Hurst index $0 < H_2 < 1$. We can construct the process X. To determine the six associated constants, we have to consider the four following cases:

- when $H_1 < \frac{1}{2}$ and $H_2 < \frac{1}{2}$, the constants are
$$\left(H_1, H_2, 1, \left(2 - 2^{2H_1 - 1}\right)\left(2 - 2^{2H_2 - 1}\right),\right.$$
$$\left. 1, \left(2 - 2^{2H_1 - 1}\right)\left(2 - 2^{2H_2 - 1}\right)\right);$$
- when $H_1 < \frac{1}{2}$ and $H_2 \geq \frac{1}{2}$, the constants are
$$\left(H_1, H_2, 2 - 2^{2H_2 - 1}, 2 - 2^{2H_1 - 1},\right.$$
$$\left. 1, \left(2 - 2^{2H_1 - 1}\right)\left(2 - 2^{2H_2 - 1}\right)\right);$$
- when $H_1 \geq \frac{1}{2}$ and $H_2 < \frac{1}{2}$, the constants are
$$\left(H_1, H_2, 2 - 2^{2H_1 - 1}, 2 - 2^{2H_2 - 1},\right.$$
$$\left. 1, \left(2 - 2^{2H_1 - 1}\right)\left(2 - 2^{2H_2 - 1}\right)\right);$$
- when $H_1 \geq \frac{1}{2}$ and $H_2 \geq \frac{1}{2}$, the constants are
$$\left(H_1, H_2, \left(2 - 2^{2H_1 - 1}\right)\left(2 - 2^{2H_2 - 1}\right),\right.$$
$$\left. 1, 1, \left(2 - 2^{2H_1 - 1}\right)\left(2 - 2^{2H_2 - 1}\right)\right).$$

4.3. The bifractional Brownian sheet

Let X_1 be a bBm with Hurst indices $0 < H_1 < 1$ and $0 < K_1 \leq 1$ as well as X_2 be a bBm with Hurst indices $0 < H_2 < 1$ and $0 < K_1 \leq 1$. We can construct the process X. Its six associated constants are

$$\left(H_1 K_1, H_2 K_2, 2^{-K_1 - K_2}, 2^{2 - K_1 - K_2}, 2^{2 - K_1 - K_2}, 1\right).$$

4.4. Other possible sheets

Following the same ideas, we can construct the sub-bifractional Brownian sheet, the generalized fractional Brownian sheet and the generalized bifractional sheet. There is no difficulty to give the six associated constants. We can also mix the different elements of the QHASI class in order to create new sheets. For example, let X_1 be a fBm with Hurst index $0 < H_1 < 1$ and X_2 be an element of the QHASI class with the associated constants $(\lambda, C_1, C_{2,} C_3, C_4)$. We can construct the process X using six associated constants

$$\left(H_1, \lambda, C_1, C_{2,} C_3, C_4\right)$$

In some sense, the influence of the fBm vanishes. This is not really surprising since the fBm has stationary increments.

4.5. Illustrations

Now we give several illustrations of an image generation, using the fractional Brownian sheet (see Fig. 1) and the subfractional Brownian sheet (see Fig.3, Fig. 5, Fig. 7, and Fig. 9). As it is possible to notice these images are similar with the pictures which one can obtain by thermal camera, say for some heated surface. Since our goal is only to augment quantity of training samples, we just suppose that minimal values of the generated process correspond to "black" pixels and maximal values corresponds to "white" pixels. Setting "red" color as a normal temperature for the heated surface, it is possible to see "overheated" areas. To make the corrupted areas more visible we apply color-based segmentation using k-means clustering (see Fig. 2, Fig. 4, Fig. 6, Fig. 8, and Fig. 10).

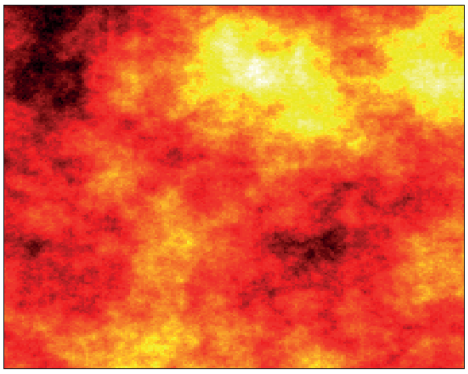

Figure 1. Test 1 - the fractional Brownian sheet with parameters $(0.75, 0.75, 1, 1, 1, 1)$

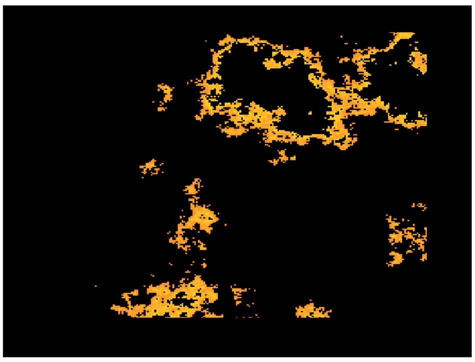

Figure 2. Segmented areas for Test 1

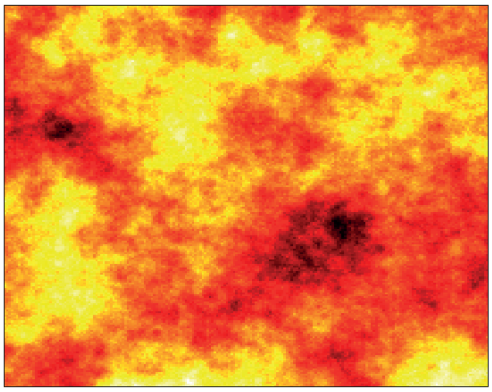

Figure 3. Test 2 – the subfractional Brownian sheet with parameters $(0.75, 0.75, 1, 0.34, 1, 0.34)$

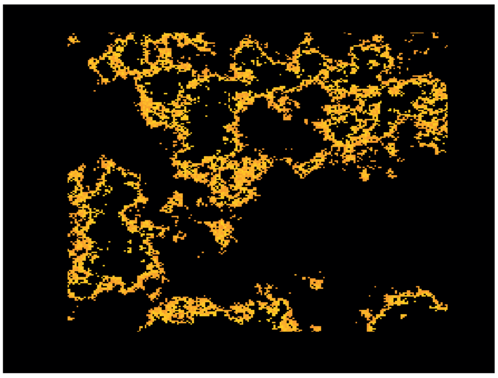

Figure 4. Segmented areas for Test 2

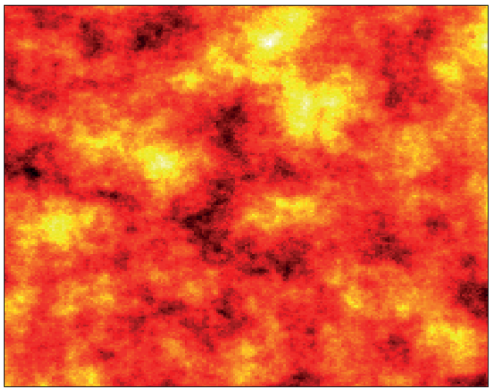

Figure 5. Test 3 – the subfractional Brownian sheet with parameters $(0.75, 0.25, 1, 0.76, 1, 0.76)$

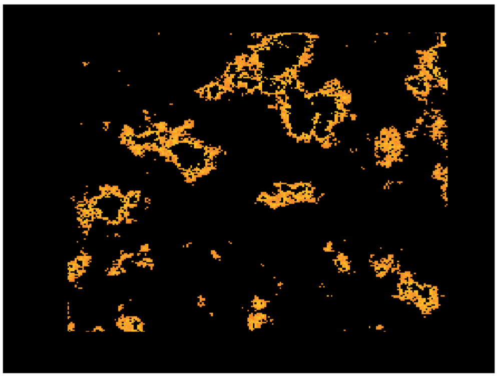

Figure 6. Segmented areas for Test 3

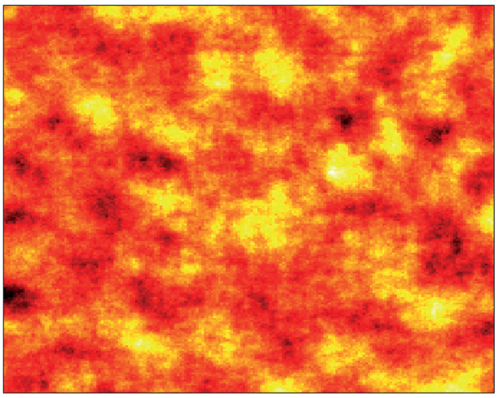

Figure 7. Test 4 – the subfractional Brownian sheet with parameters $(0.25, 0.75, 1, 0.76, 1, 0.76)$

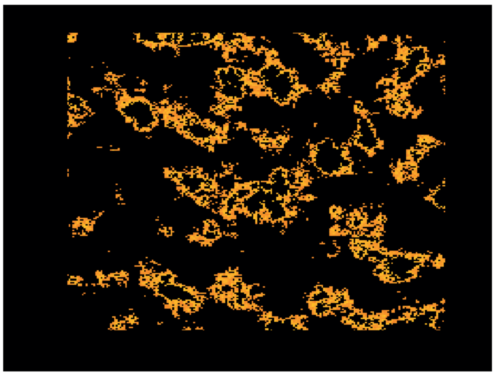

Figure 8. Segmented areas for Test 4

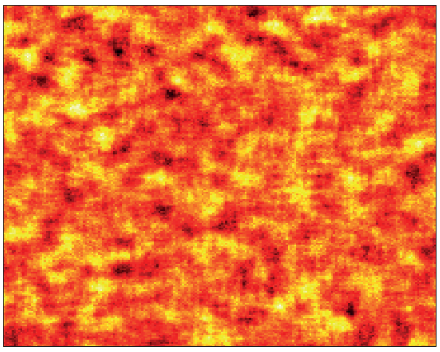

Figure 9. Test 5 – the subfractional Brownian sheet with parameters $(0.25, 0.25, 1, 1.67, 1, 1.67)$

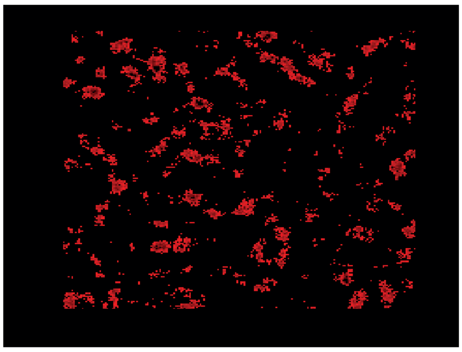

Figure 10. Segmented areas for Test 5

It is obvious that only by changing the parameters of the stochastic process we get different corruption processes for the surface. Moreover, any repetition of the generation even with the same parameters gives new image preserving the main tendency of the corruption process.

5. CONCLUDING REMARKS

We have completed previous results by proving that the gbBm is an element of the QHASI class with no condition on the parameters. When $2HK > 1$, the constant C_1 has been determined. Then we have proposed a construction of several Gaussian sheets based on the QHASI class. We have studied the main properties of these sheets such that the self-similarity one, the quasi-helix one and the approximately stationary one. The QHASI

class is therefore extended to two dimensional processes. The associated constants are determined. We have also focused our attention on new specific sheets, the well-known fractional Brownian one becoming a particular case.
We insist on the fact that a natural extension can be done for three dimensional processes. In this case, the increment Δ of X between the points

$$u_{111} = (x_1, y_1, z_1)$$

and

$$u_{222} = (x_2, y_2, z_2)$$

is defined as follows

$$\begin{aligned}\Delta = X\left(u_{222}\right) + X\left(u_{112}\right) + X\left(u_{121}\right) + X\left(u_{211}\right) \\ -X\left(u_{122}\right) - X\left(u_{212}\right) - X\left(u_{221}\right) - X\left(u_{111}\right),\end{aligned}$$

where

$$u_{ijk} = (x_i, y_j, z_k), 1 \le i, j, k \le 2$$

are points in R^3. We can also determine the seven associated constants: the first three ones deal with self-similarity whereas the last ones deal with the constants C_i, $1 \le i \le 4$. Following the same lines, we can build n dimensional processes. However, the increment Δ has no simple expression. This is why we omit this extension.
The numerical illustrations were shown for the Gaussian sheets. This generalized presentation of the class of stochastic processes was used to augment the training samples for generative adversarial networks in computer vision problem. The same approach can be used in R^3, which permits solve many applied problems devoted to default diagnostics by computer vision.

REFERENCES

1. **FilatovaD., El-Nouty Ch.** Waterproofing membranes reliability analysis by embedded and high-throughput deep learning algorithm [In:] van Gulijk, C., Zaitseva, E. (eds) Reliability Engineering and Computational Intelligence, Studies in Computational Intelligence, 2021, pp. 245 – 260, Springer.
2. **Filatova D., El-Nouty Ch., Punko U.**, High-throughput deep learning algorithm for diagnosis and defects classification of waterproofing membranes // Int. J. Comput. Civ. Struct. Eng., 2020, Vol. 16(2), pp. 26–38.
3. **Taif K., Ugail H., Mehmood I.** Cast Shadow Generation Using Generative Adversarial Networks. // [In:] Computational Science – ICCS 2020. ICCS 2020. Lecture Notes in Computer Science, Vol. 12141, 2020, pp. 481–495 Springer.
4. **El-Nouty C.**, On approximately stationary Gaussian processes // International Journal for Computational Civil and Structural Engineering, 2015, Vol. 11, pp. 15–26.
5. **Kahane J-P.**, Some random series of functions. 2nd ed. Cambridge studies in advanced mathematics, 1985, Cambridge University Press.
6. **Houdré C., Villa J.**, An example of infinite dimensional quasi-helix. In: Stochastics models, ed. by J.M. Gonzales-Barrios et al., Comtemp. Math. 336, Providence RI, 2003, pp. 195-201.
7. **Bojdecki T., Gorostiza L.G., Talarczyk A.**, Sub-fractional Brownian motion and its relation to occupation times // Statist. Probab. Lett., 2004, Vol. 69, pp. 405–419.
8. **El-Nouty C., Journé J-L.**, The sub-bifractional Brownian motion // Studia Sci. Math. Hungar., 2013, Vol. 50, pp. 67–121.
9. **Zili M.**, Generalized fractional Brownian motion // Modern Stochastics: Theory and Applications, 2017, Vol. 4, pp. 15–24.
10. **El-Nouty C.**, The generalized bifractional Brownian motion // International Journal for Computational Civil and Structural Engineering, 2 018, Vol. 14, pp. 81–89.
11. **El-Nouty C.**, The increments of a bifractional Brownian motion // *Studia Sci. Math. Hungar.*, 2009, Vol. 46, pp. 449–478.
12. **Russo F., Tudor C.A.**, On bifractional Brownian motion // Stochastic Process. Appl., 2006, Vol. 116, pp. 830–856.

13. **Li W.V., Shao Q.M.,** Gaussian Processes: Inequalities, Small Ball Probabilities and Applications, Stochastic Processes: Theory and Methods, Handbook of Statistics, 19, 2001, AMS.

СПИСОК ЛИТЕРАТУРЫ

1. **FilatovaD., El-Nouty Ch.** Waterproofing membranes reliability analysis by embedded and high-throughput deep learning algorithm [In:] van Gulijk, C., Zaitseva, E. (eds) Reliability Engineering and Computational Intelligence, Studies in Computational Intelligence, 2021, pp. 245 – 260, Springer.
2. **Filatova D., El-Nouty Ch., Punko U.**, High-throughput deep learning algorithm for diagnosis and defects classification of waterproofing membranes // Int. J. Comput. Civ. Struct. Eng., 2020, Vol. 16(2), pp. 26–38.
3. **Taif K., Ugail H., Mehmood I.** Cast Shadow Generation Using Generative Adversarial Networks. // [In:] Computational Science – ICCS 2020. ICCS 2020. Lecture Notes in Computer Science, Vol. 12141, 2020, pp. 481–495 Springer.
4. **El-Nouty C.**, On approximately stationary Gaussian processes // International Journal for Computational Civil and Structural Engineering, 2015, Vol. 11, pp. 15–26.
5. **Kahane J-P.**, Some random series of functions. 2nd ed. Cambridge studies in advanced mathematics, 1985, Cambridge University Press.
6. **Houdré C., Villa J.**, An example of infinite dimensional quasi-helix. In: Stochastics models, ed. by J.M. Gonzales-Barrios et al., Comtemp. Math. 336, Providence RI, 2003, pp. 195-201.
7. **Bojdecki T., Gorostiza L.G., Talarczyk A.**, Sub-fractional Brownian motion and its relation to occupation times // Statist. Probab. Lett., 2004, Vol. 69, pp. 405–419.
8. **El-Nouty C., Journé J-L.**, The sub-bifractional Brownian motion // Studia Sci. Math. Hungar., 2013, Vol. 50, pp. 67–121.
9. **Zili M.**, Generalized fractional Brownian motion // Modern Stochastics: Theory and Applications, 2017, Vol. 4, pp. 15–24.
10. **El-Nouty C.**, The generalized bifractional Brownian motion // International Journal for Computational Civil and Structural Engineering, 2 018, Vol. 14, pp. 81–89.
11. **El-Nouty C.**, The increments of a bifractional Brownian motion // *Studia Sci. Math. Hungar.*, 2009, Vol. 46, pp. 449–478.
12. **Russo F., Tudor C.A.**, On bifractional Brownian motion // Stochastic Process. Appl., 2006, Vol. 116, pp. 830–856.
13. **Li W.V., Shao Q.M.,** Gaussian Processes: Inequalities, Small Ball Probabilities and Applications, Stochastic Processes: Theory and Methods, Handbook of Statistics, 19, 2001, AMS.

Professor, Dr. hab. *Charles El-Nouty* works at LAGA, Université Sorbonne Paris Nord; 99 avenue J-B Clément 93430 Villetaneuse ; E-mail: elnouty@math.univ-paris13.fr, orcid.org/ /0000-0002-2321-1041

Professor, Dr. hab. *Darya Filatova* works at National Research Moscow State University of Civil Engineering, Moscow, RUSSIA, and CHART EPHE, 4-14 Rue Ferrus, 75014 Paris, France; E-mail: dvfilatova@mgsu.ru; orcid.org/0000-0001-9434-7993.

Шарль Эль-Нути – профессор, доктор физико-математических наук работает в лаборатории ЛАГА, Университет Сорбонна Париж Север; авеню Ж.-Б. Кленанта, д. 99, 94340 Вильтанез, Франция; E-mail: elnouty@math.univ-paris13.fr, orcid.org/0000-0002-2321-1041

Филатова Дарья, профессор, доктор физико-математических наук работает в Национальном исследовательском Московском государственном строительном университете, Москва, РОССИЯ, и в лаборатории Человеческого и искусственного интеллекта Практическая Школа Высших Исследований, 4–14 ул. Ферруса, 75014 Париж, Франция; E-mail: dvfilatova@mgsu.ru; orcid.org/0000-0001-9434-7993.

DOI:10.22337/2587-9618-2022-18-3-65-77

FINITE ELEMENT ANALYSIS FOR THIN-WALLED MEMBER SUBJECTED TO COMBINED LOADING

Vera V. Galishnikova [1]***, Tesfaldet H. Gebre*** [2]

[1] National Research Moscow State University of Civil Engineering, Moscow, RUSSIA
[2] Peoples' Friendship University of Russia (RUDN), Moscow, RUSSIA

Abstract. Thin-walled structures are widely used in various structural engineering applications due to their advantage of high bearing strength when compared to self-weight and used in a complex loading situation where subjected to combined loadings. When a thin-walled section is subjected to a combined load with restrained torsion, they are ineffective at resisting, resulting in a reduction in beam capacity due to torsion and additional warping stresses. A finite element calculation can be used to analyze a 3D bar of thin-walled structural sections. Different commercial software and studies commonly consider six degrees of freedom at each node of a member for a space frame without considering the effect of warping restraint at the member's ends. This paper presents a finite element calculation for thin-walled sections with restrained torsion using the 14x14 member stiffness matrix, which includes warping as an additional degree of freedom and is commonly used for open thin-walled sections. In this study, we considered two different methods for including the additional degree of freedom for the stiffness matrix, which are very close to each other for small values of characteristics number.

Keywords: Thin-walled structures, Finite element analysis, non-uniform warping, open section, stiffness matrix, restrained torsion

КОНЕЧНО-ЭЛЕМЕНТНЫЙ АНАЛИЗ ТОНКОСТЕННЫХ ЭЛЕМЕНТОВ ПОД ДЕЙСТВИЕМ КОМБИНИРОВАННЫХ НАГРУЗОК

В.В. Галишникова [1]***, Т.Х. Гебре*** [2]

[1] Национальный исследовательский московский государственный строительный университет, Москва, РОССИЯ
[2] Российский университет дружбы народов, Москва, РОССИЯ

Аннотация: Тонкостенные конструкции широко используются в различных областях проектирования конструкций благодаря своему преимуществу высокой несущей прочности по сравнению с собственным весом и используются в сложной ситуации нагрузки, когда подвергаются комбинированным нагрузкам. Когда тонкостенные секции подвергаются комбинированной нагрузке со сдержанным торсионом, они неэффективны при сопротивлении, что приводит к снижению пропускной способности балки из-за торсионных и дополнительных деформационных напряжений. Расчет конечных элементов может быть использован для анализа 3D-стержня тонкостенных структурных секций. Различные коммерческие программы и исследования обычно рассматривают шесть степеней свободы в каждом узле члена для пространственной рамки без учета эффекта деформации сдерживания на концах элемента. В данной работе представлен расчет конечных элементов для тонкостенных секций с ограниченным кручением с использованием матрицы жесткости элементов 14x14, которая включает деформацию в качестве дополнительной степени свободы и обычно используется для открытых тонкостенных секций. В данном исследовании мы рассмотрели два различных метода включения дополнительной степени свободы для матрицы жесткости, которые очень близки друг к другу для малых значений числа характеристик.

Ключевые слова: тонкостенные структуры, конечно-элементный анализ, неравномерное деформация, открытое сечение, матрица жесткости, сдержанный кручение

1. INTRODUCTION

Steel members are now manufactured as thin-wall sections because of their high strength, highly flexible, ductility, quick construction, and effective space partitioning, and they are widely used in various engineering structures. Thin-walled beams are those that are primarily prone to bending. When a thin-walled section is subjected to a combined load, it is ineffective at resisting, resulting in a reduction in the beam's capacity. The behavior is poorly described by elementary formulations that reduce the mechanical components to stretching, bending, and uniform torsion (i.e., the simplest case of a uniform distribution of cross-sectional warping along the beam axis [1-2]. Warping effects occur primarily at the points of action of concentrated torsional moments (except at free end support of beam) and at sections with free-warping restrictions, and they are accounted for by an additional degree of freedom at each nodal point in the form of the first derivative of the angle of twist of the beam's cross-section [3-5].

The analysis for extension, bending and flexure is rather straight-forward, but the analysis for the coupled deformations of torsion, warping and distortion poses a major challenge[6]. Currently, most design specifications do not provide clear guidance for combined bending and torsion design and the need exists for a simple design equation. The variation of the displacement over a section of a member is expressed with a common function for stretching, torsion and bending[7-10]. I-shaped steel beams are widely used as structural elements because of their flexural efficiency about the strong axis. It considers the cross section as completely rigid in its own plane, and the effect of shearing deformations is neglected[11]. The solutions for thin-walled section with nonuniform torsion were developed as initial works and also there are studies considered to be as a design aids for simple cases[12-13]. This is limited for a slender beam and the shear deformation in middle surface is negligible but for short-deep beam and closed thin-walled beams, the shear deformation should be considered[4,14]. However, in many applications beams are eccentrically loaded and as a result experience torsional loads in combination with bending. The importance of restrained torsion of thin-walled section has grown significantly as the deformations and stresses caused by torsion affects the behavior of the structures with open as well as closed section[15-16]. Like all open sections, I-shaped steel beams are very inefficient at resisting torsion and the interaction effects due to torsion acting in combination with bending can significantly reduce the capacity of the beam.

Many design methods have been developed to deal with combined bending and torsion, but none have been universally adopted by design standards. In the past decades, many relevant researches have been conducted and different commercial software commonly consider six degrees of freedom at each node of a member for a space frame without considering the effect of warping restraint at the ends of the member[9][17-18]. A finite element model is investigated based on a mixed variational formulation and numerical method of designing thin-walled bar systems using various theories and formulated matrices to provide an explicit way to calculate internal forces and stresses in thin-walled bar systems [19-22]. The bending and torsion behavior of cold-formed steel bars was studied experimentally based on the strengths of unbraced cold-formed steel channel beams loaded eccentrically [23-24]. Modern software packages for structural analysis use finite element types which consider up to six degrees of freedom at the structural nodes, which corresponds to the linear and angular displacements in these nodes as for the rigid bodies[25]. Moreover, various studies commonly consider with two degrees of freedom at each node of a member without considering the effect of warping restraint at node [26-27]. The warping part of the first derivative of the twist angle has been considered as the additional degree of freedom in each node at the element ends which can be regarded as part of the twist angle curvature caused by the warping moment [17][27][30]. Numerous studies developed the 14x14 member stiffness matrix including warping as an additional degree of freedom and commonly with open thin-walled section [18][25][28-29].

In this paper, a 3D frame element stiffness matrix will be presented which is more convenient for advanced structural analysis of 3D beam structures. The structures are analyzed or designed by using only the effect of Saint Venant torsion resistance thus the analysis may ignore the torsion part in the members and the design may be underestimated. To overcome this inaccuracy, several researchers tried to develop stiffness matrix with seven degrees of freedom at each node of a member for a space frame. This additional stiffness matrix considers the warping degree of freedom at the ends of the member with thin-walled section. This study deals with the Space frame finite element method regarding the first order theory based on the assumption is that the resulting deformations are small, and that the equilibrium may be formulated for the undeformed structure as an approximation. This is done by considering beam element and equation which are necessary for the computing deformations will be derived thus to calculate the displacements and internal forces and moments for frame structures.

2. METHOD

2.1. Geometry and concept of 3D thin-walled Frame

Considering Prismatic thin-walled beams of straight and of constant cross-section with y_1-axis is defined parallel to the longitudinal direction of the beam, while the y_2-axis and y_3-axis describe the transversal plane of the cross-section as shown in figure 2. The member is connected to local coordinate system and the corresponding displacement field adopted for the axial direction is v_1, while v_2 and v_3 are used for the cross-section's plane. Similarly, β_1, β_2 and β_3 are angles of rotation about the axis y_1, y_2 and y_3 and ψ is the sectional warping or twist of the section along y_1. Consider a point P with a member coordinate (y_1, y_2, y_3) in the member coordinate system. The basic assumption in the classical beam theory is that a cross-section orthogonal to the x-axis at the coordinate x remains plane and keeps its shape during deformation.

Due to the assumptions of the classical beam theory the cross-section orthogonal to the y_1-axis at the coordinate y_1 remains plane and keeps its shape during deformation and the general theory of elasticity for three-dimensional solids reduced to a special theory for space frames. The displacement of the point consists of a translation equal to that of the centroid C of section y_1 and a rotation displacement due to the rotation of the section as a rigid body about an axis through the centroid and a warping displacement normal to the section.

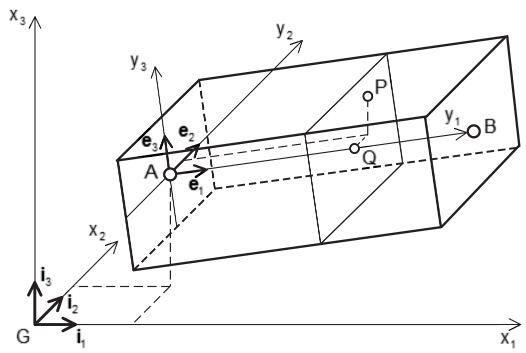

Figure 1. The orientation of coordinate systems for 3D beam section

Let S be a plane section normal to the axis of a member, which contains a point P and intersects the axis in point Q as shown in figure 1. The hypothesis for frame behavior [1] states that the shape of section S in its plane does not change under load, and that the displacement of point P is due to:

- The displacement of point Q
- A small rotation of section S about an axis passing through point Q
- A warping displacement in the y_1 direction, which is the product of a twist with a warping function

$$\begin{bmatrix} v_{1P} \\ v_{2P} \\ v_{3P} \end{bmatrix} = \begin{bmatrix} v_1 \\ v_2 \\ v_3 \end{bmatrix} + \begin{bmatrix} 0 & y_3 & -y_2 \\ -y_3 & 0 & 0 \\ y_2 & 0 & 0 \end{bmatrix} \begin{bmatrix} \beta_1 \\ \beta_2 \\ \beta_3 \end{bmatrix} + \omega \begin{bmatrix} \psi \\ 0 \\ 0 \end{bmatrix} \quad (1)$$

Where: $v_{kP}(y_1, y_2, y_3)$ the displacement coordinate of point P in the member space, $v_k(y_1)$ displacement coordinate of centroid *C* of section *y1*, $\beta_k(y_1)$, coordinate of the rotation vector of the section, $\omega(y_2, y_3)$: warping function of center of rotation C $\psi(y_1)$ twisting of the section

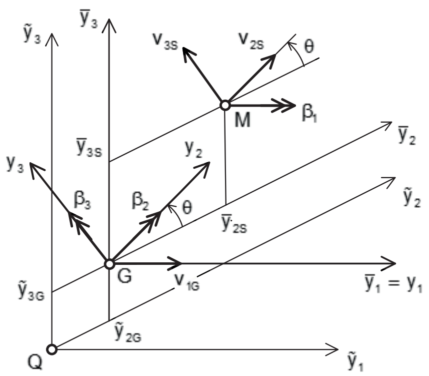

Figure 2. Beam kinematics, local and global reference systems for mass matrix

The strain coordinates are determined with the linear strain-displacement relations of the linear theory of elasticity. Because the frame hypothesis states that the shape of a section in its plane does not change, the strains are neglected.

$$\begin{aligned}
\varepsilon_{11} &= v_{1P,1} = v_{1,1} + y_3\beta_{2,1} - y_2\beta_{3,1} + \omega\psi_{,1} \\
\varepsilon_{12} &= v_{1P,2} + v_{2P,1} = -\beta_3 + \omega_{,2}\psi + v_{2,1} - y_3\beta_{1,1} \\
\varepsilon_{13} &= v_{1P,3} + v_{3P,1} = \beta_2 + \omega_{,3}\psi + v_{3,1} + y_2\beta_{1,1}
\end{aligned} \tag{2}$$

The expressions for the shear strains are rearranged so that the contributions of flexure, uniform torsion and torsion restraint are shown explicitly:

$$\varepsilon_{12} = \underbrace{(v_{2,1} - \beta_3)}_{\text{flexure}} - \underbrace{(y_3 + \omega_{,2})\beta_{1,1}}_{\text{uniform torsion}} + \underbrace{\omega_{,2}(\psi + \beta_{1,1})}_{\text{torsion restraint}} \tag{3}$$

$$\varepsilon_{13} = \underbrace{(v_{3,1} + \beta_2)}_{\text{flexure}} + \underbrace{(y_2 - \omega_{,3})\beta_{1,1}}_{\text{uniform torsion}} + \underbrace{\omega_{,3}(\psi + \beta_{1,1})}_{\text{torsion restraint}} \tag{4}$$

The constitutive hypothesis states that the strains due to the Poisson effect can be neglected in the analysis. For a linearly elastic material with modulus of elasticity *E* and shear modulus *G* the stress-strain may be calculated from equation (2) as follow:

$$\sigma_{11} = E\varepsilon_{11} = E(v_{1,1} + y_3\beta_{2,1} - y_2\beta_{3,1} + \omega\psi_{,1}) \tag{5}$$

$$\sigma_{12} = G\varepsilon_{12} = G(-\beta_3 + \omega_{,2}\psi + v_{2,1} - y_3\beta_{1,1}) \tag{6}$$

$$\sigma_{13} = G\varepsilon_{13} = G(\beta_2 + \omega_{,3}\psi + v_{3,1} + y_2\beta_{1,1}) \tag{7}$$

E modulus of elasticity

G *shear* modulus

The Virtual work of the inner forces δW_m done by the stresses σ_{11}, σ_{12} *and* σ_{13} of expressions (5)-(7), in the volume V of a member with length a, and area A due to virtual strains $\delta\varepsilon_{11}$, $\delta\varepsilon_{12}$ and $\delta\varepsilon_{13}$ is given by:

$$\delta W_m = \int_V \delta\varepsilon^T \sigma \, dv \tag{8}$$

Where: ε is state of strain vector (Voigt notation), σ state of stress vector (Voigt notation). The integrals of the products of the stress components with the geometric variables with the geometric quantities y_1, y_2, y_3 *and* ω over the area of the member are called stress resultants in the member and denoted as follows:

axial force in direction y_1 $\quad n_1 = \int_A \sigma_{11}\, dA$

transverse force in direction y_2 $\quad n_2 = \int_A \sigma_{12}\, dA$

transverse force in direction y_3 $\quad n_3 = \int_A \sigma_{13}\, dA$

bending moment about axis y_2 $\quad m_2 = \int_A \sigma_{11} y_3\, dA$

bending moment about axis y_3 $\quad m_3 = \int_A -\sigma_{11} y_2\, dA$ (9)

bimoment due to warping $\quad m_\omega = \int_A \sigma_{11}\omega\, dA$

primary torsion

$$m_{Tp} = \int_A \left(\sigma_{13}(y_2 - \omega_{,3}) - \sigma_{12}(y_3 + \omega_{,2})\right) dA\ )$$

secondary torsion

$$m_{Ts} = \int_A (\sigma_{13}\omega_{,3} + \sigma_{12}\omega_{,2})\, dA$$

The stress resultants acting on the positive face of a section are positive if they act in the positive direction of the axes of the member coordinate system. The stress resultants in the member of expression (9) are substituted into expression (8) and can be rewritten as follows:

$$\int_V \delta\boldsymbol{\varepsilon}^T \boldsymbol{\sigma}\, dv = \int_0^a \begin{pmatrix} n_1\,\delta v_1 + n_2(\delta v_{2,1} - \delta\beta_3) + \\ n_3(\delta v_{3,1} + \delta\beta_2) + \\ m_2\,\delta\beta_{2,1} + m_3\,\delta\beta_{3,1} + m_\omega\,\delta\psi_{,1} + \\ m_{Tp}\,\delta\beta_{1,1} + m_{Ts}(\delta\psi + \delta\beta_{1,1}) \end{pmatrix} dy_1 \quad (10)$$

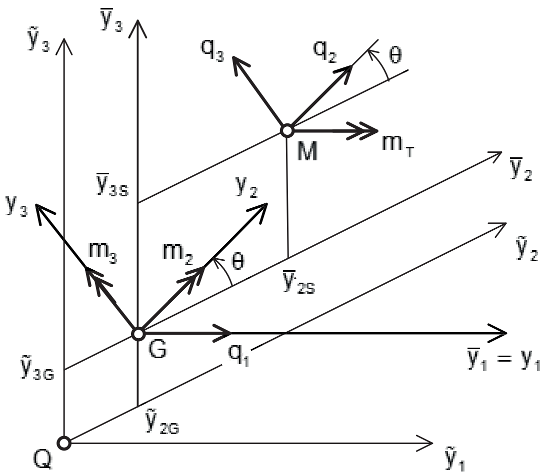

Figure 3. Local reference system and internal forces

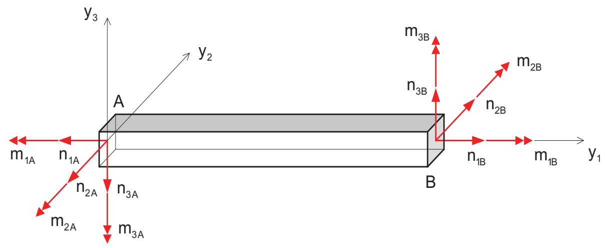

Figure 4. Positive directions of the member and nodal force coordinates

The loads acting of the volume and the surface of the member in the theory of elasticity are replaced by line loads acting at axis y_1 and by nodal forces acting at the nodes of the member, as shown in figure 3. The nodal forces acting at the end node are equal to the stress resultants defined based on equation (8). The virtual work of the nodal forces due to variations δv_k of the displacement coordinates and $\delta\beta_k$ of the rotation coordinates is given by:

$$\begin{aligned} \delta W_n = {} & m_{TpB}\,\delta\beta_{1B} - m_{TpA}\,\delta\beta_{1A} + \\ & m_{TsB}(\delta\psi_B + \delta\beta_{1B,1}) - m_{TsA}(\delta\psi_A + \delta\beta_{1A,1}) + \\ & m_{2B}\,\delta\beta_{2B} - m_{2A}\,\delta\beta_{2A} + m_{3B}\,\delta\beta_{3B} - \\ & m_{3A}\,\delta\beta_{3A} + m_{\omega B}\,\delta\psi_{B,1} - m_{\omega A}\,\delta\psi_{A,1} + \\ & \sum_{k=1}^{3}(n_{kB}\,\delta v_{kB} - n_{kA}\,\delta v_{kA}) \end{aligned} \quad (11)$$

Where δW_n is virtual work of the nodal forces

The virtual work of the inner forces in the volume of a member is expressed in terms of the strains and the virtual strains:

$$\delta W_m = \int_V (E\,\varepsilon_{11}\,\delta\varepsilon_{11} + G\,\varepsilon_{12}\,\delta\varepsilon_{12} + G\,\varepsilon_{13}\,\delta\varepsilon_{13})\, dV \quad (12)$$

Expressions (5) to (7) for the strains and the Prandtl stress function for $\beta_{2,1}$ *and* $\beta_{3,1}$ are substituted:

$$\begin{aligned} \delta W_m &= E\int_0^a\int_A h_1 h_2\, dA\, dy_1 + G\int_0^a\int_A h_3\, dA\, dy_1 \\ h_1 &= \delta v_{1,1} - y_2\delta v_{2,11} - y_3\delta v_{3,11} + \omega\,\delta\psi_{1,1} \\ h_2 &= v_{1,1} - y_2 v_{2,11} - y_3 v_{3,11} + \omega\,\psi_{1,1} \\ h_3 &= \left((y_2 - \omega_{,3})^2 + (y_3 + \omega_{,2})^2\right)\delta\beta_{1,1}\,\beta_{1,1} \end{aligned} \quad (13)$$

The integrals of functions of the coordinates and the warping function in (13) are called the shape parameters of the section or matrix section properties. To define the shape functions, we used a variable F for designations. They are defined and denoted as follows:

$$\delta W_m = E\int_0^a \delta k^T F\, k\, dy_1 + G\int_0^a J_T\,\delta\beta_{1,1}\,\beta_{1,1}\, dy_1$$

$$F = \begin{array}{|c|c|c|c|} \hline F_1 & F_2 & F_3 & F_\omega \\ \hline F_2 & F_{22} & F_{23} & F_{2\omega} \\ \hline F_3 & F_{32} & F_{33} & F_{3\omega} \\ \hline F_\omega & F_{2\omega} & F_{3\omega} & F_{\omega\omega} \\ \hline \end{array} \quad (14)$$

Where the section constants are expresses as given below:

$$F_1 = \int_A 1\, dA$$
$$F_2 = \int_A y_2\, dA \qquad F_3 = \int_A y_3\, dA$$
$$F_\omega = \int_A \omega\, dA$$
$$F_{22} = \int_A y_2^2\, dA \qquad F_{23} = \int_A y_2 y_3\, dA$$
$$F_{33} = \int_A y_3^2\, dA \qquad F_{2\omega} = \int_A y_2\,\omega\, dA$$
$$F_{3\omega} = \int_A y_3\,\omega\, dA \qquad F_{\omega\omega} = \int_A \omega^2\, dA$$
$$J_T = \int_A \left((y_2 - \omega_{,3})^2 + (y_3 + \omega_{,2})^2 \right) dA$$

The virtual work of the nodal forces due to variations of the displacement coordinates and of the rotation coordinates is given by:

$$\begin{aligned} \delta W_n \; = \; & m_{TpB}\,\delta\beta_{1B} - m_{TpA}\,\delta\beta_{1A} + \\ & m_{TsB}(\delta\psi_B + \delta\beta_{1B,1}) - \\ & m_{TsA}(\delta\psi_A + \delta\beta_{1A,1}) + \\ & m_{2B}\,\delta\beta_{2B} - m_{2A}\,\delta\beta_{2A} + m_{3B}\,\delta\beta_{3B} - \\ & m_{3A}\,\delta\beta_{3A} + m_{\omega B}\,\delta\psi_{B,1} - m_{\omega A}\,\delta\psi_{A,1} + \\ & \sum_{k=1}^{3}(n_{kB}\,\delta v_{kB} - n_{kA}\,\delta v_{kA}) \end{aligned} \tag{15}$$

δW_n virtual work of the nodal forces

The virtual work of member loads due to variations δv_k of the displacement coordinates and $\delta\beta_k$ of the rotation coordinates is given by:

$$\delta W_q = \int_0^a \left(t_\omega \psi + \sum_{i=1}^{3} (q_i\,\delta v_i + t_i\,\delta\beta_i) \right) dy_1 \tag{16}$$

q_i distributed force load in the direction of axis i
t_i distributed moment load in the direction of axis i
t_ω distributed bimoment load

2.2. Governing equations for 3D thin-walled frames

The governing equations for a member and frame are derived by applying the principle of virtual work to the frame. The sum over the members of the virtual work δW_m of the inner forces in (14) equals the sum over the members of the virtual work δW_{md} of the member loads.

The differential governing equations for the generalized member displacements are satisfied for arbitrary virtual displacements and expressed as follows:

$$\begin{aligned} & E\,A\,v_{1,1} + q_1 = 0 \\ & E\,J_3 v_{2,1111} - q_2 + m_{3,1} = 0 \\ & E\,J_2 v_{3,1111} - q_3 - m_{2,1} = 0 \\ & EJ_\omega \beta_{1,1111} - G\,J_T\,\beta_{1,11} - m_1 - m_{\omega,1} = 0 \end{aligned} \tag{17}$$

Similarly for frames, The sum over the members of the virtual work δW_m of the inner forces in (14) equals the sum over the members of the virtual work δW_{md} of the member loads and the virtual work δW_n of the nodal loads:

$$\sum_{m=1}^{M} \delta W_m = \sum_{m=1}^{M} \delta W_{md} + \delta W_n \tag{18}$$

3. RESULT AND DISCUSSION

3.1. Element *stiffness matrix for a combined load:*

Stiffness matrix as it is known, the relationship between the generalized force vector q_m and the generalized displacement vector v_m is established by the stiffness matrix K_m of the element.

$$q_m = K_m\; v_m \tag{19}$$

The displacement variation over the length of a member is related to the nodal displacements by solving the differential equations the differential governing equations for the generalized member displacements such that the values of the displacement functions at the nodes equal the unknown nodal displacement values. For non-uniform torsion, a trigonometric interpolation of rotation β_1 is used as an initial parameter and finally compared with the approximation solution.

$$v_1 = \mathbf{h}_1^T \mathbf{v}_1 \qquad 0 \le z \le 1$$

$$\mathbf{h}_1 = \begin{bmatrix} 1-z \\ z \end{bmatrix} \qquad \mathbf{v}_1 = \begin{bmatrix} v_{1A} \\ v_{1B} \end{bmatrix}$$

$$v_2 = \mathbf{h}_2^T \mathbf{v}_2$$

$$\mathbf{h}_2 = \begin{bmatrix} 1-3z^2+2z^3 \\ a\,z(1-z)^2 \\ z^2(3-2z) \\ -a\,z^2(1-z) \end{bmatrix} \qquad \mathbf{v}_2 = \begin{bmatrix} v_{2A} \\ \beta_{3A} \\ v_{2B} \\ \beta_{3B} \end{bmatrix}$$

$$v_3 = \mathbf{h}_3^T \mathbf{v}_3$$

$$\mathbf{h}_3 = \begin{bmatrix} 1-3z^2+2z^3 \\ -a\,z(1-z)^2 \\ z^2(3-2z) \\ a\,z^2(1-z) \end{bmatrix} \qquad \mathbf{v}_3 = \begin{bmatrix} v_{3A} \\ \beta_{2A} \\ v_{3B} \\ \beta_{2B} \end{bmatrix}$$

To consider the warping of the restrained member, additional degrees of freedoms are introduced at the nodes and added to member displacement vector. An interpolation function containing hyperbolic functions of y_1, which satisfies the governing differential equation (16) for torsion considered:

$$\beta_1(y_1) = g(y_1)^T b$$
$$g^T = \begin{bmatrix} g_1(y_1) & g_2(y_1) & g_3(y_1) & g_4(y_1) \end{bmatrix} \tag{20}$$
$$b^T = \begin{bmatrix} \beta_{1A} & \beta_{1,1A} & \beta_{1B} & \beta_{1,1B} \end{bmatrix}$$

$$\beta_1 = h_\omega^T C$$

$$h_\omega^T = \begin{bmatrix} \sinh\theta z \\ \cosh\theta z \\ z \\ 1 \end{bmatrix} \qquad C = \begin{bmatrix} C_1 & C_2 & C_3 & C_4 \end{bmatrix}$$

The derivatives in the integrand on the left-hand side of equation (20) are formed:

$$v_{1,1} = g_1^T v_1 \qquad v_{2,11} = g_2^T v_2 \qquad 0 \le z \le 1$$

$$g_1 = \frac{1}{a}\begin{bmatrix} -1 \\ 1 \end{bmatrix} \qquad g_2 = \frac{1}{a^2}\begin{bmatrix} 12z-6 \\ a(6z-4) \\ -(12z-6) \\ a(6z-2) \end{bmatrix}$$

$$v_{3,11} = \mathbf{g}_3^T \mathbf{v}_3$$

$$\mathbf{g}_3 = \frac{1}{a^2}\begin{bmatrix} 12z-6 \\ -a(6z-4) \\ -(12z-6) \\ -a(6z-2) \end{bmatrix}$$

The interpolation functions are substituted into the left-hand side of (18) and the integration over the length of the member is performed for axial and bending loads but separately considered for torsion as it developed based on the two different methods.

$$EA\int_0^a \delta v_1\, v_{1,1}\, dy_1 = \delta v_1^T K_1 v_1$$
$$EJ_3\int_0^a \delta v_2\, v_{2,11}\, dy_1 = \delta v_2^T K_2 v_2 \qquad EJ_2\int_0^a \delta v_3 v_{3,11}\, dy_1 = \delta v_3^T K_3 v_3$$

$$K_1 = \frac{EA}{a}\begin{bmatrix} 1 & -1 \\ -1 & 1 \end{bmatrix} = \begin{bmatrix} k_1 & k_2 \\ k_2 & k_1 \end{bmatrix}$$

$$K_2 = \frac{EJ_2}{a^3}\begin{bmatrix} 12 & 6a & -12 & 6a \\ 6a & 4a^2 & -6a & 2a^2 \\ -12 & -6a & 12 & -6a \\ 6a & 2a^2 & -6a & 4a^2 \end{bmatrix} = \begin{bmatrix} k_3 & k_4 & k_6 & k_4 \\ k_4 & k_5 & k_7 & k_8 \\ k_6 & k_7 & k_3 & k_7 \\ k_4 & k_8 & k_7 & k_5 \end{bmatrix}$$

$$K_3 = \frac{EJ_3}{a^3}\begin{bmatrix} 12 & -6a & -12 & -6a \\ -6a & 4a^2 & 6a & 2a^2 \\ -12 & 6a & 12 & 6a \\ -6a & 2a^2 & 6a & 4a^2 \end{bmatrix} = \begin{bmatrix} k_9 & k_{10} & k_{12} & k_{10} \\ k_{10} & k_{11} & k_{13} & k_{14} \\ k_{12} & k_{13} & k_9 & k_{13} \\ k_{10} & k_{14} & k_{13} & k_{11} \end{bmatrix}$$

The contribution of torsion to the internal virtual work of the governing differential equation (16) is given as the following expressions:

$$\int_0^a (EC_\omega\, \delta\beta_{1,11}\beta_{1,11} + GJ_T\, \delta\beta_{1,1}\beta_{1,1})\, dA = \delta b^T (K_{\omega 1} + K_{\omega 2})\, b$$

$K_{\omega 1}$ warping stiffness matrix
$K_{\omega 2}$ stiffness matrix for torsion with out warping restraint

Stiffness matrices $K_{\omega 1}$ and $K_{\omega 2}$ are added to the member stiffness matrix K_m in the usual manner.

$$K_T = \frac{EC_\omega}{a^3} \begin{array}{|c|c|c|c|} \hline k_{T1} & k_{T2} & k_{T3} & k_{T4} \\ \hline k_{T2} & k_{T6} & k_{T7} & k_{T8} \\ \hline k_{T3} & k_{T7} & k_{T11} & k_{T12} \\ \hline k_{T4} & k_{T8} & k_{T12} & k_{T16} \\ \hline \end{array}$$

$$K_{T1} = K_{T11} = S*\theta\sinh\theta,$$

$$K_{T6} = K_{T16} = S*(\cosh\theta - \frac{\sinh\theta}{\theta})*a^2$$

$$K_{T2} = K_{T4} = S*(\cosh\theta - 1)*a,$$

$$K_{T8} = S*\left(\frac{\sinh\theta}{\theta} - 1\right)*a^2$$

$$S = \left(\frac{\theta^2}{Q}\right), \quad Q = 2(1-\cosh\theta) + \theta\sinh\theta,$$

$$K_{T3} = -K_{T1}, \quad K_{T7} = K_{T12} = -K_{T2}$$

The above element stiffness matrix for torsion with restrain warping can be used by divided into two matrices. The parameters K_{T1}, K_{T2}, K_{T6} and K_{T8} can be replace by approximation as shown below:

$$K_{T1a} = 12 + \frac{6}{5}*\theta^2 \qquad K_{T2a} = 6 + \frac{1}{10}*\theta^2$$

$$K_{T6a} = 4 + \frac{2}{15}*\theta^2 \qquad K_{T8a} = 2 - \frac{1}{30}*\theta^2$$

Considering the above series expressions, the alternative matrices can express as shown below:

$$K_{Ta} = \frac{EC_\omega}{a^3} \begin{array}{|c|c|c|c|} \hline 12 & -6a & -12 & 6a \\ \hline 6a & 4a^2 & 6a & 2a^2 \\ \hline -12 & -6a & 12 & 6a \\ \hline 6a & 2a^2 & 6a & 4a^2 \\ \hline \end{array} + \frac{GJ}{30a} \begin{array}{|c|c|c|c|} \hline 36 & -3a & -36 & -3a \\ \hline -3a & 4a^2 & 3a & -a^2 \\ \hline -3a & 3a & 36 & 3a \\ \hline -3a & -a^2 & 3a & 4a^2 \\ \hline \end{array}$$

Comparing both methods, we can conclude that both are similar for small value of θ and which is commonly considered for open thin-walled section as their value of θ is small as shown in figure 5.

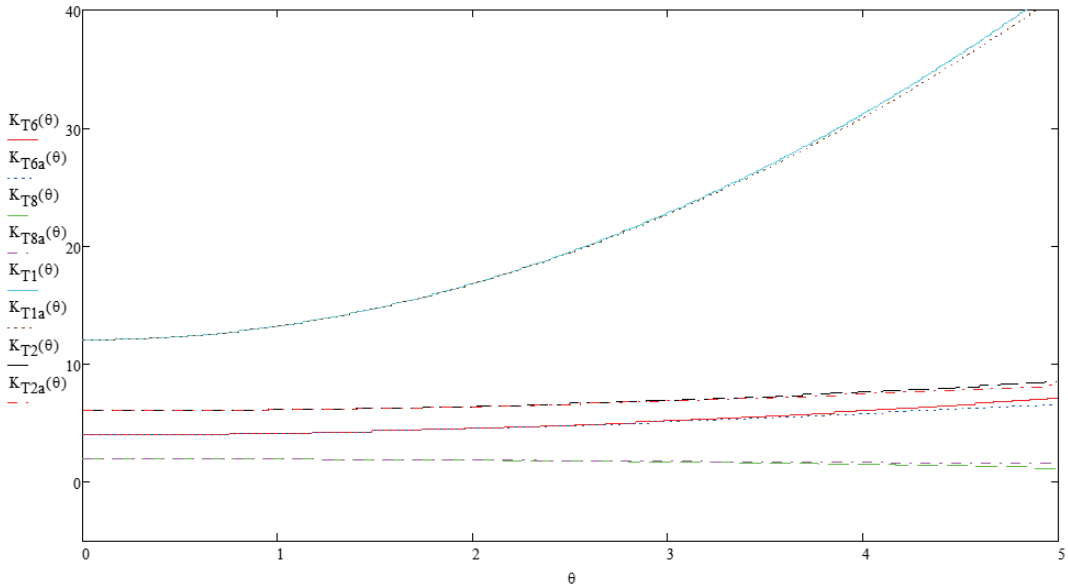

Figure 5. Evaluation of exact and approximate methods for various values of θ

If the member is free to warp, $C_w = 0$ and the torsional moment is carried by *St Venant's* torsion which is considered as uniform torsion.

Considering Expression 21, only the second part of the matrix or the uniform torsion stiffness matrix can be used as given below.

$$\mathbf{K}_T = \frac{G\,J_T}{a}\begin{array}{|c|c|}\hline 1 & -1 \\ \hline -1 & 1 \\ \hline\end{array} \quad \text{or}$$

$$\mathbf{K}_T = \frac{G\,J}{30a}\begin{array}{|c|c|c|c|}\hline 36 & -3a & -36 & -3a \\ \hline -3a & 4a^2 & 3a & -a^2 \\ \hline -3a & 3a & 36 & 3a \\ \hline -3a & -a^2 & 3a & 4a^2 \\ \hline\end{array}$$

Element load vector: Consider loads which vary linearly from start node A to end node B:

$$q_k = \mathbf{h}_1^T \mathbf{q}_k$$

$$m_k = \mathbf{h}_1^T \mathbf{m}_k \qquad \mathbf{q}_k = \begin{array}{|c|}\hline q_{kA} \\ \hline q_{kB} \\ \hline\end{array} \qquad \mathbf{m}_k = \begin{array}{|c|}\hline m_{kA} \\ \hline m_{kB} \\ \hline\end{array}$$

These loads and the interpolation functions are substituted into the right-hand side of equation (17). The integration over the length of the member is shown for q_1 *and* q_3.

$$\int_0^a q_1\,\delta v_1\,dy_1 = \int_0^a \delta\mathbf{v}_1^T\,\mathbf{h}_1\mathbf{h}_1^T\,\mathbf{q}_1\,dy_1 = \delta\mathbf{v}_1^T\,\mathbf{B}_1\mathbf{q}_1$$

$$\int_0^a q_3\,\delta v_3\,dy_1 = \int_0^a \delta\mathbf{v}_3^T\,\mathbf{h}_3\mathbf{h}_3^T\,\mathbf{q}_3\,dy_1 = \delta\mathbf{v}_3^T\,\mathbf{B}_3\mathbf{q}_3$$

$$\mathrm{B}_1 \quad \frac{a}{6}\begin{array}{|c|c|}\hline 2 & 1 \\ \hline 1 & 2 \\ \hline\end{array} = \begin{array}{|c|c|}\hline b_1 & b_2 \\ \hline b_2 & b_1 \\ \hline\end{array}$$

$$\mathrm{B}_3 = \frac{a}{60}\begin{array}{|c|c|}\hline 21 & 9 \\ \hline -3a & -2a \\ \hline 9 & 21 \\ \hline 2a & 3a \\ \hline\end{array} = \begin{array}{|c|c|}\hline b_3 & b_4 \\ \hline b_5 & b_6 \\ \hline b_4 & b_3 \\ \hline b_7 & b_8 \\ \hline\end{array}$$

The results are compared with different studies in both methods to include the aadditional degrees of freedom and are introduced at the nodes and added to member displacement vector[29][30][31]. The member variables are collected in member displacement vector V_m and member load vector q_m and the matrices are arranged correspondingly in member stiffness matrix k_m.

$\mathbf{K}_m =$

k_1							k_2						
	k_3				k_4			k_6				k_4	
		k_9		k_{10}					k_{12}		k_{10}		
			k_{T1}			k_{T2}				k_{T3}			k_{T4}
		k_{10}		k_{11}					k_{13}		k_{14}		
	k_4				k_5			k_7				k_8	
			k_{T5}			k_{T6}				k_{T7}			k_{T8}
k_2							k_1						
	k_6				k_7			k_3				k_7	
		k_{12}		k_{13}					k_9		k_{13}		
			k_{T9}			k_{T10}				k_{T11}			k_{T12}
		k_{10}		k_{14}					k_{13}		k_{11}		
	k_4				k_5			k_7				k_8	
			k_{T13}			k_{T14}				k_{T15}			k_{T16}

$$\mathbf{q}_m = \begin{array}{|c|}\hline b_1q_{1A} + b_2q_{3B} \\ \hline b_1q_{2A} + b_2q_{2B} \\ \hline b_7q_{2A} + b_8q_{2B} \\ \hline b_3q_{3A} + b_4q_{3B} \\ \hline b_5q_{3A} + b_6q_{3B} \\ \hline b_1m_{1A} + b_2m_{1B} \\ \hline b_5m_{1A} + b_6m_{1B} \\ \hline b_1q_{1A} + b_2q_{1B} \\ \hline b_7q_{2A} + b_8q_{2B} \\ \hline b_7q_{2A} + b_8q_{2B} \\ \hline b_3q_{3A} + b_4q_{3B} \\ \hline b_5q_{3A} + b_6q_{3B} \\ \hline b_1m_{1A} + b_2m_{1B} \\ \hline b_5m_{1A} + b_6m_{1B} \\ \hline\end{array} \qquad \mathbf{v}_e = \begin{array}{|c|}\hline v_{1A} \\ \hline v_{2A} \\ \hline v_{3A} \\ \hline \beta_{1A} \\ \hline \beta_{2A} \\ \hline \beta_{3A} \\ \hline \psi_A \\ \hline v_{1B} \\ \hline v_{2B} \\ \hline v_{3B} \\ \hline \beta_{1B} \\ \hline \beta_{2B} \\ \hline \beta_{3B} \\ \hline \psi_B \\ \hline\end{array}$$

4. CONCLUSION

The frequently used finite element method for thin-walled sections only considers six degrees of freedom (DOFs) in each node of a beam, but it has been demonstrated that including warping of the section as an additional DOF in structural analysis can result in a safe and optimal design. According to this study the following conclusions are drawn. The simple geometric properties of the section are used to generate the stiffness matrix for thin-walled beam sections with retrained torsion. By considering an additional degree of freedom at each node, the trigonometric and approximation solutions of an interpolation function are used to express the stiffness matrix for non-uniform torsion. The stiffness matrix for 3D thin-walled sections subjected to combined loading is presented, making advanced structural analysis bar elements more convenient. This stiffness matrix is more applicable for open thin-walled sections because the value of characteristics number for open section is very small comparing to the closed thin-walled sections. To include the additional degree of freedom both trigonometric and approximate methods are considered and for characteristics number (θ) =1 and 2 the errors range between 6.7 % to – 9.7 % which is considered reasonable and both methods are acceptable for open thin-walled sections. The length of the member is limited based on the section type and with maximum value of characteristics number (θ) less than 2.

REFERENCES

1. **Saadé K., Warzée G., Espion B.** Modeling distortional shear in thin-walled elastic beams. Thin-Walled Structures. 2006. 44(7). Pp. 808–821..
2. **Murín J., Aminbaghai M., Kutiš, V., Královič V., Sedlár T., Goga V., Mang H.** A new 3D Timoshenko finite beam element including non-uniform torsion of open and closed cross sections. Engineering Structures. 2014. 59. Pp. 153–160..
3. **Saadé K., Espion B., Warzée** G. Non-uniform torsional behavior and stability of thin-walled elastic beams with arbitrary cross sections. Thin-Walled Structures. 2004. 42(6). Pp. 857–881. DOI:10.1016/j.tws.2003.12.003.
4. S**apountzakis E.J.** Bars under Torsional Loading: A Generalized Beam Theory Approach. ISRN Civil Engineering. 2013. Pp. 1–39. DOI:10.1155/2013/916581.
5. **Kim J.H., Kim Y.Y.** One-dimensional analysis of thin-walled closed beams having general cross-sections. International Journal for Numerical Methods in Engineering. 2000. 49(5). Pp. 653–668. .
6. **Jönsson J.** Distortional theory of thin-walled beams. Thin-Walled Structures. 1999. 33(4). Pp. 269–303.
7. **Khairuzzaman M.Q.** Finite Element Analysis of Thin-Walled Structures. 4(1)2016. 64–75 p. ISBN:1851661360.
8. **Pi, Y., Trahair, N.S.** Bending and Torsion of Cold-Formed Channel Beams. 1999. 9445.
9. **Galishnikova V.V.** A Theory for Space Frames with Warping Restraint at Nodes. 1st IAA/AAS SciTech Forum on Space Flight Mechanics and Space Structures and Materials. 2020. 170. Pp. 763-784.
10. **Floros M. W.** Smith E. C. Finite element modeling of open-section composite beams with warping restraint effects. AIAA Journal. vol. 35(8). pp. 1341–1347.
11. **Vatin N., Havula J., Martikainen L., Sinelnikov A.** Thin-Walled Cross-Sections and their Joints : Tests and FEM-Modelling Thin-walled cross-sections and their joints : tests and FEM-modelling. 2014.DOI:10.4028/www.scientific.net/AMR.945-949.1211.
12. **Paul A. S., Charles J. C.** AISC Design Guide : Torsional Analysis of Structural Steel Members_Revision. Steel Design Guide Series. 2003. Pp. 116.
13. **Vlasov V. Z.**, Thin-walled Elastic Beams. Springfield, Va.: National Technical Information Service. Virginia,1984. 493p.
14. **Alwis W.A.M.,** Wang, C.M. Wagner term in flexural-torsional buckling of thin-walled open-profile columns. Engineering Structures. 1996. 18(2). Pp. 125–132.
15. **Gebre T.H., Galishnikova V. V.** The impact of section properties on thin walled beam sections with restrained torsion. Journal of Physics: Conference Series. 2020. 1687. Pp. 012020. DOI:10.1088/1742-6596/1687/1/012020.
16. **Banić D., Turkalj G., Brnić J.** Finite element stress analysis of elastic beams

under non-uniform torsion. Transactions of Famena. 2016. 40(2). Pp. 71–82.
17. **Murín J., Kutiš V**. 3D-beam element with continuous variation of the cross-sectional area. Computers and Structures. 2002. 80(3–4). Pp. 329–338.
18. **Jönsson J.** Determination of shear stresses, warping functions and section properties of thin-walled beams using finite elements. Computers and Structures. 1998. 68(4). Pp. 393–410.
19. **Lalin, V. V., Rybakov, V.A., Ivanov, S.S., Azarov, A.A.** Mixed finite-element method in semi-shear thin-walled bar theory. Magazine of Civil Engineering, 2019. 89(5). Pages 79–93. DOI: 10.18720/MCE.89.7
20. **Dyakov S.F., Lalin V.V.** Postroyeniye i analiz konechnykh elementov sterzhnya otkrytogo profilya s uchetom deformatsiy sdviga i krucheniya [Construction and investigation of open cross-section bar finite element with account of shear and torsion]. Vestnik Permskogo gosudarstvennogo tekhnicheskogo universiteta. Okhrana okruzhayushchey sredy, transport, bezopasnost zhiznedeyatelnosti. 2011. No. 2. Pp. 130–140. (Rus)
21. **Lalin V.V., Rybakov V.A.** Konechnye elementy dlya rascheta ograzhdayushchikh konstruktsiy iz tonkostennykh profiley [The finite elements for desing of building walling made of thin-walled beams]. Magazine of Civil Engineering. 2011. No. 8. Pp. 69–80. (rus)
22. **Lalin V.V., Rybakov V.A., Morozov S.A**. Issledovaniye konechnykh elementov dlya rascheta tonkostennykh sterzhnevykh sistem [The finite elements research forcalculation of thin-walled bar systems]. Magazine of Civil Engineering, 2012. No. 1 (27). Pp. 53–73. (Rus)
23. **Tusnin A.R., Tusnina O.A.** Vychislitelnaya Sistema «Stalkon» dlya rascheta i proyektirovaniya sterzhnevykh konstruktsiy iz tonkostennykh sterzhney otkrytogo profilya [Software complex “Stalkon” for analysis and design of thin-walled opened cross-section bar structures]. Promyshlennoye i grazhdanskoye stroitelstvo. 2012. No. 8. Pp. 62–64. (rus)
24. **Tusnin A.R.** Nekotoryye voprosy rascheta tonkostennykh stalnykh konstruktsiy [Some approaches of thin-walled steel structure’s analysis]. Nauchnoye obozreniye. 2015. No. 11. Pp. 79–82. (rus)
25. **Perelmuter A.**, Yurchenko, V. on the Issue of Structural Analysis of Spatial Systems From Thin-Walled Bars With Open Profiles. Metal Constructions. 2014. 20. Pp. 179–190.
26. **Wang Z.Q., Zhao J.C., Zhang D.X., Gong J.H.** Restrained torsion of open thin-walled beams including shear deformation effects. Journal of Zhejiang University: Science A. 2012. 13(4). Pp. 260–273. DOI:10.1631/jzus.A1100149.
27. **Wang Z.-Q., Zhao J.-C.** Restrained Torsion of Thin-Walled Beams. Journal of Structural Engineering. 2014. 140(11). Pp. 04014089..
28. **Tusnin A.** Finite Element for Calculation of Structures Made of Thin-Walled Open Profile Rods. Procedia Engineering. 2016. 150. Pp. 1673–1679.
29. **Xiao-Feng W., Qi-Lin Z., Qing-Shan Y.** A new finite element of spatial thin-walled beams. Applied Mathematics and Mechanics (English Edition). 2010. 31(9). Pp. 1141–1152.
30. **Murín J., Kutiš V., Královič V., Sedlár T.** 3D beam finite element including nonuniform torsion. Procedia Engineering. 2012. 48. Pp. 436–444.
31. **Sapountzakis E.J., Mokos V.G.** 3-D beam element of variable composite cross section including warping effect. Acta Mechanica. 2004. 171(3–4). Pp. 151–169.

СПИСОК ЛИТЕРАТУРЫ

1. **Saadé K., Warzée G., Espion B.** Modeling distortional shear in thin-walled elastic beams. Thin-Walled Structures. 2006. 44(7). Pp. 808–821.

2. **Murín J., Aminbaghai M., Kutiš, V., Královič V., Sedlár T., Goga V., Mang H.** A new 3D Timoshenko finite beam element including non-uniform torsion of open and closed cross sections. Engineering Structures. 2014. 59. Pp. 153–160..
3. **Saadé K., Espion B., Warzée** G. Non-uniform torsional behavior and stability of thin-walled elastic beams with arbitrary cross sections. Thin-Walled Structures. 2004. 42(6). Pp. 857–881..
4. **Sapountzakis E.J.** Bars under Torsional Loading: A Generalized Beam Theory Approach. ISRN Civil Engineering. 2013. Pp. 1–39.
5. **Kim J.H., Kim Y.Y.** One-dimensional analysis of thin-walled closed beams having general cross-sections. International Journal for Numerical Methods in Engineering. 2000. 49(5). Pp. 653–668.
6. **Jönsson J.** Distortional theory of thin-walled beams. Thin-Walled Structures. 1999. 33(4). Pp. 269–303. DOI:10.1016/S0263-8231(98)00050-0.
7. **Khairuzzaman M.Q.** Finite Element Analysis of Thin-Walled Structures. 4(1)2016. 64–75 p. ISBN:1851661360.
8. **Pi, Y., Trahair, N.S.** Bending and Torsion of Cold-Formed Channel Beams. 1999. 9445..
9. **Galishnikova V.V.** A Theory for Space Frames with Warping Restraint at Nodes. 1st IAA/AAS SciTech Forum on Space Flight Mechanics and Space Structures and Materials. 2020. 170. Pp. 763-784.
10. **Floros M. W.** Smith E. C. Finite element modeling of open-section composite beams with warping restraint effects. AIAA Journal. vol. 35(8). pp. 1341–1347.
11. **Vatin N., Havula J., Martikainen L., Sinelnikov A.** Thin-Walled Cross-Sections and their Joints : Tests and FEM-Modelling Thin-walled cross-sections and their joints : tests and FEM-modelling. 2014.DOI:10.4028/www.scientific.net/AMR.945-949.1211.
12. **Paul A. S., Charles J. C.** AISC Design Guide : Torsional Analysis of Structural Steel Members_Revision. Steel Design Guide Series. 2003. Pp. 116.
13. **Vlasov V. Z.**, Thin-walled Elastic Beams. Springfield, Va.: National Technical Information Service. Virginia,1984. 493p.
14. **Alwis W.A.M.,** Wang, C.M. Wagner term in flexural-torsional buckling of thin-walled open-profile columns. Engineering Structures. 1996. 18(2). Pp. 125–132.
15. **Gebre T.H., Galishnikova V. V.** The impact of section properties on thin walled beam sections with restrained torsion. Journal of Physics: Conference Series. 2020. 1687. Pp. 012020.
16. **Banić D., Turkalj G., Brnić J.** Finite element stress analysis of elastic beams under non-uniform torsion. Transactions of Famena. 2016. 40(2). Pp. 71–82.
17. **Murín J., Kutiš V**. 3D-beam element with continuous variation of the cross-sectional area. Computers and Structures. 2002. 80(3–4). Pp. 329–338.
18. **Jönsson J.** Determination of shear stresses, warping functions and section properties of thin-walled beams using finite elements. Computers and Structures. 1998. 68(4). Pp. 393–410.
19. **Лалин В.В., Рыбаков В.А., Иванов С.С., Азаров А.А.** Смешанный метод конечных элементов в полусдвиговой теории тонкостенных стержней В.И. Сливкера // Инженерно-строительный журнал. 2019. № 5(89). С. 79–93. DOI: 10.18720/MCE.89.7
20. **Дьяков С.Ф., Лалин В.В**. Построение и анализ конечных элементов стержня открытого профиля с учетом деформаций сдвига и кручения // Вестник Пермского государственного технического университета. Охрана окружающей среды, транспорт, безопасность жизнедеятельности. 2011. № 2. С. 130–140.
21. **Лалин В.В., Рыбаков В.А**. Конечные элементы для расчета ограждающих конструкций из тонкостенных профилей

// Инженерно-строительный журнал. 2011. № 8. С. 69–80.
22. **Лалин В.В., Рыбаков В.А., Морозов С.А**. Исследование конечных элементов для расчета тонкостенных стержневых систем // Инженерно-строительный журнал. 2012. № 1. С. 53–73.
23. **Туснин А.Р., Туснина О.А**. Вычислительная система «Сталькон» для расчета и проектирования стержневых конструкций из тонкостенных стержней открытого профиля // Промышленное и гражданское строительство. 2012. № 8. С. 62–64.
24. **Туснин А.Р.** Некоторые вопросы расчета тонкостенных стальных конструкций // Научное обозрение. 2015. № 11. С. 79–82
25. **Perelmuter A.**, Yurchenko, V. on the Issue of Structural Analysis of Spatial Systems From Thin-Walled Bars With Open Profiles. Metal Constructions. 2014. 20. Pp. 179–190.
26. **Wang Z.Q., Zhao J.C., Zhang D.X., Gong J.H.** Restrained torsion of open thin-walled beams including shear deformation effects. Journal of Zhejiang University: Science A. 2012. 13(4). Pp. 260–273. DOI:10.1631/jzus.A1100149.
27. **Wang Z.-Q., Zhao J.-C.** Restrained Torsion of Thin-Walled Beams. Journal of Structural Engineering. 2014. 140(11). Pp. 04014089. DOI:10.1061/(asce)st.1943-541x.0001010.
28. **Tusnin A.** Finite Element for Calculation of Structures Made of Thin-Walled Open Profile Rods. Procedia Engineering. 2016. 150. Pp. 1673–1679.
29. **Xiao-Feng W., Qi-Lin Z., Qing-Shan Y.** A new finite element of spatial thin-walled beams. Applied Mathematics and Mechanics (English Edition). 2010. 31(9). Pp. 1141–1152.
30. **Murín J., Kutiš V., Královič V., Sedlár T.** 3D beam finite element including nonuniform torsion. Procedia Engineering. 2012. 48. Pp. 436–444.
31. **Sapountzakis E.J., Mokos V.G.** 3-D beam element of variable composite cross section including warping effect. Acta Mechanica. 2004. 171(3–4). Pp. 151–169.

Vera V. Galishnikova, Professor, Dr.Sc.; Vice-Rector, Professor, Moscow State University of Civil Engineering (National Research University), Professor, Department of Civil Engineering, Peoples' Friendship University of Russia (RUDN University), 129337, Russia, Moscow, Yaroslavskoe Sh 26, Tel. 7 (495)025-29-38. e-mail: galishni@yandex.ru

Tesfaldet H. Gebre, PhD candidate, Assistant, Department of Civil engineering, Engineering Academy, Peoples' Friendship University of Russia (RUDN University), Moscow, Russian Federation, 117198, Russia, Moscow, Ulitsa Miklukho-Maklaya, 6, Tel +7(495) 434-53-00, e-mail: tesfaldethg@gmail.com

Галишникова Вера Владимировна, доктор технических наук, профессор, проректор, Национальный исследовательский Московский государственный строительный университет (НИУ МГСУ), профессор департамента строительства, Российский университет дружбы народов, Российская Федерация; 129337, Россия, Москва, Ярославское шоссе, 26, тел. +7 (495)025-29-38., e-mail: galishni@yandex.ru

Гебре Тесфалдет Хадгембес, аспирант, ассистент, департамента строительства, Инженерная академия, Российский университет дружбы народов (РУДН), Российская Федерация, 117198, Москва, ул. Миклухо-Маклая, д. 6, тел +7(495) 434-53-00, e-mail: tesfaldethg@gmail.com

DOI:10.22337/2587-9618-2022-18-3-78-85

CONTROL OF A NONLOCAL IN TIME FINITE ELEMENT MODEL OF THE DYNAMIC BEHAVIOR OF A COMPOSITE BEAM BASED ON THE RESULTS OF A NUMERICAL EXPERIMENT

Vladimir N. Sidorov [1,2], Elena P. Detina [1], Elena S. Badina [1,2,3]

[1] Russian University of Transport (MIIT), Moscow, RUSSIA
[2] Moscow State University of Civil Engineering, Moscow, RUSSIA
[3] Institute of Applied Mechanics of Russian Academy of Sciences, Moscow, RUSSIA

Abstract. The article presents numerical methods for controlling the parameters of temporal nonlocality of computer models of rod structures made of composite materials. The finite element method is the most widely used numerical method for solving practical problems of the analysis of mechanical systems. A nonlocal in time internal damping model is integrated into the algorithm of this method. The one-dimensional model of the Euler-Bernoulli beam is presented in the article. The equilibrium equation of a moving mechanical system is solved numerically using an implicit scheme. In the article the damping matrix obtained from the condition of stationarity of the total deformation energy was used. The article presents the study of non-local in time damping model properties. The model is integrated into the finite element method. The non-local model is algorithmized and programmed in the MATLAB software package.

Keywords: nonlocal in time damping, damping with memory, composite material, Euler-Bernoulli beam vibration, equilibrium equation, least squares technique, finite element analysis, iterative implicit scheme, structural dynamics

УПРАВЛЕНИЕ НЕЛОКАЛЬНОЙ ВО ВРЕМЕНИ КОНЕЧНО-ЭЛЕМЕНТНОЙ МОДЕЛЬЮ ДИНАМИЧЕСКОГО ПОВЕДЕНИЯ БАЛКИ ИЗ КОМПОЗИТА ПО РЕЗУЛЬТАТАМ ЧИСЛЕННОГО ЭКСПЕРИМЕНТА

В.Н. Сидоров [1,2], Е.С. Бадьина [1,2,3], Е.П. Детина [2]

[1] Российский университет транспорта (МИИТ), Москва, РОССИЯ
[2] Национальный исследовательский Московский государственный строительный университет, Москва, РОССИЯ
[3] Институт прикладной механики Российской академии наук, Москва, РОССИЯ

Аннотация. В статье представлены численные методики управления параметрами временной нелокальности расчетных моделей стержневых конструкций из композиционных материалов. Нелокальная во времени модель демпфирования интегрирована в алгоритм метода конечных элементов – наиболее широко применяемого численного метода при решении практических задач анализа механических систем. В работе рассматривается одномерная модель балки Эйлера-Бернулли. Численное решение уравнения равновесия расчётной модели конструкции в движении выполняется по неявной схеме. При этом матрица демпфирования получена из условия стационарности полной энергии деформирования движущейся механической системы. В статье приведены результаты исследования нелокальной во времени расчетной модели, реализованной в среде MATLAB.

Ключевые слова: демпфирование нелокальное во времени, демпфирование с памятью, композитный материал, колебания балок Эйлера-Бернулли, уравнение равновесия, метод наименьших квадратов, метод конечных элементов, неявная схема, динамика механических систем

INTRODUCTION

Today, the models of oscillatory processes taking place in mechanical systems can be modeled in various ways. Also the computational mathematical and algorithmic apparatus has been significantly developed. Despite this, scientists devote a special place to the issue of adequate modeling of the damping properties of structures made of structurally complex materials. For example, the papers [1, 2] present ideas of damping kernels created as a linear combination of decreasing functions. In works [3, 4, 5] study the issues of constructing the effective characteristics of a layered composite material, the layers of which are viscoelastic.

In this article, we present the results of modeling of the damping properties of structures made of structurally complex materials, built on the assumption that the material has nonlocal in time properties of internal damping. In [6, 7, 8] the matrix form of the modified equation of motion of mechanical systems was studied:

$$M \cdot \ddot{\bar{V}}(t_{i+1}) + \alpha \cdot D \cdot \dot{\bar{V}}(t_{i+1}) \cdot \\ \cdot (1-\alpha) \cdot \left(\int_{t_0}^{t_i} G(t_i - \tau) \dot{\bar{V}}(\tau) d\tau \right) \cdot \\ \cdot K \cdot \bar{V}(t_{i+1}) = F(t_{i+1}), \tag{1}$$

the integral term endows the classic computational model with the time nonlocality. Here $0 < \alpha < 1$ is the temporal nonlocality weight coefficient [7]; t_0 – initial time of the oscillatory process. Matrices of masses *M*, damping *D* and stiffness *K* of the computer model are developed from the condition of a minimum change in the total energy of a mechanical system deformed in motion [6, 8, 9]. When $\alpha = 1$ – the model preserves the locality of the time component. The function $G(t_i - \tau)$ in equation (1) is usually called the damping kernel function [7]. The Gaussian curve was taken as the damping kernel into a solution:

$$G(t_i - \tau) = e^{-\mu^2 (t_i - \tau)^2} \tag{2}$$

the parameter $\mu > 0$ in (2) characterizes the area of nonlocal properties of the time component, while regardless of the value of μ, $\int_{t_0}^{t} \frac{2\mu}{\sqrt{\pi}} \cdot e^{-\mu^2 (t-\tau)^2} d\tau = 1$; $\tau\,[sec]$ – all moments of time preceding the considered component of the time axis t_i. Reducing the value of the parameter μ increases the level of nonlocality along the time axis of the model. Such a statement of the problem endows the damping forces in the calculation model with the property of "memory" (hereinafter, this property of the model will be called "damping with memory"). Thus, in the numerical calculation of the structure according to the implicit scheme in the term (1), responsible for damping with memory, the values of the rates of change of displacements and deformations are taken into account not only at the previous computational step t_i, but also at all previous time steps up to t_i.

The use of the kernel of the internal damping operator (2) can be attributed to the mathematical idealization of the description of the distribution of the "memory" of the composite in time, which is generally not based on the features of the microstructure of the material. To use the constructed model in practical calculations, it must be calibrated based on the data of a physical or alternative, for example numerical experiment. In this case, the parameter μ in (2) becomes the main control parameter of the considered computational model, which sets the degree of nonlocality.

MODEL CALIBRATION TECHNIQUES

As an example, consider the oscillations of a beam made from the composition material. The beam is rigidly fixed at the edges and loaded with an instantly applied uniformly distributed load. The general physical and mechanical parameters of the design and the values of the momentarily applied load are presented in Table 1.

Table 1

General parameters of a fiberglass vinyl ester beam.
Young's of elasticity [Pa]: E=1720000;
Beam length [m]: L=12;
Material density [t/m^3]: ρ=1.9;
Beam cross-sectional area (constant along the entire length) [m^2]: A=0.06;
Moment of inertia [m^4]: I=4.5000e-04;
Instantaneously applied load [N/m^2]: q=-1.

To emphasize the necessity and benefit of further studies of the nonlocal in time model of damping properties of composite materials, the comparison of the results of equation (1) solution in a local statement (for $\alpha = 1$) with experimental data is presented. The fig.1 shows the time history of vertical displacements of the middle node of the beam. The solid line shows the numerical solution of the problem based on a one-dimensional local in time computational model; dotted line - data obtained as a result of a numerical experiment implemented in the finite element software package SIMULIA Abaqus (structurally complex properties of the composition were taken into account using an orthotropic material model).

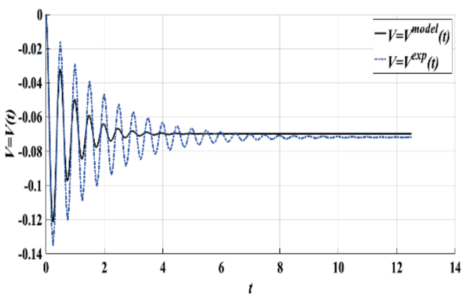

Figure 1. Vertical displacement of the middle node of the oscillating beam made of a composite material: $\bar{V}^{exp}(t)$ – experimental curve; $\bar{V}^{model}(t)$ – is a time-local curve

Based on the simulation results, it was concluded that the computer model, local in time, approximates the (dynamic) oscillatory process inside a structure made of a structurally complex material with a reliability that is not sufficient for further application in design justification process. Calculations using isotropic or local one-dimensional models for composites give a significant error, which is unacceptable in the calculation of such structures subjected to dynamic effects.

The article presents two main approaches (methodologies) to determining the optimal value of the parameter μ for a non-local in time one-dimensional model of the dynamic behavior of a structure made of composite material.

In this work the following indices are used:

$\bar{V}^{exp}(t)$ – displacement vector obtained as a result of a numerical experiment implemented in the software package SIMULIA Abaqus;

$\bar{V}^{model}(t)$ – the displacement vector obtained as a result of solving equation (1), according to the implicit scheme by the modified Newmark method [10];

$v^{synth}(t)$ – a curve synthesizing the values of the displacement vector obtained as a result of a numerical experiment.

$f^{error}(\mu)$ – a sum of squared deviations of vector elements $\bar{V}^{model}(t)$ to $\bar{V}^{exp}(t)$.

Methodology 1. Direct construction of a search model for the optimal nonlocality parameter of the dynamic properties of the composite by the least squares method (LSM).This technique provides an automated search for the value of the parameter μ, in which the sum of the squared deviations $f^{error}(\mu)$ takes the minimum value. Fig. 2 shows the dependency graph $f^{error}(\mu)$, showing the behavior of the non-local model (1) in a fairly wide range of parameter values $1 \leq \mu \leq 200$ (the value of μ was not further increased in this work). In Figure 3, we have localized the range of μ values relative to $f^{error}(\mu)$ smallest value.

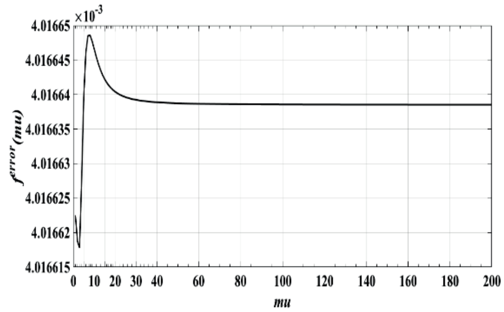

Figure 2. Dependence of f^{error} on μ. The ordinate shows the summation of the squared deviations $f^{error}(\mu)$

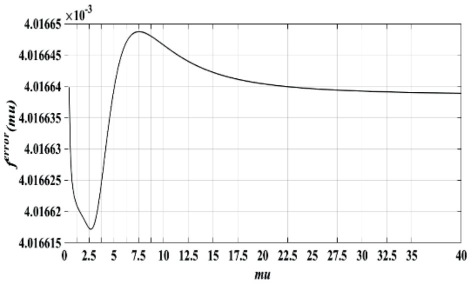

Figure 3. Dependence of f^{error} on μ, localized in the region of extreme values of μ: the abscissa shows the values of the parameter μ in the range $1 \leq \mu \leq 40$, the ordinate shows the sum of squared deviations $f^{error}(\mu)$

As a result of processing the data of the LSM experiment, we obtain $\bar{V}^{model}(t)$ with the minimum value $f^{error}(t)$, corresponding to the value $\mu = 2{,}68601$. Below, in Figure 4, there are two graphs of the vertical displacement of the middle section of an oscillating beam made of composite material: $\bar{V}^{exp}(t)$ – experimental displacement data; $\bar{V}^{model}(t)$ – displacement data based on a calibrated time-nonlocal damping model at $\mu = 2{,}68601$ sec.

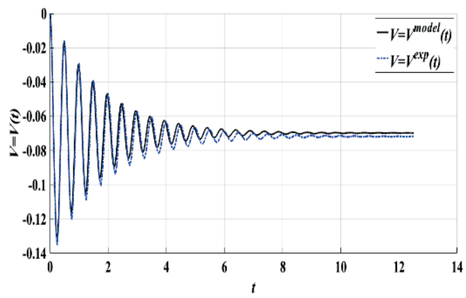

Figure 4. Time history of the composite beam middle node vertical displacement: $\bar{V}^{exp}(t)$ – experimental curve; $\bar{V}^{model}(t)$ – calibrated non-local in time curve at $\mu = 2{,}68601$ sec.

As can be seen from the fig 4., the non-local in time computational model, approximates the oscillatory process of an element made of a structurally complex material with sufficient reliability. The result of the search for the optimal nonlocality parameter value for a one-dimensional composite beam, shows the efficiency of the constructed model. However, this technique seems to be computationally difficult. Below we describe the developed alternative technique, which is simpler both in terms of computational costs and the search for the optimal value of the nonlocality parameter μ for a composite material.

Methodology 2. Search for the optimal value of the nonlocality parameter based on the least squares method using a synthesizing curve.
Under the synthesizing curve, $v^{synth}(t)$, we will mean some analytical (interpolating) curve approximating the experimental data with a satisfactory accuracy, $\bar{V}^{exp}(t)$. Below is an algorithm for constructing an expression for such a curve by the least squares method in the form of the polynomial of the fourth degree:

$$v^{synth}(t) = a_0 + a_1 \cdot t + \\ + a_2 \cdot t^2 + a_3 \cdot t^3 + a_4 \cdot t^4, \qquad (3)$$

$\{a_j\}_{j=1}^{4}$ – the desired polynomial coefficients calculated in comparison with the values of $\bar{V}^{exp}(t)$.
Representing (3) in matrix form, we find the coefficients a_j by the least squares method from the conditions for the minimum sum of squared deviations of the values $\bar{V}^{exp}(t)$ from the desired curve $v^{synth}(t)$:

$$F(a_0, a_1, a_2, a_3, a_4) = \\ = \min \sum_{i=1}^{N} \left(\bar{V}^{exp}(t_i) - v^{synth}(t_i) \right)^2, \qquad (4)$$

N – number of nodes taken along the time axis t.
Below, the minimum condition is expressed in partial derivatives $\frac{\partial F}{\partial a_j}$ equated to zero, written as a system, where $j = 0,1,2,3,4$ – is the number of the required coefficient a_j.

$$\begin{cases} a_4 \cdot \sum_{i=1}^{N} t_i^4 + a_3 \cdot \sum_{i=1}^{N} t_i^3 + a_2 \cdot \sum_{i=1}^{N} t_i^2 + a_1 \cdot \sum_{i=1}^{N} t_i + a_0 \cdot \sum_{i=1}^{N} 1 = \sum_{i=1}^{N} \bar{V}^{exp} \\ a_4 \cdot \sum_{i=1}^{N} t_i^5 + a_3 \cdot \sum_{i=1}^{N} t_i^4 + a_2 \cdot \sum_{i=1}^{N} t_i^3 + a_1 \cdot \sum_{i=1}^{N} t_i^2 + a_0 \cdot \sum_{i=1}^{N} t_i = \sum_{i=1}^{N} \bar{V}^{exp} \cdot t_i \\ a_4 \cdot \sum_{i=1}^{N} t_i^6 + a_3 \cdot \sum_{i=1}^{N} t_i^5 + a_2 \cdot \sum_{i=1}^{N} t_i^4 + a_1 \cdot \sum_{i=1}^{N} t_i^3 + a_0 \cdot \sum_{i=1}^{N} t_i^2 = \sum_{i=1}^{N} \bar{V}^{exp} \cdot t_i^2 \\ a_4 \cdot \sum_{i=1}^{N} t_i^7 + a_3 \cdot \sum_{i=1}^{N} t_i^6 + a_2 \cdot \sum_{i=1}^{N} t_i^5 + a_1 \cdot \sum_{i=1}^{N} t_i^4 + a_0 \cdot \sum_{i=1}^{N} t_i^3 = \sum_{i=1}^{N} \bar{V}^{exp} \cdot t_i^3 \\ a_4 \cdot \sum_{i=1}^{N} t_i^8 + a_3 \cdot \sum_{i=1}^{N} t_i^7 + a_2 \cdot \sum_{i=1}^{N} t_i^6 + a_1 \cdot \sum_{i=1}^{N} t_i^5 + a_0 \cdot \sum_{i=1}^{N} t_i^4 = \sum_{i=1}^{N} \bar{V}^{exp} \cdot t_i^4 \end{cases}$$

Here t_i – time coordinate; N – the number of points taken on the time axis. The system of equations (4) is represented in matrix form:

$$Koef \cdot \bar{a} = \bar{s}, \tag{5}$$

Then

$$Koef = \begin{pmatrix} \sum_{i=1}^{N} t_i^4 & \cdots & \sum_{i=1}^{N} 1 \\ \vdots & \ddots & \vdots \\ \sum_{i=1}^{N} t_i^8 & \cdots & \sum_{i=1}^{N} t_i^4 \end{pmatrix},$$

$$\bar{a} = \begin{pmatrix} a_0 \\ \vdots \\ a_4 \end{pmatrix}, \tag{6}$$

$$\bar{s} = \begin{pmatrix} \sum_{i=1}^{N} \bar{V}^{exp}(t_i) \\ \vdots \\ \sum_{i=1}^{N} \bar{V}^{exp}(t_i) \cdot t_i^4 \end{pmatrix},$$

as well as the solution of equation (5):

$$\bar{a} = Koef^{-1} \cdot \bar{s}, \tag{7}$$

The Fig. 5 graphically presents a comparison of the experimental values of dynamic vertical displacements of the middle node of the beam FE model $\bar{V}^{exp}(t)$, with the displacement values obtained using the synthesizing curve $v^{synth}(t)$.

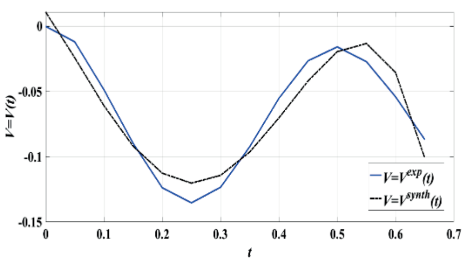

Figure 5. Graphical comparison of the numerical experimental values of the middle node vertical displacements $\bar{V}^{exp}(t)$, with the displacement values obtained using the synthesizing curve $v^{synth}(t)$ for the time period $T = 0.65$ sec.

The Fig. 5 shows some difference between the values of the experiment and the model values, which indicates the possibility of developing the presented methodology by clarifying the appropriate type of curve.

The main advantage of using the synthesizing curve lies in the "simplicity" of its further application in identifying the optimal value of the temporal nonlocality parameter of the model μ. This is also determined by the fact that the derivatives of such a synthesizing function can be represented as a functional dependence. This greatly simplifies the calculation and results analysis at the model calibration stage.

Let us substitute the expressions of the synthesizing curve $v^{synth}(t_i)$ and its derivatives $v'^{\,synth}(t_i), v''^{\,synth}(t_i)$ of the first and second order into equation (1):

$$\begin{gathered} M \cdot \left(12a_4t_i^2 + 6a_3t_i + 2a_2\right) + \\ +\alpha \cdot D \cdot \left(4a_4t_i^3 + 3a_3t_i^2 + 2a_2t_i + a_1\right) + \\ +(1-\alpha) \cdot D \cdot \int \frac{2\mu}{\sqrt{\pi}} e^{-\mu^2(t_i-\tau)^2} \cdot (4a_4(t_i - \\ \tau)^3 + 3a_3(t_i-\tau)^2 + 2a_2(t_i-\tau) + \\ +a_1)d\tau + K \cdot \left(a_4t_i^4 + a_3t_i^3 + a_2t_i^2 + \right. \\ \left. +a_1t_i + a_0\right) = F(t_i). \end{gathered} \tag{8}$$

Now we transform equation (8) in such a way that the terms containing the desired parameter μ, are located to the left side, and those free from it are to the right:

$$\begin{gathered} \frac{(1-\alpha)2\mu}{\sqrt{\pi}} \cdot D \cdot \int_{t_0}^{t_i} e^{-\mu^2(t_i-\tau)^2} \left(4a_4(t_i-\tau)^3 + \right. \\ \left. +3a_3(t_i-\tau)^2 + 2a_2(t_i-\tau) + a_1\right)d\tau = \\ = F(t_i) - M \cdot \left(12a_4t_i^2 + 6a_3t_i + 2a_2\right) - \\ -\alpha \cdot D \cdot \left(4a_4t_i^3 + 3a_3t_i^2 + 2a_2t_i + a_1\right) - \\ -K \cdot \left(a_4t_i^4 + a_3t_i^3 + a_2t_i^2 + a_1t_i + a_0\right). \end{gathered} \tag{9}$$

Let us denote in (9) by $R(t_i)$ the "effective load" vector calculated for the i moment of time:

$$\begin{gathered} R(t_i) = F(t_i) - \\ -M \cdot \left(12a_4t_i^2 + 6a_3t_i + 2a_2\right) - \\ -\alpha D \cdot \left(4a_4t_i^3 + 3a_3t_i^2 + 2a_2t_i + a_1\right) - \\ -K \cdot \left(a_4t_i^4 + a_3t_i^3 + a_2t_i^2 + a_1t_i + a_0\right). \end{gathered} \tag{10}$$

Then the total effective load vector will look like:

$$R = \sum_{i=1}^{N} R(t_i). \tag{11}$$

Now we denote by $Z(\mu, t_i)$, the integral operator in (8) - (9), calculated for the i-th moment of time and containing the nonlocality parameter of the model μ:

$$Z(\mu, t_i) = \int_{t_0}^{t_i} e^{-\mu^2 (t_i-\tau)^2} (4a_4(t_i-\tau)^3 + +3a_3(t_i-\tau)^2 + 2a_2(t_i-\tau) + a_1) d\tau, \tag{12}$$

τ – time parameter characterizing the moments of time preceding the moment t_i.
Then the total integral operator takes the form:

$$Z(\mu) = \sum_{i=1}^{N} Z(\mu, t_i). \tag{13}$$

Substituting expressions (11) and (13) into (9), we obtain an equation for an unknown quantity (the nonlocality parameter of the model μ):

$$\frac{2\mu}{\sqrt{\pi}} \cdot Z(\mu) = \frac{1}{1-\alpha} \cdot D^{-1} \cdot R. \tag{14}$$

The solution of equation (14) is algorithmized and performed in accordance with the stated method 2 and programmed in MATLAB. As a result of the numerical solution (14), we obtained the value of the nonlocality parameter in the middle node of the composite beam, equal to $\mu = 2.78328$ sec. Figure 6 shows a graph of the values of the vector $\bar{V}^{model}(t)$, of to $\mu = 2.78328$ sec, in comparison with the experimental values $\bar{V}^{exp}(t)$.

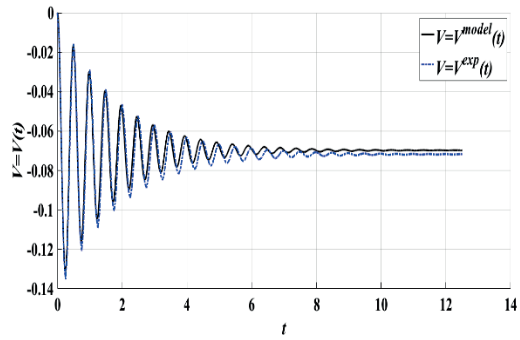

Figure 6. Vertical displacement of the composite beam middle node: $\bar{V}^{exp}(t)$ – experimental curve; $\bar{V}^{model}(t)$ – calibrated non-local in time curve at $\mu = 2.78328$ sec.

In Table 2 comparison of the calibration results of the non-local model by the two methods described with the results of the local model is presented. The average relative error is calculated by the formula $\frac{100\%}{N} \cdot \sum_{i=1}^{N} \left| \frac{\bar{V}^{exp}(t_i) - \bar{V}^{model}(t_i)}{\bar{V}^{exp}(t_i)} \right|$, where N=251 – is the number of nodal points taken along the time axis.

Table 2.

	The value of the non-locality parameter μ, [sec]	Relative calculation error, [%]
Local model	-	44,08
Non-local model calibrated by methodology 1	2.68601	4.52
Non-local model calibrated by methodology 2	2.78328	4.52

CONCLUSION

A non-local damping model applied to dynamic calculations of structures made of composite materials gives a result with a smaller relative calculation error in comparison with the experimental results than a local one.

Two techniques have been developed for controlling a non-local model of nonlocal in time damping properties according to experimental data. Those techniques are presented in the article on the example of a specific composite sample analysis. When rounding the error to a hundredth of a percent, both techniques give a result with the same reliability of calculations. To date, technique 1 seems to be basic, while technique 2 is more promising in terms of algorithmization of the process of modeling the temporal nonlocality of damping properties of composite materials. The choice of synthesizing curves suitable for real experimental data is a matter for a separate study.

ACKNOWLEDGEMENT

This research has been supported by the Russian Science Foundation (Project No 21-19-00634).

REFERENCES

1. **Oleynik O.A., Shamaev A.S., Yosifian G.A.**, 1992, Mathematical Problems in Elasticity and Homogenization. Elsevier, North-Holland.
2. **Bardzokas D.I., Zobnin A.I.**, 2003, Mathematical Modelling of Physical Processes in Composite Materials of Periodical Structures. URSS, Moscow.
3. **Shamaev A.S., Shumilova V.V.**, 2016, Asymptotic behavior of the spectrum of one-dimensional vibrations in a layered medium consisting of elastic and kelvin–voigt viscoelastic materials. Proceedings of the Steklov Institute of Mathematics 295(1), 202-212.
4. **Shamaev A. S., Shumilova V. V.**, 2016, Homogenization of the equations of state for a heterogeneous layered medium consisting of two creep materials. Proceedings of the Steklov Institute of Mathematics 295(1), 213-224.
5. **Yang X.J.**, 2019, General Fractional Derivatives: Theory, Methods and Applications. CRC Press, New York.
6. **Sidorov V.N., Badina E.S**, 2021, The Finite Element Method in Problems of Stability and Vibrations of Bar Structures. Examples of calculations in Mathcad and MATLAB. ASV Publishing House, Moscow.
7. **Sidorov V.N., Badina E.S**, 2021, Non-local damping models in dynamic calculations of structures made of composite materials. Civil engineering, №. 9, p. 66-70.
8. **Sidorov V.N., Badina E.S., Detina E.P.**, 2021, Nonlocal in time model of material damping in composite structural elements dynamic analysis. International Journal for Computational Civil and Structural Engineering, 17(4):14-21.
9. **Zenkevich O.**, 1975, Finite element methods in engineering. Mir, Moscow.
10. **Bathe K. J., Wilson E.L.,** 1976, Numerical methods in finite element analysis. Prentice Hall, New York.

СПИСОК ЛИТЕРАТУРЫ

1. **Oleynik O.A., Shamaev A.S., Yosifian G.A.**, 1992, Mathematical Problems in Elasticity and Homogenization. Elsevier, North-Holland.
2. **Bardzokas D.I., Zobnin A.I.**, 2003, Mathematical Modelling of Physical Processes in Composite Materials of Periodical Structures. URSS, Moscow.
3. **Shamaev A.S., Shumilova V.V.**, 2016, Asymptotic behavior of the spectrum of one-dimensional vibrations in a layered medium consisting of elastic and kelvin–voigt viscoelastic materials. Proceedings of the Steklov Institute of Mathematics 295(1), 202-212.
4. **Shamaev A. S., Shumilova V. V.**, 2016, Homogenization of the equations of state for a heterogeneous layered medium consisting of two creep materials. Proceedings of the Steklov Institute of Mathematics 295(1), 213-224.

5. **Yang X. J.,** 2019, General Fractional Derivatives: Theory, Methods and Applications. CRC Press, New York.
6. **Сидоров В.Н., Бадьина Е.С.**, 2021, Метод конечных элементов в задачах устойчивости и колебаний стержневых конструкций. Примеры расчетов в Mathcad и MATLAB. Издательство АСВ, Москва.
7. **Сидоров В.Н., Бадьина Е.С.**, 2021, Нелокальные модели демпфирования в динамических расчетах конструкций из композитных материалов. Промышленное и гражданское строительство, №. 9, р. 66-70.
8. **Sidorov V.N., Badina E.S., Detina E.P.**, 2021, Nonlocal in time model of material damping in composite structural elements dynamic analysis. International Journal for Computational Civil and Structural Engineering, 17(4):14-21.
9. **Зенкевич О.**, 1975, Метод конечных элементов в технике. Мир, Москва.
10. **Bathe K. J., Wilson E.L.,** 1976, Numerical methods in finite element analysis. Prentice Hall, New York.

Vladimir N. Sidorov, Corresponding Member of Russian Academy of Architecture and Construction Science, Professor, Dr.Sc, Head of the Department of Computer Science and Applied Mathematics, National Research University Moscow State University of Civil Engineering, Professor of «Building Structures, Buildings and Facilities» Department, Institute of Railway Track, Construction and Structures, Russian University of Transport (MIIT), Professor of Department «Engineering Structures and Numerical Mechanics», Perm National Research Polytechnic University; 127994, Russia, Moscow, Obraztsova st., 9, b. 9, phone: +74956814381, e-mail: sidorov.vladimir@gmail.com.

Elena S. Badina, Ph.D, Associate Professor of «Computer Aided Design» Department, Institute of Railway Track, Construction and Structures, Russian University of Transport (MIIT), Senior Researcher at the Scientific and Educational Center for Computer Modeling of Unique Buildings, Structures and Complexes of the Moscow State University of Civil Engineering, Senior Researcher at the Department of Mechanics of Structured and Heterogeneous Environment of the Institute of Applied Mechanics of the Russian Academy of Sciences;
127994, Russia, Moscow, Obraztsova st., 9, b. 9, phone: +74956092116, e-mail: shepitko-es@mail.ru.

Elena P. Detina, Research Engineer, Department of Analytical Fundamental Scientific Research on the Dynamics of Building Structures, Scientific and Educational Center for Computer Modeling of Unique Buildings, Structures and Complexes (REC KM), Lecturer at the Department of Applied Mathematics and Informatics, Moscow State University of Civil Engineering (NRU MGSU); 129337, Russia, Moscow, Yaroslavskoe shosse, 26, phone +74957819988, e-mail: detinaep@mgsu.ru

Сидоров Владимир Николаевич, член-корреспондент РААСН, профессор, доктор технических наук, заведующий кафедрой информатики и прикладной математики Национального исследовательского Московского государственного строительного университета, профессор кафедры «Строительные конструкции, здания и сооружения» Института пути, строительства и сооружений Российского университета транспорта (МИИТа); 127994, Россия, г. Москва, ул. Образцова, д.9, стр. 9, телефон: +74956814381, e-mail: sidorov.vladimir@gmail.com.

Бадьина Елена Сергеевна, кандидат технических наук, доцент кафедры «Системы автоматизированного проектирования» Института пути, строительства и сооружений Российского университета транспорта (МИИТа), старший научный сотрудник Научно-образовательного центра компьютерного моделирования уникальных зданий, сооружений и комплексов Московского государственного строительного университета, старший научный сотрудник Отдела механики структурированной и гетерогенной среды Института прикладной механики Российской академии наук,
127994, Россия, г. Москва, ул. Образцова, д.9, стр. 9, телефон: +74956092116, e-mail: shepitko-es@mail.ru.

Детина Елена Петровна, инженер-исследователь отдела аналитических фундаментальных научных исследований по динамике строительных конструкций Научно-образовательного центра компьютерного моделирования уникальных зданий, сооружений и комплексов (НОЦ КМ), преподаватель кафедры Прикладной математики и информатики Московского государственного строительного университета (НИУ МГСУ); 129337, Россия, г. Москва, Ярославское шоссе, д. 26, телефон +74957819988, e-mail: detinaep@mgsu.ru

DOI:10.22337/2587-9618-2022-18-3-86-94

ANALYSIS OF THE FILTRATION PROBLEM BY BITWISE SEARCH METHOD

Liudmila I. Kuzmina [1], Yuri V. Osipov [2], Maxim D. Astakhov [2]

[1] HSE University, Moscow, RUSSIA
[2] Moscow State University of Civil Engineering, Moscow, RUSSIA

Abstract. During the construction of ground and underground structures, filtration of a liquid grout in loose soil makes it possible to strengthen the foundation and create underground waterproof partitions. A one-dimensional problem of filtering a bidisperse suspension in a homogeneous porous medium with size-exclusion particle capture mechanism is considered. The article is devoted to the calculation of the exact solution of the problem given as the upper limit of the integral with a singularity. The proposed bitwise search method for calculating integrals makes it possible to smooth out fluctuations of the solution near the singularity. Partial and total retention profiles are analyzed.

Keywords: deep bed filtration, bidisperse suspension, retention profiles, exact solution, bitwise search method

ИССЛЕДОВАНИЕ ЗАДАЧИ ФИЛЬТРАЦИИ МЕТОДОМ ПОРАЗРЯДНОГО ПОИСКА

Л.И. Кузьмина [1], Ю.В. Осипов [2], М.Д. Астахов [2]

[1] Национальный исследовательский университет «Высшая школа экономики», Москва, РОССИЯ
[2] Национальный исследовательский Московский государственный строительный университет, Москва, РОССИЯ

Аннотация. При строительстве наземных и подземных сооружений фильтрация жидкого раствора укрепителя в рыхлом грунте позволяет укрепить фундамент и создавать подземные водонепроницаемые перегородки. Рассматривается одномерная задача фильтрации бидисперсной суспензии в однородной пористой среде с размерным механизмом захвата частиц. Статья посвящена вычислению точного решения задачи, заданного в виде верхнего предела интеграла с особенностью. Предлагаемый метод поразрядного поиска для вычисления интегралов позволяет сгладить колебания решения вблизи особенности. Исследуются частичные и полные профили концентрации осажденных частиц.

Ключевые слова: глубинная фильтрация, бидисперсная суспензия, профили осадка, точное решение, метод поразрядного поиска

1. INTRODUCTION

Filtration problems are relevant for many areas of science and technology. In construction problems, modeling the filtration of the smallest particles in a porous medium allows one to study the properties of soils and analyze the possibilities of strengthening loose soil to create a solid foundation [1–4].

The carrier fluid flows through the porous medium and carries the fine solids of suspension. During the filtration process, some particles are retained and form a deposit. There are many different mechanisms of particle capture, which are determined by the physicochemical properties of the porous medium, liquid, and suspension particles, as well as the geometry of the porous structure [5–7]. If the particle sizes and pore cross sections are of the same order, the prevailing particle capture mechanism is size-exclusion: suspended particles are transported through wide pores and get stuck at the entrance of narrow pores [8–10]. Suppose that the Newtonian fluid is incompressible, the suspended particles move at the same speed as the carrier fluid, the retained particles are stationary and cannot be knocked out of the porous frame by the fluid or suspended particles. The standard one-dimensional mathematical model of filtration of a monodisperse suspension in a homogeneous porous medium includes the balance equation for the masses of suspended and retained particles and the kinetic equation for the growth of the particles retained concentration [11–14]. The equations are considered in a dimensionless form: the concentrations of suspended and retained particles are normalized by dividing by the concentration of the suspension at the inlet of the porous medium, the length of the porous sample is taken as a unit, and the unit of time is the period of passage of a suspended particle through the porous medium from inlet to outlet. The dimensionless velocity of particles and carrier fluid is equal to 1.

When filtering in a porous medium, the deposit is unevenly distributed. The distribution of retained particles is given by the retention profile - the concentration of deposited particles at a fixed time, which depends on the coordinate. For a monodisperse suspension, the retention profile decreases monotonically: it is maximum at the inlet of the porous medium and minimum at the outlet.

If the suspension contains suspended particles of two different sizes, then the mass balance and kinetic equations of deposit growth are written separately for each type of particles. The connection between the equations for different particles is carried out by a single filtration function, which is included in both kinetic equations and depends on a linear combination of partial retained concentrations. When filtering a bidisperse suspension, the profile of large particles decreases monotonically, while the profile of small particles is nonmonotone: near the inlet of a porous medium, the profile increases, reaches a maximum, and then decreases monotonically. As time increases, the maximum point moves away from the inlet. The monotonicity or nonmonotonicity of the total retention profile depends on the model parameters. The retention profiles of a bidisperse suspension were studied numerically in [15, 16], and an analytical solution was obtained in [17].

Filtration problems, as a rule, do not have an exact analytical solution. In many works devoted to the numerical solution of filtration problems, the finite difference method is used [18–20]. Calculation using an explicit difference scheme allows you to quickly make calculations, but the presence of discontinuities significantly complicates finding a solution. If an exact solution in an implicit closed form or its asymptotics is known, it is used to numerically calculate the solution in an explicit form [21, 22]. For the problem of filtering a bidisperse suspension in a porous medium, an exact implicit solution is obtained. The solution is given in the form of integrals with variable limits, the integrand has a singularity. Finding the value of the integral near the singularity is a difficult computational problem. In this article, bitwise search method for calculation of a solution is used [23]. This method makes it possible to smooth out fluctuations in the solution that arise when calculating integrals with singularities using standard methods. The results of calculations for solving the filtration problem by the standard method and by the bitwise search method are presented. The profiles of the total retained concentration and partial retained concentrations of particles of the same size are obtained and analyzed.

2. MATHEMATICAL MODEL

In the domain $\Omega = \{x \ge 0,\ t \ge 0\}$ consider the system

$$\frac{\partial c_i}{\partial t} + \frac{\partial c_i}{\partial x} + \frac{\partial s_i}{\partial t} = 0, \qquad (1)$$

$$\frac{\partial s_i}{\partial t} = (1-b)\lambda_i c_i,\ b = B_1 c_1^0 s_1 + B_2 c_2^0 s_2,\ \ i = 1,2\,. \qquad (2)$$

Here λ_i, B_i, c_i^0 are positive constants, $\lambda_1 > \lambda_2$, $c_1^0 + c_2^0 = 1$. The unknowns c_i, s_i, $i = 1,2$ are the suspended and retained particles concentrations, respectively, b is the concentration of occupied sites, B_i is the individual area that an attached particle occupies at the rock surface, and c_i^0 are the particle concentrations in the injected suspension.

For the uniqueness of the solution of problem (1), (2), the conditions are set at the inlet of the porous medium and at the initial moment:

$$x = 0 : c_i = c_i^0, \ \ t = 0 : c_i = 0, \ s_i = 0, \ i = 1,2. \quad (3)$$

The solutions $c_1(x,t)$, $c_2(x,t)$ have a discontinuity on the characteristic line $t = x$, because the initial and boundary conditions do not match at the origin. The line $t = x$ is the concentration front Γ of the suspended and retained particles which divides the interior of the domain Ω into two zones. In the domain $\Omega_0 = \{x > 0,\ 0 < t < x\}$ the problem has a zero solution; in the domain $\Omega_1 = \{x > 0,\ t > x\}$ the solution is positive. In the domain Ω_1 the solutions $c_1(x,t)$, $c_2(x,t)$ are related by the formulae

$$c_1 = c_1^0 \left(\frac{c_2}{c_2^0} \right)^{\lambda_1/\lambda_2}, \quad c_2 = c_2^0 \left(\frac{c_1}{c_1^0} \right)^{\lambda_2/\lambda_1} \quad (4)$$

and are given in implicit form

$$\begin{aligned} &\int_{c_1^-}^{c_1} \frac{dc}{c\left(B_1 c_1^0 (c_1^0 - c) + B_2 c_2^0 \left(c_2^0 - c_2^0 \left(\frac{c}{c_1^0} \right)^{\lambda_2/\lambda_1} \right) \right)} = \lambda_1 (t - x), \\ &\int_{c_2^-}^{c_2} \frac{dc}{c\left(B_1 c_1^0 \left(c_1^0 - c_1^0 \left(\frac{c}{c_2^0} \right)^{\lambda_1/\lambda_2} \right) + B_2 c_2^0 \left(c_2^0 - c \right) \right)} = \lambda_2 (t - x), \end{aligned} \quad (5)$$

where

$$c_i^- = c_i(x,x) = c_i^0 e^{-\lambda_i x} \quad (6)$$

is the solution on the concentration front Γ.

For known $c_1(x,t)$, $c_2(x,t)$ concentrations of retained particles are given by the formula

$$s_i = \frac{c_i - c_i^-}{B_1 c_1^0 (c_1^0 - c_1^-) + B_2 c_2^0 (c_2^0 - c_2^-)}, \quad i = 1,2. \quad (7)$$

In particular, at the inlet $x = 0$ solution (7) takes the form

$$\begin{aligned} &s_i^0(t) = \frac{\lambda_i c_i^0}{B} (1 - e^{-Bt}), \quad i = 1,2, \\ &B = \lambda_1 B_1 (c_1^0)^2 + \lambda_2 B_2 (c_2^0)^2. \end{aligned} \quad (8)$$

Consider the properties of retention profiles given by formula (7) at fixed time *t*.

- The partial retention profile $s_1(x,t)$ decreases monotonically for all $t > x$;
- The partial retention profile $s_2(x,t)$ decreases monotonically for $x < t < t_0$ and increases monotonically for $t > t_0$;
-The total retention profile $s(x,t)$ decreases monotonically for all $t > x$ if $B_1 c_1^0 < B_2 c_2^0$; decreases monotonically at $x < t < T_0$ and increases monotonically at $t > T_0$ if $B_1 c_1^0 > B_2 c_2^0$.

So, any non-monotonic retention profile has a maximum point. As time increases, the maximum point shifts from the inlet of the porous medium.

3. BITWISE SEARCH METHOD

Obtained exact solution makes it possible to perform calculations using formulae (5) without a numerical solution of the original problem (1)–(3). Calculation of the implicit solution – the upper limit of integration in integrals (5) was performed by the bitwise search method [24, 25]. Finding the solution numerically is complicated by the fact that the upper limit of integration is close to the singularity of the integrand. Calculations by standard methods lead to oscillations of the solution and increase of an error, since the derivative solutions are limited. To obtain a smooth solution, the bitwise search method was chosen as one of the direct search methods that does not use derivatives in calculations. With a large error in calculating the values of the function, the bitwise search method makes it possible to avoid an excessive number of iterations.

The profile is constructed by calculating the profiles of suspended particles concentrations $c_1(x,t)$, $c_2(x,t)$ at each point of the porous medium at a fixed time *t*. Formulae (4) set a relation for concentrations and make it possible to implement two approaches to computation of a solution. You can use one profile as a basic one, calculating it by formula (5), and obtain the second profile algebraically by formula (4). If we calculate both profiles by formulae (5), algebraic formulae (4) can be used to check the accuracy of the solutions found.

The input parameters of the program are:

- x_step – step by x,
- t – time for which the solution profile is calculated,
- accuracy – obtained accuracy of the solution c_n,
- *calc* – list of profiles, which are calculated by formulae (5).

Denote the following variables:

- $Need_n$ – the right side of equation (5), the value of the integral,
- *Depth* – the current bit of the search for c_n, called the search depth,
- S – the calculated value of the integral at the current iteration,
- Res_n – the last obtained profile value,
- *Best* – a pair of variables:
    - *Best*[0] = *Delta* – deviation between the values of the integral *S* and *Need*,
    - *Best*[1] = c_n – the calculated solution,
- Plus – flag storing the search direction:
    - true (1) – in the direction of increase of c_n,
    - false (0) – in the direction of decrease of c_n.

The first step is to calculate the right side $Need_n = \lambda_n(t-x)$ of the integral (5), then the condition $Need > 0$ is checked, which means that the solution behind the front $t > x$ is positive. If $Need \le 0$, the point *x* belongs to the front and $c_n = c_n^-$. Otherwise, we proceed to the calculation for one of the basic profiles.

The search depth (Depth) for the next step in *x* is calculated using the linear interpolation formula

$$Depth = -\log_{10}\left|Res_n - c_n\right| - 1 .$$

The search depth determines in which bit the next value of c_n can be obtained, and reduce the number of iterations of the algorithm.

Then it is checked that the upper integration limit cannot be less than the lower one: $Res_n \ge c_n^-$, otherwise $Res_n = c_n^-$.

The condition $Res_n \le c_n^0$ is also checked, which means that the concentration cannot exceed the initial concentration of the suspension, otherwise $Res_n = c_n^-$.

Let's start the calculation of c_n at a given point *x*, setting Res_n as the initial value. The algorithm includes the following steps.

1. Calculate the integral on the left side of formula (5) with the current value c_n using the Simpson method.
2. Calculate $Delta = \left|S - Need\right|$.

3. If $Delta \le Best[0]$, then $Best = \{Delta, c_n\}$.
4. If $Delta \le 10^{-(accuracy)}$, then the value of the integral is found with the required accuracy, go to step 1 with the next value of x.
5. If $S > Need$ and Plus = true, change the search direction (Plus = false) and increase the search bit (Depth +=1).
6. If $S < Need$ and Plus = false, change the search direction (Plus = true) and increase the search bit (Depth +=1).
7. If $Depth > accuracy$, then the specified accuracy of the solution is reached, go to step 1 with the next value of x.
8. Let's take the next step $\begin{cases} c_n = c_n + 10^{-Depth}, \text{ if } Plus = false, \\ c_n = c_n - 10^{-Depth}, \text{ if } Plus = true. \end{cases}$
9. Check that the value of c_n does not go beyond the limits of the interval $[c_n^-, c_n^0]$.

If $c_n \notin [c_n^-, c_n^0]$, then take a step back $\begin{cases} c_n = c_n - 10^{-Depth}, \text{ if } Plus = false, \\ c_n = c_n + 10^{-Depth}, \text{ if } Plus = true. \end{cases}$, and increase Depth +=1, then return to step 8.

10. Increase x by one step and go to step 1.

At the end of the loop, the result of the calculation is Best[1].

Dependent profile is calculated by formula (4).

If both profiles were calculated by formulae (5), then with the help of (4) the calculation error is determined - the discrepancy between the values of the same profiles is calculated.

4. NUMERICAL SIMULATION

Figure 1 shows the profiles of partial and total concentration of retained particles at different time for the parameters $\lambda_1 = 25$, $\lambda_2 = 5$, $B_1 = 0.125$, $B_2 = 0.025$, $c_1^0 = 0.5$, $c_2^0 = 0.5$.

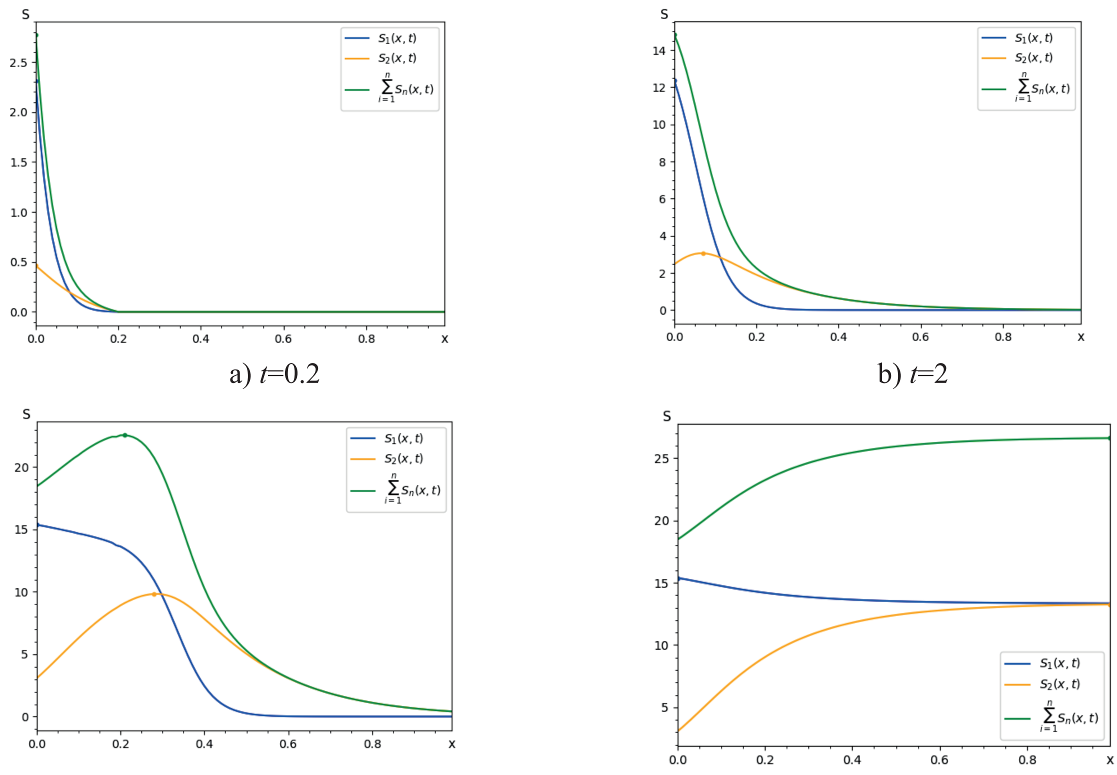

a) t=0.2 b) t=2

c) t=10 d) t=40

Figure 1. Retained concentration profiles

According to Fig. 1 profiles of large and small particles are separated at a long time. Large particles are mainly deposited near the inlet of the porous medium, while small particles are deposited near the outlet. The monotonicity of the total sediment profile depends on the parameters of the problem.

The graphs of solutions obtained without the procedure for smoothing oscillations have kinks and oscillating nonmonotonic sections that are unacceptable in smooth solutions (Fig. 2).

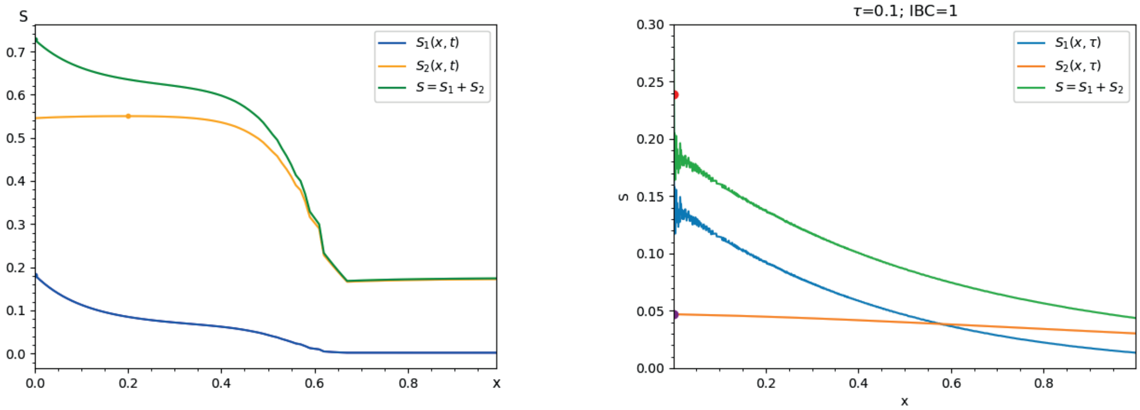

Figure 2. Unacceptable non-smooth retention profiles

5. CONCLUSION

For the filtration model of bidisperse suspension in a homogeneous porous medium

- Implicit exact solutions are found in the form of integrals with singularities.
- Bitwise search method is used to calculate the smoothed solution.
- The algorithm of the bitwise search method is described.
- Smooth numerical solutions are obtained.
- Retention profiles of total and partial deposit concentrations are constructed.

REFERENCES

1. **Zhou Z., Zang H., Wang S., Du X., Ma D., Zhang J.** Filtration Behavior of Cement-Based Grout in Porous Media // Transport in Porous Media, 2018, vol. 125, pp. 435–463.
2. **Tsuji M., Kobayashi S., Mikake S., Sato T., Matsui H.** Post-Grouting Experiences for Reducing Groundwater Inflow at 500 m Depth of the Mizunami Underground Research Laboratory, Japan // Procedia Engineering, 2017, vol. 191, pp. 543–550.
3. **Zhu G., Zhang Q., Liu R., Bai J., Li W., Feng X.** Experimental and Numerical Study on the Permeation Grouting Diffusion Mechanism considering Filtration Effects // Geofluids, 2021, 6613990.
4. **Wang X.; Cheng H.; Yao Z.; Rong C.; Huang X.; Liu X.** Theoretical Research on Sand Penetration Grouting Based on Cylindrical Diffusion Model of Tortuous Tubes // Water, 2022, vol. 14, 1028, pp. 1-15.
5. **Ramachandran V., Fogler H.S.** Plugging by hydrodynamic bridging during flow of stable colloidal particles within cylindrical pores // Journal of Fluid Mechanics, 1999, vol. 385, pp. 129–156.
6. **Rabinovich A., Bedrikovetsky P., Tartakovsky D.** Analytical model for gravity segregation of horizontal multiphase flow in porous media // Physics of Fluids, 2020, vol. 32(4), pp. 1–15.
7. **Tartakovsky D.M., Dentz M.** Diffusion in Porous Media: Phenomena and Mechanisms // Transport in Porous Media, 2019, vol. 130, pp. 105–127.

8. **Elimelech M., Gregory J., Jia X., Williams, R.** Particle deposition and aggregation: measurement, modelling, and simulation, revised ed., Butterworth-Heinemann, New-York, 2013.
9. **Santos A., Bedrikovetsky P.** Size exclusion during particle suspension transport in porous media: stochastic and averaged equations // Computational and Applied Mathematics, 2004, vol. 23(2-3), pp. 259–284.
10. **Kuzmina L.I, Osipov Yu.V., Zheglova Yu.G.** Analytical model for deep bed filtration with multiple mechanisms of particle capture // International Journal of Non-Linear Mechanics, 2018, vol. 105, pp. 242–248.
11. **Herzig J.P., Leclerc, D.M., Goff, P.Le.** Flow of suspensions through porous media—application to deep filtration // Industrial & Engineering Chemistry Research, 1970, vol. 62(8), pp. 8–35.
12. **Kuzmina L.I., Osipov Y.V., Gorbunova T.N.** Asymptotics for filtration of polydisperse suspension with small impurities // Applied Mathematics and Mechanics (English Edition), 2021, vol. 42(1), pp. 109–126.
13. **Nazaikinskii V.E., Bedrikovetsky P.G., Kuzmina L.I., Osipov, Y.V** Exact solution for deep bed filtration with finite blocking time. // SIAM Journal on Applied Mathematics, 2020, vol. 80(5), pp. 2120–2143.
14. **Safina G.**L. Filtration problem with nonlinear filtration and Concentration functions. // International Journal for Computational Civil and Structural Engineering, 2022, vol. 18(1), pp. 129–140.
15. **Malgaresi, G., Collins, B., Alvaro, P., Bedrikovetsky, P.** Explaining non-monotonic retention profiles during flow of size-distributed colloids // Chemical Engineering Journal, 2019, vol. 375, 121984.
16. **Safina G.L.** Calculation of retention profiles in porous medium // Lecture Notes in Civil Engineering, 2021, vol. 170, pp. 21–28.
17. **Kuzmina L.I., Osipov Yu.V., Astakhov M.D.** Filtration of 2-particles suspension in a porous medium // Journal of Physics: Conference Series, 2021, vol. 1926, 012001.
18. **Osipov Yu., Safina G., Galaguz Yu.** Calculation of the filtration problem by finite differences methods // MATEC Web Conference, 2018, vol. 251(3), 04021.
19. **Safina G.L.** Numerical solution of filtration in porous rock // E3S Web of Conferences, 2019, vol. 97, 05016.
20. **Galaguz Yu., Safina G.** Modeling of fine migration in a porous medium // MATEC Web Conference, 2016, vol. 86, 03003.
21. **Kuzmina L.I., Osipov Yu.V.** Asymptotics of the filtration problem with almost constant coefficients // International Journal for Computational Civil and Structural Engineering, 2021, vol. 17(2), pp. 43–49.
22. **Kuzmina L.I., Osipov Yu.V.** Determining the Lengmur coefficient of the filtration problem // International Journal for Computational Civil and Structural Engineering, 2020, vol. 16(4), pp. 48–54.
23. **Knuth D.E.** The Art of Computer Programming, vol.3. Sorting and Searching.— 2 ed., Addison-Wesley, Reading, Massachusetts, 1998.
24. **Ramachandran, R.** Radix Search – an Alternative to Linear Search // Journal of E-Technology, 2011, vol. 2(4), pp. 154–158.
25. **Leis V., Kemper A., Neumann T.** The adaptive radix tree: ARTful indexing for main-memory databases // 2013 IEEE 29th International Conference on Data Engineering (ICDE), 2013, pp. 38–49.

СПИСОК ЛИТЕРАТУРЫ

1. **Zhou Z., Zang H., Wang S., Du X., Ma D., Zhang J.** Filtration Behavior of Cement-Based Grout in Porous Media // Transport in Porous Media, 2018, vol. 125, pp. 435–463.
2. **Tsuji M., Kobayashi S., Mikake S., Sato T., Matsui H.** Post-Grouting Experiences for Reducing Groundwater Inflow at 500 m Depth of the Mizunami Underground Research Laboratory, Japan // Procedia Engineering, 2017, vol. 191, pp. 543–550.
3. **Zhu G., Zhang Q., Liu R., Bai J., Li W., Feng X.** Experimental and Numerical Study on the Permeation Grouting Diffusion Mechanism considering Filtration Effects // Geofluids, 2021, 6613990.
4. **Wang X.; Cheng H.; Yao Z.; Rong C.; Huang X.; Liu X.** Theoretical Research on Sand Penetration Grouting Based on Cylindrical Diffusion Model of Tortuous Tubes // Water, 2022, vol. 14, 1028, pp. 1-15.
5. **Ramachandran V., Fogler H.S.** Plugging by hydrodynamic bridging during flow of stable colloidal particles within cylindrical pores // Journal of Fluid Mechanics, 1999, vol. 385, pp. 129–156.
6. **Rabinovich A., Bedrikovetsky P., Tartakovsky D.** Analytical model for gravity segregation of horizontal multiphase flow in porous media // Physics of Fluids, 2020, vol. 32(4), pp. 1–15.
7. **Tartakovsky D.M., Dentz M.** Diffusion in Porous Media: Phenomena and Mechanisms // Transport in Porous Media, 2019, vol. 130, pp. 105–127.
8. **Elimelech M., Gregory J., Jia X., Williams, R.** Particle deposition and aggregation: measurement, modelling, and simulation, revised ed., Butterworth-Heinemann, New-York, 2013.
9. **Santos A., Bedrikovetsky P.** Size exclusion during particle suspension transport in porous media: stochastic and averaged equations // Computational and Applied Mathematics, 2004, vol. 23(2-3), pp. 259–284.
10. **Kuzmina L.I, Osipov Yu.V., Zheglova Yu.G.** Analytical model for deep bed filtration with multiple mechanisms of particle capture // International Journal of Non-Linear Mechanics, 2018, vol. 105, pp. 242–248.
11. **Herzig J.P., Leclerc, D.M., Goff, P.Le.** Flow of suspensions through porous media—application to deep filtration // Industrial & Engineering Chemistry Research, 1970, vol. 62(8), pp. 8–35.
12. **Kuzmina L.I., Osipov Y.V., Gorbunova T.N.** Asymptotics for filtration of polydisperse suspension with small impurities // Applied Mathematics and Mechanics (English Edition), 2021, vol. 42(1), pp. 109–126.
13. **Nazaikinskii V.E., Bedrikovetsky P.G., Kuzmina L.I., Osipov, Y.V.** Exact solution for deep bed filtration with finite blocking time. // SIAM Journal on Applied Mathematics, 2020, vol. 80(5), pp. 2120–2143.
14. **Сафина Г.Л.** Задача фильтрации с нелинейными функциями фильтрации и концентрации // International Journal for Computational Civil and Structural Engineering, 2022, т. 18(1), с. 129–140.
15. **Malgaresi, G., Collins, B., Alvaro, P., Bedrikovetsky, P.** Explaining non-monotonic retention profiles during flow of size-distributed colloids // Chemical Engineering Journal, 2019, vol. 375, 121984.
16. **Safina G.L.** Calculation of retention profiles in porous medium // Lecture Notes in Civil Engineering, 2021, vol. 170, pp. 21–28.
17. **Kuzmina L.I., Osipov Yu.V., Astakhov M.D.** Filtration of 2-particles suspension in a porous medium // Journal of Physics: Conference Series, 2021, vol. 1926, 012001.
18. **Osipov Yu., Safina G., Galaguz Yu.** Calculation of the filtration problem by finite differences methods // MATEC Web Conference, 2018, vol. 251(3), 04021.

19. **Safina G.L.** Numerical solution of filtration in porous rock // E3S Web of Conferences, 2019, vol. 97, 05016.
20. **Galaguz Yu., Safina G.** Modeling of fine migration in a porous medium // MATEC Web Conference, 2016, vol. 86, 03003.
21. **Кузьмина Л.И., Осипов Ю.В.** Асимптотика задачи фильтрации с почти постоянными коэффициентами // International Journal for Computational Civil and Structural Engineering, 2021, т. 17(2), с. 43–49.
22. **Кузьмина Л.И., Осипов Ю.В.** О нахождении коэффициента Ленгмюра задачи фильтрации // International Journal for Computational Civil and Structural Engineering, 2020, т. 16(4), с. 48–54.
23. **Knuth D.E.** The Art of Computer Programming, vol.3. Sorting and Searching.— 2 ed., Addison-Wesley, Reading, Massachusetts, 1998.
24. **Ramachandran, R.** Radix Search – an Alternative to Linear Search // Journal of E-Technology, 2011, vol. 2(4), pp. 154–158.
25. **Leis V., Kemper A., Neumann T.** The adaptive radix tree: ARTful indexing for main-memory databases // 2013 IEEE 29th International Conference on Data Engineering (ICDE), 2013, pp. 38–49.

Liudmila I. Kuzmina, Candidate of Physical and Mathematical Sciences, Associate Professor, Department of Applied Mathematics, National Research University Higher School of Economics, 101000, Russia, Moscow, Myasnitskaya st., 20, tel. +7(495) 77295 90 * 15219, e-mail: lkuzmina@hse.ru.

Yuri V. Osipov, Candidate of Physical and Mathematical Sciences, Associate Professor, Department of Computer Science and Applied Mathematics, Moscow State University of Civil Engineering, 129337, Russia, Moscow, Yaroslavskoe Shosse, 26, tel. +7(499)1835994, e-mail: yuri-osipov@mail.ru.

Maxim D. Astakhov, 3rd year bachelor's degree student of the direction of training 09.03.02 of the Institute IDTMC of the National Research Moscow State University of Civil Engineering; 129337, Russia, Moscow, Yaroslavskoe shosse, 26; tel. +7(499)1834674; e-mail: work@astakhovmd.ru.

Кузьмина Людмила Ивановна, доцент, кандидат физико-математических наук, Департамент прикладной математики, Национальный исследовательский университет «Высшая школа экономики»; 101000, г. Москва, ул. Мясницкая, д. 20, тел. +7(495) 77295 90 *15219; e-mail: lkuzmina@hse.ru.

Осипов Юрий Викторович, доцент, кандидат физико-математических наук, кафедра информатики и прикладной математики Национального исследовательского Московского государственного строительного университета; 129337, Россия, г. Москва, Ярославское шоссе, д. 26; тел. +7(499)1835994; e-mail: yuri-osipov@mail.ru.

Астахов Максим Денисович, студент 3 курса бакалавриата направления подготовки 09.03.02 института ИЦТМС Национального исследовательского Московского государственного строительного университета; 129337, Россия, г. Москва, Ярославское шоссе, д. 26; тел. +7(499)1834674; e-mail: work@astakhovmd.ru.

DOI:10.22337/2587-9618-2022-18-3-95-113

MODELING AND MONITORING OF STRUCTURAL SAFETY OF LONG-OPERATING UNDERGROUND STRUCTURES OF THE SEWAGE SYSTEM IN THE CONDITIONS OF INCREASING ANTHROPOGENIC ACTIONS IN ORDER TO PROVIDE SUSTAINABLE LIFECYCLE OF ENGINEERING INFRASTRUCTURE OF THE MEGACITY (THE EXPERIENCE OF ST. PETERSBURG)

***Nickolai A. Perminov* [1], *Rashid A. Mangushev* [2]**

[1] Emperor Alexander I Saint-Petersburg State Transport University, Saint-Petersburg, RUSSIA
[2] Saint-Petersburg State Architecture and Construction University, Saint-Petersburg, RUSSIA

Abstract. Long-term operation in difficult engineering-geological conditions of unique underground sewage facilities creates the danger of violating their structural safety. A long-term study of the dynamics of changes in a technical state of large pumping stations and deep sewage tunnels made it possible to establish patterns of influence of intensive anthropogenic and dynamic actions on this process. The developed discrete and continuous diagnostic models of defect development in tunnel structures allow identifying potentially hazardous areas subjected to manifestation of critical failures and methods of their localization. On the basis of numerical modeling the boundaries of defect-free joint operation of the system “source of impact – geo-mass – sewage underground structure” have been determined. The geotechnical and structural calculations are used to simulate the interaction of the facilities with the soil environment and predict adaptive stress-strain control system parameters. With increasing external anthropogenic and dynamic impacts, modeling zones of urban areas with potentially dangerous sections of underground sewage facilities constitute the basis for development of regulatory documents on monitoring methods and safe development of the geotechnical infrastructure of a megacity.

Keywords: unique underground sewer structures, structural safety, complex ground conditions, modeling and monitoring, man-made impacts

МОДЕЛИРОВАНИЕ И МОНИТОРИНГ КОНСТРУКЦИОННОЙ БЕЗОПАСНОСТИ ДЛИТЕЛЬНО ЭКСПЛУАТИРУЕМЫХ ПОДЗЕМНЫХ СООРУЖЕНИЙ СИСТЕМЫ ВОДООТВЕДЕНИЯ В УСЛОВИЯХ ВОЗРАСТАЮЩИХ ТЕХНОГЕННЫХ ВОЗДЕЙСТВИЙ В ЦЕЛЯХ ОБЕСПЕЧЕНИЯ УСТОЙЧИВОГО ЖИЗНЕННОГО ЦИКЛА ИНЖЕНЕРНОЙ ИНФРАСТРУКТУРЫ МЕГАПОЛИСА (ОПЫТ САНКТ-ПЕТЕРБУРГА)

***Н.А. Перминов* [1], *Р.А. Мангушев* [2]**

[1] Санкт-Петербургский государственный университет путей сообщения имени императора Александра I, Санкт-Петербург, РОССИЯ
[2] Санкт-Петербургский государственный архитектурно-строительный университет, Санкт-Петербург, РОССИЯ

Аннотация. Длительная эксплуатация в сложных инженерно-геологических условиях уникальных подземных канализационных сооружений создает опасность нарушения их конструкционной безопасности. Многолетнее изучение динамики изменения технического состояния крупногабаритных насосных станций и туннелей глубокого заложения позволило установить закономерности влияния интенсивных антропогенных и динамических воздействий на этот процесс. Разработанные дискретные и непрерывные диагностические модели развития дефектов конструкций тоннелей позволяют выявить потенциально опасные участки, подверженные проявлению критических отказов и способы их локализации. На основе численного моделирования определены границы бездефектной совместной работы системы "источник воздействия – геомассив – подземное канализационное сооружение. Посредством совместного выполнения геотехнических и конструкторских расчетов моделируются процессы взаимодействия оборудования с грунтовой средой и прогнозируются параметры адаптивного управления напряженно-деформированным состоянием системы. При возрастающих внешних антропогенных и динамических воздействий моделирование зон городских территорий с потенциально опасными участками подземных канализационных сооружений является основой для разработки нормативных документов по методам мониторинга и безопасному развитию геотехнической инфраструктуры мегаполиса.

Keywords: уникальные подземные сооружения, конструкционная безопасность, сложные грунтовые условия, моделирование и мониторинг, техногенные воздействия

1. INTRODUCTION. GENERAL FEATURES OF THE PROBLEM UNDER SOLUTION

At development of big cities unique underground sewage structures require special protection against anthropogenic actions. Sewage pump stations and tunnels as the facilities of an increased level of responsibility should meet the requirements of safe operation excluding the risk of emerging dangerous failures [1, 2]. The analysis of data on a current technical state of large pump stations (the depth of lowering - down to 71 m, the diameter - up to 66 m) and deep sewage tunnels (the total length – more than 2500 km) in more than ten largest cities of Russia with developed historical downtowns allowed developing methods of evaluation of their technical state, make a classification and a catalogue of defects.

In order to identify causes of defects at operation of underground pump stations (violation of integrity of a structure shell, force cracks, corrosion of concrete and reinforcement due to leakages) there were analyzed processes of construction and lowering of a large RC shell. During the sinking of large-size tempering structures, specific conditions of their interaction with the ground massif manifest themselves. Due to the inclusion of the scale effect (factor) (by the hyper size of the side surface area of the shell interacting with heterogeneous soil S=14500m2 and its super large mass G=1,2•106кН) creating a powerful kinetic momentum at instantaneous, most often sudden, landings of the lowering structure [3, 4]. The joint manifestation of these factors is responsible for the specific, non-linear behavior of the structure during sinking and the host soil mass. The strength and deformability of a large-scale massive structure, its geometric variability should be calculated not only for the final stage of construction. Still for the entire history of immersion, taking into account the history of the interaction of the shell with the soil massif during immersion and consequently the effect of stage-by-stage inheritance of the stress. That can only be done using nonlinear problem solving and computer modeling.

The analysis of the experimental results presented in the article showed that the main defects leading to failure of shell integrity and cracking occurred during the erection of the underground part in the soil mass. Thus, the main task is to ensure the operation of the structure in up to the limit modes at the stage of its life cycle during the erection. In order to be able to realise these conditions, it is crucial to assess the actual structural performance taking into account the process of its stage-by-stage erection in the soil mass under the non-linear material properties of the structure and the ground. These conditions can be taken into account to build a correct model of the interaction history of the shell during its step-by-step insertion into the soil mass. Calculated justification of the range of preliminarily changes in the stress-strain state of the mega massive shell when it is immersed in heterogeneous soils will ensure a defect-free life cycle of the underground structure at the stage of erection [5]. The analysis of the shell loading history at the stage of its erection taking into account the effect of VAT inheritance allows to create an adequate calculation and analytical model of the underground structure and to choose a rational calculation method for predicting the dynamics and spatial boundaries of stress-strain state (SSS) changes in the reinforced concrete shell structure, ensuring defect-free structure at all stages of its immersion.

The methodological approach proposed in the article allows you to move from the previously adopted method of calculation on the sinking (Handbook of geotechnics. Edited by V.A. Ilyichev and R.A. Mangushev, 2016) of large-size underground water disposal facilities erected by tempering method to the concept of modeling and prediction of defect-free life cycle at the stage of their construction. The results of experimental and theoretical studies represented in the article convincingly show that modeling and calculated justification of preventive protection parameters by geotechnical methods of underground construction at the stage of erection will ensure its safety and stability to man-made impacts at subsequent stages of the life cycle during long-term operation.

The paper draws special attention to investigation of structural safety of deep sewage tunnels, long-operating in the bulk of unstable soils of different strength at growing anthropogenic and dynamic actions. For almost most of the cities under consideration, the network of tunnel collectors has an average value of the physical deterioration degree more than 60% with a development dynamic of 0.6-1.2% per year. It was found that for the cities where the operation of the engineering infrastructure is carried out in complex engineering and geological conditions typical, for example, for St. Petersburg, the degree of the tunnels wear is significantly greater, reaching 83% with a higher development dynamic of up to 1.6-2.1 % per year. Development of a methodology for identifying the potentially dangerous sections of tunnels operated for a long time in difficult soil conditions, with their subsequent modeling and monitoring, will ensure their structural safety with increasing man-induced dynamic impacts.

2. THE METHODS OF MONITORING AND GEOTECHNICAL EVALUATION OF NON-STATIONARY INTERACTION OF A LARGE SHELL WITH HETEROGENEOUS SOIL MILIEU

According to the results of field and calculated-experimental works and data of complex system of geotechnical monitoring (Figure 1) of large-sized (D=50÷60m and H=55÷71m) sinking wells the peculiarities of their interaction with heterogeneous soil medium during sinking were studied. The heterogeneity of soil strata is characterized as follows: the upper stratum is represented by quaternary strata to a depth of 14.0-25.0 m (dusty sands of medium density, water-saturated, E = 11 MPa, C = 0.005 MPa, φ = 30°; dusty loamy sandy loam, E = 4 MPa, C = 0.01 MPa, φ = 15°; dusty loamy layered fluid plastic, E = 9 MPa, C = 0.025 MPa, φ = 16°; dusty loamy semi-solid with gravel, pebbles, E = 14 MPa, C = 0.028 MPa, φ = 28°), the lower one - the roof of Proterozoic clays of dislocated solids (E = 19 MPa, C = 0.04÷0.06 MPa, φ = 18÷21°).

The geomonitoring structure included: 1) program complex of calculations and the geomassive stress under different erection modes; 2) technical means of instrumental observations and SSS control of the separate elements of the system "structure - geomassive"; 3) information-measuring system of gathering, processing, storage and identification of parameters (data) of observations and control; 4) geotechnical methods of the influence on the geometric massif and soil and structure stress.

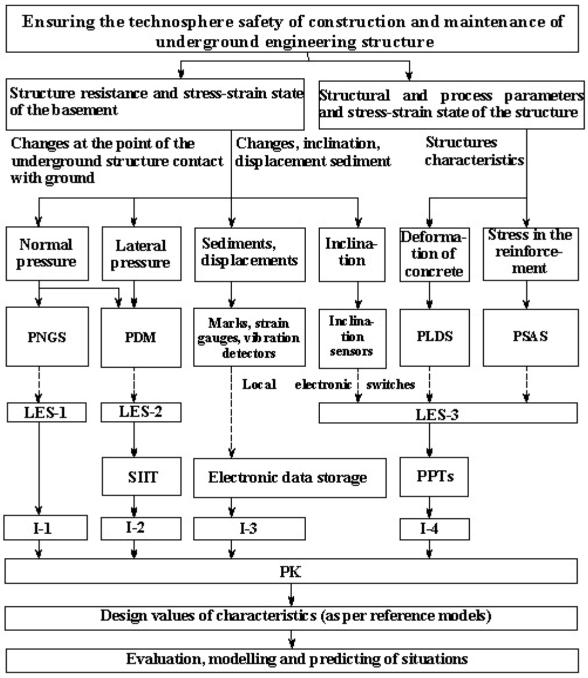

Figure 1. Geocomplex of monitoring and regulating stress-strain behavior of an embedding geobulk.

The monitoring established the peak values of horizontal stresses at the moment of "roll", exceeding the calculated values by more than 2.5 times. This can cause the appearance of microcracks in the concrete structure, which will inevitably lead to violations of waterproofing of the structure. The consequences of this circumstance were noted after 15-20 years of culverts' operation by the inevitable failure of their airtightness (Figure 2).

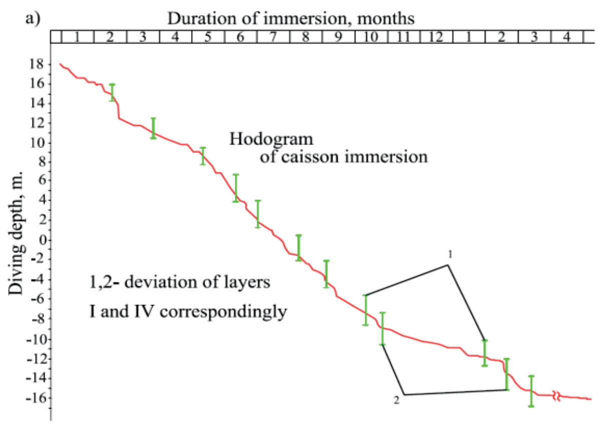

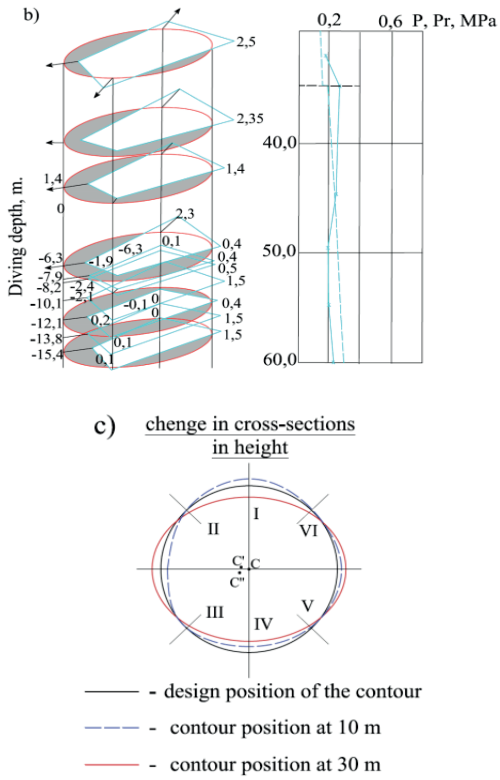

Figure 2. Sinking stages and monitoring of the stress-strain state of the large-sized sinking well: a - sinking hodogram; b, c - volume diagram of the shell displacement and the stress-strain state (SSS) of the shell

According to the analysis of sinking process and stress-strain state of large-sized shell, different, even alternating, stress-strain state of "large-sized shell-soil mass" system and different types of pressures (SP22.13330) of ground medium on the shell, including resting pressure, active and passive pressure (see Figure 3) are observed at different sinking stages.

The strength and deformability of a large-scale massive structure, its geometric variability, must be calculated not only for the final stage of construction, but for the entire history of immersion, taking into account the history of the interaction of the shell with the ground massif during immersion.

According to the general theory the ground pressure on the walls of the well at rest can be determined from the expression:

$$\sigma_o(z) = \sigma_x(z,u_x)\big|_{u_x=0} = \lambda_0\gamma z \qquad (1)$$

where λ_0 - coefficient of lateral pressure of the ground at rest; γ - specific weight of the ground; z - distance from the ground surface to the point in question.

At displacements of the manhole shell wall > 0.005h (SP22.133 p.9.21) from the ground at depth z, the active pressure on the enclosure, σ_a which corresponds to the minimum pressure value, is realized. The passive pressure σ_p, is realized at much larger displacements of the wall on the ground ($U_p = 0{,}01 - 0{,}02h$) and corresponds to the maximum value of pressure.

If there is no load on the ground surface, the expressions for determining the active and passive pressures are as follows:

$$\sigma_a(z) = \lambda_a \gamma z - c\lambda_{ac} \tag{2}$$

$$\sigma_p(z) = \lambda_p \gamma z + c\lambda_{pc} \tag{3}$$

where: λ_a - coefficient of active ground pressure; - λ_{ac} coefficient for the influence of ground cohesion on the active pressure; λ_p - coefficient of passive ground pressure; - λ_{pc} coefficient for the influence of ground cohesion on passive pressure; c - specific ground cohesion.

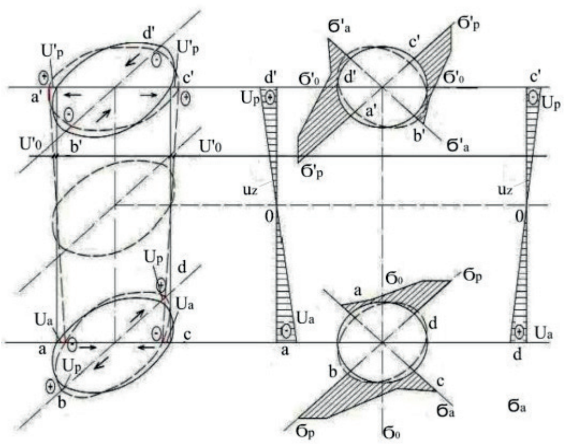

Figure 3. Asymmetric deformation (displacement) of the KGOK shell

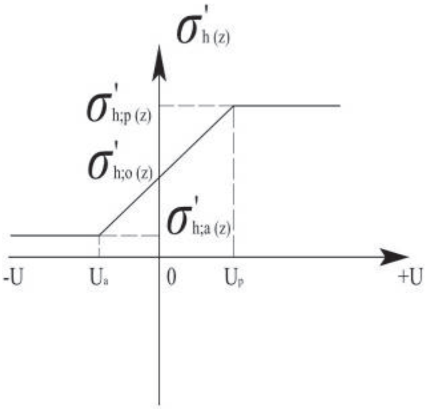

Figure 4. Dependence of lateral soil pressure on the shell on displacements $u_x \in (u_p, u_a)$ according to clause 9.21 (SP 22.13330)

The dependence of the effective horizontal pressure of the ground on the retaining structure in the interval u_x (u_p, u_a) has a complex character (Figure 4).

The active and passive pressures of the ground on the enclosure constitute the pressure limits, that is, the effective pressure is always in the range:

$$\sigma_a(z) \le \sigma_x(z, u_x) \le \sigma_p(z) \tag{4}$$

The dependence of the effective horizontal ground pressure on the holding structure in the interval $u_x \in (u_p, u_a)$ has a complex character (Figure 4).

In Figure 3 and considering Figure 4 we show the character of asymmetric deformations (displacements) of the shell contour according to the diagram of dependence of horizontal soil pressure on the walls of the well depending on the character of its displacement (asymmetric contraction-expansion of the shell in its upper and lower parts) and the diagram of lateral soil pressure, when approximating it by piecewise linear function.

The function of change of pressure value σ_x at some depth z from displacements can be represented as follows:

$$\sigma_x(u_x) = \begin{cases} \sigma_p, & u_x \le u_p \\ f(u_x), & u_p < u_x < u_a \\ \sigma_a, & u_a \le u_x \end{cases} \tag{5}$$

With some assumptions, the function

$$f(u_x) = \sigma_0 - ku_x \tag{6}$$

where k is the stiffness coefficient of the ground; σ_0 - ground pressure at rest.

The ground stiffness coefficient can be used as the ground stiffness coefficient.

The resulting pressure along the bottom and top sections of the well wall is the sum of the effective pressures on both sides of the enclosure. Let us present in the form of two graphs the effective ground pressure on the wall of the well from the ground (left) and the excavation (right) depending on the horizontal displacement of the well shell (Figure 3).

Construct the function as a $\sigma_x(z,u_x)$ piecewise given function for any value of z.

To describe the effective pressures $\sigma_x(z,u_x)$ for individual sections of the diagram between the active and passive pressure limits $\sigma_a(z) = \lambda_a \gamma z - c\lambda_{ac}$ $\sigma_p(z) = \lambda_p \gamma z + c\lambda_{pc}$, instead of (a), (b), (c), (d) we will use (1), (2), (3), (4), adding indices "l","r"for the terms relating to the axis of contraction and expansion of the well diameter. In the case where the knife part of the wall of the well is surrounded on both sides by the soil mass $\sigma_x(z,u_x)$ will take the form of:

$$\sigma_x(z,u_x) = \begin{cases} \sigma_p^l(z) - \sigma_a^r(z-h_k), & u_x \le u_1 \\ \sigma_0^l(z) - \sigma_a^r(z-h_k) - u_x k^l, & u_1 < u_x < u_2 \\ \sigma_0^l(z) - \sigma_a^r(z-h_k) - u_x(k^l + k^r), & u_2 \le u_x \le u_3 \\ \sigma_a^l(z) - \sigma_0^r(z-h_k) - u_x k^r, & u_3 < u_x < u_4 \\ \sigma_a^l(z) - \sigma_p^r(z-h_k), & u_4 \le u_x \end{cases} \tag{7}$$

If we separately consider the resultant pressures on the shell up to the face ($z \le h_k$), expression (7) will take the form:

$$\sigma_x(z,u_x) = \begin{cases} \sigma_p^l(z), & u_x \le u_1 \\ \sigma_0^l(z) - k^l u_x, & u_1 < u_x < u_3 \\ \sigma_a^l(z), & u_3 \le u_x \end{cases} \tag{8}$$

Let us substitute expressions (1), (2), (3) in (7) and (8):

$$\sigma_x(z,u_x) = \begin{cases} \lambda_{pl}\gamma z + c\lambda_{pcl}, & u_x \le u_1 \\ \lambda_{0l}\gamma z - k_l u_x, & u_1 < u_x < u_3 \\ \lambda_{al}\gamma z + c\lambda_{acl}, & u_3 \le u_x \end{cases} \tag{9}$$

$$\sigma_x(z,u_x) = \begin{cases} \lambda_p^l\gamma z - \lambda_a^r\gamma(z-h_k) + c\lambda_{pc}^l + c\lambda_{ac}^r, & u_x \le u_1 \\ \lambda_0^l\gamma z - \lambda_a^r\gamma(z-h_k) + c\lambda_{ac}^r - u_x k^l, & u_1 < u_x < u_2 \\ \lambda_0^l\gamma z - \lambda_a^r\gamma(z-h_k) - u_x(k^l + k^r), & u_2 \le u_x \le u_3 \\ \lambda_a^l\gamma z - \lambda_0^r\gamma(z-h_k) - c\lambda_{ac}^l - u_x k^r, & u_3 < u_x < u_4 \\ \lambda_a^l\gamma z - \lambda_p^r\gamma(z-h_k) - c\lambda_{ac}^l - c\lambda_{pc}^r, & u_4 \le u_x \end{cases} \tag{10}$$

The analysis of formulas (9) and (10) describing resultant pressures shows that practically independent of properties of the host soil mass, the sum of effective pressures on the asymmetric deformed shell (Figure 3) both in the opposite axial directions and in the lower and upper parts of the shell exhibit a high degree of nonuniformity. As comparative calculations show, the non-uniformity of the resulting pressures can be of the order of one unit (see Figure 5) or more, either on both sides of it, or along the formations of the lower and upper sections of the manhole walls. It is impossible to predict such character of the stress-strain state (SSS) of the "sinking structure-soil massif" system using the recommended calculation approach, as it was noted, and it is also impossible to ensure verticality and uniformity of sinking by applying previously known methods of geotechnology [6], as evidenced by hodograms (see Figure 2a).

The analysis of the conditions of interaction between a massive large-sized shell and the ground massif when immersed in heterogeneous strata testifies to the manifestation of non-stationarity effects in the parameters reflecting this process. In order to be able to study the regularities of manifestation and conditions for preventing their prohibitive development in our further studies, it is necessary to use simulation of shell immersion modes, solving for this purpose the problems in linear and nonlinear formulations.

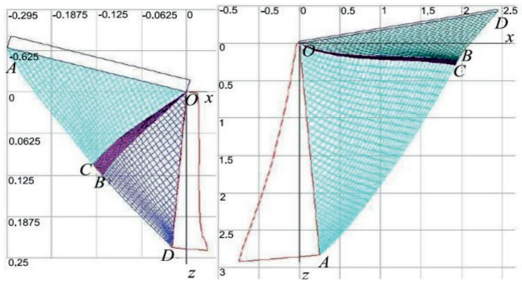

Figure 5. Slip lines for active and passive pressures on the retaining wall (by Korolev K.V.) 10Ea<<En

The strength and deformability of a large-scale massive structure, its geometric variability should be calculated not only for the final stage of construction. Still for the entire history of immersion, taking into account the history of the interaction of the shell with the soil massif during immersion and consequently the effect of stage-by-stage inheritance of the stress. That can only be accomplished using nonlinear problem solving, nonlinear models, and computer-based nonlinear modeling.

3. THE RESULTS OF MODELING AND ANALYSIS OF REGULATED MODES OF LOWERING OF A MASSIVE SHELL IN HETEROGENEOUS SOIL USING THE METHODS OF GEOTECHNOLOGY

3.1 Numerical modeling of the process of correcting a tilt of a massive embedded structure

In engineering practice, it is known that during the construction of large-diameter manholes there are often problems associated with the deviation of the structure from the design position. The causes of uneven sinking of the well, as it was found in section 2, are peculiarities of interaction of the large-sized shell with heterogeneous soil medium at the stage of its sinking and non-stationary nature of the stress-strain state of the system "large-sized lowering shell - the host soil mass".

By means of numerical geotechnical calculations it is proposed to choose technically possible geotechnological methods for controlling the sinking process: change of the geomassivation in the base of the structure and on the side surface, for example, by methods of prestressing the soil mass, by means of loading leader screens, regulation of the soil resistance on the side surface and other protective geotechnological measures,

In order to assess the effectiveness of geotechnical measures to correct the roll, several series of calculations were carried out on the ground massif with a buried structure. In the initial series of calculations, the soil base was modeled as a linearly deformable medium. In the subsequent series, the nonlinearly deformable material. As a linear medium, a model with a Hooke coupling between stresses and strains was used [7, 8]. An incremental model based on generalized Hooke's law was used to simulate nonlinear material.

Description of the nonlinear ground model

An incremental strain-type model was used as the computational ground model to solve the nonlinear problem. The relationship between stresses and strains in the model is taken separately for the volumetric and shear components of the stress tensor:

$$\left.\begin{aligned} dS_{ij} &= 2G^{\partial} \cdot de_{ij} \\ d\delta_{cp} &= 3K^{\partial} \cdot d\varepsilon_{cp} \end{aligned}\right\} \qquad (11)$$

Where: dS_{ij} - increment of the deviatoric component of the stress tensor; de_{ij} - increment of the deviatoric component of the strain tensor; $d\delta_{cp}$ - increment of the average stress; $d\varepsilon_{cp}$ - increment of the average strain; K^{∂} - differential volume strain; G^{∂} - differential shear strain.

The mathematical approximation of deviator loading is taken as a linear polynomial of two variables:

- under the condition of loading by the deviatoric component of the stress tensor

$$G_H^{\partial} = A_0 + A_1 \cdot \delta_{cp} + A_2 \cdot \tau_i \qquad (12)$$

- under the condition of unloading by the deviatoric component of the stress tensor

$$G_P^{\partial} = A_0 + A_1 \cdot \delta_{cp} \qquad (13)$$

Approximation of the differential volume strain modulus under the condition of loading by the spherical component of the stress tensor is carried out by a second-order power polynomial:

$$K_H^{\partial} = B_0 + B_1 \cdot \delta_{cp} + B_2 \cdot \delta_{cp}^2 \quad (14)$$

at "unloading": $K_P = const$

where: τ_i - tangential stress intensity; δ_{cp} - average stress; $A_0; A_1; A_2; K_p; B_0; B_1; B_2$ - model design parameters.

Parameters of the computational model $A_0; A_1; A_2; K_p; B_0; B_1; B_2$ (12-14) were determined from the data of three-axis tests in the stabilometer. The tested soil is a sandy soil of medium coarseness with density Pd=1.65g/cm3 and humidity W=10%.

The procedure for solving the nonlinear problem was reduced to the well-known method of variable stiffness [9, 10], according to which the stiffness matrix was reshaped at each step of the solution according to the current level of SSS and the orientation of the overload vector.

As measures for leveling the roll of a buried structure can be chosen the method of regulation of ground resistance by electroosmosis or the transfer of horizontal pressure on the ground, based on immersion in an array of soil elastic shell, in which by special technology creates excessive pressure, transmitted through the walls of the shell on the ground [11]. The elastic casings are placed to some depth along the wall of the buried structure on the outer side. Then pressure is transferred to the inner cavity of the shell, which is transferred to the wall of the structure on one side and to the ground on the other side.

The calculation scheme is a soil mass measuring 296.0 m (horizontal) by 115, 0 m (vertical). In the central part of the scheme is a rigid buried structure having a length of 50.0 m in plan and is buried at 45.0 m.

The computational scheme is discretized into 246 quadrangular isoparametric elements. The total number of nodes was 282. The computational domain is represented by two groups of elements with different deformation characteristics. The elements of the first group (rigid buried structure) are represented by an elastic material with an elastic modulus E=30000.0MPa and Poisson's coefficient V=0.18.

The surrounding structure space is represented by a group of linearly deformable elements No. 2 with strain modulus E=30.0 MPa and Poisson's coefficient V=0.33.

In solving the problem, it is assumed that the structure has an initial roll, as shown in Fig. 6 (left to right). To correct for uneven subsidence on the right side of the structure is applied additional load intensity Q on the section of length L = 12.5 m.

The load Q in the solved problems was taken equal to 0.3; 0.6 and 0.9 MPa.

Numerical solution of geotechnical problems allowed to obtain the following results. Moving the contour of the dip well in a continuous elastic medium while adjusting the action of the lateral additional load Q and simultaneously adjusting the soil resistance on the lateral surface provided predicted prevention of rolls when sinking in heterogeneous soils. The displacements of the structure according to the solution of the nonlinear problem are shown in Figure 6. The greatest prevention of absolute horizontal displacement at a load of Q=0.9 MPa is as follows:

1st series of calculations - 48 cm; 2nd series of calculations - 67 cm; 3rd series of calculations - 80 cm; 4th series of calculations - 16 cm.

Table of displacements of corner points of the structure

№ points	Q = 0,3 kg/cm²		Q = 0,6 kg/cm²		Q = 0,9 kg/cm²	
	U_y [cm]	U_z [cm]	U_y [cm]	U_z [cm]	U_y [cm]	U_z [cm]
1	-6,7	9,16	-13,4	18,3	-20,2	27,5
2	-16,0	9,17	-32,0	18,3	-48,0	27,5
3	-6,7	-1,08	-13,3	-2,1	-20,0	3,2
4	-16,0	-1,06	-31,9	-2,1	-47,8	3,2

E = 30 MPa
$\nu = 0,33$

Moving the structure in a controlled immersion mode

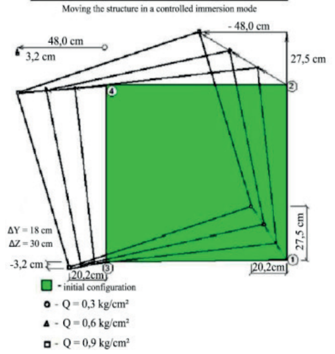

Figure 6. Contour displacement of the dip well in a solid elastic medium under the action of lateral load: Q=0.3; 0.6; 0.9 (MPa)

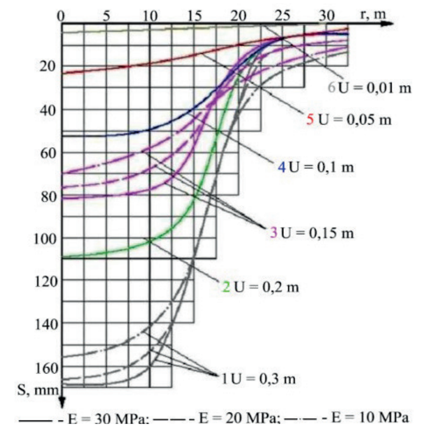

Figure 7. Influence of horizontal displacements of manhole walls U_k on ground surface settlements under roll

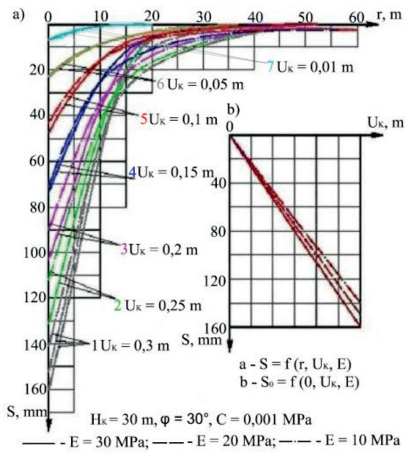

Figure 8. Influence of U_k value control on ground surface settlement in the mode of controlled structure landing

For all solved problems, without the application of geotechnical regulation methods, the irregularity of sinking of the lowered structure was observed: vertical movements (raising (+); lowering (-)) of the left and right contour of the buried structure with the corresponding sign is given below:

Series 1 calculations -3.2 and +27.5 cm; Series 2 calculations -12.5 and +36.4 cm; Series 3 calculations -25.7 and +41.1cm; Series 4 calculations -3.2 and +15.9cm.

When the zones with a reduced deformation modulus are taken into account in the calculations (the drilling zone), the horizontal displacement of the upper part of the structure has increased almost 2 times.

By comparing the results for different sizes of the drilling area, it can be seen that for the same E*, the increase in size by 2 times leads to a displacement increase of about 15-30%.

The geometric dimensions and configuration of the SSS control zones were selected by analyzing the displacement calculation data (Figure 7, 8). When solving the nonlinear problem (4th series of calculations), the displacements were obtained significantly less than when solving elastic problems. This fact can be explained by the considerable deformation heterogeneity in the soil surrounding the buried structure when solving the non-linear problem. The strain modulus when solving a nonlinear problem depends significantly on the stress state. Because of this, the strain modulus increases with depth. We also note that for the nonlinear solution there was no drilling zone, as well as the thixotropic jacket located around the structure was not modeled

3.2 Modeling of conditionally instantaneous failure of a massive shell when it is immersed in an inhomogeneous soil medium

Using the software package Autodesk Robot Structural Analysis Professional [12], we analyzed the performance of the casing structure during its sudden uncontrolled slip (fall) to the bottom of an open soil cavity from a height of 1.3 - 1.5 m at angles of deviation from the vertical axis of 0.5°-5°.

In developing the calculation model (Figure 9) it was taken into account that the structure of the shell consists of two cylinders stacked on each other: Upper cylinder: outer radius R = 36 m, inner radius R = 30.5 m, height H1 = 46 m; Lower cylinder: outer radius R = 36 m, inner radius R = 30 m, height H2 = 25 m. Thus, the outer diameter of the shell was D = 72 m, the height of the shell was H = 71 m. Concrete class B30.

To simulate the magnitude of the impact force at failure of the shell in the model, the cylinder fell from a height H = 150-250cm. under the action of its own weight with an angle of inclination of 0.5 °-5 ° on the compliant soil (clay greenish-gray: φ = 21 °, C = 0,04 MPa, E = 19 MPa). Spatial shell design scheme was modeled: weight G = 210000 t; number of knots 16944; volume finite elements 12496; number of static degrees of freedom: 50828; number of loads 27; free fall acceleration g = 9.81 m/kV.s; fall time t=√(2*H/g); Δt=0.30-0.54 sec. Because of the angle of the slope, the frictional forces were applied at the top of the well on one side and at the bottom on the opposite side.

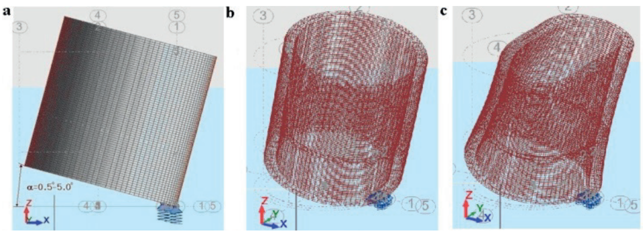

Figure 9. Schematics of calculation models and submersible shell simulation results at different angles of its deviation from the vertical axis: a - static support at roll; b,c - failure and slippage at deviation from the vertical axis (roll), respectively: calculation form "N4" at a=1°; ΔH=1.25m (n=0.56, Δ=26.1cm-limited VAT), calculation form "N22" at a=3.5°; ΔH=2.5m (n=1.94, Δ=183. 4cm-limited SSS)

During the analysis of the shell's deflectivity, we used the coefficient of forbidden state n, defined as the ratio of the equivalent stress of the shell structure according to Mises to the ultimate resistance of concrete of class B30.
Since the simulation of the stalling processes at different deflection angles of the shell from the -α-axis and the drop heights -ΔH was performed in a rather large range, Figure 9 shows only fragments of the calculated forms "NN4 and 22" and the most characteristic results that were taken for analysis. The total calculation table of the integration results of the motion equations of the shell at stall (fall) at velocity VZ, VX, VY (cm/sec), acceleration AZ, AX, AY (cm/sec2) and displacement UZ, UX, UY (cm) was 186385 lines.

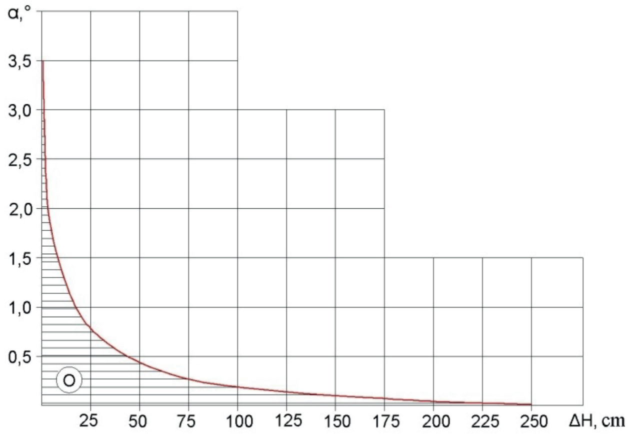

Figure 10. Area of maximum permissible values of conditionally instantaneous landings (failures) ΔH of the shell with diameter D=61m, height H=71m, weight G=210000t, at various angles of deviation of the structure from the vertical axis a° (concrete class B30; φ = 21°, C = 0,04 MPa, E = 19 MPa)

According to the results of modeling (Figure 10), the acceptable parameters of the spatial position of the shell and the range of its conditionally instantaneous disruptions, providing up to the limit value of the shell's SSS were established.
The simulation results show that for large-sized shells, the recommendations of normative documents have limited application and need to be confirmed by computational modeling.

4. MODELING AND MONITORING OF POTENTIALLY DANGEROUS PARTS OF SEWAGE TUNNELS

4.1 The methods of studying potentially dangerous parts of sewage tunnels

The most interesting from the point of view of studying potentially dangerous sections of sewer tunnels is the system and network of tunnel collectors of St. Petersburg, which, with an undeveloped redundancy scheme, has a length of about 275 km. The system of sewer tunnels consists of pipelines with a diameter of 1.2 to 5.6 m and a depth of 8 to 70 m. Most (up to 75%) of the waste line length is located in the central historical part of the city in extremely difficult technogenic and engineering-geological conditions. The main part of the territory is covered by a stratum of Quaternary deposits (Q) that are unstable to technogenic impacts. Among the latter, it should be especially noted water-saturated clay soils belonging to lake-sea, lake-glacial and moraine deposits. Up to a depth of 30-120 m, soil strata are represented by silty sands of medium density, water-saturated E=7-11 MPa, C=0-0.005MPa, j=27-30°; silty plastic sandy loam E=3-5 MPa, C=0.01-0.02 MPa, j=12-17°; silty layered fluid plastic loams E=5-8 MPa, C=0.015-0.025 MPa, j=10-16° [13]. Long-term waste line operation in these conditions negatively affects their technical condition.

This factor is especially true for the continuously operating tunnel sewer collectors under the conditions of increasing man-induced impacts, first of all, to static from the large-sized complexes under construction in the influence zone with a developed underground part (see Figure. 11) and vibro-dynamic from the construction and transport equipment [14]. To identify the potentially dangerous areas, instrumental surveys of tunnels are carried out using a special technique. Technical instrumental surveys included: full-scale tachymetric survey of the spatial position of the tunnel in the intervals between mines, scanning the inner surface conditions of the tunnel with an assessment of its continuity with a GPR; taking cores and carrying out tests using the pull-off method with scanning to determine the strength characteristics of concrete, taking samples for chemical and biochemical analyzes, assessing the degree of corrosion and reinforcement by non-destructive methods, vibro-dynamic testing of vibrations of internal tunnel structures from external and construction vibration effects [15].

The uniqueness of the observation materials for the tunnels' state lies in the fact that the technical inspection of the structures has been carried out for a long time from the end of the 70s up to the present (2021). During this period, the same reservoir intervals have been surveyed for several times. At the same time, as a rule, after the examination, their conditions were monitored for several years. Thus, it became possible to trace the dynamics of the defects' development.

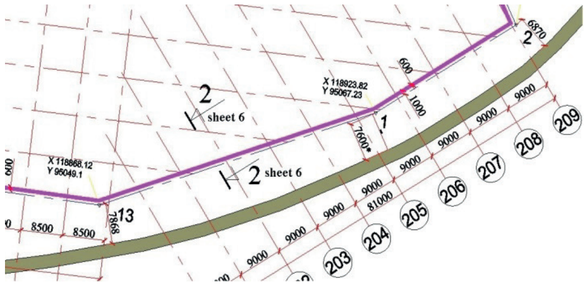

Figure 11. Scheme of a potentially dangerous section of a sewer tunnel in the zone with man-induced impacts from a complex under construction in St. Petersburg

The observation time range was divided into 3 periods:

a) 70-80s; b) 80-2000s; c) 2000-2020s. The most typical revealed defects affecting the operational reliability and bearing capacity of the tunnel were grouped into 7 classes: d1 - shrinkage cracks in the concrete jacket; d2 - signs of gas corrosion; d3 - drip leaks; d4 - force cracks in the arch and on the lateral surface of the tunnel; d5 - signs of biological corrosion of concrete; d6 - reinforcement corrosion, tray abrasion; d7- the presence of pressure leaks.

Analysis of the defects' development manifestation and dynamics structure show that in the initial period of the tunnel collectors' operation, defects were observed in the form of shrinkage cracks in the concrete jacket with the manifestation of drip leaks and signs of gas corrosion. The nature of the defects prevailing in the first 15-20 years of the tunnels' operation and their influence on the bearing capacity and operational reliability of structures can be taken as insignificant, and their technological state can be recognized as workable according to the RF "GOST" and "BC" regulations.

Defect-free waste line functioning in these conditions requires a calculated justification of the structural safety of the tunnel and monitoring its technical condition when choosing a method

and a mode of carrying out the measures to restore the bearing capacity and operational reliability of the structure.
Within the framework of this study, we faced the task of the safe level external anthropogenic impacts' geotechnical provision on the tunnel structure, taking into account its residual bearing capacity.

4.2 Modeling, monitoring and geotechnical substantiation of protective measures for potentially dangerous parts of deep sewage tunnel

The measures to protect potentially dangerous sections of tunnel collectors and ensure their reliability and structural safety were proposed on the basis of modeling and determining the boundary of the defect-free joint operation of the system "source of impact – geo-mass - sewer tunnel", but the main requirement that they must certainly meet, is the possibility of preventive use, justified by geotechnical and design calculations.
The results of geotechnical modeling to ensure the waste line structural safety typical for a large city with a developed engineering and transport infrastructure under difficult engineering and geological conditions of construction and operation are presented below (Table 1) as one of the examples [16].

Table 1. The results of the calculation substantiation of geotechnical measures to protect potentially dangerous sections of tunnels from unacceptable impacts

<table>
<tr><th>Characte of technogenic impacts</th><th colspan="3">Geotechnical and structural measures</th></tr>
<tr><td colspan="4">Arrangement of a protective screen made of fixed soil to prevent the foundation pit bottom from elevation</td></tr>
<tr><td rowspan="2">Unloading the soil mass when trenching the excavation for the tunnel</td><td>Vertical deformations of the soil mass after the excavation of the construction pit, without preliminary fixing - 37mm</td><td colspan="2">Vertical deformations of the soil mass after excavation of a construction pit with soil fixing above the collector using Jet Grouting technology (3.0 m thick) - 3.2 mm</td></tr>
<tr><td>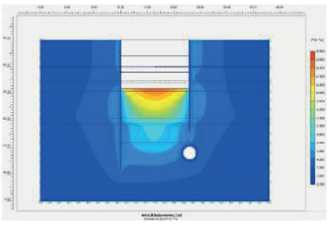</td><td colspan="2">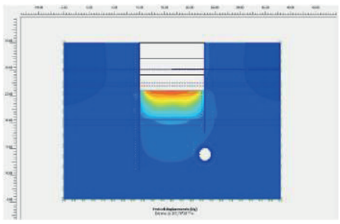</td></tr>
<tr><td colspan="2">Calculation option</td><td>Construction stage</td><td>Collector deformation, mm.</td></tr>
<tr><td colspan="2">Without Propping</td><td>-</td><td>+37</td></tr>
<tr><td colspan="2" rowspan="2">Propping the foundation pit using Jet Grouting technology. Power 2.0m.</td><td>soil reinforcement</td><td>-2.1</td></tr>
<tr><td>excavation</td><td>+10.1</td></tr>
</table>

<table>
<tr><td colspan="2" rowspan="2">Propping the foundation pit using Jet Grouting technology. Power 3.0m.</td><td>soil reinforcement</td><td>-3.0</td></tr>
<tr><td>excavation</td><td>+3.6</td></tr>
<tr><td colspan="2" rowspan="2">Propping the soils above the collector using Jet Grouting technology. Power 2.0m.</td><td>soil reinforcement</td><td>-2.6</td></tr>
<tr><td>excavation</td><td>+8.3</td></tr>
<tr><td colspan="2" rowspan="2">Propping the soils above the collector using Jet Grouting technology. Power 3.0m.</td><td>soil reinforcement</td><td>-2.9</td></tr>
<tr><td>excavation</td><td>+3.2</td></tr>
<tr><td colspan="4">Structural waste line reinforcement winding technology to increase the maximum permissible tunnel displacements</td></tr>
<tr><td rowspan="4">Increasing the zone of maximum permissible waste line displacements with one-sided unloading of the soil mass during the embankment reconstruction.</td><td>General calculated displacements during excavation under the protection of sheet piling</td><td colspan="2">General calculated displacements during excavation with the device of a geotechnical barrier</td></tr>
<tr><td>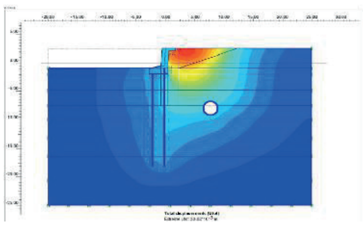</td><td colspan="2">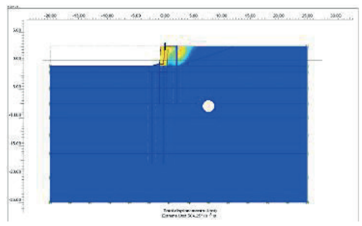</td></tr>
<tr><td>Additional horizontal deformations of the collector were 54mm</td><td colspan="2">Additional horizontal deformations of the collector were 7mm</td></tr>
<tr><td colspan="3"></td></tr>
<tr><td colspan="4">Structural waste line reinforcement by lining and spiral-wound technology to restore the bearing capacity of the tunnel to the design level</td></tr>
<tr><td rowspan="2">Increase in static and dynamic loads on waste line from the action of heavy vehicles and trams</td><td>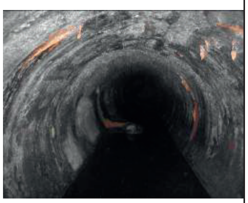</td><td>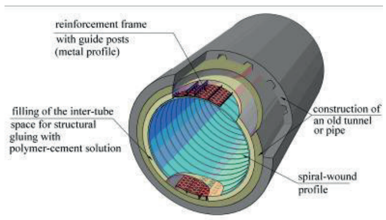</td><td></td></tr>
<tr><td>Condition of a potentially dangerous waste line area before renovation</td><td>Structural scheme and solution to strengthen the tunnel section</td><td>Technical condition of the tunnel after restoration and repair</td></tr>
</table>

The second example of the numerical implementation of measures to protect the collector from external influences is the potentially hazardous area noted above (see Figure 11).

The customer set the task to ensure the safe operation of a sewer collector located in soft soils, near which the construction of a high-rise building had started.

The modeling task was to determine the permissible horizontal displacements of the tunnel sections when performing work near the structure.

For normal operation of the collector tunnel, it is necessary to exclude the formation of cracks in the structure of the lining caused by its displacement towards the pit during the work.

The criterion for the structure safety is the maximum permissible tensile stresses of concrete at the characteristic points of the lining.

The design of the collector tunnel lining is a two-layer cylinder. The outer layer is a prefabricated reinforced concrete structure made of tubing. The inner layer is a monolithic reinforced concrete jacket (see Figure 12).

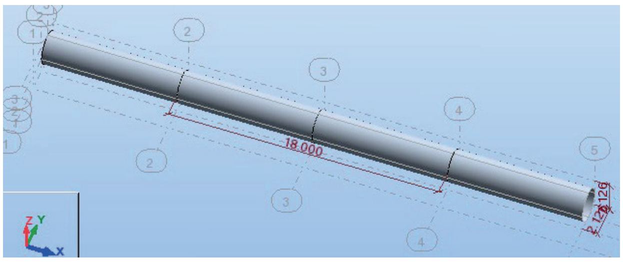

Figure 12. Design of the collector tunnel potentially dangerous section's lining

The tunnel sections with different lengths of the influence zone and the structure reinforcement degree were modeled (see Figure 13). Geotechnical calculations simulated the measures to reduce the impact on the displacement of the tunnel using a wall in the ground between the tunnel and the wall under construction in the ground made of low-modulus material.

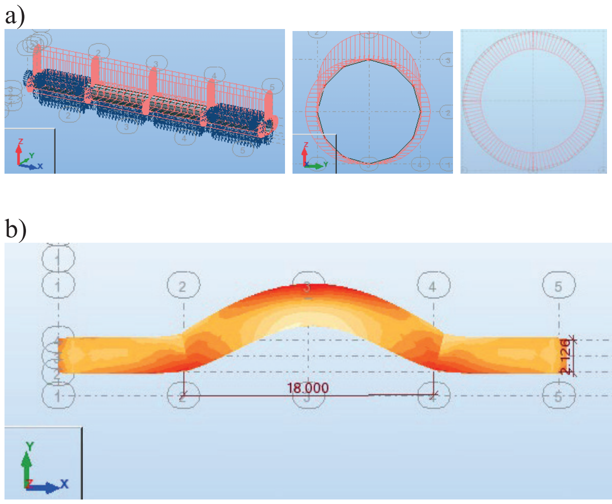

Figure 13. Fragment of the calculated potentially dangerous section of the collector with a length of 18 m: a) with loads and elastic rebound; b) the transcendent SSS tunnel zones: 1 - in the middle; 2 - at the ends of the displacement section

Numerical calculations were used to obtain the permissible displacement values of the lining, taking into account the presence of a screen made of low modulus material and depending on the tunnel deformable section length. Carrying out of work related to man-induced impacts, the project provided monitoring the tunnel and geo-massif structure [17].

The calculation substantiation of geotechnical protective measures was carried out according to the algorithm: collection of loads and impacts, determination of physical and mechanical characteristics, determination by geotechnical calculations of the permissible level of external anthropogenic impacts on the tunnel, taking into account its residual bearing capacity. Figure 14.a shows fragments of the tunnels' maximum permissible displacements computational modeling results (before the application of protective measures and after the implementation of protective measures) and Figure 14.b shows the data of monitoring observations.

a)

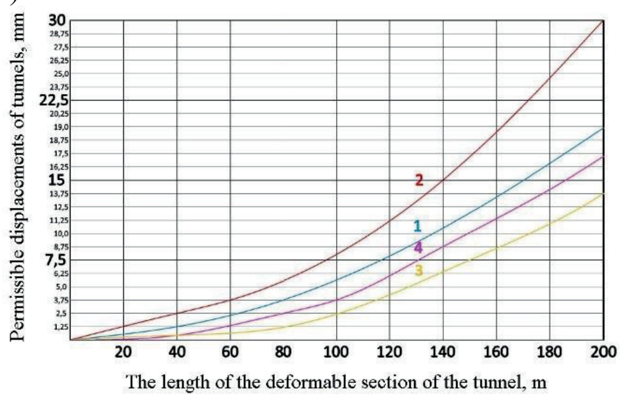

b)

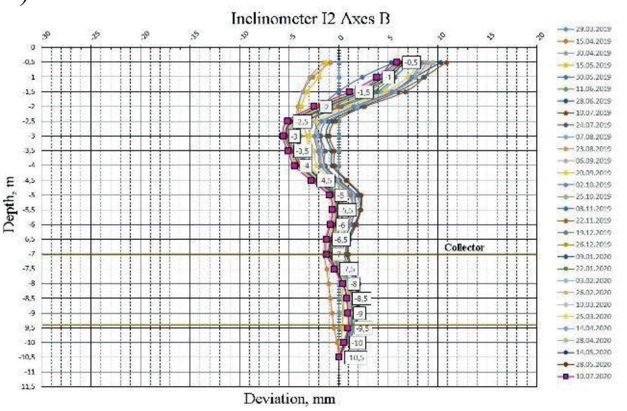

<u>Figure 14.</u> Maximum permissible displacement of a tunnel falling into the zone of man-induced influences: a) calculated values of the maximum permissible displacement of sewer tunnels D=1.5 and D=2.5 before (1.3) and after (2.4) strengthening the structure using winding technology; b) data of monitoring control by the inclinometers readings to prevent exceeding the maximum permissible displacement of the tunnel D=2.5m with the length of the deformable section 70m

To ensure the bearing capacity of the tunnel, the SATURN winding method was used, developed and adapted for the specific conditions of St. Petersburg: intervals between mines up to 1000m and more; irregularity of the working section along the length of the collector associated with the dynamic influences and subsidence of the tunnel in weak thixotropic soils. The sewage tunnel with inter-shaft spacing up to 850m and diameters D= 2,5 m and D= 1,5 m is embedded at the depth down to 17 m, it has been operating for more than 40 years and, according to the survey results, had a wear rate of more than 79%, subsidence at the intersection of streets up to 25 mm. Based on the GPR scanning results, it was found everywhere that the concrete jacket was peeled off from the tubing lining with the formation of pressure leaks. The scope of work operations included: tunnel cleaning and surface preparation; structural bonding of the concrete jacket and tubing lining by injecting SikaDur; reinforcement of the surface of the vault with structural reinforcement with SikaWrap carbon fiber; lining the surface of the tunnel with a winding profile made of PVC; polymer cement mortar injection (P_{comp}=65MPa) into the annular space for structural bonding of the shell made of PVC with tunnel construction.

This method was applied to make a geotechnical prediction of dangerous parts of tunnels long-operating in difficult soil conditions (see figure 15), the numerical modeling defined a rational method of geotechnical protection of these sections in order to provide their structural safety at growing anthropogenic and dynamic actions.

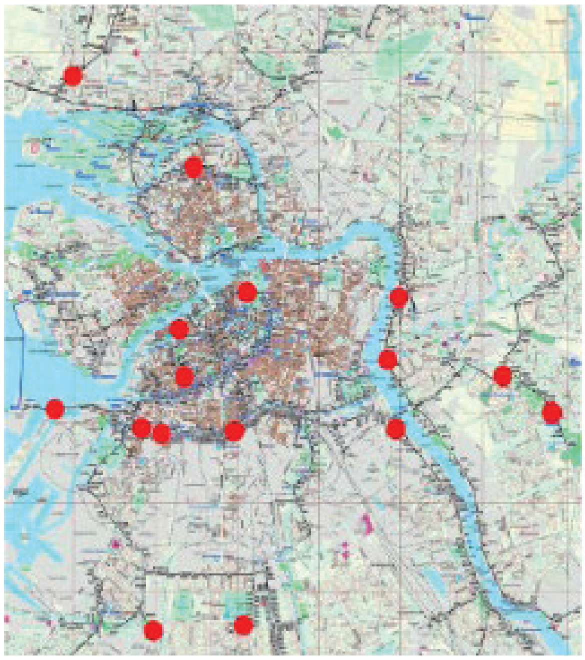

<u>Figure 15.</u> Geotechnical prediction of potentially dangerous sections of sewage tunnels in St. Petersburg which require protection of structural safety

According to the monitoring carried out on the restored potentially dangerous sections of the tunnel, it was established: vibration dynamic tests of the tunnel before and after repair showed the changes in the period of natural collector vibrations of 0.54 s. up to 0.19 s. so, by 58%, and the amplitude of natural vibrations decreased from A = 300 μm to A = 15 μm, i.e., by almost double. This indicates the structure integrity restoration and the joint work of its layers during continuous operation.

5. CONCLUSIONS

Difficult engineering and geological conditions and the increasing influence of technogenic factors have led to the wear of long-operated tunnel collectors in large cities of Russia up to 66%. For St. Petersburg, characterized by vibration-resistant enclosing waste line massifs of soils, the level of wear reaches 83% with a high dynamic of development up to 1.5 hours 2% per year.

Potentially dangerous sections of the tunnels have been identified by the methods of diagnostics and modeling of technical conditions

Proposed and geotechnically sound waste line protection methods, including technologies of structural reinforcement and rehabilitation in the conditions of wastewater transportation, accompanied by a monitoring system, ensure structural waste line safety and their operational reliability.

Methods for ensuring structural safety developed and substantiated by waste line geotechnical modeling are recommended for use in large cities with difficult soil conditions, with heavily worn-out sewers with potentially dangerous sections of tunnels and, as a result, to increase their reliability during long-term operation in conditions of urban infrastructure development.

This work was supported by a grant of RAACS No. 2020-SN-7.4.1.

REFERENCES

1. **Alexeev M.I., Baranov L.A., Ermolin Yu.A.** Risk-based approach to evaluate the reliability of a city sewer network // Water and Ecology: Problems and Solutions, 2020, №3 (83), pp. 3-7 (in Russian).
2. **Perminov A., Perminov N.** Geotechnical and geo ecological fundamentals of sustainable life cycle of unique long-operated underground structures of water disposal systems in difficult soil conditions (the experience of St. Petersburg) // Geotechnics fundamentals and applications in construction: new materials, structures, technologies and calculations Proceedings of the International Conference on Geotechnics Fundamentals and Applications in Construction: New Materials, Structures, Technologies and Calculations, GFAC 2019, pp. 231-234.
3. **Travush V.I., Shulyat'ev O.A**. Analysis of the results of geotechnical monitoring of "Lakhta Center" Tower // Soil Mechanics and Foundation Engineering, 2019, Vol. 56, № 2, pp. 98-106.
4. **Perminov N.** Unsteady interaction simulation of a large RC shell with heterogeneous soil milieu for a gradually increasing caisson structure // IOP conference series: materials science and engineering Institute of Physics Publishing, 2018, Paper № 012059.
5. **Mangushev R.A.,** Osokin A.I. The experience of the underground construction for the complex of buildings on a soft soil in the center of St. Petersburg // International Journal for Computational Civil and Structural Engineering, 2020, Vol . 16, № 3, pp. 47-53.
6. **Protosenya A.G., Karasev M.A., Belyakov N.A., Lebedev M.O.** Geomechanics of low-subsidence construction during the development of underground space in large cities and megalopolises // International Journal of Mechanical and Production

Engineering Research and Development, 2019, Vol. 9, № 5, pp. 1005-1014.
7. **Karasev M.A., Tai Tien N., Vil'ner M.A.** Forecast of the stress-strain state of the prefabricated lining of underground tunnels of curvilinear cross-section // Bulletin of the Ural State Mining University, 2019, № 4 (56), pp. 90-97.
8. **Protosenya A.G., Karasev M.A., Belyakov N.A.** Elastoplastic problem for noncircular openings under coulomb's criterion // Journal of Mining Science, 2016, Vol. 52, № 1, pp. 53-61.
9. **Perelmuter A.V., Fialko S.Y.** Inelastic analysis of reinforced concrete structures in SCAD // International Journal for Computational Civil and Structural Engineering Publishing House ASV, LTD (Moscow), 2019, Vol. 15, № 1, pp. 54-60.
10. **Merzlyakov V.P., Vlasov A.N.** Effect of polygonal crack nets on the deformation characteristics of rocks // Soil mechanics and foundation engineering, 1993, № 30(3), pp. 85-91.
11. **Ulitsky, V., Bogov, S.** Restoration engineering of historic structures: Case study of building 12 on new Holland Island in Saint-Petersburg // Geotechnics Fundamentals and Applications in Construction: New Materials, Structures, Technologies and Calculations - Proceedings of the International Conference on Geotechnics Fundamentals and Applications in Construction: New Materials, Structures, Technologies and Calculations, GFAC 2019, pp. 390-395.
12. **Lebedev M.O., Bezrodny K.P., Larionov R.I.** Ensuring safety during construction of double-track subway tunnels in quaternary deposits // In the collection:Tunnels and Underground Cities: Engineering and Innovation meet Archaeology, Architecture and Art- Proceedings of the WTC 2019 ITA-AITES World Tunnel Congress, 45th. 2019, pp. 941-951.
13. **Dashko R.E., Alekseev I.V.** Main features of engineering-geological and geotechnical research of microbiota influence on hard rocks in the urban underground space // Conference Proceedings. 19th International Multidisciplinary Scientific Geoconference Sgem., 2019, pp. 369-376.
14. **Voznesensky E.A., Sentsova E.A., Nikitin M.S.** Sandy soils dynamic strength parameters according to triaxial tests // Engineering Geology, 2019, №2. Vol.14, pp. 24-33 (in Russian).
15. **Voznesensky E.A., Kushnareva E.S.** Methodological aspects of experimental evaluation of dynamic stability of sands in geotechnical survey // Article in the proceedings of the conference. Saint Petersburg 2008: Geosciences - From New Ideas to New Discoveries. 2008.
16. **Perminov N.** Simulation of defectless lifecycle of unique underground structures of the sewage system at the stage of their construction in difficult soil conditions // International Journal for Computational Civil and Structural Engineering Publishing House ASV, LTD (Moscow), 2019, Vol. 15, № 1, pp. 119-130.
17. **Frolov, Y.S., Konkov, A.N., Larionov, A.A.** Scientific Substantiation of Constructive-technological Parameters of St. Petersburg Subway // Underground Structures Procedia Engineering, 2017, pp. 673-680.

СПИСОК ЛИТЕРАТУРЫ

1. **Алексеев М.И., Баранов Л.А., Ермолин Ю.** Риск ориентированный подход к оценке надежности городской канализационной сети // Водоснабжение и экология: проблемы и решения, 2020, №3 (83), с. 3-7.
2. **Perminov A., Perminov N.** Geotechnical and geo ecological fundamentals of sustainable life cycle of unique long-operated underground structures of water disposal systems in difficult soil conditions (the experience of St. Petersburg) //

Geotechnics fundamentals and applications in construction: new materials, structures, technologies and calculations Proceedings of the International Conference on Geotechnics Fundamentals and Applications in Construction: New Materials, Structures, Technologies and Calculations, GFAC 2019, pp. 231-234.
3. **Travush V.I., Shulyat'ev O.A**. Analysis of the results of geotechnical monitoring of "Lakhta Center" Tower // Soil Mechanics and Foundation Engineering, 2019, Vol. 56, № 2, pp. 98-106.
4. **Perminov N.** Unsteady interaction simulation of a large RC shell with heterogeneous soil milieu for a gradually increasing caisson structure // IOP conference series: materials science and engineering Institute of Physics Publishing, 2018, Paper № 012059.
5. **Mangushev R.A.,** Osokin A.I. The experience of the underground construction for the complex of buildings on a soft soil in the center of St. Petersburg // International Journal for Computational Civil and Structural Engineering, 2020, Vol . 16, № 3, pp. 47-53.
6. **Protosenya A.G., Karasev M.A., Belyakov N.A., Lebedev M.O.** Geomechanics of low-subsidence construction during the development of underground space in large cities and megalopolises // International Journal of Mechanical and Production Engineering Research and Development, 2019, Vol. 9, № 5, pp. 1005-1014.
7. **Karasev M.A., Tai Tien N., Vil'ner M.A.** Forecast of the stress-strain state of the prefabricated lining of underground tunnels of curvilinear cross-section // Bulletin of the Ural State Mining University, 2019, № 4 (56), pp. 90-97.
8. **Protosenya A.G., Karasev M.A., Belyakov N.A.** Elastoplastic problem for noncircular openings under coulomb's criterion // Journal of Mining Science, 2016, Vol. 52, № 1, pp. 53-61.
9. **Perelmuter A.V., Fialko S.Y.** Inelastic analysis of reinforced concrete structures in SCAD // International Journal for Computational Civil and Structural Engineering Publishing House ASV, LTD (Moscow), 2019, Vol. 15, № 1, pp. 54-60.
10. **Merzlyakov V.P., Vlasov A.N.** Effect of polygonal crack nets on the deformation characteristics of rocks // Soil mechanics and foundation engineering, 1993, № 30(3), pp. 85-91.
11. **Ulitsky, V., Bogov, S.** Restoration engineering of historic structures: Case study of building 12 on new Holland Island in Saint-Petersburg // Geotechnics Fundamentals and Applications in Construction: New Materials, Structures, Technologies and Calculations - Proceedings of the International Conference on Geotechnics Fundamentals and Applications in Construction: New Materials, Structures, Technologies and Calculations, GFAC 2019, pp. 390-395.
12. **Lebedev M.O., Bezrodny K.P., Larionov R.I.** Ensuring safety during construction of double-track subway tunnels in quaternary deposits // In the collection:Tunnels and Underground Cities: Engineering and Innovation meet Archaeology, Architecture and Art- Proceedings of the WTC 2019 ITA-AITES World Tunnel Congress, 45th. 2019, pp. 941-951.
13. **Dashko R.E., Alekseev I.V.** Main features of engineering-geological and geotechnical research of microbiota influence on hard rocks in the urban underground space // Conference Proceedings. 19th International Multidisciplinary Scientific Geoconference Sgem., 2019, pp. 369-376.
14. **Вознесенский Е.А., Сенцова Е.А., Никитин М.С.** Параметры динамической прочности песчаных грунтов по данным трехосных испытаний // Инженерная геология, 2019, №2, Вып.14,с.24-33.
15. **Voznesensky E.A., Kushnareva E.S.** Methodological aspects of experimental

evaluation of dynamic stability of sands in geotechnical survey // Article in the proceedings of the conference. Saint Petersburg 2008: Geosciences - From New Ideas to New Discoveries. 2008.

16. **Perminov N.** Simulation of defectless lifecycle of unique underground structures of the sewage system at the stage of their construction in difficult soil conditions // International Journal for Computational Civil and Structural Engineering Publishing House ASV, LTD (Moscow), 2019, Vol. 15, № 1, pp. 119-130.
17. **Frolov, Y.S., Konkov, A.N., Larionov, A.A.** Scientific Substantiation of Constructive-technological Parameters of St. Petersburg Subway // Underground Structures Procedia Engineering, 2017, pp. 673-680.

Nicolay A. Perminov, C.T.Sc., Chief specialist of the Institute SUE "Lengiproingproekt", docent «Emperor Alexander I St. Petersburg State Transport University», 9, Moskovsky prospect, St. Petersburg, 190031, Russia; phone +7 (812) 315-26-21; fax: +7 (812) 315-26-21; E-mail: perminov-n@mail.ru.

Перминов Николай Алексеевич, кандидат технических наук, главный специалист института ГУП «Ленгипроинжпроект», доцент «Петербургского государственного университета путей сообщения Императора Александра I»; 190031, Россия, г. Санкт-Петербург, пр. Московский, д. 9, тел. +7 (812) 315-26-21; факс +7 (812) 315-26-21; E-mail: perminov-n@mail.ru.

Mangushev Rashid Abdullovich, Corresponding Member of the Russian Academy of Architecture and Construction Sciences, Professor, Doctor of Technical Sciences; Head of Geotechnical Department, Saint-Petersburg State Architecture and Construction University, Russia, Saint-Petersburg, 2-ya Krasnoarmeyskaya 4; E-mail: ramangushev@yandex.ru.

Мангушев Рашид Абдуллович, член-корреспондент РААСН, профессор, доктор технических наук; заведующий кафедрой геотехники Санкт-Петербургского государственного архитектурно-строительного университета (СПбГАСУ), Россия, Санкт-Петербург, 2-я Красноармейская 4; E-mail: ramangushev@yandex.ru.

DOI:10.22337/2587-9618-2022-18-3-114-125

MODELING OF SEISMIC WAVES STRESSES IN A HALF-PLANE WITH A VERTICAL CAVITY FILLED WITH WATER (THE RATIO OF WIDTH TO HEIGHT IS ONE TO TEN)

Vyacheslav K. Musayev

National Research Moscow State University of Civil Engineering, Moscow, RUSSIA
Russian University of transport, Moscow, RUSSIA
Mingachevir state University, Mingachevir, AZERBAIJAN

Abstract. The problem of mathematical modeling of unsteady seismic waves in an elastic half-plane with a vertical rectangular cavity filled with water is considered. The problem of modeling problems of the transition period is an actual scientific problem. A quasi-regular approach is proposed to solve a system of linear ordinary differential equations of the second order in displacements with initial conditions and to approximate the region under study. The method is based on the schemes: a point, a line and a plane. An algorithm and a set of programs for solving flat (two-dimensional) problems that allow obtaining a stress-strain state in complex objects have been developed. To assess the reliability of the developed methodology, algorithm and software package, the problem of the effect of a plane longitudinal wave in the form of a Heaviside function on an elastic half-plane was solved. The numerical solution corresponds quantitatively to the analytical solution. The problem of mathematical modeling of unsteady elastic stress waves in a half-plane with a cavity filled with water (the ratio of width to height is one to ten) under seismic influence is solved. A system of equations consisting of 8016008 unknowns is solved. Contour stresses and components of the stress tensor are obtained in the characteristic areas of the problem under study. A cavity filled with water, with a width-to-height ratio of one to ten, reduces the amount of elastic contour stress.

Keywords: wave theory of seismic safety, wave propagation, elastic half-plane, Heaviside function, vertical rectangular cavity, water medium, contour stresses

МОДЕЛИРОВАНИЕ СЕЙСМИЧЕСКИХ ВОЛН НАПРЯЖЕНИЙ В ПОЛУПЛОСКОСТИ С ВЕРТИКАЛЬНОЙ ПОЛОСТЬЮ ЗАПОЛНЕННОЙ ВОДОЙ (СООТНОШЕНИЕ ШИРИНЫ К ВЫСОТЕ ОДИН К ДЕСЯТИ)

В.К. Мусаев

Национальный исследовательский Московский государственный строительный университет, Москва, РОССИЯ
Российский университет транспорта, Москва, РОССИЯ
Мингячевирский государственный университет, Мингячевир, АЗЕРБАЙДЖАН

Аннотация. Рассматривается задача о математическом моделировании нестационарных сейсмических волн в упругой полуплоскости с вертикальной прямоугольной полостью, заполненной водой. Проблема моделирования задач переходного периода является актуальной научной задачей. Предложен квазирегулярный подход к решению системы линейных обыкновенных дифференциальных уравнений второго порядка в перемещениях с начальными условиями и к аппроксимации исследуемой области. Методика основывается на схемах: точка, линия и плоскость. Разработаны алгоритм и комплекс программ для решения плоских (двумерных) задач, которые позволяют получать напряженно-деформированное состояние в сложных объектах. Для оценки достоверности разработанной методики, алгоритма и комплекса программ была решена задача о воздействии плоской продольной волны в виде функции Хевисайда на упругую полуплоскость. Численное решение количественно соответствует аналитическому решению. Решена задача о математическом моделировании нестационарных упругих волн напряжений в полуплоскости с полостью заполненной водой (соотношение ширины к высоте один к десяти) при сейсмическом воздействии. Решается система уравнений из 8016008 неизвестных. В характерных областях исследуемой задачи получены контурные напряжения и компоненты тензора напряжений. Полость заполненной водой, с соотношением ширины к высоте один к десяти, уменьшает величину упругого контурного напряжения.

Ключевые слова: волновая теория сейсмической безопасности, распространение волн, упругая полуплоскость, функция Хевисайда, вертикальная прямоугольная полость, водная среда, контурные напряжения

1. STATEMENT OF THE PROBLEM OF NONSTATIONARY WAVE EFFECTS IN DEFORMABLE BODIES

Unsteady elastic stress waves propagating in a deformable body interact with each other [1–8, 15–16, 18–29, 31].

After several passes and reflection of stress waves in the body, the process of propagation of disturbances becomes steady, the body is in oscillatory motion [1–8, 15–16, 18–29, 31].

The formulation of some problems of deformable solid mechanics is given in the following works [1–31].

In [9–13], some information is given about the formulation, analysis and technology for developing optimal algorithms for numerical modeling of structural mechanics problems.

The application of the considered numerical method, algorithm and software package for solving non-stationary wave problems in deformable bodies is given in the following works [7–8, 18 –29, 31].

Verification (evaluation of accuracy and reliability) of the considered numerical method, algorithm and software package is given in the following works [7–8, 18–21, 23–29, 31].

To solve the problem of modeling elastic unsteady stress waves in deformable regions of complex shape, we consider a certain body Γ in a rectangular cartesian coordinate system XOY, to which at the initial moment of time $t=0$ a mechanical non-stationary pulse effect is reported [1, 3–5, 7–8, 18–19].

Suppose that a certain body Γ is made of a homogeneous isotropic material obeying the elastic Hooke law for small elastic deformations [1, 3–5, 7–8, 18–19].

The exact equations of the two-dimensional (plane stress state) dynamic theory of elasticity have the following form [1, 3–5, 7–8, 18–19]

$$\frac{\partial \sigma_x}{\partial x} + \frac{\partial \tau_{xy}}{\partial y} = \rho \frac{\partial^2 u}{\partial t^2},$$

$$\frac{\partial \tau_{yx}}{\partial x} + \frac{\partial \sigma_y}{\partial y} = \rho \frac{\partial^2 v}{\partial t^2}, \; (x,y) \in \Gamma,$$

$$\sigma_x = \rho C_p^2 \varepsilon_x + \rho (C_p^2 - 2C_s^2)\varepsilon_y,$$

$$\sigma_y = \rho C_p^2 \varepsilon_y + \rho (C_p^2 - 2C_s^2)\varepsilon_x,$$

$$\tau_{xy} = \rho C_s^2 \gamma_{xy},$$

$$\varepsilon_x = \frac{\partial u}{\partial x}, \; \varepsilon_y = \frac{\partial v}{\partial y},$$

$$\gamma_{xy} = \frac{\partial u}{\partial y} + \frac{\partial v}{\partial x}, \; (x,y) \in (\Gamma \cup S), \quad (1)$$

where: σ_x, σ_y и τ_{xy} – components of the elastic stress tensor; ε_x, ε_y и γ_{xy} – components of the elastic strain tensor; u and v – components of the vector of elastic displacements along the axes OX and OY accordingly; ρ – material density; $C_p = \sqrt{\frac{E}{\rho(1-\nu^2)}}$ – the velocity of the longitudinal elastic wave; $C_s = \sqrt{\frac{E}{2\rho(1+\nu)}}$ – the velocity of the transverse elastic wave; ν – Poisson's ratio; E – modulus of elasticity; S $(S_1 \cup S_2)$ – the boundary contour of the body Γ.

System (1) in the area occupied by the body Γ, should integrate under initial and boundary conditions [1, 3–5, 7–8, 18–19].

2. DEVELOPMENT OF THE METHODOLOGY AND ALGORITHM

To solve a two-dimensional plane dynamic problem of the theory of elasticity with initial and boundary conditions (1), we use the finite element method in displacements [7–8, 19]. The problem is solved by the method of end-to-end counting, without highlighting gaps [7–8, 18–19].

The main relations of the finite element method are obtained using the principle of possible displacements [7–8, 18–19].

Taking into account the definition of the stiffness matrix, the inertia vector and the vector of external forces for the body Γ, we write down the approximate value of the equation of motion in the theory of elasticity [7–8, 18–19]

$$\overline{H}\ddot{\vec{\Phi}} + \overline{K}\vec{\Phi} = \vec{R}\,,$$
$$\vec{\Phi}\big|_{t=0} = \vec{\Phi}_0\,,\ \dot{\vec{\Phi}}\big|_{t=0} = \dot{\vec{\Phi}}_0 \qquad (2)$$

where: $\overline{H}$ – diagonal inertia matrix; $\overline{\mathrm{K}}$ – stiffness matrix; $\vec{\Phi}$ – vector of nodal elastic displacements; $\dot{\vec{\Phi}}$ – vector of nodal elastic displacement velocities; $\ddot{\vec{\Phi}}$ – vector of nodal elastic accelerations; $\vec{R}$ – vector of external nodal elastic forces.

Thus, using the finite element method, a linear problem with initial and boundary conditions (1) was led to a linear Cauchy problem (2).

We determine the elastic contour stress at the boundary of the region free from loads [7–8, 18–19].

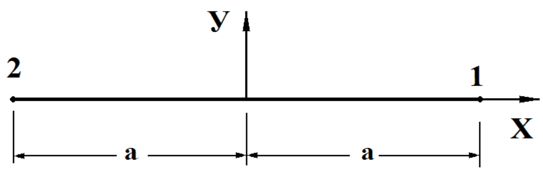

Figure 1. Contour end element with two node points

Using the degeneracy of a rectangular finite element with four nodal points, we obtain a contour finite element with two nodal points (fig. 1).

When turning the axis x on corner α counterclockwise, we get an elastic contour stress σ_k in the center of gravity of a contour finite element with two nodal points [7–8, 18–19]

$$\sigma_k = (E/(2a(1-\nu^2)))((u_1 - u_2)\cos\alpha +$$
$$+ (v_1 - v_2)\sin\alpha) \qquad (3)$$

To integrate equation (2) with a finite element version of the Galerkin method, we reduce it to the following form [7–8, 18–19]

$$\overline{H}\frac{d}{dt}\dot{\vec{\Phi}} + \overline{K}\vec{\Phi} = \vec{R}\,,\ \frac{d}{dt}\vec{\Phi} = \dot{\vec{\Phi}}\,. \qquad (4)$$

Integrating the relation (4) over the time coordinate using a finite-element version of the Galerkin method, we obtain an explicit two-layer scheme for internal and boundary node points [7–8, 18–19]

$$\dot{\vec{\Phi}}_{i+1} = \dot{\vec{\Phi}}_i + \Delta t \overline{H}^{-1}(-\overline{K}\vec{\Phi}_i + \vec{R}_i)\,,$$
$$\vec{\Phi}_{i+1} = \vec{\Phi}_i + \Delta t \dot{\vec{\Phi}}_{i+1}\,. \qquad (5)$$

The main relations of the finite element method in displacements are obtained using the principle of possible displacements and a finite element version of the Galerkin method [7–8, 18–19].

The general theory of numerical equations of mathematical physics requires for this purpose the imposition of certain conditions on the ratio of steps along the time coordinate Δt and by spatial coordinates, namely [7–8, 18–19]

$$\Delta t = k\frac{\min \Delta l_i}{C_p} \quad (i = 1,\ 2,\ 3,...)\,, \qquad (6)$$

where: Δl – the length of the side of the end element.

The results of the numerical experiment showed that at $k = 0{,}5$ the stability of the explicit two-layer scheme for internal and boundary node points on quasi-regular grids is ensured [7–8, 18–19].

For the study area consisting of materials with different physical properties, the minimum step along the time coordinate is selected (6).

On the basis of the finite element method in displacements, a technique is developed, an algorithm is developed and a set of programs is compiled for solving two-dimensional wave problems of the dynamic theory of elasticity [7–8, 18–19].

3. LONGITUDINAL WAVES IN AN ELASTIC HALF-PLANE WHEN EXPOSED AS A HEAVISIDE FUNCTION

The problem of the effect of a flat longitudinal wave in the form of a Heaviside function (fig. 3) on an elastic half-plane (fig. 2) is considered to assess the physical reliability and mathematical accuracy [7–8, 18–19].

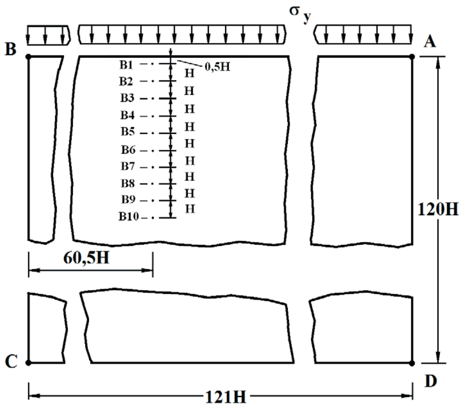

Figure 2. Statement of the problem of propagation of plane longitudinal waves in the form of a Heaviside function in an elastic half-plane

The calculations were carried out for the following units of measurement: kilogram-force (kgf); centimeter (cm); second (s). The following assumptions were made for switching to other units of measurement: 1 kgf/cm^2 ≈ 0,1 MPa; 1 kgf s^2/cm^4 ≈ 10^9 kg/m^3.

On the boundary of the half-plane AB (fig. 2) a normal voltage σ_y is applied, which at $0 \le n \le 11 \, (n = t/\Delta t)$ changes linearly from 0 to P, and at $n \ge 11$ is equal to P ($P = \sigma_0$, $\sigma_0 =$ -0,1 MPa (-1 kgf/cm^2)). Boundary conditions for a contour $BCDA$ on $t > 0$ $u = v = \dot{u} = \dot{v} = 0$. Reflected waves from the contour $BCDA$ they do not reach the studied points when $0 \le n \le 100$.

The calculations were carried out with the following initial data: $H = \Delta x = \Delta y$; $\Delta t =$ 1,393·10^{-6} s; E = 3,15·10^4 MPa (3,15·10^5 kgf/cm^2); $\nu =$ 0,2; $\rho =$ 0,255·10^4 kg/m^3 (0,255·10^{-5} kgf s^2/cm^4); C_p = 3587 m/s; C_s = 2269 m/s.

The studied computational domain has 14762 nodal points. A system of equations consisting of 59048 unknowns is solved.

The calculation results are obtained at characteristic points $B1$ - B10 (fig. 2).

As an example, a change in the normal voltage is given $\bar{\sigma}_y$ ($\bar{\sigma}_y = \sigma_y / |\sigma_0|$) (fig. 4) in time n at the point $B1$ (1 – numerical solution; 2 – analytical solution).

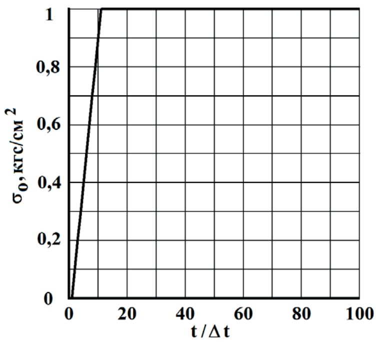

Figure 3. Impact in the form of a Heaviside function

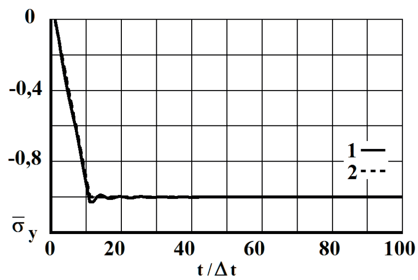

Figure 4. Change in elastic normal stress $\bar{\sigma}_y$ (the problem of propagation of plane longitudinal waves in the form of a Heaviside function in an elastic half-plane) in time $t/\Delta t$ at the point $B1$: 1 – numerical solution; 2 – analytical solution

In this case, you can use the conditions on the plane wave front, which are described in the paper [5].
At the front of a plane longitudinal wave, there are the following analytical dependences for a plane stress state $\sigma_y = -|\sigma_0|$. From here we see that the exact solution of the problem corresponds to the impact σ_0 (fig. 3).

4. MODELING OF STRESS WAVES IN A HALF-PLANE WITH A LIQUID-FILLED CAVITY (THE RATIO OF WIDTH TO HEIGHT IS ONE TO TEN) IN CASE OF SEISMIC IMPACT

The problem of the impact of a plane longitudinal unsteady seismic wave (fig. 6) parallel to the free surface of an elastic half-plane, with a cavity filled with water (the ratio of width to height is one to ten) is considered (fig. 5).
The problem under consideration was solved for the first time by V.K. Musayev using the developed methodology, algorithm and software package [7–8, 18–19].
The calculations were carried out for the following units of measurement: kilogram-force (kgf); centimeter (cm); second (s). The following assumptions were made for switching to other units of measurement: 1 kgf/cm^2 ≈ 0,1 MPa; 1 kgf s^2/cm^4 ≈ 10^9 kg/m^3.
From a point F parallel to the free surface $ABEFG$ voltage normal applied (fig. 5), which on $0 \le n \le 11$ ($n = t/\Delta t$) changes linearly from 0 before P, and when $n \ge 11$ is equal to P ($P = \sigma_0, \sigma_0 = 0{,}1$ MPa (1 kgf/cm^2)).
Boundary conditions for a contour $GHIA$ on $t > 0$ $u = v = \dot{u} = \dot{v} = 0$.
Reflected waves from the contour $GHIA$ they do not reach the studied points when $0 \le n \le 1000$.
Contour $ABEFG$ free from loads, except for the point F.
The calculations were carried out with the following initial data.

For the region $ABCDEFGHI$: $H = \Delta x = \Delta y$; $\Delta t = 1{,}393 \cdot 10^{-6}$ s; $E = 3{,}15 \cdot 10^4$ MPa ($3{,}15 \cdot 10^5$ kgf/cm^2); $\nu = 0{,}2$; $\rho = 0{,}255 \cdot 10^4$ kg/m^3 ($0{,}255 \cdot 10^{-5}$ kgf s^2/cm^4); C_p = 3587 m/s; $C_s = 2269$ m/s.
For the region $BEDC$: $H = \Delta x = \Delta y$; Δt = $3{,}268 \cdot 10^{-6}$ s; ρ = $1{,}045 \cdot 10^3$ кг/м^3 ($1{,}045 \cdot 10^{-6}$ кгс с^2/см^4); C_p = 1530 м/с.

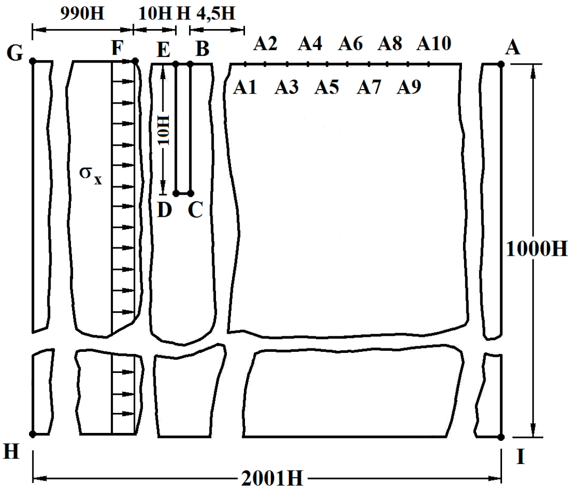

Figure 5. Statement of the problem of the effect of a plane longitudinal seismic wave on an elastic half-plane with a cavity filled with water (the ratio of width to height is one to ten)

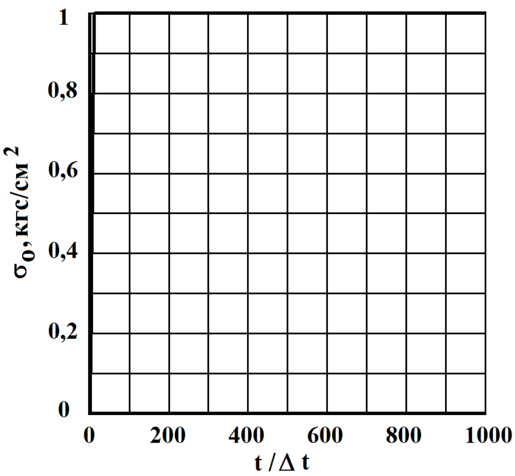

Figure 6. Impact in the form of a Heaviside function

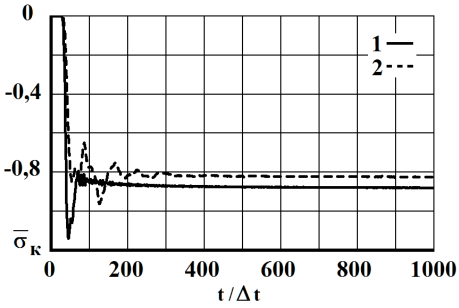

Figure 7. Changing the elastic contour stress $\overline{\sigma}_k$ in time $t/\Delta t$ at the point $A1$: 1 – in a problem without a cavity; 2 – in the problem with a cavity filled with water (the ratio of width to height is one to ten)

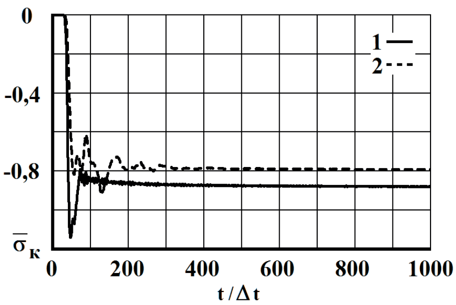

Figure 8. Changing the elastic contour stress $\overline{\sigma}_k$ in time $t/\Delta t$ at the point $A2$: 1 – in a problem without a cavity; 2 – in the problem with a cavity filled with water (the ratio of width to height is one to ten)

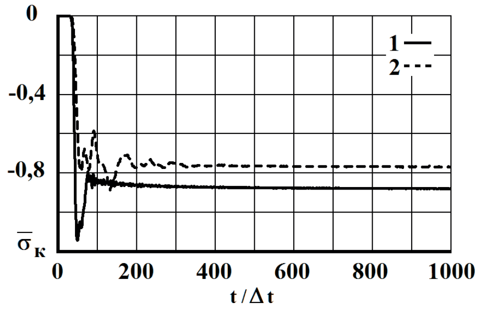

Figure 9. Changing the elastic contour stress $\overline{\sigma}_k$ in time $t/\Delta t$ at the point $A3$: 1 – in a problem without a cavity; 2 – in the problem with a cavity filled with water (the ratio of width to height is one to ten)

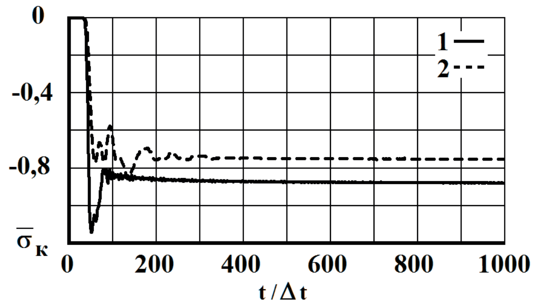

Figure 10. Changing the elastic contour stress $\overline{\sigma}_k$ in time $t/\Delta t$ at the point $A4$: 1 – in a problem without a cavity; 2 – in the problem with a cavity filled with water (the ratio of width to height is one to ten)

When calculating, the minimum time step is taken Δt = 1,393·10^{-6} s.

At the boundary of materials with different properties, the conditions of continuity of displacements are assumed.

The studied computational domain has 2004002 nodal points. A system of equations consisting of 8016008 unknowns is solved.

As an example, fig. 7-11 shows the change in the elastic contour stress $\overline{\sigma}_k$ ($\overline{\sigma}_k = \sigma_k / |\sigma_0|$) in time n in points $A1$ - A5 (рис. 5), located on the free surface of an elastic half-plane: 1 – in the problem without a cavity; 2 – in the problem with a cavity filled with water (the ratio of width to height is one to ten).

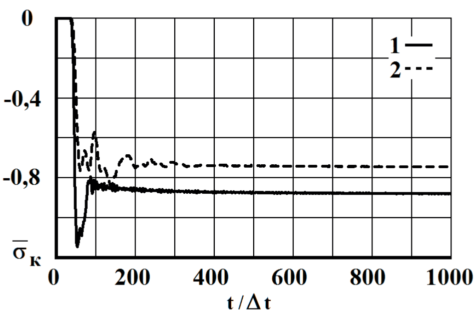

Figure 11. Changing the elastic contour stress $\overline{\sigma}_k$ in time $t/\Delta t$ at the point $A5$: 1 – in a problem without a cavity; 2 – in the problem with a cavity filled with water (the ratio of width to height is one to ten)

The distance between the points: $A1$ and $A2$ is H; $A2$ and $A3$ are H; $A3$ and $A4$ are H; $A4$ and $A5$ are H; $A5$ and $A6$ are H; $A6$ and $A7$ are H; $A7$ and $A8$ are H; $A8$ and $A9$ are H; $A9$ and $A10$ are H)

5. CONCLUSIONS

1. On the basis of the finite element method, a methodology, an algorithm and a set of programs for solving linear two-dimensional plane problems have been developed, which allow solving complex problems with non-stationary wave effects on complex objects. The main relations of the finite element method are obtained using the principle of possible displacements. The elasticity matrix is expressed in terms of the velocity of longitudinal waves, the velocity of transverse waves and the density.
2. A linear dynamic problem with initial and boundary conditions in the form of partial differential equations, for solving problems under wave effects, using the finite element method in displacements, is reduced to a system of linear ordinary differential equations with initial conditions, which is solved by an explicit two-layer scheme.
3. To predict the seismic safety of an object, under non-stationary wave effects, numerical modeling of the equations of mechanics of a deformable solid is used. A method, algorithm and a set of programs for solving linear two-dimensional (flat) problems for solving problems of safety in terms of bearing capacity (strength) in multiphase deformable bodies under non-stationary wave influences have been developed.
4. The area under study is divided by spatial variables into triangular and rectangular finite elements of the first order. According to the time variable, the area under study is divided into linear finite elements of the first order. Two displacements and two velocities of displacements at the node of the finite element are taken as the main unknowns.
5. A system with an infinite number of unknowns is reduced to a system with a finite number of unknowns. A quasi-regular approach is proposed to solve a system of linear ordinary differential equations of the second order in displacements with initial conditions and to approximate the region under study. The method is based on the schemes: a point, a line and a plane.
6. The problem of the effect of a plane longitudinal wave in the form of a Heaviside function on an elastic half-plane is solved. The computational domain under study has 14762 nodal points and 14520 finite elements. A system of equations consisting of 59048 unknowns is solved. A comparison was made with the results of the analytical solution, which showed that the discrepancy for the maximum compressive elastic normal stress $\overline{\sigma}_y$ is 2,8 %.
7. The problem of mathematical modeling of unsteady elastic stress waves in a half-plane with a cavity filled with water (the ratio of width to height is one to ten) under seismic influence is solved. At the boundary of materials with different properties, the conditions of continuity of displacements are assumed. The studied computational domain has 2004002 nodal points. A system of equations consisting of 8016008 unknowns is solved. A cavity filled with water, with a width-to-height ratio of one to ten, reduces the value of the elastic contour stress on the free surface of the elastic half-plane under non-stationary wave seismic influences.

REFERENCES

1. **Kolsky G.** Volny napryazhenij v tverdyh telah [Stress waves in solids]. Moscow, Inostrannaya literatura, 1955, 192 pages (in Russian).
2. **Napetvaridze Sh.G.** Sejsmostojkost' gidrotekhnicheskih sooruzhenij [Earthquake resistance of hydraulic structures]. Moscow, Gosstrojizdat, 1959, 216 pages (in Russian).
3. **Ionov V.I., Ogibalov P.M.** Napryazheniya v telah pri impul'sivnom nagruzhenii. [Stresses in bodies under impulsive load-

ing]. Moscow, Vysshaya shkola, 1975, 464 pages (in Russian).

4. **Novatsky V.** Teoriya uprugosti [Theory of elasticity]. Moscow, Mir, 1975, 872 pages (in Russian).
5. **Timoshenko S.P., Gudyer D.** Teoriya uprugosti [Theory of elasticity]. Moscow, Nauka, 1975, 576 pages (in Russian).
6. **Bate K., Vilson Ye.** CHislennye metody analiza i metod konechnyh elementov [Numerical methods of analysis and the finite element method]. Moscow, Strojizdat, 1982, 448 pages (in Russian).
7. **Musayev V.K.** Structure design with seismic resistance foundations // Proceedings of the ninth European conference on earthquake engineering. Moscow, TsNIISK, 1990, V. 4–A, pp. 191–200.
8. **Musayev V.K.** Testing of stressed state in the structure-base system under non-stationary dynamic effects // Proceedings of the second International conference on recent advances in geotechnical earthquake engineering and soil dynamics. Sent-Louis: University of Missouri-Rolla, 1991, V. 3, pp. 87–97.
9. **Zolotov A.B., Akimov P.A.** Diskretno-kontinual'nyj metod konechnyh elementov dlya opredeleniya napryazhenno-deformirovannogo sostoyaniya trekhmernyh konstrukcij [Discrete-continuous finite element method for determining the stress-strain state of three-dimensional structures]. // Nauka i tekhnika transporta, 2003, No. 3, pp. 72–85 (in Russian).
10. **Zolotov A.B., Akimov P.A.** Pryamoj diskretno-kontinual'nyj metod granichnyh elementov dlya opredeleniya napryazhenno-deformirovannogo sostoyaniya trekhmernyh konstukcij [A direct discrete-continuum method of boundary elements for determining the stress-strain state of three-dimensional constuctions]. // Nauka i tekhnika transporta, 2004, No. 3, pp. 70–77 (in Russian).
11. **Zolotov A.B., Akimov P.A.** Nekotorye analitiko-chislennye metody resheniya kraevyh zadach stroitel'noj mekhaniki [Some analytical and numerical methods for solving boundary value problems of structural mechanics]. Moscow, ASV, 2004, 200 pages (in Russian).
12. **Zolotov A.B., Akimov P.A.** Diskretno-kontinual'nye metody rascheta stroitel'nyh konstrukcij, zdanij i sooruzhenij [Discrete-continuous methods of calculation of building structures, buildings and structures]. // Vestnik MGSU, 2006, No. 3, pp. 97–107 (in Russian).
13. **Akimov P.A., Sidorov V.N., Kozyrev O.A.** Opredelenie sobstvennyh znachenij i sobstvennyh funkcij kraevyh zadach stroitel'noj mekhaniki na osnove diskretno-kontinual'nogo metoda konechnyh elementov [Determination of eigenvalues and eigenfunctions of boundary value problems of structural mechanics based on the discrete-continuous finite element method]. // Vestnik MGSU, 2009, No. 3, pp. 255–259 (in Russian).
14. **Kuznetsov S.V.** Seismic waves and seismic barriers // International Journal for Computational Civil and Structural Engineering. 2012, Volume 8, Issue 1, pp. 87–95.
15. **Nemchinov V.V.** Diffraction of a plane longitudinal wave by spherical cavity in elastic space // International Journal for Computational Civil and Structural Engineering, 2013, Volume 9, Issue 1, pp. 85–89.
16. **Nemchinov V.V.** Numerical methods for solving flat dynamic elasticity problems // International Journal for Computational Civil and Structural Engineering, 2013, Volume 9, Issue 1, pp. 90–97.
17. **Kuznetsov S.V., Terentyeva E.O.** Lamb problems: a review and analysis of methods and approaches // International Journal for Computational Civil and Structural Engineering, 2014, Volume 10, Issue 1, pp. 78–93.
18. **Musayev V.K.** Estimation of accuracy of the results of numerical simulation of unsteady wave of the stress in deformable objects of complex shape // International Journal for Computational Civil and Structural Engineering, 2015, Volume 11, Issue 1, pp. 135–146.
19. **Musayev V.K.** On the mathematical modeling of nonstationary elastic waves stresses

in corroborated by the round hole // International Journal for Computational Civil and Structural Engineering, 2015, Volume 11, Issue 1, pp. 147–156.

20. **Dikova Ye.V.** Dostovernost' chislennogo metoda, algoritma i kompleksa programm Musaeva V.K. pri reshenii zadachi o rasprostranenii ploskih prodol'nyh uprugih voln (voskhodyashchaya chast' – linejnaya, niskhodyashchaya chast' – chetvert' kruga) v poluploskosti [Reliability of the numerical method, algorithm and software package of Musayev V.K. when solving the problem of propagation of plane longitudinal elastic waves (the ascending part is linear, the descending part is a quarter of a circle) in a half-plane]. // Mezhdunarodnyj zhurnal eksperimental'nogo obrazovaniya, 2016, No. 12–3, pp. 354–357 (in Russian).
21. **Musayev V.K.** Mathematical modeling of seismic nonstationary elastic waves stresses in Kurpsai dam with a base (half-plane) // International Journal for Computational Civil and Structural Engineering, 2016, Volume 12, Issue 3, pp. 73–83.
22. **Musayev V.K.** Numerical simulation of non-stationary seismic stresses in elastic waves dam Koyna with base (half-plane) // International Journal for Computational Civil and Structural Engineering, 2016, Volume 12, Issue 3, pp. 84–94.
23. **Starodubtsev V.V., Akatyev S.V., Musayev A.V., Shiyanov S.M., Kurantsov O.V.** Modelirovanie uprugih voln v vide impul'snogo vozdejstviya (voskhodyashchaya chast' – chetvert' kruga, niskhodyashchaya chast' – chetvert' kruga) v poluploskosti s pomoshch'yu chislennogo metoda Musaeva V.K. [Modeling of elastic waves in the form of a pulse action (the ascending part is a quarter of a circle, the descending part is a quarter of a circle) in a half-plane using the numerical method of Musayev V.K.]. // Problemy bezopasnosti rossijskogo obshchestva, 2017, No. 1, pp. 36–40 (in Russian).
24. **Starodubtsev V.V., Akatyev S.V., Musayev A.V., Shiyanov S.M., Kurantsov O.V.** Modelirovanie s pomoshch'yu chislennogo metoda Musaeva V.K. nestacionarnyh uprugih voln v vide impul'snogo vozdejstviya (voskhodyashchaya chast' – chetvert' kruga, srednyaya – gorizontal'naya, niskhodyashchaya chast' – linejnaya) v sploshnoj deformiruemoj srede [Modeling using the numerical method of Musayev V.K. of non-stationary elastic waves in the form of a pulsed effect (the ascending part is a quarter of a circle, the middle part is horizontal, the descending part is linear) in a continuous deformable medium]. // Problemy bezopasnosti rossijskogo obshchestva, 2017, No. 1, pp. 63–68 (in Russian).
25. **Kurantsov V.A., Starodubtsev V.V., Musayev A.V., Samoylov S.N., Kuznetsov M.E.** Modelirovanie impul'sa (pervaya vetv': voskhodyashchaya chast' – chetvert' kruga, niskhodyashchaya chast' – linejnaya; vtoraya vetv': treugol'nik) v uprugoj poluploskosti s pomoshch'yu chislennogo metoda Musaeva V.K. [Modeling of a pulse (the first branch: the ascending part is a quarter of a circle, the descending part is linear; the second branch is a triangle) in an elastic half-plane using the numerical method of Musayev V.K.]. // Problemy bezopasnosti rossijskogo obshchestva, 2017, No. 2, pp. 51–55 (in Russian).
26. **Musayev V.K.** Primenenie volnovoj teorii sejsmicheskogo vozdejstviya dlya modelirovaniya uprugih napryazhenij v Kurpsajskoj plotine s gruntovym osnovaniem pri nezapolnennom vodohranilishche [Application of the wave theory of seismic impact for modeling elastic stresses in the Kurpsay dam with a soil base with an unfilled reservoir]. // Geologiya i geofizika YUga Rossii, 2017, No. 2, pp. 98–105 (in Russian).
27. **Dzhinchvelashvili G.A., Popadeykin V.V., Aksenov V.A., Blinnikov V.V., Doronin F.L.** O fizicheskoj dostovernosti i matematicheskoj tochnosti modelirovaniya nestacionarnyh voln napryazhenij v deformiruemyh telah s pomoshch'yu chislennogo metoda, algoritma i kompleksa programm Musaeva V.K. [On the physical reliability and mathematical accuracy of modeling non-

stationary stress waves in deformable bodies using a numerical method, algorithm and software package Musayev V.K.]. // Tekhnosfernaya bezopasnost', nadezhnost', kachestvo, energo i resursosberezhenie: T38. Materialy Mezhdunarodnoj nauchno-prakticheskoj konferencii. Vypusk XIX. V 2 t. Tom 2. Rostov-on-Don: Donskoj gosudarstvennyj tekhnicheskij universitet, 2017, pp. 55–63 (in Russian).
28. **Starodubtsev V.V., Musayev A.V., Shepelina P.V., Akatyev S.V., Kuznetsov M.E.** Modelirovanie prodol'nyh, otrazhennyh, interferencionnyh, difrakcionnyh, izgibnyh, poverhnostnyh i stoyachih voln s pomoshch'yu chislennogo metoda, algoritma i kompleksa programm Musaeva V.K. [Modeling of longitudinal, reflected, interference, diffraction, bending, surface and standing waves using the numerical method, algorithm and software package Musayev V.K.]. // Tekhnosfernaya bezopasnost', nadezhnost', kachestvo, energo i resursosberezhenie: T38. Materialy Mezhdunarodnoj nauchno-prakticheskoj konferencii. Vypusk XIX. V 2 t. Tom 2. Rostov-on-Don, Donskoj gosudarstvennyj tekhnicheskij universitet, 2017, pp. 230–238. (in Russian).
29. **Akatyev S.V.** Reshenie zadachi o rasprostranenii impul'snogo vozdejstviya (voskhodyashchaya chast' – linejnaya, srednyaya – gorizontal'naya, niskhodyashchaya chast' – chetvert' kruga) v uprugoj poluploskosti s pomoshch'yu chislennogo metoda Musaeva V.K. [The solution of the problem of the propagation of an impulse action (the ascending part is linear, the middle part is horizontal, the descending part is a quarter of a circle) in an elastic half-plane using the numerical method of Musayev V.K.]. // Vysshaya shkola. Novye tekhnologii nauki, tekhniki, pedagogiki: materialy Vserossijskoj nauchno-prakticheskoj konferencii «Nauka – Obshchestvo – Tekhnologii – 2018». Moscow, Moskovskij politekh, 2018, pp. 9–16 (in Russian).
30. **Avershyeva A.V., Kuznetsov S.V.** Numerical simulation of Lamb wate propagation isotropic layer // International Journal for Computational Civil and Structural Engineering, 2019, Volume 15, Issue 2, pp. 14–23.
31. **Musayev V.K.** Ocenka dostovernosti chislennogo metoda pri interferencii uprugih voln napryazhenij v beskonechnoj plastinke (vozdejstvie v vide stupenchatoj funkcii) [Estimation of the reliability of the numerical method for interference of elastic stress waves in an infinite plate (impact in the form of a step function)]. // Problemy bezopasnosti rossijskogo obshchestva, 2020, No. 1, pp. 49–54 (in Russian).

СПИСОК ЛИТЕРАТУРЫ

1. **Кольский Г.** Волны напряжений в твердых телах. М.: Иностранная литература, 1955, 192 с.
2. **Напетваридзе Ш.Г.** Сейсмостойкость гидротехнических сооружений. М.: Госстройиздат, 1959, 216 с.
3. **Ионов В.И., Огибалов П.М.** Напряжения в телах при импульсивном нагружении. М.: Высшая школа, 1975, 464 с.
4. **Новацкий В.** Теория упругости. М.: Мир, 1975, 872 с.
5. **Тимошенко С.П., Гудьер Д.** Теория упругости. М.: Наука, 1975, 576 с.
6. **Бате К., Вилсон Е.** Численные методы анализа и метод конечных элементов. М.: Стройиздат, 1982, 448 с.
7. **Musayev V.K.** Structure design with seismic resistance foundations // Proceedings of the ninth European conference on earthquake engineering. Moscow: TsNIISK, 1990, V. 4–A, pp. 191–200.
8. **Musayev V.K.** Testing of stressed state in the structure-base system under non-stationary dynamic effects // Proceedings of the second International conference on recent advances in geotechnical earthquake engineering and soil dynamics. Sent-Louis: University of Missouri-Rolla, 1991, V. 3, pp. 87–97.
9. **Золотов А.Б., Акимов П.А.** Дискретно-континуальный метод конечных элемен-

тов для определения напряженно-деформированного состояния трехмерных конструкций // Наука и техника транспорта, 2003, № 3, с. 72–85.
10. **Золотов А.Б., Акимов П.А.** Прямой дискретно-континуальный метод граничных элементов для определения напряженно-деформированного состояния трехмерных констукций // Наука и техника транспорта, 2004, № 3, с. 70–77.
11. **Золотов А.Б., Акимов П.А.** Некоторые аналитико-численные методы решения краевых задач строительной механики. М.: АСВ, 2004, 200 с.
12. **Золотов А.Б., Акимов П.А.** Дискретно-континуальные методы расчета строительных конструкций, зданий и сооружений // Вестник МГСУ, 2006, № 3, с. 97–107.
13. **Акимов П.А., Сидоров В.Н., Козырев О.А.** Определение собственных значений и собственных функций краевых задач строительной механики на основе дискретно-континуального метода конечных элементов // Вестник МГСУ, 2009, № 3, с. 255–259.
14. **Kuznetsov S.V.** Seismic waves and seismic barriers // International Journal for Computational Civil and Structural Engineering, 2012, Volume 8, Issue 1, pp. 87–95.
15. **Nemchinov V.V.** Diffraction of a plane longitudinal wave by spherical cavity in elastic space // International Journal for Computational Civil and Structural Engineering, 2013, Volume 9, Issue 1, pp. 85–89.
16. **Nemchinov V.V.** Numerical methods for solving flat dynamic elasticity problems // International Journal for Computational Civil and Structural Engineering, 2013, Volume 9, Issue 1, pp. 90–97.
17. **Kuznetsov S.V., Terentyeva E.O.** Lamb problems: a review and analysis of methods and approaches // International Journal for Computational Civil and Structural Engineering. 2014, Volume 10, Issue 1, pp. 78–93.
18. **Musayev V.K.** Estimation of accuracy of the results of numerical simulation of unsteady wave of the stress in deformable objects of complex shape // International Journal for Computational Civil and Structural Engineering, 2015, Volume 11, Issue 1, pp. 135–146.
19. **Musayev V.K.** On the mathematical modeling of nonstationary elastic waves stresses in corroborated by the round hole // International Journal for Computational Civil and Structural Engineering, 2015, Volume 11, Issue 1, pp. 147–156.
20. **Дикова Е.В.** Достоверность численного метода, алгоритма и комплекса программ Мусаева В.К. при решении задачи о распространении плоских продольных упругих волн (восходящая часть – линейная, нисходящая часть – четверть круга) в полуплоскости // Международный журнал экспериментального образования, 2016, № 12–3, с. 354–357.
21. **Musayev V.K.** Mathematical modeling of seismic nonstationary elastic waves stresses in Kurpsai dam with a base (half-plane) // International Journal for Computational Civil and Structural Engineering, 2016, Volume 12, Issue 3, pp. 73–83.
22. **Musayev V.K.** Numerical simulation of non-stationary seismic stresses in elastic waves dam Koyna with base (half-plane) // International Journal for Computational Civil and Structural Engineering, 2016, Volume 12, Issue 3, pp. 84–94.
23. **Стародубцев В.В., Акатьев С.В., Мусаев А.В., Шиянов С.М., Куранцов О.В.** Моделирование упругих волн в виде импульсного воздействия (восходящая часть – четверть круга, нисходящая часть – четверть круга) в полуплоскости с помощью численного метода Мусаева В.К. // Проблемы безопасности российского общества, 2017, № 1, с. 36–40.
24. **Стародубцев В.В., Акатьев С.В., Мусаев А.В., Шиянов С.М., Куранцов О.В.** Моделирование с помощью численного метода Мусаева В.К. нестационарных упругих волн в виде импульсного воздействия (восходящая часть – четверть круга, средняя – горизонтальная, нисхо-

дящая часть – линейная) в сплошной деформируемой среде // Проблемы безопасности российского общества, 2017, № 1, с. 63–68.
25. **Куранцов В.А., Стародубцев В.В., Мусаев А.В., Самойлов С.Н., Кузнецов М.Е.** Моделирование импульса (первая ветвь: восходящая часть – четверть круга, нисходящая часть – линейная; вторая ветвь: треугольник) в упругой полуплоскости с помощью численного метода Мусаева В.К. // Проблемы безопасности российского общества, 2017, № 2, с. 51–55.
26. **Мусаев В.К.** Применение волновой теории сейсмического воздействия для моделирования упругих напряжений в Курпсайской плотине с грунтовым основанием при незаполненном водохранилище // Геология и геофизика Юга России, 2017, № 2, с. 98–105.
27. **Джинчвелашвили Г.А., Попадейкин В.В., Аксенов В.А., Блинников В.В., Доронин Ф.Л.** О физической достоверности и математической точности моделирования нестационарных волн напряжений в деформируемых телах с помощью численного метода, алгоритма и комплекса программ Мусаева В.К. // Техносферная безопасность, надежность, качество, энерго и ресурсосбережение: Т38. Материалы Международной научно-практической конференции. Выпуск XIX. В 2 т. Том 2. Ростов-на-Дону: Донской государственный технический университет, 2017, с. 55–63.
28. **Стародубцев В.В., Мусаев А.В., Шепелина П.В., Акатьев С.В., Кузнецов М.Е.** Моделирование продольных, отраженных, интерференционных, дифракционных, изгибных, поверхностных и стоячих волн с помощью численного метода, алгоритма и комплекса программ Мусаева В.К. // Техносферная безопасность, надежность, качество, энерго и ресурсосбережение: Т38. Материалы Международной научно-практической конференции. Выпуск XIX. В 2 т. Том 2. Ростов-на-Дону: Донской государственный технический университет, 2017, с. 230–238.
29. **Акатьев С.В.** Решение задачи о распространении импульсного воздействия (восходящая часть – линейная, средняя – горизонтальная, нисходящая часть – четверть круга) в упругой полуплоскости с помощью численного метода Мусаева В.К. // Высшая школа. Новые технологии науки, техники, педагогики: материалы Всероссийской научно-практической конференции «Наука – Общество – Технологии – 2018». М.: Московский политех, 2018, с. 9–16.
30. **Avershyeva A.V., Kuznetsov S.V.** Numerical simulation of Lamb wate propagation isotropic layer // International Journal for Computational Civil and Structural Engineering, 2019, Volume 15. Issue 2, pp. 14–23.
31. **Мусаев В.К.** Оценка достоверности численного метода при интерференции упругих волн напряжений в бесконечной пластинке (воздействие в виде ступенчатой функции) // Проблемы безопасности российского общества, 2020, № 1, с. 49–54.

Мусаев Вячеслав Кадыр оглы – почетный работник высшего профессионального образования Российской Федерации, доктор технических наук, профессор, профессор кафедры Комплексной безопасности в строительстве Национального исследовательского Московского государственного строительного университета, 129337, г. Москва, Ярославское шоссе, 26, РОССИЯ, тел. +7(926)5670558. E-mail: musayev-vk@yandex.ru

Musayev Vyacheslav Kadyr ogly – honorary worker of higher professional education of the Russian Federation, doctor of technical Sciences, Professor, Professor of the Department of Integrated Safety in Construction of the National Research Moscow State University of Civil Engineering, Yaroslavl Highway, 26, Moscow, 129337, RUSSIA, tel. +7(926) 5670558. E-mail: musayev-vk@yandex.ru

DOI:10.22337/2587-9618-2022-18-3-126-136

SIMPLIFIED MODEL FOR DETERMINING THE STRESS-STRAIN STATE IN MASSIVE MONOLITHIC FOUNDATION SLABS DURING CONSTRUCTION

Anton S. Chepurnenko, Grigory V. Nesvetaev, Yuliya I. Koryanova, Batyr M. Yazyev

Don State Technical University, Rostov-on-Don, RUSSIA

Abstract. The article proposes the simplified method for determining stresses in massive monolithic foundation slabs arising from the heat release of concrete during the hardening process. The proposed technique makes it possible to reduce a three-dimensional problem to a one-dimensional one based on the features of the distribution of stresses and strains in the structures under consideration, identified during finite element modeling in a three-dimensional setting. The resulting resolving equations take into account the creep and shrinkage of concrete, the coefficient of reinforcement of the structure. The strength and deformation characteristics of concrete are assumed as functions of the degree of maturity of the concrete, which in turn is determined by the time and temperature of curing. Approbation of the developed model is carried out by comparison with the calculation in a three-dimensional setting in the ANSYS software package. The influence of creep and contraction shrinkage of concrete, the degree of concrete maturity and the coefficient of reinforcement on the stress-strain state of structures is investigated.

Keywords: thermal stresses, massive monolithic structures, foundation slab, reinforced concrete, creep, shrinkage

УПРОЩЕННАЯ МОДЕЛЬ ОПРЕДЕЛЕНИЯ НАПРЯЖЕННО-ДЕФОРМИРОВАННОГО СОСТОЯНИЯ В МАССИВНЫХ МОНОЛИТНЫХ ФУНДАМЕНТНЫХ ПЛИТАХ В ПРОЦЕССЕ ВОЗВЕДЕНИЯ

А.С. Чепурненко, Г.В. Несветаев, Ю.И. Корянова, Б.М. Языев

Донской государственный технический университет, Ростов-на-Дону, РОССИЯ

Аннотация. В статье предлагается упрощенная методика определения напряжений в массивных монолитных фундаментных плитах, возникающих вследствие тепловыделения бетона в процессе твердения. Предлагаемая методика позволяет свести трехмерную задачу к одномерной на основе особенностей распределения напряжений и деформаций в рассматриваемых конструкциях, выявленных при конечно-элементном моделировании в трехмерной постановке. В полученных разрешающих уравнениях учитывается ползучесть и усадка бетона, коэффициент армирования конструкции. Прочностные и деформативные характеристики бетона принимаются функциями от степени зрелости бетона, которая в свою очередь определяется временем и температурой твердения. Выполняется апробация разработанной модели путем сравнения с расчетом в трехмерной постановке в программном комплексе ANSYS. Исследуется влияние ползучести и контракционной усадки бетона, степени зрелости бетона и коэффициента армирования на напряженно-деформированное состояние конструкций.

Ключевые слова: температурные напряжения, массивные монолитные конструкции, фундаментная плита, железобетон, ползучесть, усадка

INTRODUCTION

For massive monolithic structures, which include foundation slabs, the problem of early cracking at the construction stage is relevant. This problem primarily arises because of uneven heating of structures, which in turn is due to the internal heat release of concrete during hardening and heat exchange with the environment [1-4].

Predicting the risk of early cracking is possible using computer simulation methods.

When modeling rectangular in plane massive foundation slabs, as a rule, a quarter of the structure is considered together with the soil massif [5] (Fig. 1).

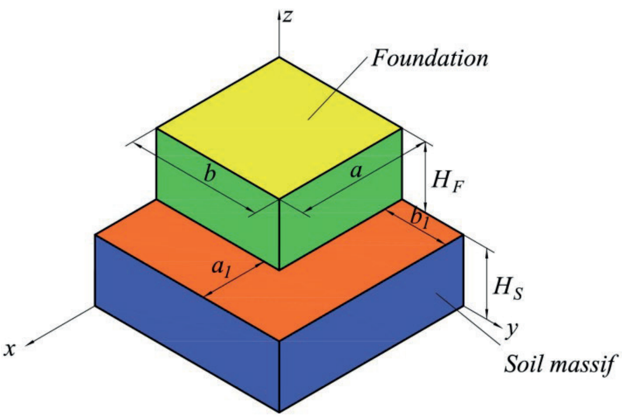

Figure 1. Calculation scheme of the foundation

The temperature field is determined from the solution of the differential equation of heat conduction [6]:

$$\lambda\left(\frac{\partial^2 T}{\partial x^2}+\frac{\partial^2 T}{\partial y^2}+\frac{\partial^2 T}{\partial z^2}\right)+Q=\rho c\frac{\partial T}{\partial t}, \tag{1}$$

where λ is the coefficient of thermal conductivity, T is the temperature, Q is the density of internal heat sources (W/m^3), ρ is the material density, c is the specific heat, t is the time.

In the presence of convective heat exchange with the environment (on the upper and side surfaces of the foundation, the upper surface of the soil), the boundary conditions are written as:

$$\lambda\frac{\partial T}{\partial n}+h\left(T-T_\infty\right)=0, \tag{2}$$

where n is the surface normal, h is the heat transfer coefficient, T_∞ is the ambient temperature.

On the side surfaces of the soil mass at a sufficient distance from the foundation, the temperature can be considered given:

$$T_g\left(t\right)=f\left(t\right). \tag{3}$$

The thermal conductivity coefficient and the specific heat capacity of concrete in equation (1) are generally functions of time. However, this factor cannot be taken into account in existing software systems (ANSYS, Abaqus, etc.)

According to [7], the thermal conductivity coefficient λ is the function of the hydration degree ξ:

$$\lambda\left(\xi\right)=\lambda_\infty\left(1.33-0.33\xi\right). \tag{4}$$

The hydration degree is determined from the differential equation [8]:

$$\frac{\partial\xi}{\partial t}=f\left(\xi\right)\exp\left(-\frac{E_a}{RT}\right), \tag{5}$$

where E_a is the activation energy, R is the universal gas constant.

For the function $f(\xi)$, the empirical formula can be used [8]:

$$f\left(\xi\right)=\frac{m}{n_0}\left(\frac{A}{m\xi_\infty}+\xi\right)\left(\xi_\infty-\xi\right)\exp\left(-\frac{\overline{n}\xi}{\xi_\infty}\right), \tag{6}$$

Here A_0, m, n_0 and $\overline{n}$ are the material constants depending on the type of cement.

When modeling the stress-strain state, it is necessary to take into account the dependence of the strength and deformation characteristics of concrete on time. One of the few authors that take this factor into account is T.C. Nguyen [9-

11]. For the elastic modulus, an explicit dependence on time is taken in the form

$$E(t) = E_0(1 - e^{-at}). \tag{7}$$

Formula (6) is not the only option for describing the dependence of the elastic modulus on time. Some other formulas can be found, for example, in [12, 13].

However, this approach is rather simplified, since the physical and mechanical characteristics of concrete at each point depend not only on the hardening time, but also on the history of temperature changes over time. More perfect is the concept of expressing the physical and mechanical characteristics of concrete through the degree of its maturity *DM* [14], determined by the integral:

$$DM(t) = \int_0^t T(\tau)\,d\tau. \tag{8}$$

The ultimate compressive strength of concrete at time *t* can be determined by the empirical formula [15]:

$$R_b = R_{28}\exp(0.35\left(1 - \left(\frac{15800 - 122.5\overline{T}}{\overline{T}t}\right)^{0.55}\right)) \tag{9}$$

where R_{28} is the strength of concrete at the age of 28 days (MPa), $\overline{T} = DM/t$, *t* is the age of concrete in hours.

The elastic modulus of concrete *E* (MPa) at time *t* can be represented as a function of the compressive strength R_b at time *t* [16]:

$$E = 1000\frac{0.04R_b + 57}{1 + \dfrac{29}{3.8 + 0.8R_b}}. \tag{10}$$

Accounting for the degree of maturity of concrete by standard means of the existing finite element software is also very difficult. In addition, since the temperature is different at each point of the structure, the modulus of elasticity becomes a function not only of time, but also of coordinates. Thus, the problem of the mechanics of an inhomogeneous body takes place.

In addition to taking into account the dependence of material characteristics on time, the determination of the stress-strain state of massive monolithic structures in the process of erection requires taking into account creep deformations and contraction shrinkage.

The purpose of this work is to develop a methodology for calculating the stress-strain state of massive monolithic foundation slabs in the process of construction, taking into account the above factors. A simplified technique is proposed, which, based on the characteristic features of the stress-strain state, makes it possible to reduce a three-dimensional problem to a one-dimensional one.

DERIVATION OF THE RESOLVING EQUATIONS

Finite element modeling of the temperature field in a three-dimensional formulation shows that for massive foundation slabs, with the exception of the edges, the temperature distribution is one-dimensional, i.e. the temperature does not depend on the *x*, *y* coordinates, and is a function of the *z* coordinate only. (Fig. 2)

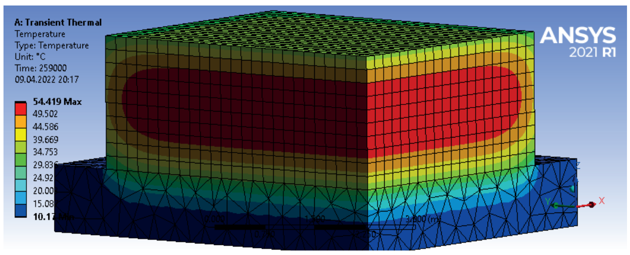

Figure 2. Temperature distribution in the foundation slab due to internal heat release of concrete during construction

Simulation of the stress-strain state in a three-dimensional setting shows that, with the exception of the edges, the stresses σ_z, τ_{xz}, τ_{xy}

and τ_{yz} are close to zero, and the stresses σ_x and σ_y are approximately equal to each other, even if the sides of the foundation are not equal to each other (Fig. 3-7).

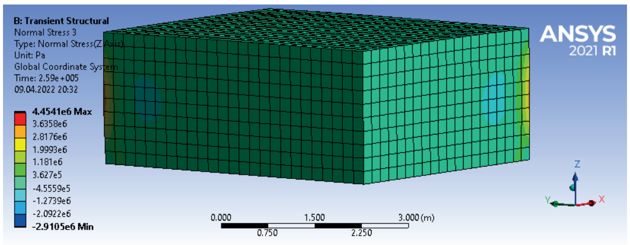

Figure 3. Stress σ_z distribution

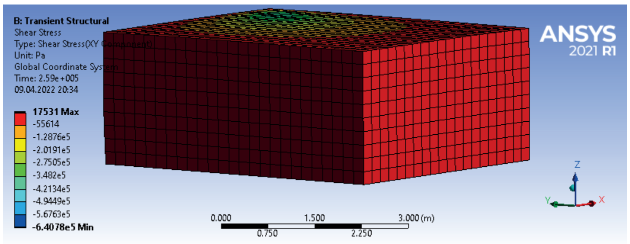

Figure 4. Stress τ_{xy} distribution

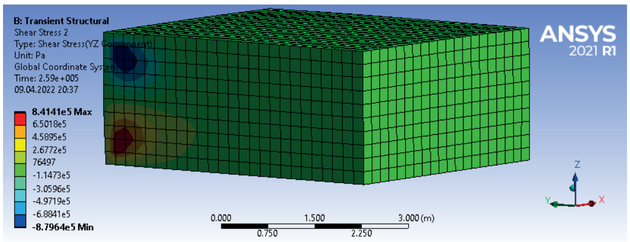

Figure 5. Stress τ_{yz} distribution

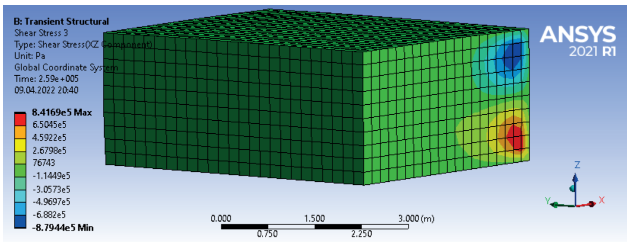

Figure 6. Stress τ_{xz} distribution

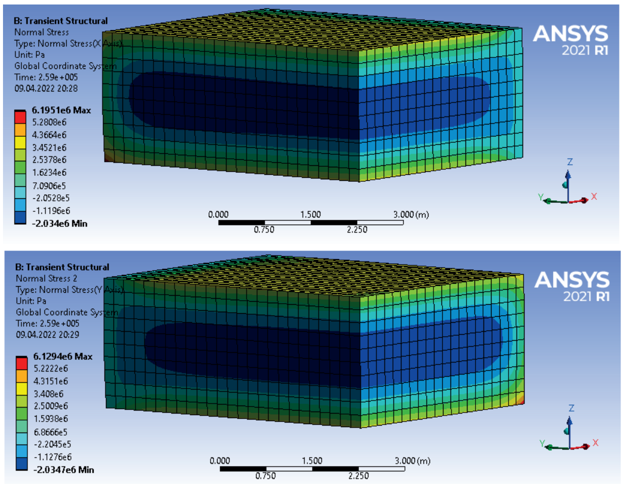

Figure 7. Stress distribution for σ_x (top) and σ_y (bottom)

Total deformations ε_x and ε_y, with the exception of the edges, are almost constant throughout the thickness of the slab, equal to each other and do not depend on the coordinates *x* and *y* (Fig. 8)

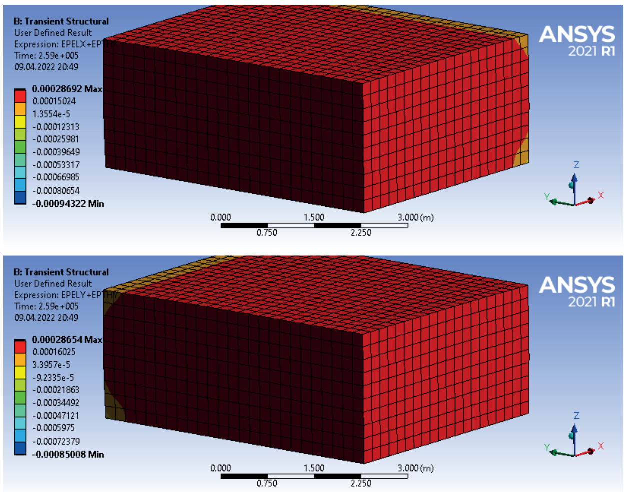

Figure 8. Total strain distribution for ε_x (top) and ε_y (bottom)

Based on these features, we propose the simplified method for calculating the stress-strain state.

In a biaxial stress state, the relationship between stresses and strains can be represented as:

$$\varepsilon_x = \frac{1}{E}(\sigma_x - \nu\sigma_y) + \varepsilon_f; \qquad \varepsilon_y = \frac{1}{E}(\sigma_y - \nu\sigma_x) + \varepsilon_f, \tag{11}$$

Here, the modulus of elasticity is taken as a function of coordinates, ε_f are the forced deformations, representing the sum of temperature deformations, contraction shrinkage deformations and creep strains:

$$\varepsilon_f = \alpha\Delta T + \varepsilon_{sh} + \varepsilon_{cr}. \tag{12}$$

At $\sigma_x = \sigma_y = \sigma$ and $\varepsilon_x = \varepsilon_y = \varepsilon$, expressing stresses from (11) in terms of strains, we obtain:

$$\sigma = \frac{E}{1-\nu}(\varepsilon - \varepsilon_f). \tag{13}$$

We assume that the soil under foundation slab does not prevent the free expansion of the foundation in the directions x and y. The ε value can be found from the condition that the axial forces $N = N_x = N_y = 0$:

$$N = \int_0^h \sigma dz = 0, \tag{14}$$

where h is the foundation slab thickness.
Substituting (13) into (14), we get:

$$\frac{1}{1-\nu}\left(\varepsilon \int_0^h E(z)dz - \int_0^h E(z)\varepsilon_f(z)dz\right) = 0, \tag{15}$$

From (15) it is possible to find ε:

$$\varepsilon = \frac{\int_0^h E(z)\varepsilon_f(z)dz}{\int_0^h E(z)dz}. \tag{16}$$

The proposed approach also makes it possible to take into account the reinforcement of the structure in the case when the coefficients of reinforcement along the x and y axes are the same.
The deformation of the i-th reinforcement layer can be written as:

$$\varepsilon_{s,i} = \frac{\sigma_{s,i}}{E_s} + \alpha_s \Delta T_{s,i}, \tag{17}$$

where α_s is the coefficient of linear thermal expansion of steel, E_s is the modulus of elasticity of steel.
We express from (17) the stress in the reinforcement and take into account that the reinforcement and concrete work together ($\varepsilon_{s,i} = \varepsilon$):

$$\sigma_{s,i} = E_s(\varepsilon - \alpha_s \Delta T_{s,i}). \tag{18}$$

The axial force represents the sum of the forces perceived by the reinforcement and concrete:

$$N = \int_0^h \sigma dz + \sum \sigma_{s,i} A_{s,i} = 0, \tag{19}$$

where $A_{s,i}$ is the cross-sectional area of the reinforcement of the i-th layer per 1 meter of the length of the slab.
Substituting (13) and (18) into (19), we obtain the following formula for ε:

$$\varepsilon = \frac{\int_0^h E(z)\varepsilon_f(z)dz + (1-\nu)\sum E_s \alpha_s \Delta T_{s,i} A_{s,i}}{\int_0^h E(z)dz + (1-\nu)\sum E_s A_{s,i}}. \tag{20}$$

CALCULATION ALGORITHM

The first step in calculating the stress-strain state of foundation slabs is to determine the temperature field. As mentioned earlier, with the exception of the edges of the foundation slab, the temperature distribution is one-dimensional, and to determine the function $T(z,t)$, instead of equation (1), one can use the equation:

$$\lambda(z,t)\frac{\partial^2 T}{\partial z^2}+Q=\rho c\frac{\partial T}{\partial t}. \qquad (17)$$

To solve equation (17), a grid in z and t is introduced. When solving this equation by the finite element method, the problem is reduced to a system of differential equations

$$[C]\frac{\partial\{\mathrm{T}\}}{\partial t}+[K]\{T\}+\{F\}=0, \qquad (18)$$

where $[C]$ is the damping matrix, $[K]$ is the thermal conductivity matrix, $\{F\}$ is the load vector.
The integration of system (18) is carried out together with the solution of differential equation (5) using the Euler method or other difference schemes.
Further, at each time step, the stress-strain state is calculated.
Contraction shrinkage ε_{sh} is determined by the empirical formula [17]:

$$\varepsilon_{sh}(t)=-\left(0.2B-2\right)\left(a\ln t-b\right)\cdot 10^{-5}\le 0, \qquad (17)$$

where B is the concrete class (MPa), a and b are the empirical coefficients
For quick hardening concrete $a=0.31$ and $b=0.4$, for slow hardening concrete $a=0.41$ and $b=0.85$.
To determine creep strains, a viscoelastic model of hereditary aging of concrete is used [13]. In the case of a biaxial stress state, the creep law is written as:

$$\begin{aligned}\varepsilon_x&=\frac{1}{E(t)}(\sigma_x(t)-\nu\sigma_y(t))-\\&-\int_0^t(\sigma_x(\tau)-\nu\sigma_y(\tau))\cdot\frac{\partial C(t,\tau)}{\partial\tau}d\tau.\end{aligned} \qquad (19)$$

The measure of creep was used in the form:

$$\begin{aligned}C(t,\tau)&=\frac{\varphi(\tau)}{E(t)}(1-e^{-\gamma(t-\tau)}),\\ \varphi(\tau)&=\frac{8000}{E(\tau)^{0.785}},\quad \gamma=0.05\,days^{-1}.\end{aligned} \qquad (20)$$

From (18), the creep deformation, taking into account the equality of stresses σ_x and σ_y can be written as:

$$\varepsilon_{cr}=-(1-\nu)\int_0^t\sigma(\tau)\cdot\frac{\partial C(t,\tau)}{\partial\tau}d\tau. \qquad (21)$$

The stress calculation is carried out step by step. The creep strains in the next step are determined from the strains and stresses in the previous step. If the forced deformation ε_f in each node is known at the current step, one can find the value ε using formula (20). And then the stress in each node can be calculated using formula (11).

RESULTS AND DISCUSSION

To test the developed technique, a test problem was solved for a foundation slab with dimensions $a=8$ m, $b=10$ m, H_f = 2 m. The initial temperature of the concrete mix, the ambient temperature, and the initial temperature of the soil were assumed to be the same and equal to 10.5 ^{0}C for simplicity. B25 class concrete was assumed with thermophysical properties: λ_∞ = 2.67 W/(m·^{0}C), ρ = 2500 kg/m^3, c = 1000 J/(kg·^{0}C). Thermal properties of the soil were: λ = 1.5 W/(m·^{0}C), ρ = 1600 kg/m^3, c = 1875 J/(kg·^{0}C). Heat transfer coefficients on the upper surface of the soil and on the top of the foundation were 25 W/(m^2·^{0}C) and 4.5 W/(m^2·^{0}C) respectively. The time interval from 0 to 72 hours was considered. Thermal expansion coefficient of concrete was α = 10^{-5} 1/^{0}C.

We have used for concrete the time dependence of the density of internal sources which is shown in Fig. 9.

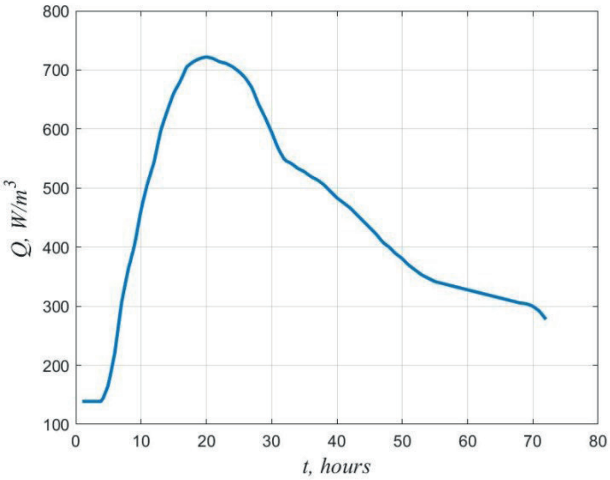

Figure 9. Dependence of the density of internal heat sources of concrete on time

The comparison was carried out with the solution in the ANSYS software package in a three-dimensional formulation. When calculating in ANSYS, the modulus of elasticity of concrete was assumed to be constant in time and equal to 2.45×10^4 MPa, which corresponded to the average value of the modulus of elasticity over the thickness of the slab at the age of 72 hours.

Figure 10 shows the change in time of the maximum temperature in the foundation and the temperature on the upper surface, obtained from the solution of a one-dimensional problem, taking into account the dependence of the thermal conductivity coefficient on the degree of hydration. The dashed lines correspond to the solution in the ANSYS software package in a three-dimensional setting at a constant thermal conductivity coefficient. From the graphs presented, it can be seen that, firstly, the conditions on the side surfaces of the foundation do not affect the temperature distribution in the center, and, secondly, the change in the thermal conductivity coefficient over time can be neglected.

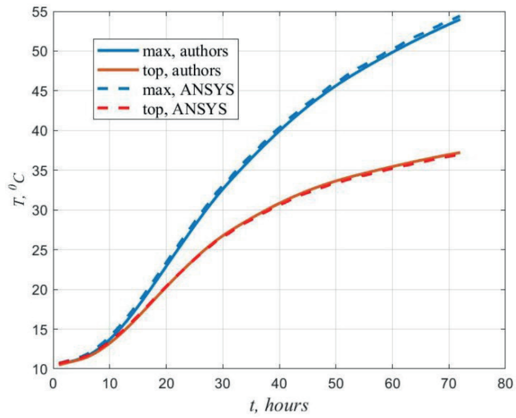

Figure 10. Time change of temperatures in the foundation

Fig. 11 and 12 show the change in time of stresses σ_x in the center of the foundation at the upper and lower surfaces respectively (at points with the highest tensile stresses). Curve 1 corresponds to the solution according to the author's method at a constant modulus of elasticity without taking into account creep and contraction shrinkage. Curve 2 corresponds to the solution taking into account the dependence of the elasticity modulus on the degree of concrete maturity, but without taking into account creep and contraction shrinkage. Curve 3 takes into account the dependence of the elastic modulus on time, creep, and contraction shrinkage. Curve 4 was plotted taking into account the factors listed above and a reinforcement factor of 2%. The dashed line shows the solution in the ANSYS software package.

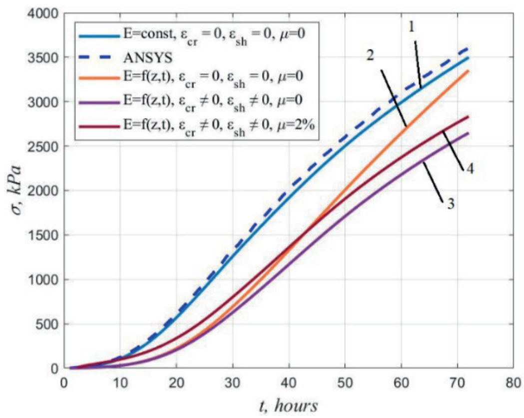

Figure 11. Change in stresses σ_x at the upper surface of the foundation

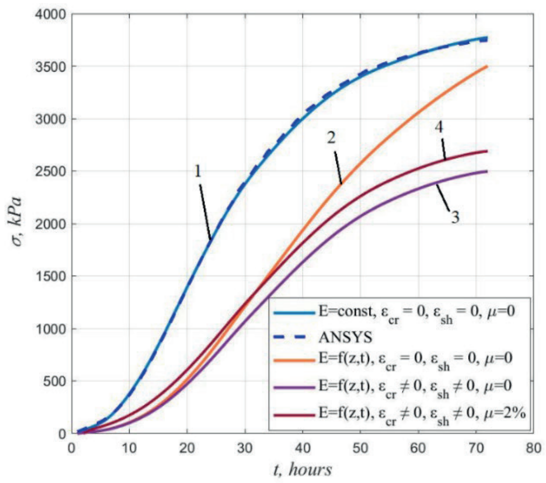

Figure 12. Stress σ_x change at the bottom surface of the foundation

Figures 11-12 show the following:

1. The results obtained with E = const according to the author's method and in the ANSYS software package differ slightly.
2. Neglecting the dependence of the elasticity modulus of concrete on the degree of its maturity leads to an overestimation of stresses in concrete.
3. Neglect of the concrete creep also leads to overestimation of stresses.
4. When reinforcement is taken into account, the stresses in concrete at the stage of construction are higher, which, firstly, can be explained by the presence of a small difference between the coefficients of linear thermal expansion of steel and concrete (α_s = 1.15·10^{-5} and α_b = 1·10^{-5}), and secondly by the contraction shrinkage of concrete.
5. With the accepted initial data, the tensile stresses in concrete during the curing process can reach almost 3 MPa. Similar results were obtained earlier in the works [14,18]. Obviously, concretes of mass classes (B25-B35) are not able to withstand such stresses, especially at the stage of structure formation, and measures are needed to reduce the risk of early cracking. Such measures include the regulation of the kinetics of heat release of concrete [19, 20] and the parameters of heat transfer on surfaces [21], the installation of cooling systems [22], etc.

CONCLUSIONS

A simplified, but at the same time effective method for determining the stress-strain state of massive monolithic foundation slabs during the construction process was proposed.

It was shown that the problem of calculating thermal stresses in massive monolithic foundation slabs can be reduced to a one-dimensional one without compromising the accuracy of the results.

The developed technique was tested by comparison with the results of calculations in the ANSYS software package in a three-dimensional formulation. The discrepancy between the results is insignificant.

The proposed method makes it possible to take into account the dependence of the modulus of elasticity of concrete on the degree of its maturity, creep, contraction shrinkage, and reinforcement coefficient.

It has been established that neglect of creep and changes in the modulus of elasticity of concrete over time leads to overestimated stress values. The contraction shrinkage of concrete and the difference in the coefficients of linear thermal expansion of concrete and reinforcement lead to the fact that with an increase in the coefficient of reinforcement, the stresses in concrete at the stage of construction increase.

REFERENCES

1. **Castilho E. et al.** FEA model for the simulation of the hydration process and temperature evolution during the con-creting of an arch dam // Engineering Structures. – 2018. – Vol. 174. – Pp. 165-177.
2. **Korotchenko I. et al.** Thermal stressed state in massive concrete structures in the winter building period // MATEC Web of

Conferences. – 2016. – Vol. 53. – Article 01001.

3. **Abeka H., Agyeman S., Adom-Asamoah M.** Thermal effect of mass concrete structures in the tropics: Experimental, modelling and parametric studies // Cogent Engineering. – 2017. – Vol. 4. – Article 1278297.
4. **Xu J. et al.** Finite element simulation of prevention thermal cracking in mass concrete // International Journal of Computing Science and Mathematics. – 2019. – Vol. 10. – Pp. 327-339.
5. **Havlásek P. et al.** Thermo-mechanical simulations of early-age concrete cracking with durability predictions // IOP Conference Series: Materials Science and Engineering. – 2017. – Vol. 236. – Article 012052.
6. **Semenov K. et al.** Unsteady temperature fields in the calculation of crack resistance of massive foundation slab during the building period // International Scientific Conference on Energy, Environmental and Construction Engineering. Springer, Cham, 2019; pp. 455-467.
7. **Kuriakose B., Rao B. N., Dodagoudar, G. R.** Early-age temperature distribution in a massive concrete foundation // Procedia Technology. – 2016. – Vol. 25. – Pp. 107-114.
8. **Kuryłowicz-Cudowska A.** Determination of thermophysical parameters involved in the numerical model to predict the temperature field of cast-in-place concrete bridge deck // Materials. – 2019. – Vol. 12. – Article 3089.
9. **Nguyen T.C., Luu, X.B.** Reducing temperature difference in mass concrete by surface insulation // Magazine of Civil Engineering. – 2019. – Vol. 88(4). – Pp. 70–79.
10. **Nguyen T. C., Huynh T. P., Tang V. L.** Prevention of crack formation in massive concrete at an early age by cooling pipe system // Asian Journal of Civil Engineering. – 2019. – Vol. 20. – Pp. 1101-1107.
11. **Aniskin N., Nguyen T. C.** Influence factors on the temperature field in a mass concrete // E3S Web of Conferences. – 2019. – Vol. 97. – Article 05021.
12. **Chuc N. T., Aniskin N.** The effect of formworks on the temperature regime in the mass concrete // Magazine of Civil Engineering. – 2020. – №. 7 (99). – Article 9911.
13. **Tamrazyan A. G., Esayan S. G.** Concrete creep mechanics. – Moscow: MGSU. – 2012. – 524 p. (In Russian)
14. Basis for and practical approaches to stress calculations and crack risk estimation in hardening concrete structures. State of the art. COIN Project report 31 - 2011. SINTEF Building and Infrastructure. 135 p.
15. **Nesvetayev G. V., Koryanova Yu. I., Sukhin D. P.** On the influence temperature conditions during concreting of massive monolithic reinforced concrete structures on the strength of concrete // Engineering Journal of Don. – 2021. – №. 10 (82). – URL: http://ivdon.ru/en/magazine/archive/n10y2021/7228 (In Russian)
16. **Mailyan D.R., Nesvetaev G.V.** Rigidity and strength analysis of reinforced concrete beams by varying elasticity modulus // Vestnik Tomskogo gosudarstvennogo arkhitekturno-stroitel'nogo universiteta. Journal of Construction and Architecture. – 2018. – Vol. (4). – Pp. 86-93. (In Russian)
17. **Nesvetaev G., Koryanova Y., Zhilnikova T.** On effect of superplasticizers and mineral additives on shrinkage of hardened cement paste and concrete // MATEC Web of Conferences. – 2018. – Vol. 196. – Article 04018.
18. **Diaz F., Johansson R.** Early-Age Thermal Cracking in Concrete, A FE-Modelling approach. Master's Thesis in the Master's Programme Structural Engineering and Building Technology, Department of Civil and Environmental Engineering, Göteborg, Sweden, 2016.
19. **Van Lam T. et al.** Effect of natural pozzolan on strength and temperature distribution of heavyweight concrete at early ages //

MATEC Web of Conferences. – 2018. – Vol. 193. – Article 03024.
20. **Van Lam T. et al.** Composition calculation and cracking estimation of concrete at early ages // Magazine of Civil Engineering. – 2018. – Vol. 6(82). – Pp. 136-148.
21. **Chuc N. T. et al.** The effects of insulation thickness on temperature field and evaluating cracking in the mass concrete // Electronic Journal of Structural Engineering. – 2018. – Vol. 18. – Pp. 128-132.
22. **Tasri A., Susilawati A.** Effect of material of post-cooling pipes on temperature and thermal stress in mass concrete // Structures. – 2019. – Vol. 20. – Pp. 204-212.

СПИСОК ЛИТЕРАТУРЫ

1. **Castilho E. et al.** FEA model for the simulation of the hydration process and temperature evolution during the concreting of an arch dam // Engineering Structures. – 2018. – Vol. 174. – Pp. 165-177.
2. **Korotchenko I. et al.** Thermal stressed state in massive concrete structures in the winter building period // MATEC Web of Conferences. – 2016. – Vol. 53. – Article 01001.
3. **Abeka H., Agyeman S., Adom-Asamoah M.** Thermal effect of mass concrete structures in the tropics: Experimental, modelling and parametric studies // Cogent Engineering. – 2017. – Vol. 4. – Article 1278297.
4. **Xu J. et al.** Finite element simulation of prevention thermal cracking in mass concrete // International Journal of Computing Science and Mathematics. – 2019. – Vol. 10. – Pp. 327-339.
5. **Havlásek P. et al.** Thermo-mechanical simulations of early-age concrete cracking with durability predictions // IOP Conference Series: Materials Science and Engineering. – 2017. – Vol. 236. – Article 012052.
6. **Semenov K. et al.** Unsteady temperature fields in the calculation of crack resistance of massive foundation slab during the building period // International Scientific Conference on Energy, Environmental and Construction Engineering. Springer, Cham, 2019; pp. 455-467.
7. **Kuriakose B., Rao B. N., Dodagoudar, G. R.** Early-age temperature distribution in a massive concrete foundation // Procedia Technology. – 2016. – Vol. 25. – Pp. 107-114.
8. **Kuryłowicz-Cudowska A.** Determination of thermophysical parameters involved in the numerical model to predict the temperature field of cast-in-place concrete bridge deck // Materials. – 2019. – Vol. 12. – Article 3089.
9. **Нгуен Ч.Ч., Лыу С.Б.** Уменьшение разницы температур в монолитном бетоне за счет поверхностной изоляции // Инженерно-строительный журнал. 2019. № 4(88). С. 70–79.
10. **Nguyen T. C., Huynh T. P., Tang V. L.** Prevention of crack formation in massive concrete at an early age by cooling pipe system // Asian Journal of Civil Engineering. – 2019. – Vol. 20. – Pp. 1101-1107.
11. **Aniskin N., Nguyen T. C.** Influence factors on the temperature field in a mass concrete // E3S Web of Conferences. – 2019. – Vol. 97. – Article 05021.
12. **Chuc N. T., Aniskin N.** The effect of formworks on the temperature regime in the mass concrete //Magazine of Civil Engineering. – 2020. – №. 7 (99). – Article 9911.
13. **Тамразян А. Г., Есаян С. Г.** Механика ползучести бетона //М.: МГСУ. – 2012. – 524 с.
14. Basis for and practical approaches to stress calculations and crack risk estimation in hardening concrete structures. State of the art. COIN Project report 31 - 2011. SINTEF Building and Infrastructure. 135 p.

15. **Несветаев Г.В., Корянова Ю.И., Сухин Д.П.** О влиянии условий выдерживания при возведении массивных монолитных железобетонных конструкций на прочность бетона // Инженерный вестник Дона. – 2021. – №. 10 (82). – URL: http://ivdon.ru/ru/magazine/archive/n10y2021/7228
16. **Маилян Д.Р., Несветаев Г.В.** Регулирование жесткости и прочности железобетонных балок варьированием модуля упругости бетона // Вестник Томского государственного архитектурно-строительного университета. – 2018. – Т. 20. – №. 4. – С. 86-93.
17. **Nesvetaev G., Koryanova Y., Zhilnikova T.** On effect of superplasticizers and mineral additives on shrinkage of hardened cement paste and concrete // MATEC Web of Conferences. – 2018. – Vol. 196. – Article 04018.
18. **Diaz F., Johansson R.** Early-Age Thermal Cracking in Concrete, A FE-Modelling approach. Master's Thesis in the Master's Programme Structural Engineering and Building Technology, Department of Civil and Environmental Engineering, Göteborg, Sweden, 2016.
19. **Van Lam T. et al.** Effect of natural pozzolan on strength and temperature distribution of heavyweight concrete at early ages // MATEC Web of Conferences. – 2018. – Vol. 193. – Article 03024.
20. **Ван Лам Т., Нгуен Ч.Ч., Булгаков Б.И., Ань Ф.Н.** Расчет состава и оценка трещинообразования бетона в раннем возрасте // Инженерно-строительный журнал. – 2018. – № 6(82). – С. 136–148.
21. **Chuc N.T. et al.** The effects of insulation thickness on temperature field and evaluating cracking in the mass concrete // Electronic Journal of Structural Engineering. – 2018. – Vol. 18. – Pp. 128-132.
22. **Tasri A., Susilawati A.** Effect of material of post-cooling pipes on temperature and thermal stress in mass concrete // Structures. – 2019. – Vol. 20. – Pp. 204-212.

Chepurnenko Anton Sergeevich, DSc, Associate Professor of the Department of Strength of Materials, Don State Technical University, 344000, Russia, Rostov-on-Don, Gagarin sq., 1, tel. +7 (863) 201-91-36, e-mail: anton_chepurnenk@mail.ru

Nesvetaev Grigory Vasilievich, DSc, Professor of the Department of Technology of Construction Production, Don State Technical University, 344000, Russia, Rostov-on-Don, Gagarin sq., 1, tel. +7 (863) 201-94-64 , e-mail: nesgrin@yandex.ru

Koryanova Yulia Igorevna, PhD, Associate Professor of the Department of Technology of Construction Production, Don State Technical University, 344000, Russia, Rostov-on-Don, Gagarin sq., 1, tel. +7 (863) 201-94-64 , e-mail: koryanova.yi@mail.ru

Yazyev Batyr Meretovich, DSc, Professor of the Department of Strength of Materials, Don State Technical University, 344000, Rostov-on-Don, Gagarin sq., 1, tel. +7 (863) 201-91-36 , e-mail: ps62@yandex.ru

Чепурненко Антон Сергеевич, доктор технических наук, доцент кафедры «Сопротивление материалов» Донского государственного технического университета, 344000, г. Ростов-на-Дону, пл. Гагарина, 1, тел. +7 (863) 201-91-36 , e-mail: anton_chepurnenk@mail.ru

Несветаев Григорий Васильевич, доктор технических наук, профессор кафедры «Технология строительного производства» Донского государственного технического университета, 344000, г. Ростов-на-Дону, пл. Гагарина, 1, тел. +7 (863) 201-94-64 , e-mail: nesgrin@yandex.ru

Корянова Юлия Игоревна, кандидат технических наук, доцент кафедры «Технология строительного производства» Донского государственного технического университета, 344000, г. Ростов-на-Дону, пл. Гагарина, 1, тел. +7 (863) 201-94-64 , e-mail: koryanova.yi@mail.ru

Язьев Батыр Меретович, доктор технических наук, профессор кафедры «Сопротивление материалов» Донского государственного технического университета, 344000, г. Ростов-на-Дону, пл. Гагарина, 1, тел. +7 (863) 201-91-36 , e-mail: ps62@yandex.ru

DOI:10.22337/2587-9618-2022-18-3-137-146

FORMATION OF COMPUTATIONAL SCHEMES OF ADDITIONAL TARGETED CONSTRAINTS THAT REGULATE THE FREQUENCY SPECTRUM OF NATURAL OSCILLATIONS OF ELASTIC SYSTEMS WITH A FINITE NUMBER OF DEGREES OF MASS FREEDOM, THE DIRECTIONS OF MOVEMENT OF WHICH ARE PARALLEL, BUT DO NOT LIE IN THE SAME PLANE PART 2: THE FIRST SAMPLE OF ANALYSIS

Leonid S. Lyakhovich [1], Pavel A. Akimov [2], Nikita V. Mescheulov [1]

[1] Tomsk State University of Architecture and Civil Engineering, Tomsk, RUSSIA
[2] National Research Moscow State University of Civil Engineering, Moscow, RUSSIA

Abstract: For some elastic systems with a finite number of degrees of freedom of masses, in which the directions of mass movement are parallel and lie in the same plane (for example, rods), special methods have been developed for creating additional constraints, the introduction of each of which purposefully increases the value of only one natural frequency and does not change any from the natural modes. The method of forming a matrix of additional stiffness coefficients that characterize such targeted constraint in this problem can also be applied when solving a similar problem for elastic systems with a finite number of degrees of mass freedom, in which the directions of mass movement are parallel, but do not lie in the same plane (for example, plates). At the same time, for such systems, only the requirements for the design schemes of additional targeted constraints are formulated, and not the methods for their creation. The distinctive paper is devoted to solution of corresponding sample of plate analysis with the use of approach that allows researcher to create computational schemes for additional targeted constraints for such systems.

Keywords: natural frequency, natural modes, generalized additional targeted constraint, sample of analysis

ФОРМИРОВАНИЕ РАСЧЕТНЫХ СХЕМ ДОПОЛНИТЕЛЬНЫХ СВЯЗЕЙ, ПРИЦЕЛЬНО РЕГУЛИРУЮЩИХ СПЕКТР ЧАСТОТ СОБСТВЕННЫХ КОЛЕБАНИЙ УПРУГИХ СИСТЕМ С КОНЕЧНЫМ ЧИСЛОМ СТЕПЕНЕЙ СВОБОДЫ МАСС, У КОТОРЫХ НАПРАВЛЕНИЯ ДВИЖЕНИЯ ПАРАЛЛЕЛЬНЫ, НО НЕ ЛЕЖАТ В ОДНОЙ ПЛОСКОСТИ ЧАСТЬ 2: ПЕРВЫЙ ТЕСТОВЫЙ ПРИМЕР

Л.С. Ляхович [1], П.А. Акимов [2], Н.В. Мещеулов [1]

[1] Томский государственный архитектурно-строительный университет, Томск, РОССИЯ
[2] Национальный исследовательский Московский государственный строительный университет, Москва, РОССИЯ

Аннотация. Для некоторых упругих систем с конечным числом степеней свободы масс, у которых направления движения масс параллельны и лежат в одной плоскости, (например, стержни) разработаны методы создания дополнительных связей, введение каждой из которых прицельно увеличивает значение только одной собственной частоты и не изменяет ни одну из форм собственных колебаний. Метод формирования матрицы дополнительных коэффициентов жесткости, характеризующих в этой задаче такую прицельную связь, может быть применен и при решении аналогичной задачи для упругих систем с конечным числом степеней свободы масс, у которых направления движения масс параллельны, но не лежат в одной плоскости (например, пластины). Вместе с тем для таких систем сформулированы лишь требования к расчетным схемам дополнительных прицельных связей, а не методы их создания. В данной статье рассматривается пример применения для пластин разработанного подхода, позволяющего создавать расчётные схемы дополнительных прицельных связей и для таких систем.

Ключевые слова: частота собственных колебаний, форма собственных колебаний, обобщенная прицельная дополнительная связь, пример расчета

THE FIRST SAMPLE

Let us consider a hinged rectangular plate [4, 10-14, 19, 20] 6 *m* by 6 *m* in size, carrying concentrated masses (Fig. 1*a* [4])

$$m[1] = 1000\,kg,\ \ m[2] = 1100\,kg,$$
$$m[3] = 1150\,kg,\ \ m[4] = 1200\,kg\ .$$

The thickness of the plate is 0.12 *m*. The modulus of elasticity of the plate material

$$E = 24 \cdot 10^9\ N/m^2 = 24 \cdot 10^9\ Pa\,.$$

Poisson's ratio $\nu_0 = 0.2$.

We choose the main system of the displacement method (Fig. 1b) [17], form the corresponding system of equations (1) from the paper [4] (matrices $A = \|r[i,k]\|$, $M = \|m[i]\|$). From equation (2) given in [4], we determine the eigenfrequencies and eigenmodes of the plate vibrations. The values of the eigenfrequencies of the plate and the coordinates of the eigenmodes corresponding to them are given in Table 1 (columns are the eigenfrequencies and coordinates of the eigenmodes).

Assume that it is required to increase the value of the first frequency of natural oscillations up to 100 s^{-1} (or up to 100 *Hz*, respectively). To do this, in accordance with formulas (7), (8), (9) given in [4], we form a matrix of additional stiffness coefficients (4) (see [4]). All the data necessary to use dependencies (7), (8), (9) from [4] are given in Table 1. After forming the matrix of additional stiffness factors, taking into account their influence, we determine from equation (10) given in [4], the modified spectrum eigenfrequencies and their corresponding vibration modes [1-6, 13]. The modified spectrum of natural frequencies and their corresponding forms are shown in Table 2.

It can be seen from the table that taking into account the additional stiffness factors did not change any of the modes of natural oscillations of the plate, but only increased the value of one of the frequencies from 61.6965 s^{-1} to the specified value of 100 s^{-1}.

The generalized targeted constraint must correspond to the matrix of additional stiffness coefficients.

One of the variants of the computational scheme of the targeted constraint is shown in Figure 1*a* and Figure 1*b*. The accepted version is once statically indeterminate and does not contain additional racks. Thus, its geometry is determined only by the lengths of the main vertical members, that is, by the values $l_{st}[i]$.

As noted above, now the problem is reduced to finding in the computation scheme of targeted constraint the lengths of the main vertical members $l_{st}[i]\ (i = 1,2,..,4)$ from the conditions for the occurrence of forces $N_{st}[i],\ i = 1,..,4$ in them, the ratios between which will be proportional to the ratios between the forces $R_0[i] = m[i]v[i,1],\ i = 1,..,4$. The values $m[i]$ are shown in the initial data of the distinctive sample, and the values $v[i,1]$ are given in the first column of Table 1 and Table 2. The forces are shown in Table 3.

In order to use the algorithm for the formation of the computational scheme of targeted constraint, researcher must firstly select the base vertical member and set its length. For the base we will take the vertical member of the first node and set $l_{st}[1]=2.45\,m$. We will take the initial values of other variable lengths $l_{st}[2]=2.30\,m$, $l_{st}[3]=2.00\,m$, $l_{st}[4]=2.6\,m$.

Table 1. Values of eigenfrequencies (natural vibration frequencies) of the plate and coordinates of their corresponding eigenmodes (natural modes) (the first example).

ω	61.6965	141.4295	146.2905	205.4514
1	0.4908	0.0001	0.7080	-0.5893
2	0.4965	-0.7093	0.0895	0.5154
3	0.5058	-0.0676	-0.7003	-0.4432
4	0.5068	0.7016	0.0181	0.4367

Table 2. Modified frequency spectrum of natural vibrations of the plate and coordinates, corresponding to them natural forms (the first example).

ω	100.00	141.4295	146.2905	250.00
1	0.4908	0.0001	0.7080	-0.5893
2	0.4965	-0.7093	0.0895	0.5154
3	0.5058	-0.0676	-0.7003	-0.4432
4	0.5068	0.7016	0.0181	0.4367

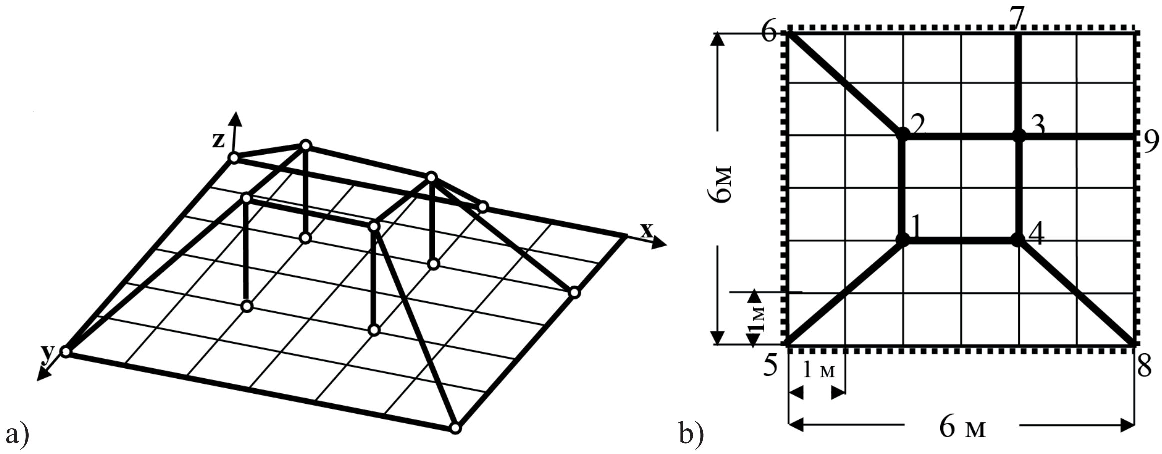

Figure 1. The first sample: variant of the computational targeted constraint: a) three-dimensional visualization; b) top view.

Table 3. To the analysis of the targeted constraint in the computational scheme (the first example).

i	1	2	3	4
$m[i]$	1000	1100	1150	1200
$v[i,1]$	0.4908	0.4965	0.5058	0.5068
$R_0[i]$	490.7597	546.1499	581.6800	608.1056

It is also necessary to set the force in one of the vertical members. Let's accept

$$N_{st}[1]=R_0[1]=490.7597\,kg.$$

To find the minimum of the objective function (12), described in [4], the method of steepest descent in the space of varying lengths of vertical members $l_{st}[i]$, $i=2,3,4$ was used. The formation of the computational scheme of the targeted constraint according to the above mentioned algorithm was carried out without restrictions on the length of the vertical members. Equilibrium equations were constructed for nodes located at the tops of the vertical members.

Table 4. The lengths of vertical members of targeted constraint and corresponding forces in them (the first sample).

$l_{st0}[1]=2.4500$	$N_{st}[1]=-490.7597$	$l_p[8,4]=3.7680$	$N_p[8,4]=747.1761$
$l_{st}[2]=2.3855$	$N_{st}[2]=-546.1499$	$l_p[9,3]=2.7948$	$N_p[9,3]=554.1850$
$l_{st}[3]=1.9521$	$N_{st}[3]=-581.6800$	$l_p[1,2]=2.0010$	$N_p[1,2]=396.7919$
$l_{st}[4]=2.4896$	$N_{st}[4]=-608.1056$	$l_p[2,3]=2.0464$	$N_p[2,3]=405.7875$
$l_p[5,1]=3.7420$	$N_p[5,1]=742.0097$	$l_p[3,4]=2.0710$	$N_p[3,4]=410.6569$
$l_p[6,2]=3.7001$	$N_p[6,2]=733.6948$	$l_p[1,4]=2.0004$	$N_p[1,4]=396.6633$
$l_p[7,3]=2.7948$	$N_p[7,3]=554.1850$		

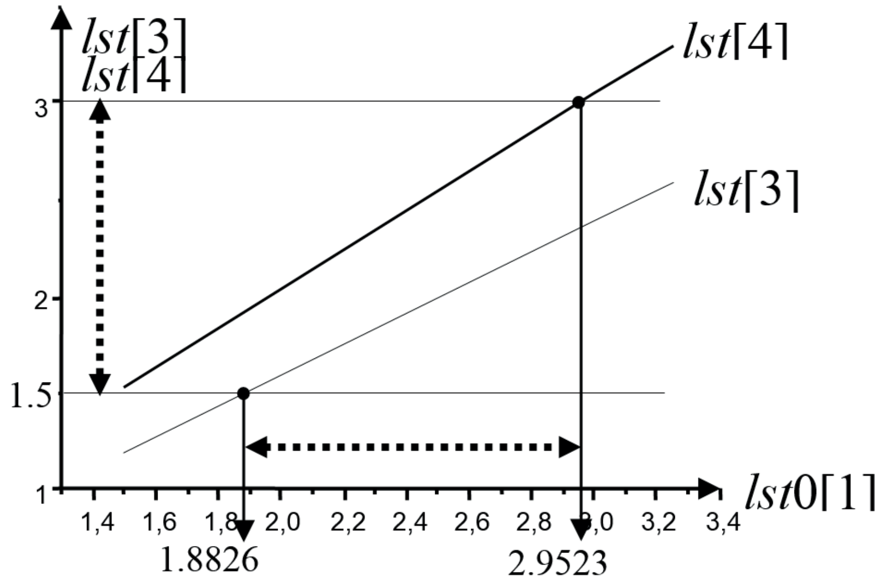

Figure 2. The first sample: parameters of targeted constraint.

The found lengths of the vertical members of targeted constraint and the forces in them are shown in Table 4.

From Table 4 it can be seen that the forces in the vertical member by absolute values coincide with the forces $R_0[i]$. This circumstance confirms the minimum of the objective function (12) [7-9, 15, 16, 18, 21-23] from [4] and the fulfillment of the requirement that the ratios between the forces $N_{st}[i]$ are proportional to the ratios between the values $R_0[i]$.

The cross-sectional areas of the vertical members of targeted constraint can be found from the condition that its stiffness coincides with the stiffness determined by the matrix of additional coefficients (4) from [4]. These conditions are realized by dependencies (9), (14), (15) from [4]. Since there are no additional vertical members in the computational scheme of the targeted constraint, then in (14) from [4] only the values

$$F_{st}[i]=F\alpha[i], \quad F_P[j]=F\beta[j]$$

remain, and in the brackets of expression (15) from [4] we have only the first two terms.

When minimizing the volume of the material of the targeted constraint from [4], researcher normally consider the case when, according to the design conditions

$$\alpha[i] = 2, \quad \beta[i] = 1.$$

All vertical members are solid round rods. The modulus of elasticity of the material of the vertical members in equal to $E = 2.06 \cdot 10^{11}\, Pa$. Then, using (13), (14), (15) and (16) from [4], we obtain

$$F_{st}[i] = 0.00057357\, m^2, \quad D_{st} = 0.027024\, m,$$
$$F_p[i] = 0.00028678\, m^2,\ D_p = 0.0191088\, m,$$
$$V_{SV} = 0.012467\, m^3,$$

where D_{st} and D_p are respectively, the diameters of the rods of the vertical members and belts of targeted constraint.

As noted above, when the length of the base vertical member changes, the ratios between the lengths of the base vertical members do not change, that is, the values χ_1 and χ_2 (see [4]) remain constant. Therefore, when changing the length of the base vertical member, the greatest length remains at the vertical member of the fourth node, and the smallest at the vertical member of the third node. Thus, when minimizing the function V_{SV} (see [4]), the values

$$\chi_1 = l_{st}[1]/l_{st}[4] = 0.9841;$$
$$\chi_2 = l_{st}[1]/l_{st}[3] = 1.551,$$

computed with the use of data from Table 4 do not change. Figure 2 shows the dependences of the lengths $l_{st}[3]$ and $l_{st}[4]$ on the change in the length of the base vertical member $l_{st0}[1]$.

On Figure 2 also shows in the direction of the *y*-axis the restrictions

$$3\, m \geq l_{st}[i] \geq 1.5\, m, \quad i = 1, 2, 3, 4$$

on the expression (17) from [4], and in the direction of the abscissa shows the range of permissible values of variable length $l_{st0}[1]$ according to the expression (18) from [4].

The targeted constraint was formed at an arbitrarily chosen value of the length of the base vertical member $l_{st}[1] = 2.45\,м$. By varying the length of the base vertical member $l_{st0}[1]$, the researcher can use the one-dimensional search method to achieve the minimization of material consumption when creating targeted constraint. In this case, the values of variable length should be chosen in the range of admissible values (17), (18) from [4]. Table 5 lists seven options for choosing the length of the base vertical member. For each option, the values of the lengths of the remaining racks and the amount of sighting material are given V_{SV}.

Let's consider three options for forming restrictions on the lengths of the vertical members and, accordingly, the area of admissible values of the length of the base vertical member $l_{st0}[1]$. variable while minimizing the amount of sighting material:

1) $3\,м \geq lst[i] \geq 1.5m, \quad i = 1, 2, 3, 4$ (17) from [1];
$2.9523\, m \geq l_{st0}[1] \geq 1.8826\,м$ (18) from [1];
2) $2.1848\, m \geq l_{st}[i] \geq 1.5\,м$ (17) from [1];
$2.15\, m \geq l_{st0}[1] \geq 1.8826\,м$ (18) from [1];
3) $3\, m \geq l_{st}[i] \geq 2.1\, m$ (17) from [1];
$2.9523\ m \geq l_{st0}[1] \geq 2.6356\, m$ (18) from [1].

In all variants, cases were considered when, according to the design conditions, we have

$$\alpha[i] = 2, \quad \beta[i] = 1.$$

On Figure 3 shows a graph of the change in the volume of material of targeted constraint depending on the length of the base vertical member $l_{st0}[1]$. Figure 3 also shows the ranges of acceptable values of the variable value of the three above options. In each area, the minimum volume values V_{SV} are marked.

The results of minimizing the volume for the first version of the restrictions are shown in the fourth row of Table 5. Here, the minimum value $V_{SV} = 0.01247\,m^3$ for $l_{st0}[1] = 2.45\,m$ is within the range of acceptable values $l_{st0}[1]$, that is, the global extremum is found. The areas and diameters of the sections of the vertical members of targeted constraint are equal to

Table 4. The parameters of targeted constraint (the first sample).

No.	$l_{st0}[1]$	$l_{st}[2]$	$l_{st}[3]$	$l_{st}[4]$	V_{SV}
1	1	0.9737	0.7968	1.0162	0.02495
2	1.5	1.4606	1.1952	1.5242	0.01567
3	2.15	2.0934	1.7131	2.1848	0.01268
4	2.45	2.3855	1.9521	2.4896	0.01247
5	2.6356	2.5662	2.1000	2.6782	0.01254
6	3.0	2.9211	2.3904	3.0485	0.01300
7	3.25	3.1645	2.5896	3.3025	0.01351

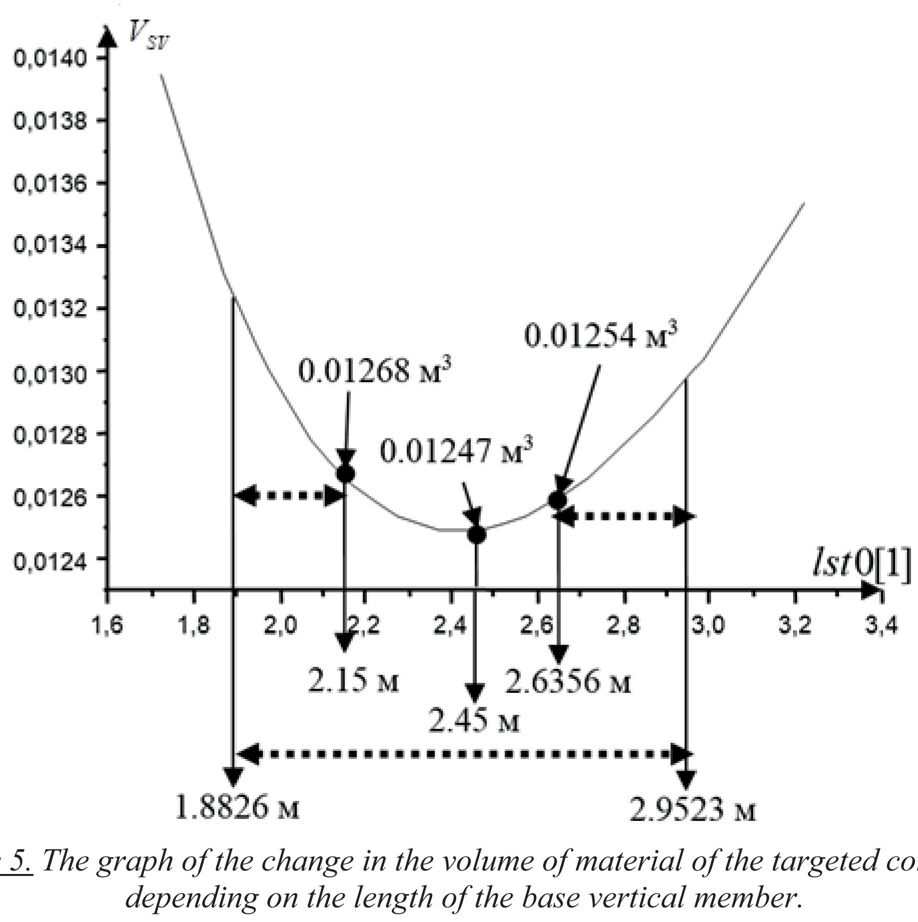

Figure 5. The graph of the change in the volume of material of the targeted constraint depending on the length of the base vertical member.

$F_{st} = 0.0005734\,m^2$, $D_{st} = 0.0270\,m$,

$F_p = 0.0002868\,m^2$, $D_p = 0.0191\,m$.

The results of the second variant are presented in the third row of Table 5. The minimum value $V_{SV} = 0.01268\,m^3$ is on the border of the range of acceptable values $l_{st0}[1]$, that is, the boundary optimum is found at $l_{st0}[1] = 2.15m$. The areas and diameters of the sections of the vertical members of targeted constraints are equal to

$$F_{st} = 0.0006295\,m^2,\ D_{st} = 0.02381\,m,$$
$$F_p = 0.0003148\,m^2,\ D_p = 0.02002\,m.$$

The results of the third variant are presented in the fifth row of Table 5. The minimum value $V_{SV} = 0.01254\,m^3$ is on the border of the range of acceptable values $l_{st0}[1]$, that is, the boundary optimum is found at $l_{st0}[1] = 2.635m$. The areas and diameters of the sections of the vertical members of targeted constraints are equal to

$$F_{st} = 0.0005513\,m^2,\ D_{st} = 0.02649\,m,$$
$$F_p = 0.0002756\,m^2,\ D_p = 0.01873\,m.$$

The results obtained were checked (verified) with the use of “LIRA-SAPR” software package. The eigenfrequencies and coordinates of the vibration modes of the plate with impact coupling, obtained using LIRA-SAPR [8], coincided with the data in Table 2.

REFERENCES

1. **Akimov P.A, Lyahovich L.S.** Pricel'noe regulirovanie spektra chastot sobstvennyh kolebanij uprugih plastin s konechnym chislom stepenej svobody mass putem vvedenija dopolnitel'nyh obobshhennyh svjazej i obobshhennyh kinematicheskih ustrojstv [Precision control for eigenfrequency of elastic plates with finite number of mass degrees of freedom by using additional generalized connections and kinematic devices]. // Vestnik Tomskogo gosudarstvennogo arkhitekturno-stroitel'nogo universiteta. Journal of Construction and Architecture, 2021, Vol. 23, No. 4, pp. 57-67 (In Russian).
2. **Giterman D.M., Lyahovich L.S., Nudel'man Ja.L.** Algoritm sozdanija rezonansno-bezopasnyh zon pri pomoshhi nalozhenija dopolnitel'nyh svjazej [Algorithm for creating resonantly safe zones by imposing additional bonds]. // Dinamika i prochnost' mashin, Vypusk 39. – Kharkov, Vishha shkola, 1984, pp. 63-69 (In Russian).
3. **Lyahovich L.S.** Osobye svojstva optimal'nyh sistem i osnovnye napravlenija ih realizacii v metodah rascheta sooruzhenij [Special properties of optimal systems and the main directions of their implementation in the methods of structural analysis]. Tomsk, TGASU, 2009. – 372 pages (In Russian).
4. **Lyakhovich L.S., Akimov P.A.** Formation of Computational Schemes of Additional Targeted ConstraintsThat Regulate The Frequency Spectrum of Natural Oscillations of Elastic Systems With a Finite Number of Degrees of Mass Freedom, the Directions of Movement of Which are Parallel, But Do Not Lie in the Same Plane. Part 1: Theoretical Foundations. // International Journal for Computational Civil and Structural Engineering, 2022, Volume 18, Issue 2, pp. 183-193.
5. **Lyahovich L.S., Maletkin O.Ju.** O pricel'nom regulirovanii sobstvennyh chastot uprugih system [On targeted control of natural frequencies of elastic systems]. // Izvestija vuzov. Stroitel'stvo i arhitektura, 1990, No. 1, pp. 113-117 (In Russian).
6. **Nudel'man Ja.L., Lyahovich L.S., Giterman D.M.** O naibolee podatlivyh svjazjah naibol'shej zhestkosti [On the most pliable bonds of the greatest rigidity]. // Voprosy prikladnoj Mehaniki i matematiki. Tomsk, TGU, 1981, pp. 113-126 (In Russian).
7. **An H.H., Jung M.H., Kim N.H., Lee E.B., Shin K.B.** Study on the Automated Size Optimization and Structural Analysis Program for Composite Lattice Structures. // Transactions of the Korean Society of Mechanical Engineers, 2022, Volume 66, Issue 3, pp. 77-83.

8. **Dmitrieva T., Ulambayar Kh.** Algorithm for Building Structures Optimization Based on Lagrangian Functions. // Magazine of Civil Engineering, 2022, Volume 109, Issue 1, pp. 10910.
9. **Hinz M., Magoules F., Rozanova-Pierrat A., Rynkovskaya M., Teplyaev A.** On the Existence of Optimal Shapes in Architecture. // Applied Mathematical Modelling, 2021, Volume 94, pp. 676-687.
10. **Koreneva E.B.** Analysis of Combined Plates With Allowance for Contact With Elastic Foundation. // International Journal for Computational Civil and Structural Engineering, 2019, Volume 15, Issue 4, pp. 83-87.
11. **Koreneva E.B.** Unsymmetric Oscillations of Anisotropic Plate Having an Additional Mass. // International Journal for Computational Civil and Structural Engineering, 2021, Volume 17, Issue 1, pp. 48-54.
12. **Koreneva E.B., Grosman V.R.** Equation Decomposition Method for Solving of Problems of Statics, Vibrations and Stability of Thin-Walled Constructions. // International Journal for Computational Civil and Structural Engineering, 2020, Volume 16, Issue 2, pp. 63-70.
13. **Lyakhovich L.S., Akimov P.A.** Aimed control of the frequency spectrum of eigenvibrations of elastic plates with a finite number of degrees of freedom of masses by superimposing additional constraints. // International Journal for Computational Civil and Structural Engineering, 2021, Volume 17, Issue 2, pp. 76-82.
14. **Manuylov G.A., Kosytsyn S.B., Grudtsyna I.E.** Influence of Buckling Forms Interaction of Stiffened Plate Bearing Capacity. // International Journal for Computational Civil and Structural Engineering, 2020, Volume 16, Issue 2, pp. 83-93.
15. **Pan C., Han Y., Lu J.** Design and Optimization of Lattice Structures: A Review. // Applied Sciences, 2020, Volume 10, Issue 18, pp. 1-36.
16. **Peleshko I.D., Yurchenko V.V.** Parametric Optimization of Metal Rod Structures Using the Modified Gradient Projection Method. // Internal Applied Mechanics, 2021, Volume 57, Issue 4, pp. 440-454.
17. **Potapov A.N.** The Elastoplastic Calculation of Frames Using the Displacement Method. // International Journal for Computational Civil and Structural Engineering, 2019, Volume 15, Issue 3, pp. 120-130.
18. **Senatore G., Reksowardojo A.P.** Force and Shape Control Strategies for Minimum Energy Adaptive Structures. // Frontiers in Build Environment, 2020, Volume 6, p. 105.
19. **Shitikova M.V., Kandu V.V.** Analysis of Forced Vibrations of Nonlinear Plates in a Viscoelastic Medium Under the Conditions of the Different Combinational Internal Resonances. // International Journal for Computational Civil and Structural Engineering, 2019, Volume 15, Issue 3, pp. 131-148.
20. **Shitikova M.V., Krusser A.I.** Force Driven Vibrations of Nonlinear Plates on a Viscoelastic Winkler Foundation Under the Harmonic Moving Load. // International Journal for Computational Civil and Structural Engineering, 2021, Volume 17, Issue 4, pp. 161-180.
21. **Xu Y., Chen H., Wang X.** Buckling Analysis and Configuration Optimum Design of Grid-Stiffened Composite Panels. // AIAA Journal, 2020, Volume 58, Issue 8, pp. 3653-3664.
22. **Yankovskaya Y., Merenkov A.** Problems of Optimization of Design Solutions of Residential Structures and Their Elements // Lecture Notes in Civil Engineering, 2022, Volume 227, pp. 339-350.
23. **Yurchenko V.V., Peleshko I.D.** Searching for Optimal Prestressing of Steel Bar Structures Based on Sensitivity Analysis. // Archives of Civil Engineering, 2020, Volume 66, Issue 3, pp. 526-540.

СПИСОК ЛИТЕРАТУРЫ

1. **Акимов П.А, Ляхович Л.С.** Прицельное регулирование спектра частот собственных колебаний упругих пластин с конечным числом степеней свободы масс путем введения дополнительных обобщенных связей и обобщенных кинематических устройств. // Вестник Томского государственного архитектурно-строительного университета, 2021, том 23, № 4, с. 57-67.
2. **Гитерман Д.М., Ляхович Л.С., Нудельман Я.Л.** Алгоритм создания резонансно-безопасных зон при помощи наложения дополнительных связей. // Динамика и прочность машин, Выпуск 39. - Харьков: "Вища школа", 1984, с. 63-69.
3. **Ляхович Л.С.** Особые свойства оптимальных систем и основные направления их реализации в методах расчета сооружений. Монография. - Томск: Издательство ТГАСУ, 2009. - 372 с.
4. **Lyakhovich L.S., Akimov P.A.** Formation of Computational Schemes of Additional Targeted ConstraintsThat Regulate The Frequency Spectrum of Natural Oscillations of Elastic Systems With a Finite Number of Degrees of Mass Freedom, the Directions of Movement of Which are Parallel, But Do Not Lie in the Same Plane. Part 1: Theoretical Foundations. // International Journal for Computational Civil and Structural Engineering, 2022, Volume 18, Issue 2, pp. 183-193.
5. **Ляхович Л.С., Акимов П.А.** Формирование расчетных схем дополнительных связей, прицельно регулирующих спектр частот собственных колебаний упругих систем с конечных числом степеней свободы масс, у которых направления движения параллельны, но не лежат в одной плоскости. Часть 1: Теоретические основы подхода. Статья в настоящем номере.
6. **Ляхович Л.С., Малеткин О.Ю.** О прицельном регулировании собственных частот упругих систем. // Известия вузов. Строительство и архитектура, 1990, № 1, с. 113-117.
7. **Нудельман Я.Л., Ляхович Л.С., Гитерман Д.М.** О наиболее податливых связях наибольшей жесткости. // Вопросы прикладной Механики и математики. - Томск: Издательство ТГУ, 1981, с. 113-126.
8. **An H.H., Jung M.H., Kim N.H., Lee E.B., Shin K.B.** Study on the Automated Size Optimization and Structural Analysis Program for Composite Lattice Structures. // Transactions of the Korean Society of Mechanical Engineers, 2022, Volume 66, Issue 3, pp. 77-83.
9. **Dmitrieva T., Ulambayar Kh.** Algorithm for Building Structures Optimization Based on Lagrangian Functions. // Magazine of Civil Engineering, 2022, Volume 109, Issue 1, pp. 10910.
10. **Hinz M., Magoules F., Rozanova-Pierrat A., Rynkovskaya M., Teplyaev A.** On the Existence of Optimal Shapes in Architecture. // Applied Mathematical Modelling, 2021, Volume 94, pp. 676-687.
11. **Koreneva E.B.** Analysis of Combined Plates With Allowance for Contact With Elastic Foundation. // International Journal for Computational Civil and Structural Engineering, 2019, Volume 15, Issue 4, pp. 83-87.
12. **Koreneva E.B.** Unsymmetric Oscillations of Anisotropic Plate Having an Additional Mass. // International Journal for Computational Civil and Structural Engineering, 2021, Volume 17, Issue 1, pp. 48-54.
13. **Koreneva E.B., Grosman V.R.** Equation Decomposition Method for Solving of Problems of Statics, Vibrations and Stability of Thin-Walled Constructions. // International Journal for Computational Civil and Structural Engineering, 2020, Volume 16, Issue 2, pp. 63-70.
14. **Lyakhovich L.S., Akimov P.A.** Aimed control of the frequency spectrum of eigenvibrations of elastic plates with a finite number of degrees of freedom of masses by

superimposing additional constraints. // International Journal for Computational Civil and Structural Engineering, 2021, Volume 17, Issue 2, pp. 76-82.
15. **Manuylov G.A., Kosytsyn S.B., Grudtsyna I.E.** Influence of Buckling Forms Interaction of Stiffened Plate Bearing Capacity. // International Journal for Computational Civil and Structural Engineering, 2020, Volume 16, Issue 2, pp. 83-93.
16. **Pan C., Han Y., Lu J.** Design and Optimization of Lattice Structures: A Review. // Applied Sciences, 2020, Volume 10, Issue 18, pp. 1-36.
17. **Peleshko I.D., Yurchenko V.V.** Parametric Optimization of Metal Rod Structures Using the Modified Gradient Projection Method. // Internal Applied Mechanics, 2021, Volume 57, Issue 4, pp. 440-454.
18. **Potapov A.N.** The Elastoplastic Calculation of Frames Using the Displacement Method. // International Journal for Computational Civil and Structural Engineering, 2019, Volume 15, Issue 3, pp. 120-130.
19. **Senatore G., Reksowardojo A.P.** Force and Shape Control Strategies for Minimum Energy Adaptive Structures. // Frontiers in Build Environment, 2020, Volume 6, p. 105.
20. **Shitikova M.V., Kandu V.V.** Analysis of Forced Vibrations of Nonlinear Plates in a Viscoelastic Medium Under the Conditions of the Different Combinational Internal Resonances. // International Journal for Computational Civil and Structural Engineering, 2019, Volume 15, Issue 3, pp. 131-148.
21. **Shitikova M.V., Krusser A.I.** Force Driven Vibrations of Nonlinear Plates on a Viscoelastic Winkler Foundation Under the Harmonic Moving Load. // International Journal for Computational Civil and Structural Engineering, 2021, Volume 17, Issue 4, pp. 161-180.
22. **Xu Y., Chen H., Wang X.** Buckling Analysis and Configuration Optimum Design of Grid-Stiffened Composite Panels. // AIAA Journal, 2020, Volume 58, Issue 8, pp. 3653-3664.
23. **Yankovskaya Y., Merenkov A.** Problems of Optimization of Design Solutions of Residential Structures and Their Elements // Lecture Notes in Civil Engineering, 2022, Volume 227, pp. 339-350.
24. **Yurchenko V.V., Peleshko I.D.** Searching for Optimal Prestressing of Steel Bar Structures Based on Sensitivity Analysis. // Archives of Civil Engineering, 2020, Volume 66, Issue 3, pp. 526-540.

Leonid S. Lyakhovich, Full Member of the Russian Academy of Architecture and Construction Sciences, Professor, DSc, Head of Department of Structural Mechanics, Tomsk State University of Architecture and Building; 2, Solyanaya St., 2, Tomsk, 634003, Russia; E-mail: lls@tsuab.ru

Pavel A. Akimov, Full Member of the Russian Academy of Architecture and Construction Sciences, Professor, Dr.Sc.; Rector of National Research Moscow State University of Civil Engineering; 26, Yaroslavskoe Shosse, Moscow, 129337, Russia; phone +7(495) 651-81-85; Email: AkimovPA@mgsu.ru, pavel.akimov@gmail.com.

Nikita V. Mescheulov, Ph.D., Director of Scientific & Educational Center of Computer Modelling of Structures and Systems, Tomsk State University of Architecture and Building; 2, Solyanaya St., 2, Tomsk, 634003, Russia; phone +7(962)788-41-21; E-mail: ckm.tsuab@mail.ru.

Ляхович Леонид Семенович, академик РААСН, профессор, доктор технических наук, профессор кафедры строительной механики, Томский государственный архитектурно-строительный университет; 634003, Россия, г. Томск, Соляная пл. 2; E-mail: lls@tsuab.ru

Акимов Павел Алексеевич, академик РААСН, профессор, доктор технических наук; ректор Национального исследовательского Московского государственного строительного университета; 129337, г. Москва, Ярославское шоссе, д. 26; тел. +7(495) 651-81-85; Email: AkimovPA@mgsu.ru, pavel.akimov@gmail.com.

Мещеулов Никита Владимирович, кандидат технических наук, директор Научно-образовательного центра «Компьютерное моделирование строительных конструкций и систем», Томский государственный архитектурно-строительный университет; 634003, Россия, г. Томск, Соляная пл. 2; тел. +7(962)788-41-21; E-mail: ckm.tsuab@mail.ru.

DOI:10.22337/2587-9618-2022-18-3-147-158

NORMAL VIBRATIONS OF SAGGING CONDUCTORS OF OVERHEAD POWER LINES

Airat A. Valiullin [1], ***Alexander N. Danilin*** [2], ***Valery A. Feldshteyn*** [3]

[1] Moscow Institute of Physics and Technology (National Research University), Moscow, RUSSIA
[2] Institute of Applied Mechanics of the Russian Academy of Sciences, Moscow, RUSSIA
[3] JSC "Central Research Institute for Machine Building", Moscow, RUSSIA

Abstract. The phenomenon of self-excitation of thermomechanical vibrations of current-carrying conductors, experimentally discovered by academician A.F. Ioffe, is of practical interest as a possible explanation of the phenomenon of galloping conductors of overhead power transmission lines (OHL) – low-frequency vibrations with frequencies of ~ 1 Hz and with amplitudes of the order of the static conductor sagging. To build the theoretical foundations of this phenomenon, as a special class of self-oscillating systems, it is necessary, first of all, a model of conductor vibrations in the OHL span. With regard to the most studied type of conductor vibrations, high-frequency aeolian vibration, excited by sign-alternating aerodynamic forces from the Karman vortex street, the classical model of a straight string is reasonably applied. However, to study low-frequency vibrations of the galloping type, it is necessary to take into account the effect of sagging of the conductor, the associated elastic tension and, in some cases, the nonlinear nature of the vibrations. The article presents two models for calculating the natural vibrations of sagging conductors (cables) within the framework of the technical theory of flexible threads, assuming the constancy of the tension force along the length. The first model describes linear oscillations of an elastic conductor in the sagging plane. For a system of equations with respect to the displacement components given in natural coordinates, an exact solution of the Sturm-Liouville problem with estimates of the frequency ranges arising is obtained. The second model describes nonlinear vibrations of an elastic conductor in the sagging plane and pendulum vibrations accompanied by an exit from it. The solution of the problem is based on the principle of possible displacements using the Ritz method. The structure of the frequency spectrum and the natural forms of transverse vibrations are studied. The developed models are intended for further investigation of thermomechanical vibrations of conductor and flexible cable systems.

Keywords: sagging conductor, cable, flexible elastic thread, frequencies and modes of normal vibrations, Ritz method, spectrum structure

СОБСТВЕННЫЕ КОЛЕБАНИЯ ПРОВИСАЮЩИХ ПРОВОДОВ ВОЗДУШНЫХ ЛИНИЙ ЭЛЕКТРОПЕРЕДАЧИ

А.А. Валиуллин [1], ***А.Н. Данилин*** [2], ***В.А. Фельдштейн*** [3]

[1] Московский физико-технический институт (национальный исследовательский университет), Москва, РОССИЯ
[2] ФГБУН Институт прикладной механики Российской академии наук, Москва, РОССИЯ
[3] АО «Центральный научно-исследовательский институт машиностроения», Москва, РОССИЯ

Аннотация. Явление самовозбуждения термомеханических колебаний токонесущих проводников, экспериментально обнаруженное академиком А.Ф. Иоффе, представляет практический интерес в качестве возможного объяснения феномена пляски проводов воздушных линий электропередачи (ВЛЭ) – низкочастотных колебаний с частотами ~1 Гц и с амплитудами порядка стрелы статического провисания провода. Для построения теоретических основ этого явления, как особого класса автоколебательных систем, необходима, прежде всего, модель колебаний провода в пролете ВЛЭ. Применительно к наиболее изученному виду колебаний проводов, высокочастотной эоловой вибрации, возбуждаемой знакопеременными аэродинамическими силами со стороны вихревой дорожки Кармана, обоснованно применяется классическая модель прямолинейной струны. Однако для исследования низкочастотных колебаний типа пляски необходимо учитывать эффект провисания провода, связанное с этим упругое растяжение и, в ряде случаев, нелинейный характер колебаний. В статье представлены две модели для расчёта собственных колебаний провисающих проводов (тросов) в рамках технической теории гибких нитей, предполагающей постоянство силы натяжения по длине. Первая модель описывает линейные колебания упругого тяжелого провода в плоскости провисания. Для системы уравнений относительно компонент перемещения, заданных в естественных координатах, получено точное решение задачи Штурма-Лиувилля с оценками возникающих частотных диапазонов. Вторая модель описывает нелинейные колебания упругого провода, совершающего колебания в плоскости провисания и маятниковые колебания, сопровождающиеся выходом из нее. Решение задачи строится на основе принципа возможных перемещений с использованием метода Ритца. Изучена структура спектра частот и форм собственных поперечных колебаний провода. Разработанные модели предназначены для дальнейшего исследования термомеханических колебаний проводов и гибких тросовых систем.

Ключевые слова: провисающий провод, трос, гибкая упругая нить, частоты и формы собственных колебаний, метод Ритца, структура спектра

INTRODUCTION

Works [1-5] are devoted to the construction of a theory explaining the self-excitation of thermomechanical self-oscillations of a conductor that heats up when included in an electrical circuit. In [5], there are indications of the repetition of the experiment of A.F. Ioffe. A practical interest is the question of whether the self-excitation of thermomechanical vibrations is related to the phenomenon of the conductor galloping – low-frequency vibrations with frequencies of ~ 1 Hz and with amplitudes of the order of the static sagging [6,7].

In the cited works, such an assumption was made, but it has not yet received reasonable confirmation: there is no transfer of the effect, modeled theoretically and observed in a laboratory model, to the full-scale OHL conductors.

The purpose of this work is to study the normal frequencies and modes of a conductor in the OHL span, necessary for the mathematical model to determine the conditions for self-excitation of the galloping of full-scale conductors, based on the thermo-mechanical model.

1. A MODEL OF COUPLED LONGITUDINAL-TRANSVERSE VIBRATIONS OF A CONDUCTOR IN THE SAGGING PLANE

The natural oscillations of an OHL conductor in the plane of its sagging in a homogeneous field of gravity are considered. The conductor is considered as a flexible elastic heavy thread. The coordinate system and the selected natural basis are shown in Figure 1.

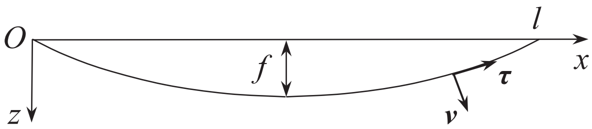

Figure 1. Orientation of the natural basis in the coordinate system Oxz

Conductor parameters: l – the distance between the suspension points (span length); m – linear mass; B – tensile stiffness; T_0 – static tension; k_0, f – the curvature of the static curve and its sag. By $\boldsymbol{p} = m\boldsymbol{g}$ denote the vertical linear load, where $\boldsymbol{g}$ is the vector of gravity acceleration. With small sag $(f << l)$, which is typical for most spans of OHL, tension $T_0 = B\varepsilon$ and curvature $k_0 = 8f/l^2$ can be considered constant along the length and related by the ratio:

$$T_0 = mg/k_0 = mgl^2/8f\ .$$

Conductor oscillation equation

$$(T\tau)' + \mathrm{p} - m(\ddot{u}\tau + \ddot{w}\nu) = 0$$

represent in projections onto the associated basis, using the Frenet formulas for a flat curve

$$\begin{aligned} T' - m\ddot{u} &= 0, \\ -kT + mg - m\ddot{w} &= 0. \end{aligned} \qquad (1)$$

During vibrations, the conductor has an additional elongation deformation $\tilde{\varepsilon} = u' + kw$, increments of curvature $k = k_0 - w''$ and tension $T = T_0 + B\tilde{\varepsilon}$. Substituting these values into (1), limiting ourselves to a linear approximation and excluding time by substitution $u \to ue^{i\omega t}$, $w \to we^{i\omega t}$, we obtain

$$Bu'' + Bk_0 w' = -m\omega^2 u,$$
$$T_0 w'' - Bk_0 u' - Bk_0^2 w = -m\omega^2 w$$
$$x = 0, l:\ u = w = 0.$$

Here and below, the dashes denote the derivative with respect to the arc coordinate s, which, due to the flatness of the sag curve, is identified with the x coordinate on the horizontal projection.

Let us pass to dimensionless variables, choosing as the scales of length and frequency, respectively l and $\sqrt{T_0/m}/l$:

$$u'' + \alpha w' = \varepsilon\omega^2 u,$$
$$w'' - \frac{\alpha}{\varepsilon}\left(u' + \alpha w\right) = -\omega^2 w, \quad (2)$$

where indicated: $\varepsilon = T_0/B$, $\alpha = k_0 l = 8f/l$. The parameter ε represents the deformation of the conductor elongation in the state of equilibrium and can be considered small. Note that equations (1) are similar to the equations of vibrations of an elongated cylindrical shell (panel with curvature k_0) with a vanishingly small bending stiffness [8]. The parameter α defines the connection between the longitudinal and transverse displacements of the wire section. At small values of this parameter, which are characteristic of a strongly stretched wire, system (2) breaks up into two independent equations: longitudinal vibrations of the rod and transverse vibrations of the string.

Assuming in (2) $u = Ue^{i\lambda x}$, $w = We^{i\lambda x}$, let's move on to the system

$$\left(\varepsilon\omega^2 - \lambda^2\right)U + i\alpha\lambda W = 0,$$
$$-\frac{i\alpha\lambda}{\varepsilon}U + \left(\omega^2 - \lambda^2 - \frac{\alpha^2}{\varepsilon}\right)W = 0. \quad (4)$$

Let's write an equation for determining wavenumbers λ with respect to $z = \lambda^2$:

$$z^2 - z\omega^2\left(1+\varepsilon\right) + \varepsilon\omega^4 - \alpha^2\omega^2 = 0. \quad (5)$$

At $\omega > \alpha/\sqrt{\varepsilon}$ (conditionally large frequencies) the roots $z_{1,2} > 0$ and all wavenumbers are real. At $\omega < \alpha/\sqrt{\varepsilon}$ (relatively low frequencies) $z_1 > 0$, $z_2 < 0$; in this case, one pair of wavenumbers is real, the other is imaginary. The frequency $\omega_{cr} = \alpha/\sqrt{\varepsilon}$, that delimits the low- and high-frequency regions is further called critical. From (4) follow the relationship between the displacement components (distribution coefficients) for each λ_k $(k = 1,...,4)$:

$$U_k = W_k \frac{i\alpha\lambda_k}{\lambda_k^2 - \varepsilon\omega^2} = W_k i\eta_k. \quad (6)$$

In the general case, the roots of equation (5) are:

$$z_{1,2} = \frac{\omega^2}{2}\left(1+\varepsilon\right) \pm$$
$$\pm\frac{\omega^2}{2}\left(1-\varepsilon\right)\sqrt{1 + \frac{4\alpha^2}{\omega^2\left(1-\varepsilon\right)^2}}. \quad (7)$$

Let's first consider the high-frequency range: $\omega > \alpha/\sqrt{\varepsilon}$. Given the strong inequality, we assume that

$$\sqrt{1 + 4\alpha^2/\omega^2\left(1-\varepsilon\right)^2} \approx 1 + 2\alpha^2/\omega^2.$$

It follows that

$$z_1 \approx \omega^2 + \alpha^2,\ z_2 \approx \varepsilon\omega^2 - \alpha^2$$

and the wavenumbers and distribution coefficients are equal to:

$$\lambda_{1,2} = \pm\chi_1, \ \lambda_{3,4} = \pm\chi_2; \qquad (8)$$
$$\eta_{1,2} = \pm\delta_1, \ \eta_{3,4} = \mp\delta_2.$$

Here the notations are used:

$$\chi_1 = \sqrt{\omega^2 + \alpha^2}, \quad \chi_2 = \sqrt{\varepsilon\omega^2 - \alpha^2},$$
$$\delta_1 = \alpha/\chi_1, \quad \delta_2 = \chi_2/\alpha.$$

The general solution of system (2), taking into account correlation (6), has the form:

$$w = \sum_{k=1}^{4} A_k e^{i\lambda_k x}, \ u = \sum_{k=1}^{4} A_k \eta_k i e^{i\lambda_k x} \qquad (9)$$

or in trigonometric form:

$$w = B_1 \cos\chi_1 x + B_2 \sin\chi_1 x +$$
$$+ B_3 \cos\chi_2 x + B_4 \sin\chi_2 x,$$
$$u = -B_1\delta_1 \sin\chi_1 x + B_2\delta_1 \cos\chi_1 x +$$
$$+ B_3\delta_2 \sin\chi_2 x - B_4\delta_2 \cos\chi_2 x.$$

Subjecting the obtained solution to boundary conditions, we come to a homogeneous system of equations with respect to: B_k :

$$B_1 + B_3 = 0,$$
$$B_1 \cos\chi_1 + B_2 \sin\chi_1 +$$
$$+ B_3 \cos\chi_2 + B_4 \sin\chi_2 = 0, \qquad (10)$$
$$B_2\delta_1 - B_4\delta_2 = 0,$$
$$-B_1\delta_1 \sin\chi_1 + B_2\delta_1 \cos\chi_1 +$$
$$+ B_3\delta_2 \sin\chi_2 - B_4\delta_2 \cos\chi_2 = 0.$$

The condition for the existence of a nontrivial solution gives the frequency equation –

$$\Delta_1(\omega) = 2\delta_1\delta_2(1 - \cos\chi_1 \cos\chi_2) + \qquad (11)$$
$$+ (\delta_1^2 + \delta_2^2)\sin\chi_1 \sin\chi_2 = 0.$$

Assuming $B_2 = 1$ and defining the remaining integration constants from the first three equations of system (10), we represent the eigenfunctions (normal modes) in the form:

$$w = \frac{1}{\delta_2}\left[\varphi_1(x) - \mu_1\psi_1(x)\right], \qquad (12)$$
$$u = \delta_1\psi_1(x) + \mu_1\theta_1(x).$$

It is indicated here:

$$\varphi_1(x) = \delta_2 \sin\chi_1 x + \delta_1 \sin\chi_2 x,$$
$$\psi_1(x) = \cos\chi_1 x - \cos\chi_2 x,$$
$$\theta_1(x) = \nu \sin\chi_1 x + \sin\chi_2 x,$$
$$\nu = \delta_1/\delta_2, \ \mu_1 = \varphi_1(1)/\psi_1(1).$$

Consider the low-frequency range, when $\omega < \alpha/\sqrt{\varepsilon}$. In this case, the wavenumbers and distribution coefficients are equal to

$$\lambda_{1,2} = \pm\chi_1, \ \lambda_{3,4} = \pm i\chi_3;$$
$$\eta_{1,2} = \pm\delta_1, \ \eta_{3,4} = \mp i\delta_2.$$

where now: $\chi_2 = \sqrt{\alpha^2 - \varepsilon\omega^2}$, $\delta_2 = \chi_2/\alpha$.
The general solution (9) takes the form:

$$w = B_1 \cos\chi_1 x + B_2 \sin\chi_1 x +$$
$$+ B_3 \operatorname{ch}\chi_2 x + B_4 \operatorname{sh}\chi_2 x,$$
$$u = -B_1\delta_1 \sin\chi_1 x + B_2\delta_1 \cos\chi_1 x -$$
$$- B_3\delta_2 \operatorname{sh}\chi_2 x - B_4\delta_2 \operatorname{ch}\chi_2 x.$$

Frequency equation is

$$\Delta_2(\omega) = 2\delta_1\delta_2(1 - \cos\chi_1 \operatorname{ch}\chi_2) + \qquad (13)$$
$$+ (\delta_1^2 - \delta_2^2)\sin\chi_1 \operatorname{sh}\chi_2 = 0.$$

Note that the boundary frequency $\omega_b = \alpha/\sqrt{\varepsilon}$ simultaneously satisfies both frequency equations (11) и (13) and, therefore, is a natural frequency. Native functions:

$$w = \frac{1}{\delta_2}\left[\varphi_2(x) - \mu_2\psi_2(x)\right],$$
$$u = -\delta_1\psi_2(x) + \mu_2\theta_2(x). \tag{14}$$

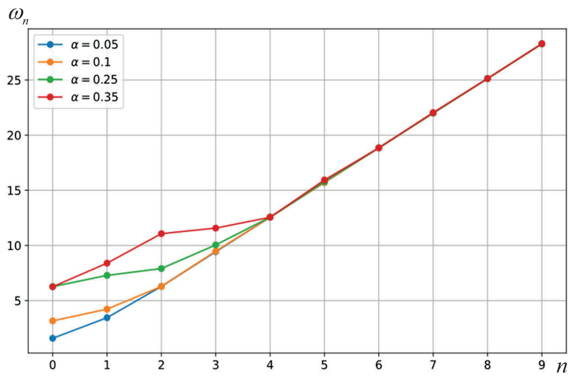

Figure 2. Natural frequency spectra for various α and $\varepsilon = 10^{-3}$

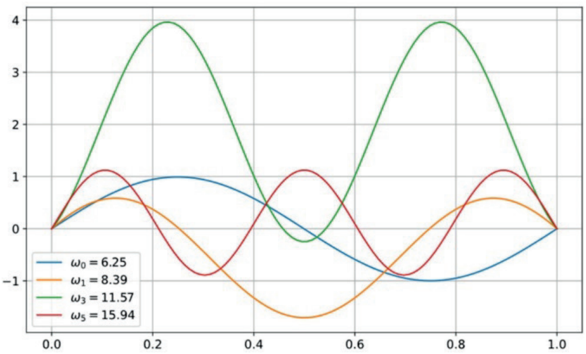

Figure 3. Characteristic forms of transverse vibrations of the lower (n=0, 1) *and upper* (n=3, 5) *harmonics; here $\alpha = 0.35$, $\varepsilon = 10^{-3}$, critical frequency $\omega_{cr} = 11.07$*

It is indicated here:

$$\varphi_2(x) = \delta_2 \sin \chi_1 x + \delta_1 \mathrm{sh}\chi_2 x,$$
$$\psi_2(x) = \mathrm{ch}\chi_2 x - \cos \chi_1 x,$$
$$\theta_2(x) = \mathrm{sh}\chi_2 x - \nu \sin \chi_1 x;$$
$$\mu_1 = \varphi_1(1)/\psi_1(1).$$

Note that for small sag $(\alpha \to 0)$, the high-frequency equation (11) transforms into $\sin\chi_1 \sin\chi_2 = 0$ and the spectrum splits into groups of quasi-transverse (string) and quasi-longitudinal frequencies: $\omega_n = \pi n$ and $\omega_n = \pi n/\sqrt{\varepsilon}$.

The low-frequency equation (13) takes the form $\sin\chi_1 \mathrm{sh}\chi_2 = 0$ and defines only transverse frequencies. For high harmonics, string asymptotic is manifested for all, not necessarily small values α. The spectrum features are characterized by Figure 2, which shows the frequencies of the modes corresponding to the harmonics with a number n calculated for different α and $\varepsilon = 10^{-3}$.

The structure of the spectrum, which is quite complex in the low-frequency region, becomes regular with the growth of the harmonic number. The forms of vibrations in the low-frequency region differ significantly from the forms of transverse vibrations of a string and a beam: the difference is that the amplitudes of adjacent half-waves (of different signs) vary greatly in amplitude, which is not typical for a string. This difference decreases with the growth of the harmonic number, as follows from the graphs in Figure 3, and for high harmonics, the shapes do not differ from the shapes of the string.

2. MODEL OF SPATIAL VIBRATIONS

Let's introduce the coordinate system $Oxyz$, directing the axis Ox through the conductor fixing points, as shown in Figure 2.

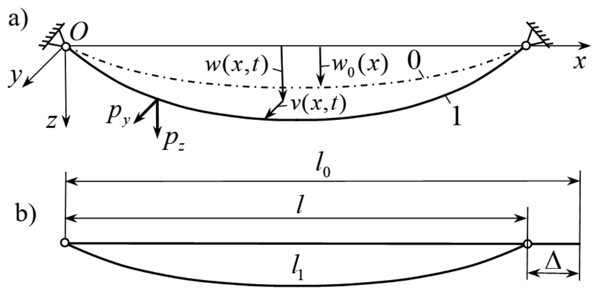

Figure 4. Parameters of static (0) and dynamic (1) states: a) displacements and components of the external load (a); lengths of the initial and current states (b)

Let $u(x,t)$, $v(x,t)$, $w(x,t)$ be the displacements of the points of the conductor axial line along the axes Ox, Oy, and Oz respectively. As before, the conductor is considered as a weighty elastic thread, fixed at the ends in a stretched state. Denote by p_y the given lateral linear load in the plane Oxy, by $p_z = mg$ the linear load of gravity forces in the plane Oxz.

The positive directions of the entered values are shown in the Figure 4 a). Figure 4 (b) shows: l – span length; l_0 – the conductor length in the span without elastic deformation at normal temperature; l_1 – the length of the stretched conductor; initial elongation –

$$\Delta = l_0(1+\alpha T) - l, \qquad (15)$$

where T is the increment of temperature relative to its normal value, α is the coefficient of linear thermal expansion.

Neglecting the longitudinal inertial forces, we assume that the tensile force T and tensile stiffness B are constant along the conductor length. It follows that the deformation of the conductor is also constant along the length, i.e. $\varepsilon(x,t) \approx \varepsilon(t)$. Using this assumption, we determine the longitudinal deformation in a quadratic approximation. It's obvious that

$$\begin{aligned} dl_1^2 &= \left(dx+du\right)^2 + dv^2 + dw^2 = \\ &= \left[\left(1+u'\right)^2 + v'^2 + w'^2\right]dx^2. \end{aligned}$$

Here and below, primes denote the derivative with respect to x. Neglecting the square of a small value du, we have

$$dl_1 ; \quad \sqrt{1+2u'+v'^2+w'^2}\, dx .$$

Expanding the last expression into a Taylor series and restricting ourselves to the first two terms, we obtain

$$dl_1 \approx \left[1+u'+\frac{1}{2}\left(v'^2+w'^2\right)\right]dx .$$

Integrating the last expression by x gives

$$l_1 - l = u_1 - u_0 + \frac{1}{2}\int_0^l \left(v'^2+w'^2\right)dx .$$

This makes it possible to determine the deformation of the conductor elongation in the form

$$\begin{aligned} \varepsilon &= \frac{l_1-l_0}{l_0} = \frac{l_1-l}{l_0} - \frac{\Delta}{l_0} = \\ &= \frac{1}{2l_0}\int_0^l \left(v'^2+w'^2\right)dx - \frac{\Delta}{l_0}. \end{aligned} \qquad (16)$$

where Δ is determined by expression (15) and it is taken into account that at the fixing points $u_0 = u_1 = 0$.

2.1. Nonlinear vibration equations

We will obtain the conductor vibration equations based on the principle of possible displacements in generalized coordinates with nonlinear elastic forces [9-11]:

$$\delta U - \delta A_p - \delta A_{in} = 0 . \qquad (17)$$

where δU is the variation of the potential energy of the system; δA_p, δA_{in} are the variation of the work of external and inertial forces. It is assumed that the initial configuration is known from the solution of static equilibrium equations.

We will search for displacements using the Ritz method:

$$\begin{aligned} \overline{w}(x,t) &= \frac{w}{l} = \sum_i \left(\overline{q}_{0i} + \overline{q}_i(t)\right)\sin\frac{i\pi x}{l}, \\ \overline{v}(x,t) &= \frac{v}{l} = \sum_j \overline{r}_i(t)\sin\frac{j\pi x}{l}. \end{aligned} \qquad (18)$$

where $\overline{q}_{0i}$ are the generalized coordinates of the static (initial) state; $\overline{q}_i$, $\overline{r}_i$ are generalized coordinates describing the dynamic process.
Let us determine the axial deformation by formula (16) in the form:

$$\varepsilon = \frac{l}{l_0}\left(\frac{\pi}{2}\right)^2\left[\sum_i i^2\left(\overline{q}_{0i}+\overline{q}_i\right)^2 + \right. \\ \left. + \sum_j j^2\overline{r}_j^2\right] - \frac{\Delta}{l_0}. \tag{19}$$

Then the potential energy of longitudinal deformation and its variation are respectively equal to

$$\Pi = \frac{l_0}{2}B\varepsilon^2; \\ \delta\Pi = \sum_i \frac{\partial\Pi}{\partial\overline{q}_i}\delta\overline{q}_i + \sum_j \frac{\partial\Pi}{\partial\overline{r}_j}\delta\overline{r}_j. \tag{20}$$

Here:

$$\frac{\partial\Pi}{\partial\overline{q}_i} = l_0 T\frac{\partial\varepsilon}{\partial\overline{q}_i} = lT\frac{(i\pi)^2}{2}\left(\overline{q}_{0i}+\overline{q}_i\right), \\ \frac{\partial\Pi}{\partial\overline{r}_j} = l_0 T\frac{\partial\varepsilon}{\partial\overline{r}_j} = lT\frac{(j\pi)^2}{2}\overline{r}_j; \quad T = B\varepsilon,$$

where the deformation ε is determined by the nonlinear expression (19).
We now write down the variations of the work of inertial and external forces:

$$\delta A_{in} = -\frac{l^3 m^*}{2}\left(\sum_i \ddot{\bar{q}}_i\delta\bar{q}_i + \sum_j \ddot{\bar{r}}_j\delta\bar{r}_j\right), \\ \delta A_p = l\left(\textstyle\sum_i (Q_{0i}+Q_i)\delta\bar{q}_i + \sum_j R_j\delta\bar{r}_j\right), \tag{21}$$

using the notations

$$m^* = m\left(1+\frac{\Delta}{l}\right); \quad Q_{0i} = lm^* g\frac{1-\cos i\pi}{i\pi}, \\ Q_i = \int_0^l p_y \sin\frac{i\pi x}{l}dx, \quad R_j = \int_0^l p_z \sin\frac{j\pi x}{l}dx.$$

The equations of spatial oscillations of the conductor follow from the variational principle of possible displacements (17) taking into account expressions (20), (21). As a result, we have

$$m^* l^2\ddot{\bar{q}}_i + T(i\pi)^2(\bar{q}_{0i}+\bar{q}_i) = 2(Q_{0i}+Q_i), \\ m^* l^2\ddot{\bar{r}}_j + T(j\pi)^2\bar{r}_j = 2R_j; \\ i,j = 1,2,3,\ldots. \tag{22}$$

Let's omit the terms in the first equation, the sum of which turns to zero due to static conditions. To do this, we will write the longitudinal deformation in the form (19) as the sum of the static and dynamic components:

$$\varepsilon(t) = \varepsilon_0 + \varepsilon_d(t), \tag{23}$$

where

$$\varepsilon_0 = \frac{l}{l_0}\left(\frac{\pi}{2}\right)^2\sum_i i^2\overline{q}_{0i}^2 - \frac{\Delta}{l_0}, \\ \varepsilon_d = \frac{l}{l_0}\left(\frac{\pi}{2}\right)^2\left[\sum_i i^2\left(2\overline{q}_{0i}\overline{q}_i + \overline{q}_i^2\right) + \sum_j j^2\overline{r}_j^2\right].$$

Substituting expression (23) into the first equation of system (22), we obtain nonlinear equations of spatial vibrations of the wire in the form:

$$m^* l^2\ddot{\bar{q}}_i + B(i\pi)^2(\varepsilon_d\bar{q}_{0i} + \varepsilon\bar{q}_i) = 2Q_i, \\ m^* l^2\ddot{\bar{r}}_j + (j\pi)^2\varepsilon\bar{r}_j = 2R_j; \\ i,j = 1,2,3,\ldots,$$

where ε is determined by formula (23). Passing to the quantities

$$\tau = t\sqrt{\frac{B}{m^* l^2}}; \quad \overline{Q}_i = 2\frac{Q_i}{B}, \quad \overline{R}_j = 2\frac{R_j}{B},$$

we obtain the final form of the equations in dimensionless form:

$$\frac{d^2\bar{q}_i}{d\tau^2} = \bar{Q}_i - (i\pi)^2 \left(\varepsilon_d \bar{q}_{0i} + \varepsilon \bar{q}_i\right),$$
$$\frac{d^2\bar{r}_j}{d\tau^2} = \bar{R}_j - (j\pi)^2 \varepsilon \bar{r}_j; \qquad (24)$$
$$i, j = 1,2,3,....$$

2.2. Solution of the static problem

In this case, instead of expressions (18), (19) we have

$$w_0(x) = \sum_k q_{0k} \sin\frac{k\pi x}{l};$$
$$\varepsilon_0 = \frac{l}{l_0}\left(\frac{\pi}{2}\right)^2 \sum_k \left(k\bar{q}_{0k}\right)^2 - \frac{\Delta}{l_0}.$$

The equilibrium equation follows from (22):

$$l\frac{(k\pi)^2}{2} T_0 k^2 \bar{q}_{0k} = -l^2 m^* g \frac{1}{k\pi}\left(1 - \cos k\pi\right),$$

whence it follows that $\bar{q}_{0k} = 0$ at $k = 2,4,6,...$. We rewrite the last equation in the form:

$$\frac{k\pi}{2}\bar{q}_{0k} = -\frac{2}{(k\pi)^2}\frac{l\,m^* g}{N_0} \quad (k = 1,3,5,...)$$

and substitute in the expression for deformation (24). As a result, we get

$$\varepsilon_0 = \frac{l}{l_0}\left(\frac{2l\,m^* g}{\pi^2 EF\varepsilon_0}\right)^2 \sum_{k=1,3,...}\frac{1}{k^4} - \frac{\Delta}{l_0},$$

whence it follows that the deformation ε_0 is determined from the solution of the cubic equation $\varepsilon_0^3 + b\varepsilon_0^2 + d = 0$, where

$$b = \frac{\Delta}{l_0} \ge 0,\ \ d = -\frac{l}{l_0}\left(\frac{2l\,m^* g}{\pi^2 B}\right)^2 \sum_{k=1,3,...}\frac{1}{k^4} < 0,$$

the solution of which is found by the Cardano formula.

As an example, a wire fixed at the ends with the characteristics given in Table 1 is considered. Table 2 shows the results of calculations for $n = 1,3,...,9$.

2.3. Natural vibrations

The linearization of equations (24) leads to a system of linear equations

$$\frac{d^2\bar{q}_i}{d\tau^2} + (i\pi)^2\left(\varepsilon_d \bar{q}_{0i} + \varepsilon_0 \bar{q}_i\right) = 0,$$
$$\frac{d^2\bar{r}_j}{d\tau^2} + (j\pi)^2 \varepsilon_0 \bar{r}_j = 0; \quad i, j = 1,2,3,..., \qquad (25)$$

where ε_0, $\bar{q}_{0i}$ are determined from the solution of a static problem; $\varepsilon_d = \frac{l}{l_0}\frac{\pi^2}{2}\sum_i i^2 \bar{q}_{0i}\bar{q}_i$.

Equations (25) will be written in matrix form by introducing column vectors

$$\bar{\boldsymbol{q}} = \left(\bar{q}_1\ ...\ \bar{q}_n\right)^T,\ \bar{\boldsymbol{r}} = \left(\bar{r}_1\ ...\ \bar{r}_m\right)^T$$

and a diagonal matrix K with elements $\kappa_{ii} = i^2$. For simplicity, we will assume that $n = m$. Then instead of equations (25) we have two unrelated matrix equations

$$\frac{d^2\bar{\boldsymbol{q}}}{d\tau^2} + \mathrm{M}^q \bar{\boldsymbol{q}} = 0,\quad \frac{d^2\bar{\boldsymbol{r}}}{d\tau^2} + \mathrm{M}^r \bar{\boldsymbol{r}} = 0, \qquad (26)$$

where

$$\mathrm{M}^q = \pi^2 \mathrm{K}\left(\frac{l}{l_0}\frac{\pi^2}{2}\bar{\boldsymbol{q}}\,\bar{\boldsymbol{q}}^T \mathrm{K} + \varepsilon_0 \mathrm{E}\right),\ \mathrm{M}^r = \pi^2 \varepsilon_0 \mathrm{K};$$

E – unit matrix.

The solution of equations (26) is represented as

$$\bar{\mathrm{q}} = \mathrm{A}\,\widetilde{\sin\omega}\,\tau,\ \bar{\mathrm{r}} = \mathrm{C}\,\widetilde{\sin\omega}\,\tau;$$
$$\widetilde{\omega} = \omega\sqrt{\frac{m^* l^2}{B}}. \qquad (27)$$

Substituting expressions (27) into equations (25) leads to two unrelated systems of algebraic equations

$$(M^q - \tilde{\omega}^2 E)\mathrm{A} = 0,\ (M^r - \tilde{\omega}^2 E)\mathrm{C} = 0, \quad (28)$$

Since the matrix M^r is diagonal, the eigenvalues of the second equation are the values $\tilde{\omega}_j^2 = (j\pi)^2\varepsilon_0$. Then the frequency spectrum of the natural vibrations of the conductor in the horizontal direction is a sequence $\tilde{\omega}_j = j\pi\sqrt{\varepsilon_0}$, $j = 1, 2, ..., n$.

From the condition of non-triviality of the solution of the first equation of system (28), a frequency equation follows for determining the frequency spectrum of natural vibrations in the vertical direction:

$$det\|M^q - \tilde{\omega}^2 E\| = 0.$$

The vibration modes $\boldsymbol{A}$ are determined from the solution of the first equation (28) with the normalization condition $\sqrt{\boldsymbol{A}^T\boldsymbol{A}} = 1$. The vibration modes $\boldsymbol{C}$ are trivial as a sequence $(1\,0...0)$, $(0\,1...0)$, …, $(0\,0...1)$.

As an example, consider a conductor with characteristics from Table 1 for $n = 5$. The solution of the static problem is given in Table 2. The calculation results are shown in Table 3.

The first frequency of horizontal oscillations can be estimated using the equation of oscillations of a physical pendulum $J\,d^2\varphi/dt^2 = M$, where J is the moment of inertia of the sagging conductor about the axis Ox, M is the total moment of the gravitational load.

Table 1. Conductor parameters

Tensile stiffness	$B = 7.3 \cdot 10^6$ N
Linear mass	$m = 0.23$ kg/m
Conductor length	$l_0 = 21$ m
Span length	$l = 20$ m
Gravity acceleration	$g = 9.81$ m/s^2

Table 2. Results of solving a static problem

n	1	3	5	7	9
D	$-6.59 \cdot 10^{-18}$	$-6.67 \cdot 10^{-18}$	$-6.68 \cdot 10^{-18}$	$-6.68 \cdot 10^{-18}$	$-6.68 \cdot 10^{-18}$
ε_0	$5.88 \cdot 10^{-6}$	$5.92 \cdot 10^{-6}$	$5.92 \cdot 10^{-6}$	$5.92 \cdot 10^{-6}$	$5.92 \cdot 10^{-6}$
q_{01}	0.14236	0.14149	0.14138	0.14135	0.14134
q_{03}	-	0.00524	0.00523	0.00523	0.00523
q_{05}	-	-	0.00113	0.00113	0.00113
q_{07}	-	-	-	0.00041	0.00041
q_{09}	-	-	-	-	0.00019

Table 3. Frequencies and waveforms for $n = 5$

Vertical vibrations					Horizontal vibrations				
Natural frequencies, Hz									
0.669	0.957	1.338	1.646	45.202	0.335	0.669	1.004	1.338	1.673
Vibration modes									
0	0.932	0	0.930	0.932	1	0	0	0	0
1	0	0	0	0	0	1	0	0	0
0	0.311	0	0.310	0.310	0	0	1	0	0
0	0	1	0	0	0	0	0	1	0
0	0.189	0	0.195	0.187	0	0	0	0	1

Using the expansion

$$w_0(x) = \sum_k q_{0k} \sin(k\pi x/l),$$

we get

$$J = \frac{m^* l^3 \tilde{J}}{2}, M = -\frac{2m^* l^2 g \tilde{S} \phi}{\pi},$$

where $\tilde{J} = \sum_{i=1,3,...} \bar{q}_{0i}^2, \tilde{S} = \sum_{i=1,3,...} \frac{\bar{q}_{0i}}{i}$.

For the angle of rotation of the pendulum (sagging wire) in the form $\varphi = A \sin \omega t$ from the condition of non-triviality of the solution of the equation of vibrations, we obtain a formula for calculating the circular frequency of oscillations $\omega = \sqrt{\frac{4g\tilde{S}}{\pi l \tilde{J}}}$ or in Hertz $f = \frac{1}{\pi} \cdot \sqrt{\frac{g\tilde{S}}{\pi l \tilde{J}}}$.

The calculation for the above example gives the value $f = 0.333$ Гц, which is completely consistent with the first oscillation frequency in the horizontal direction $f = 0.335$ Гц.

CONCLUSION

When constructing the theory of self-excitation of conductor vibrations, classified in operational OHL practice as a galloping, it is necessary to proceed from the model of a flexible heavy thread that performs spatial vibrations. Galloping modes are observed in the frequency range of the order of 1 Hz, which in the typical OHL spans correspond to the first 1-3 harmonics [6, 7]. Model experiments have shown [5] that vibrations in the vertical plane, which excite parametric vibrations with exit from the sag plane, are essential for such processes. The model of self-excitation should be based on the data of the modal analysis of the system as its basic characteristics.

The methods developed and described in the article for calculating the natural frequencies and vibration modes of the OHL conductors reflect the features of the conductors that determine their tendency to self-excitation of vibrations. It is shown that in the frequency domain of interest, transverse stretching vibrations and pendulum vibrations are essential; longitudinal elastic waves do not play a significant role.

The developed methods of modal analysis of conductor vibrations will be used in the construction of a model of self-excitation of vibrations of OHL conductors of both thermomechanical and aerodynamic nature.

ACKNOWLEDGMENT

The work was supported by a grant from the Russian Science Foundation No 22-19-00678.

REFERENCES

1. **Landa P.S.** Nelinejnye kolebaniya i volny [Nonlinear vibrations and waves]. Moscow,

Fizmatlit, Nauka Publ., 1997, 495 p. (in Russian).
2. **Babitsky V.I., Landa P.S.** Avtokolebaniya v sistemah s inercionnym vozbuzhdeniem [Self-vibrations in systems with inertial excitation] // Dokl. USSR Academy of Sciences, 1982, Vol. 266, No. 5, pp. 1087–1089 (in Russian).
3. **Penner D.I., Duboshinsky Ya.B., Duboshinsky D.B., Petrosov V.A., Porotnikov A.A.** Parametricheskie termomekhanicheskie kolebaniya [Parametric thermomechanical vibrations]. In book: Nekotorye voprosy vozbuzhdeniya nezatuhayushchih kolebanij [Some issues of excitation of undamped oscillations]. Vladimir, VGPI Publ., 1974, pp. 168–183 (in Russian).
4. **Galkin Yu.V., Duboshinsky D.B., Vermel A.S., Penner D.I.** Vertikal'nye termomekhanicheskie kolebaniya [Vertical thermomechanical vibrations]. Ibid, pp. 150–158 (in Russian).
5. **Feldshteyn V.A.** Termomekhanicheskie kolebaniya tokonesushchih provodnikov [Thermomechanical vibrations of current-carrying conductors] // Journal of Applied Mechanics and Technical Physics, 2017, Vol. 58, No. 6, pp. 158–166 (in Russian). DOI: 10.15372/PMTF20170615
6. **Yakovlev L.V.** Plyaska provodov na vozdushnyh liniyah elektroperedachi i sposoby bor'by s neyu [Galloping of overhead power lines conductors and ways to deal with it]. Moscow, NTF "Energoprogress", "Energetik" Publ., 2002, 96 p. (in Russian).
7. **Alexandrov G.P.** (ed.) Proektirovanie linij elektroperedachi sverhvysokogo napryazheniya [Design of ultra-high voltage power transmission lines]. St. Petersburg, "Energoatomizdat" Publ., 1993, 368 p. (in Russian).
8. **Volmir A.S.** Ustojchivost' deformiruemyh system [Stability of deformable systems]. Moscow, Fizmatlit, Nauka Publ., 1967, 984 p. (in Russian).
9. **Grishanina T.V., Shklyarchuk F.N.** Dynamics of plane motion of a body with a system of flexible inextensible rods connected in series by elastoviscous joints at large angles of rotation // Mechanics of Solids, 2011, Vol. 46, pp. 248–255. DOI: 10.3103/S0025654411020130
10. **Danilin A.N.** Dynamics of multilink rod system with constraints: a plane problem in finite element formulation // PNRPU Mechanics Bulletin, 2016, No. 4, pp. 338-363. DOI: 10.15593/perm.mech/2016.4.20
11. **Danilin A.N., Kurdyumov N.N., Shavnya R.A.** Wake-Induced Oscillations of Two Bundle Conductors Connected at Intervals by Spacers // AIP Conference Proceedings 2343, 120005 (2021). DOI: 10.1063/5.0048305

СПИСОК ЛИТЕРАТУРЫ

1. **Ланда П.С.** Нелинейные колебания и волны. Москва: Наука, Физматлит, 1997, 495 с.
2. **Бабицкий В.И., Ланда П.С.** Автоколебания в системах с инерционным возбуждением, ДАН СССР, 1982, Т. 266, № 5. С. 1087–1089.
3. **Пеннер Д.И., Дубошинский Я.Б., Дубошинский Д.Б., Петросов В.А., Поротников А.А.** «Параметрические термомеханические колебания». В кн. Некоторые вопросы возбуждения незатухающих колебаний. Владимир: изд. ВГПИ, 1974. С. 168–183.
4. **Галкин Ю.В., Дубошинский Д.Б., Вермель А.С., Пеннер Д.И.** «Вертикальные термомеханические колебания», там же. С. 150–158.
5. **Фельдштейн В.А.** «Термомеханические колебания токонесущих проводников», ПМТФ, 2017, Т. 58, № 6. С. 158–166.
6. **Яковлев Л.В.** Пляска проводов на воздушных линиях электропередачи и способы борьбы с нею. Москва: НТФ “Энергопрогресс”, “Энергетик”, 2002, 96 с.

7. **Александров Г.П.** (ред.). Проектирование линий электропередачи сверхвысокого напряжения. С-Пб., «Энергоатомиздат», 1993, 368 с.
8. **Вольмир А.С.** Устойчивость деформируемых систем. М., Наука, Физматлит, 1967, 984 с.
9. **Гришанина Т.В., Шклярчук Ф.Н.** Динамика плоского движения тела с системой последовательно соединённых упруговязкими шарнирами гибких нерастяжимых стержней при больших углах поворота // Изв. РАН. МТТ. 2011. № 2. С. 109–117.
10. **Данилин А.Н.** Динамика стержневой системы со связями: плоская задача в конечно-элементной формулировке // Вестник ПНИПУ. Механика. 2016. № 4. С. 338–363.
11. **Danilin A.N., Kurdyumov N.N., Shavnya R.A.** Wake-Induced Oscillations of Two Bundle Conductors Connected at Intervals by Spacers // AIP Conference Proceedings 2343, 120005 (2021).

Valiullin Airat A., student of the Moscow Institute of Physics and Technology (National Research University) (MIPT); 9, Institutsky Lane, Dolgoprudny, Moscow region, 141701; +7 (495) 408-45-54; valiullin.aa@phystech.edu

Валиуллин Айрат Анасович, студент Московского физико-технического института (национального исследовательского университета) (МФТИ); 141701, Московская область, г. Долгопрудный, Институтский пер., д. 9; +7 (495) 408-45-54; valiullin.aa@phystech.edu

Danilin Alexander N., Doctor of Physical and Mathematical Sciences, Chief Researcher of the Institute of Applied Mechanics of the Russian Academy of Sciences (IAM RAS), Deputy Director of IAM RAS for Scientific Work, Professor of the Moscow Aviation Institute; 125040, Moscow, Leningradsky Prospekt, 7, p. 1; +7 (495) 946-18-06; andanilin@yandex.ru

Данилин Александр Николаевич, доктор физико-математических наук, главный научный сотрудник Института прикладной механики РАН (ИПРИМ РАН), заместитель директора ИПРИМ РАН по научной работе, профессор Московского авиационного института; 125040, г. Москва, Ленинградский проспект, д. 7, стр. 1; +7 (495) 946-18-06; andanilin@yandex.ru

Feldshteyn Valery A., Doctor of Technical Sciences, Chief Research Associate of JSC "Central Research Institute for Machine Building" (JSC "TsNIIMash"), Professor at MIPT; Russia, 141070, Moscow region, Korolev, Pionerskaya str., 4; +7 (495) 513-59-51; dinpro@mail.ru

Фельдштейн Валерий Адольфович, доктор технических наук, главный научный сотрудник АО «Центральный научно-исследовательский институт машиностроения» (АО "ЦНИИМаш"), профессор МФТИ; Россия, 141070, Московская область, г. Королёв, ул. Пионерская, д. 4; +7 (495) 513-59-51; dinpro@mail.ru